INVESTIGATION OF THE BIOLOGICAL EFFECT OF EIF4A REDUCTION AND INHIBITION

BY

RICHARD JOHN LITTLE

A thesis

submitted to the Victoria University of Wellington

in fulfilment of the requirements for the degree of

Doctor of Philosophy

Victoria University of Wellington

2020

Abstract

Translation initiation has been identified as a therapeutic target for many diseases including cancers, Alzheimer's disease, viral infections and cachexia. One protein involved in this process is the eukaryotic initiation factor 4A (eIF4A), an RNA helicase that is integral for cap-dependent translation initiation. Multiple drugs that inhibit the normal function of eIF4A have been identified, with one currently entering clinical trials. Recent investigations into the effects of eIF4A inhibitor treatment, however, have used concentrations that significantly hinder cell proliferation and survival. However, applications in Alzheimer's disease, viral infections and cachexia require much lower inhibitor concentrations. Current evidence shows that under these conditions, inhibition of eIF4A leads to disruption of translation of individual transcripts in a manner that is dependent on their sequence and structure. However, the cell-wide effects of eIF4A inhibition at these low concentrations is still not known, and so the mechanisms through which treatments for these diseases will function are not fully elucidated.

Using an expression-based analysis, we investigated the effects of mild perturbation of eIF4A through gene deletion mutations in yeast and low doses of the eIF4A inhibitor pateamine on human cells. With both these approaches we identify a range of expression changes in proteins throughout the proteostatic network, relating to processes such as translation, amino acid production, ribosome biogenesis, protein folding and protein degradation. Processes further removed from translation initiation were also found to be affected but differed between yeast and human cell line models, with energy metabolism being affected in yeast, and telomere maintenance and mRNA metabolism being affected in human cells. We also identified an mRNA 5' untranslated region sequence that appears to confer a disproportionate reduction in expression only seen in pateamine treatment conditions. Through this approach we identify the key cellular effects of altered eIF4A function and demonstrate differences between reduced eIF4A function and pateamine inhibition.

Acknowledgements

To my parents, John and Julie, and my sister, Tracey, thank you for all your love and support over the years. I know that you put a lot into raising me and made a large investment into my education early on when I was struggling, I would not be where I am today without you. I appreciate that when I was unwell, you were there for me and helped me to get back on my feet. I hope I've made you proud.

My amazing partner Charlie, I don't know how to convey just how much I value and appreciate you and the sacrifices you have made for me. The last few years have been incredibly intense and not at all what you thought you were signing up for. Despite this you have been an amazing partner throughout my studies and my sickness and stuck by me and supported me more than I could have ever hoped. I've seen that you are an incredibly strong and brave person and I know we can rely on each other for all of life's challenges. I love you and I'm so excited to spend the rest of my life with you. I know I've hardly made a dent in the number of roasts I owe you but I'll get there.

My supervisor Paul, you have been a guiding hand throughout my studies giving insights and encouragement whenever it was needed. I have found your advice to be invaluable and I am thankful for all the time you have spent on me and my project. I really appreciate how patient you have been, especially with my writing and when I had to take a break. I hope to keep in touch in the years ahead.

My supervisor Lifeng, thank you for all you have taught me about mass spectrometry analysis and methodology and your help with editing. I really appreciate that you were always happy to help and give advice whenever I knocked on your office door.

James, your guidance when I was starting out in research was invaluable, you taught me a great deal and gave me the foundations I needed to build this project

Peter, thank you for your help when I was getting my head around analysis with your GFP scripts and good times at BYOs.

Dini, thank you for all your help with fixing and maintaining the microscope despite how non-compliant it was, and for you company in the evenings. You are a great scientist and a dear friend.

To everyone else from the lab past and present you have all helped me in your own way, whether you gave advice on a technique or were good company, I appreciate how you contributed.

Table of contents

Table of figures

Table of tables

Table of abbreviations

Abbreviation	Word
APP	Amyloid precursor protein
APS	Ammonium persulfate
ATP	Adenosine triphosphate
CID	Collision-induced dissociation
dH2O	Distilled water
DMDA	Des-methyl, des-amino
DMSO	Dimethyl sulfoxide
DTT	Dithiothreitol
EDTA	Ethylenediaminetetraacetic acid
eIF	Eukaryotic initiation factor
EJC	Exon junction complex
FDR	False discovery rate
FTMS	Fourier transform mass spectrometry
GFP	Green fluorescent protein
GOAT	Gradient optimization analysis tool
HPLC	High Performance Liquid Chromatography
iBAQ	Intensity-based absolute quantification
IC	Inhibitory concentration (followed by degree of inhibition)
iNOS	Inducible NO Synthase
IRES	Internal ribosome entry sites
LPS	Lipopolysaccharide
MTT	3-(4,5-dimethylthiazol-2-yl)-2,5-diphenyltetrazolium bromide
Nano LC	Nano liquid chromatography

nt	Nucleotide
ORFs	Open reading frames
P-bodies	Processing bodies
PEG	Polyethylene glycol
PMA	Para-methoxyamphetamine
RAN	Repeat associated non-AUG
RFP	Red fluorescence protein
SC	Synthetic complete
SC	Synthetic complete
SD	Synthetic deficient
SD	Synthetic deficient
SDS	Sodium dodecyl sulphate
TBE	Tris boric acid EDTA
TE	Tris EDTA
TEMED	Tetramethylethylenediamine
TIC	Total ion current
TIF	Translation initiation factor
TOP	Terminal oligopyrimidine tract
uORF	Upstream open reading frame
WT	Wild type

Chapter 1 – Introduction

1.1. Background

Many human diseases are the result of a protein-driven physiological imbalance or accumulation of aberrantly synthesised proteins. The process through which proteins are produced from mRNA transcripts is called translation. One of the key steps in this process is translation initiation, where many cellular components are brought together and organised for translation to begin. Recent studies have led to the identification of several small molecules which inhibit translation initiation providing a new target for therapeutic strategies. At present, the first translation initiation targeting drugs are entering clinical trials as a therapeutic strategy (Cunningham et al., 2018; Effector_Therapeutics, 2019). Complete inhibition of this process renders a cell unviable and cell death will follow. However, not all chemical inhibitor treatments have such a general, global effect. Our research focuses on the function of eukaryotic initiation factor 4A (eIF4A) and the small molecule inhibitor pateamine. Pateamine has been demonstrated to have powerful anti-proliferative effects in cancers as well as having positive effects that may be harnessed in treatment of cachexia (Di Marco et al., 2012; Parikh et al., 2012). There are additional suggestions of the value of eIF4A inhibitors, such as pateamine, in treatment of Alzheimer's disease, Huntington's disease, and viral infections (Banez-Coronel et al., 2015; Bottley et al., 2010; Slaine et al., 2017a). Despite the promise of pateamine as a potential therapeutic agent, the model that explains these effects is still being refined, and there is still a major lack of understanding of what other broad effects, either beneficial or detrimental, eIF4A inhibition could have on biological systems.

The aim of the work reported in this thesis is to examine and refine the model that explains the effect of eIF4A inhibitors, in terms of global protein changes. Through measuring gene expression at the protein level, both direct and indirect consequences of inhibition can be evaluated to identify key features dictating expression changes. This will give a greater overall understanding of the mechanisms involved in the actions of eIF4A inhibitors and the follow-on effects of eIF4A depletion and inhibition.

1.2. Pateamine

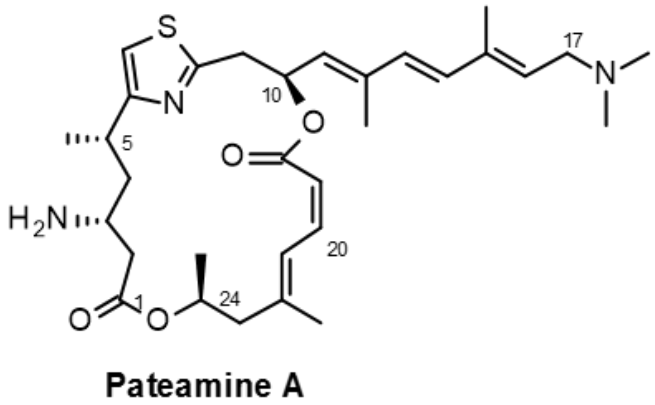

Figure 1. Chemical structure of pateamine A

Pateamine A (Figure 1) was first reported in 1991 as a natural product isolated from the marine sponge *Mycale Heranceli* by the Blunt and Munro research group. It was initially identified through the use of activity-directed purification (Northcote et al., 1991). Pateamine A was identified to have immunomodulatory effects. By treating a mixed lymphocyte reaction it was demonstrated that pateamine inhibited the synthesis of IL-2 in T-cells at sub cytotoxic concentrations (Romo et al., 1998). Pateamine was found to affect human cells at much lower concentrations than required to have an effect on yeast, and it has no effect on prokaryotes (Northcote et al., 1991). Treatment was also found to induce stress granule formation in mammalian cells (Dang et al., 2006). The target of pateamine, eIF4A, was identified concurrently by two different research teams. A collaboration between McGill University and Victoria University of Wellington research teams identified pateamine as an inhibitor of translation through a high throughput reporter chemical screen and in parallel through affinity isolation of pateamine-binding proteins (Bordeleau et al., 2005; Low et al., 2005). It was also found that binding of pateamine to eIF4A enhanced both the ATPase and RNA binding affinity of the protein, which ultimately causes a decrease in catalytic turnover (Bordeleau et al., 2005). Since identifying the target of pateamine, interest in the compound as a therapeutic agent has gained momentum. Research reported in 2009 showed pateamine exhibited significantly increased apoptosis-inducing activity when treating proliferating cells compared to cells in quiescence, making it a compound of interest for cancer therapy (Kuznetsov et al., 2009). In addition to its anticancer potential, research into pateamine is also of interest for other human diseases as it, or other inhibitors of eIF4A, have been shown to

retard viral proliferation and prevent the production of toxic proteins associated with several neurodegenerative diseases (Biedenkopf et al., 2017; Bottley et al., 2010; Kearse et al., 2016; Slaine et al., 2017a; Yanguez et al., 2011).

Unfortunately, research into pateamine and its effects has been slow moving. A major contributor to this is the limited availability of pateamine. The compound abundance is highly variable between samples of *Mycale.* In general, it is either not produced by a sample, or is found only in very small amounts. The highest abundance samples have come from extremely remote locations in the rugged Fiordland regions of New Zealand, meaning supply of pateamine from a natural source is very limited. The variable availability is consistent with pateamine being produced by a symbiotic bacterium and to date attempts to culture pateamine producers have failed.

To increase the availability of pateamine it has also been produced using synthetic chemistry. The first synthesis of pateamine was reported in 1998 (Romo et al., 1998). The second complete synthesis followed in 2004 (Pattenden, 2004). In both cases, the synthesis contained more than 20 steps in its longest linear sequence, with an overall yield below 0.2%. Although a 2018 synthesis from Zhuo and Furstner (2018) has increased the overall yield to 5.3%, the very limited availability of the natural form of pateamine has substantially limited its development for clinical use (Zhuo and Furstner, 2018). In an effort to enhance production efficiency a number of analogues of pateamine have also been produced. The alteration and/or removal of some structural motifs of pateamine can significantly reduce the cost of reagents and reduce the number of reaction steps required to produce the final molecule. The most successful pateamine analogue so far is des-methyl, des-amino (DMDA) pateamine A, again produced by the Romo lab. Due to the structural simplification inherent in DMDA pateamine, it was synthesized in fewer steps than pateamine giving an overall yield of almost 4% (Romo et al., 2004). Fürstner's 2018 publication also provides a dramatically improved synthesis of DMDA pateamine A, which can be accessed through his methodology in a reported >18% overall yield (Zhuo and Furstner, 2018). This molecule is much less costly to produce yet still retains biological activity close to that of pateamine. Given the improved yield through Furstner's synthesis and that other eIF4A inhibitors are expected to reach clinical trials in the near future, there is an urgent need to characterise the downstream effects of eIF4A inhibition.

1.2.1. Potential covalent inhibition

There are indications that pateamine may form a covalent interaction with its target, eIF4A. Experimentation with pateamine-linked sepharose columns determined that removal of eIF4A proved to be difficult, requiring harsh treatments for elution. Additionally, in experiments involving treatment with pateamine, subsequent washing to remove the drug does not result in rescue of the cells from apoptosis, suggesting that pateamine is inactivating eIF4A in a permanent manner. If a covalent bond is formed between pateamine and eIF4A, this could arise through reaction of the electrophilic α,β-unsaturated lactone motif which is known to be the motif responsible for formation of the covalent bond between syringolin A and the β5 proteasome subunit (Kitahata et al., 2017). Inhibitors that form a covalent bond with their target, initially interact non-covalently much like a normal small molecule inhibitor. A combination of non-covalent interactions lead to the inhibitor interacting closely with the target protein. Once in the correct conformation a nucleophilic motif on the protein can attack an electrophilic reside on the inhibitor. There are several advantages to inhibitors that function in this way: inhibition of the target protein will be retained even after concentrations of the inhibitor in solution has decreased and can be given at lower concentrations as, unlike noncovalent treatments, there is no equilibrium to maintain. This can mean effective treatment with reduced side effects (Singh et al., 2011). However, only some amino acid residues are nucleophiles, giving a potential mechanism for acquiring resistance (Singh et al., 2011).

1.3. Other translation initiation inhibitors

Although Pateamine was the first drug-like compound found to modulate functions of eIF4A, several other eIF4A-modulating molecules have since been discovered.

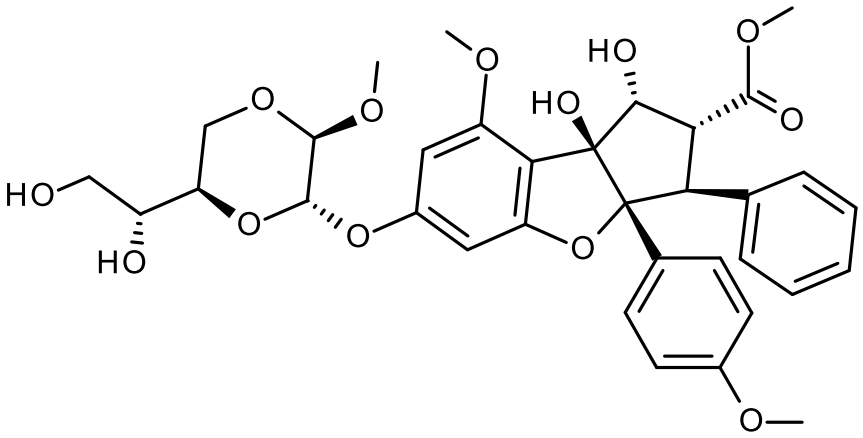

Figure 2. The chemical structure of silvestrol

Silvestrol (Figure 2) is a flavagline, or rocaglate derivative, which was originally identified in the fruits and twigs of *Aglaia foveolate,* a tree found in Southeast Asia. Although it is structurally very different from pateamine, silvestrol has also been shown to elicit its inhibitory functions by increasing the RNA binding affinity of eIF4A leading to a reduction of enzymatic turnover (Bordeleau et al., 2008). Investigations in mouse models have shown silvestrol could be used as an effective treatment against hormone-dependent human prostate cancer (Kim et al., 2007). Silvestrol has a number of attributes which make it a poor candidate for being a clinical therapeutic. However, modifications to the structure of silvestrol through chemical synthesis, has led to the production of several structural analogues. Alterations at carbons 2, 4 and 6 of silvestrol has resulted in the improvement of exposure, potency and efflux profiles of the drug as well as simplification of the synthesis (Liu et al., 2012). The synthetically designed compound eFT226, now known as zotatifin, is also a modified flavagline and a selective inhibitor of eIF4A. Much like pateamine and silvestrol eFT226 has been shown to elicit its effects by inducing a strong binding interaction between eIF4A and the mRNA strand. This tight binding prevents translation initiation. *In vitro* eFT226 is effective at inhibiting the proliferation of several cancer cell lines including lymphoma, breast, and lung cancer, at low nanomolar concentrations (Thompson, 2017). Western blot analysis showed treatment resulted in reduced expression of key oncogenes including c-MYC

and BCL2 (Thompson, 2017). *In vivo*, when treated with eFT266, multiple mouse xenograft human tumour models showed a marked decrease in tumour size. Of particular note were TMD8 B-cell lymphoma xenografts which exhibited a 97% tumour size reduction when treated at 1 mg/kg for 15 days (Thompson, 2017). Zotatifin is now entering clinical trials in patients with pancreatic adenocarcinoma or certain other tumours driven by HER2, ERBB3, FGFR1, FGFR2, or KRAS (Therapeutics, 2019). These early trials will primarily determine the safety, pharmacokinetics, and pharmacodynamics of zotatifin, providing an indication of doses suitable for use in further clinical trials.

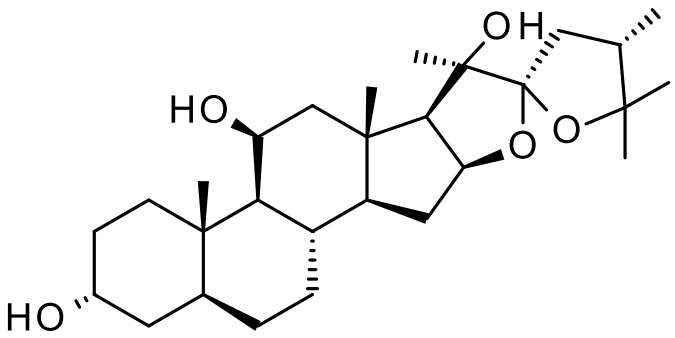

Figure 3. The chemical structure of Hippuristanol

Hippuristanol (Figure 3) is a natural product isolated from the coral *Isis hippuris*. Hippuristanol acts as a small molecule inhibitor which targets the function of eIF4A. However, unlike pateamine and silvestrol, which induce strong binding of eIF4A with its substrates, hippuristanol induces its effects by causing eIF4A to remain in a closed conformation (Sun et al., 2014). When in this conformation the RNA binding site is allosterically inhibited, resulting in a loss of function. Hippuristanol is primarily an eIF4AI and II inhibitor, it does also inhibit eIF4AIII but at concentrations 10-fold higher (Lindqvist et al., 2008). Hippuristanol, much like pateamine, has been found to have strong anti-proliferative effects on viruses. A 2006 study investigating the effects of hippuristanol used HeLa cells infected with polio virus. When treated with the drug, cells needed to be incubated for two hours longer than cells not treated with hippuristanol, for viral proteins to reach detectable levels (Bordeleau et al., 2006). Hippuristanol has also been demonstrated to be a potential treatment for certain types of cancer including Human T-cell leukaemia virus induced anti-adult T-cell leukaemia (Tsumuraya et al., 2011).

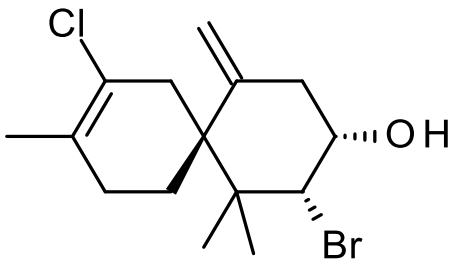

Figure 4. Elatol chemical structure

Elatol (Figure 4) is a compound isolated from a number of marine species, including the red algae *Laurencia rigida*. It was discovered through a screen searching for translation initiation inhibitors. It has been identified as an ATP-mimic competitive inhibitor, which results in inhibition of the helicase activity of eIF4A. In cell culture experiments, elatol has been shown to inhibit eIF4AI at low μM concentrations but it is so far unclear if it also affects eIF4AII and eIF4AIII. Elatol was found to be effective at inhibiting the growth of 344/924 cancers screened with leukaemia and lymphoma cell lines in particular being overrepresented. Murine xenograft models show daily injections of elatol halts tumour growth, however tumour growth resumes after injections cease. Unfortunately, treatment was not well tolerated in mice, with treated tumour-bearing animals developing damage to heart and liver (Peters et al., 2018).

A final inhibitor, 6-aminocholestanol, was originally identified for its antifungal activity by inhibiting the biosynthesis of ergosterol (Beuchet et al., 1998). However, more recently 6-aminocholestanol has been shown to inhibit both mouse eIF4A and a suspected leishmania parasite eIF4A homologue. This inhibition is achieved by competitively inhibiting the RNA binding and ATPase activity of eIF4A, resulting in the protein being unable to carry out its helicase activity. Interestingly, 6-aminocholestanol was shown to enhance the RNA unwinding activity of mouse eIF4AI/II in the absence of ATP. This suggests the enzyme can be locked in a closed conformation when bound by the drug, similar to pateamine. The predicted binding pocket of 6-aminocholestanol on eIF4A is the same pocket hippuristanol is known to bind in. This is unsurprising as the compounds share structural similarity but interesting as hippuristanol inhibits RNA binding instead of enhancing it (Abdelkrim et al., 2018; Lindqvist et al., 2008).

1.4. eIF4A

Translation involves concerted function and regulation of many factors. The processes of translation begins after an RNA transcript exits the nucleus through the nuclear pore into the cytoplasm. The transcript is then bound by translation initiation factors in order to facilitate the binding of the ribosome which ultimately leads to the production of a new protein. Of particular interest to us is the group of initiation factor proteins which bind to the *N*7-methylguanylate cap of the RNA template and prepares the site for the binding of the 40S ribosomal subunit. The major complex involved in this process, the eIF4F complex, is responsible for carrying out a number of processes required for translation initiation. This complex is comprised of three proteins each with its own role. The cap-binding protein eIF4E binds tightly to the *N*7-methylguanylate cap of the mRNA strand and holds the complex in the correct position. Our protein of interest, eIF4A, is an RNA helicase. It interacts with the mRNA stand causing the strand to lose its secondary structure which then allows the ribosome preinitiation complex to bind. Lastly, eIF4G functions as a scaffold protein which binds eIF4A and eIF4E, ensuring these proteins are in the correct conformation. It positions and induces conformational changes in the other enzymes to enhance their activity. In addition to interacting with other members of the eIF4F complex, eIF4G interacts with eIF3 and the Poly(A)-binding protein (PABP) recruiting them to the cap to initiate ribosomal scanning (Figure 5)

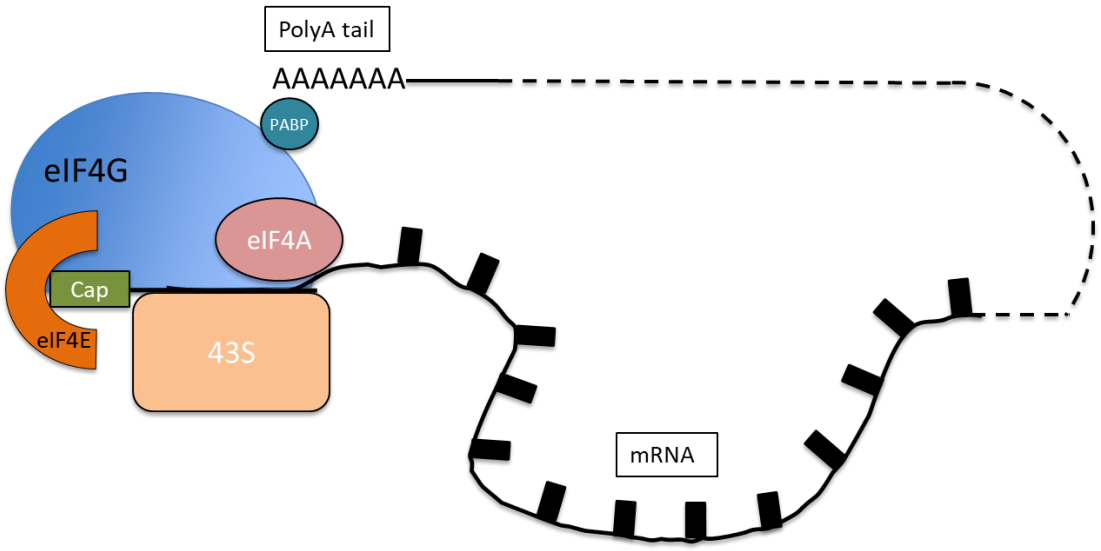

Figure 5. A schematic of the pre-translation initiation complex. The eIF4E protein binds the N*7-methylguanylate cap of the mRNA anchoring the complex. The eIF4G protein acts as a scaffold recruiting and holding the other factors in place and enhancing their activity. The mRNA transcript is the unwound by eIF4A allowing binding of the 43S ribosome and scanning of the start site with tRNA.*

1.4.1. eIF4A structure and function

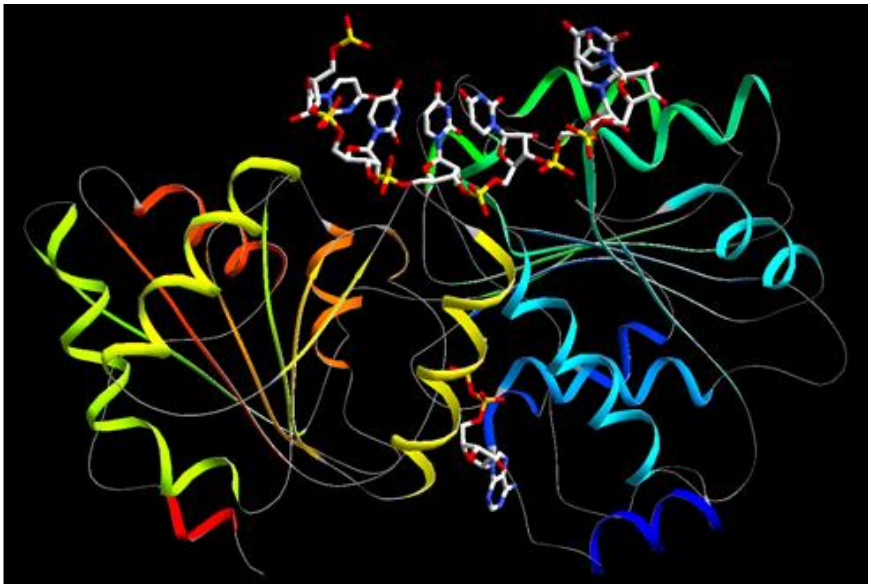

Figure 6. Schematic of the eIF4AIII protein. eIF4AIII bound to RNA (top) and ATP (bottom) from 3EX7 pdb file. The protein is represented as a ribbon that is colour coded from blue (N-terminus) to red (C-terminus).

The structure of eIF4A consists of two RecA-like lobe structures with a flexible linker amino acid string between them. When inactive, eIF4A adopts an open conformation with the two lobes independent of each other. This conformation changes when eIF4A interacts the other members of the eIF4F complex inducing it form a 'half-open' conformation, greatly increasing its affinity for RNA and ATP (Hilbert et al., 2011; Korneeva et al., 2005) and increasing the helicase and ATPase activity of the enzyme (Andreou and Klostermeier, 2014). When RNA and ATP bind, the flexible linker region of eIF4A then bends to allow the two lobes to interact with each other to adopt a closed conformation which results in the formation of the ATPase and helicase catalytic sites (Figure 6).

Human eIF4As are encoded by 3 different genes, eIF4AI and II proteins function in a cyclical manner in translation initiation; first the two lobes are brought together through the binding of ATP and an mRNA duplex, to form a closed conformation. This binding activates the enzyme, causing it to manipulate the bound RNA. Any duplex of RNA strands which are interacting with the chain of the transcript bound to eIF4A are forced into energetically unfavourable conformations, causing them to dissociate and be released from the complex. ATP is hydrolysed, and release of the phosphate group causes the conformation of the protein to adopt a more open state. The remaining segment of the mRNA strand is then expelled from its binding site on eIF4A and ADP can dissociate (Andreou and Klostermeier, 2013). The eIF4A

molecule is now returned to its initial state having removed the mRNA secondary structure. This process prepares the 5' untranslated region (UTR) end of the mRNA transcript for binding of the ribosome. The cap binding complex remains bound to mRNA strand and guides the 40S ribosome subunit on to the stand to form the 43S preinitiation complex (Figure 5). Once the complex has scanned for the start codon translation begins.

A point of difference with eIF4A is that, unlike the other translation initiation proteins, different mRNAs have varying requirements for eIF4A function. Experimentation using a dominant-negative eIF4A mutant has demonstrated the requirement for eIF4A is directly proportional to mRNA structure. Transcripts with highly structured 5' UTRs, particularly when the structure was proximal to the 5' cap, were found to be more susceptible to translation inhibition by the mutant eIF4A (Svitkin et al., 2001). This attribute presents the possibility that partial inhibition of eIF4AI or II will reduce expression of certain transcripts, leading to therapeutic benefits, while leaving many protein levels unchanged.

1.4.2. eIF4AIII

The function of eIF4AIII differs greatly from eIF4AI and II. In contrast to the cytosolic location of eIF4AI and II, the highest abundance of eIF4AIII is located in the nucleus where it is involved in mRNA maturation and nonsense mediated decay. In the nucleus, eIF4AIII acts as a component of the spliceosome complex. Much like eIF4AI and II, eIF4AIII functions by binding mRNA strands but in this case, it is utilized by the cell as a molecular anchoring device. The eIF4AIII protein interacts with exon junction complex (EJC) components MLN51 and the Magoh/Y14 heterodimer (Singh et al., 2013). This activates its helicase activity and can then bind to the pre-mRNA transcript. Moreover as with eIF4AI and II, eIF4AIII binds and hydrolyses ATP but when interacting with MAGO-Y14 eIF4AIII does not allow the release of ADP and the phosphate group. This causes eIF4AIII to clamp tightly to the mRNA anchoring the EJC in place. This binding remains after mRNA maturation has occurred and it is suspected that the EJC functions to enhance nuclear export of the mRNA through the nuclear pore (Le Hir et al., 2001). Once in the cytoplasm, translation is initiated. As the ribosome travels along the mRNA transcript, the EJCs on the strand are removed until the ribosome reaches a stop codon. In a normal cellular setting, all EJCs on the mRNA will be removed. However, if there is a frameshift mutation which leads to a premature stop codon in the gene being expressed, not all EJCs will be removed. An mRNA strand which still has an EJC bound after an initial translation step will

be bound by Upf3 recruiting the nonsense mediated decay machinery and degrading the strand (He and Jacobson, 2015).

1.4.3. Endogenous eIF4A inhibition

Initiation is the rate limiting step of translation. As a result, this process is highly regulated and the effects of inhibitors on this process can cause major changes in a cell's expression profile. Given the involvement of eIF4A in many types of cancers and other diseases, it is no surprise that there are internal cellular mechanisms in place to regulate its function and induce apoptosis if these mechanisms fail. Programmed cell death 4 protein (PDCD4) is an inhibitor of cap-dependent translation. It carries out this function by binding directly to eIF4AI and preventing it from interacting with eIF4G to form the eIF4F complex, preventing translation initiation. The expression of PDCD4 is linked to the prognosis of several cancers. It has been observed that PDCD4 expression is often repressed in in high-grade tumours compared to low-grade tumours with decreased PDCD4 expression being an indicator of poor outcomes (Chen et al., 2003). Development of a therapeutic capable of inhibiting the actions of eIF4A could be particularly effective on cancers supressing PDCD4 expression by re-inducing translational control. This has been demonstrated in human breast cancers that overexpress MUC1-C which causes the degradation of PDCD4. Treatment with silvestrol resulted in a marked decrease in MUC1-C expression and inhibited cell growth (Jin et al., 2013).

1.4.4. Dose dependent effects of eIF4A inhibitors

The complete inhibition of all eIF4A has a relatively indiscriminate effect on translation. With the exception of a small number of genes which utilise select cap-independent internal ribosome entry sites (IRES), translation initiation cannot be carried out without functional eIF4A. As mentioned above, what differentiates eIF4A inhibition from most other translation inhibitors is that at sub-complete inhibition concentrations certain inhibitors exhibit mRNA-selective characteristics in a dose dependent manner (Iwasaki et al., 2016; Iwasaki et al., 2019; Wolfe et al., 2014). At low concentrations of inhibitors many proteins are synthesized at relatively normal levels but a small number of proteins exhibit a much larger decrease in abundance (Wolfe, 2014; Iwasaki, 2016). This is likely a result of two causes; an mRNA transcript's 5' UTR secondary structure and mRNA containing specific 5' UTR nucleotide sequences. The former can be explained by an individual mRNA's requirement for eIF4A. An mRNA transcript which forms a highly stable secondary structure must be unwound before translation can occur. When cellular levels of functional eIF4A are reduced, translation is likely to preferentially stall on these structured mRNAs compared to mRNA with relatively little secondary structure. The latter cause is likely explained by the very specific effect some select inhibitors have on eIF4A. Most chemical inhibitors elicit their effects by disrupting functions of the target molecule, however pateamine, silvestrol, and rocaglamide A have been shown to act as enhancers of the RNA binding functions of eIF4A. This interaction causes a strong interaction between eIF4A and RNA. It is likely that the effects observed during treatment is the result of the eIF4A protein having preferred substrate sequences and being unable to release these RNA strands and be recycled, resulting in an RNA-specific dominant-negative effect.

1.4.5. G-quadruplexes & purine tetramer

Figure 7. The silvestrol-sensitive motif identified by Wolfe et al. (2014)capable of forming G-quadruplex structures

Previous research into inhibiting eIF4A has utilized ribosome profiling to investigate where the ribosome stalls upon treatment with an eIF4A inhibitor (Iwasaki et al., 2016; Wolfe et al., 2014). These studies have focused on the positioning of stalled polysomes on certain mRNA transcripts. This has led to the identification of sequences in the 5' UTR which result in a greater than average inhibitory effect when treating with rocaglamide A. Two main nucleotide motifs have been identified with this method. The first is the G-quadruplex motif identified by Wolfe et al. (2014). This motif consists of a repeating sequence of two guanidine nucleotides next to each other with a spacer (usually a cytosine) for four or more repeats (Figure 7). This motif can coil on itself to form highly stable structures called G-quadruplexes by adopting Hoogsteen base-pairing (Fay et al., 2017). It is easy to understand why this motif may be disproportionately affected by eIF4A inhibition. As described above, eIF4A is a helicase which functions to remove the secondary structure of the mRNA strand, so the ribosome can bind and proceed along the transcript. If a particular mRNA transcript has a stronger, more stable structure in its 5' UTR it stands to reason that it will have a greater requirement for eIF4A in order for the ribosome to proceed to the start site. This motif has been identified in number of oncogenes' 5' UTRs suggesting eIF4A inhibition could be an effective cancer treatment strategy (Wolfe et al., 2014).

Figure 8. One of many possible arrangements a rocaglamide A-sensitive polypurine motif

Another nucleotide motif was identified part-way through this project which consists of purine-rich stretch identified by Iwasaki et al. (2016; 2019). This motif consists of a length of adenosine and guanidine bases four or more nucleotides long (Figure 8). Pull down and

mutant eIf4A studies show that this binding is the result of rocaglamide A inducing eIF4A to bind tightly to the polypurine motif and not allowing the preinitiation complex to form. Inhibition of translation of transcripts with this motif is the result of a tight binding of eIF4A to target transcripts rather than depletion of useable eIF4A. Recently, there has been progress in understanding the mechanism of inhibition for these select sequences. The interaction of rocaglamide A with eIF4A and RNA has been revealed with the use of X-ray crystallography. Binding of eIF4A to RNA results in a cavity formed by the helicase and the bent RNA strand. When this cavity formation occurs, a single molecule of rocaglamide A can position inside of this cavity and interact with both the protein and RNA molecule, stabilising the interaction and preventing dissociation from occurring (Figure 9). Interestingly the formation of the correct molecular cavity was only observed when the RNA strand contains a stretch of four or more purine nucleotides and sequences containing pyrimidines form a cavity that was unable to accommodate the inhibitor (Iwasaki et al., 2019). This interaction was shown to be sequence length dependent with polypurine stretches 10 nucleotide (nt) long showing a far greater affinity for eIF4A in the presence of Rocaglamide A than those 4 nt long. The stabilization of eIF4A and the RNA strand being sequence dependent demonstrates that it is possible that this inhibition can result in a reduction in expression of certain transcripts at very low concentrations of inhibitor, whilst leaving most transcripts unaffected. These sequence and concentration effects are summarised in Figure 10.

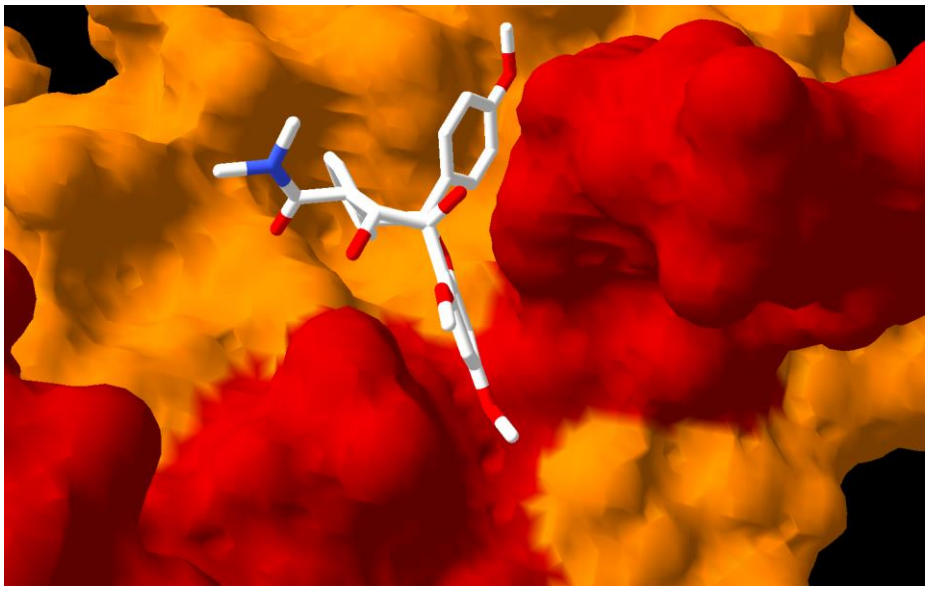

Figure 9. Image of the interaction between eIF4A and the mRNA strand being "locked" in place by rocaglamide A. Image was produced using the 5ZC9 pdb file using the Swiss PDB viewer. The orange surface is from the eIF4A protein; RNA is shown as a deep red surface; rocaglamide is shown as a stick structure.

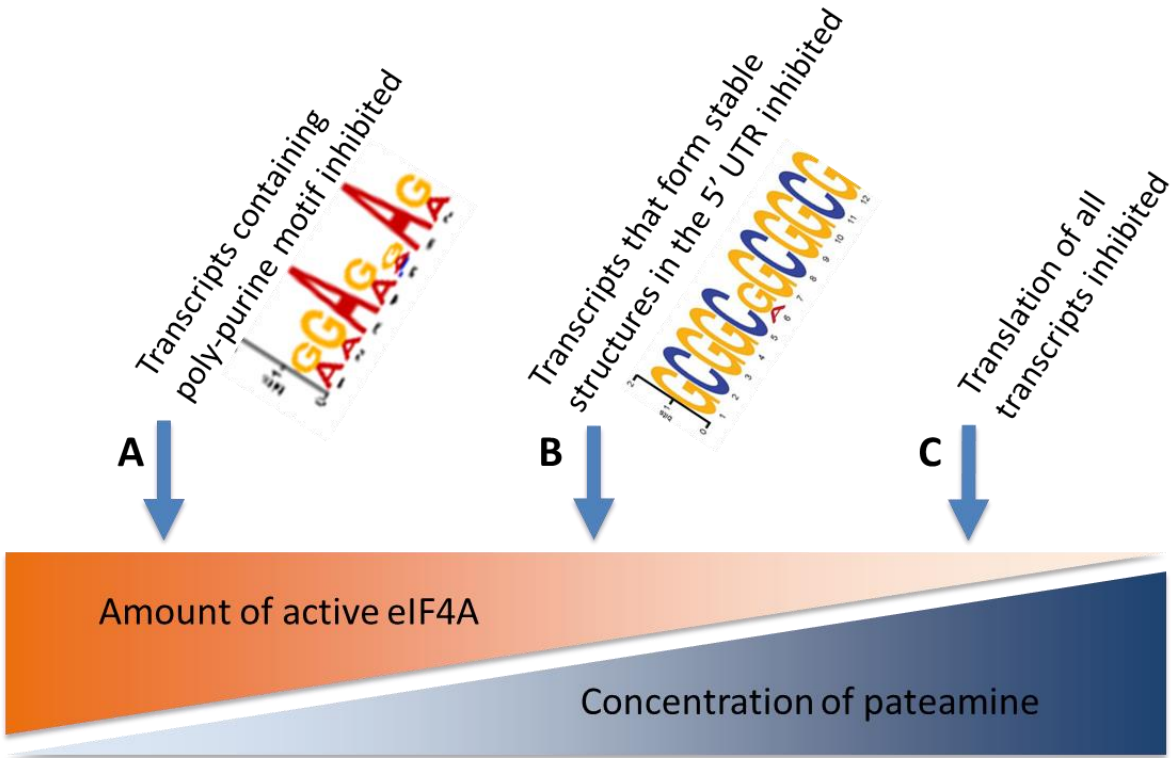

Figure 10. A diagram demonstrating the hypothesised *relationship between amount of pateamine and active eIF4A, and the mRNA transcripts affected. At lower concentrations of pateamine there is still an abundance of active eIF4A, only transcripts with specific motifs that pateamine-affected eIF4A "clamps" to are affected (**A**). At higher concentrations of pateamine significant amounts of eIF4A are inactivated leading to transcripts with higher structure no longer being sufficiently unwound to be expressed (**B**). At very high concentrations of pateamine all eIF4A is inhibited resulting in the suppression of all transcripts (**C**).*

1.5. eIF4A and disease

1.5.1. Cancer

Cancer is a disease characterised by the uncontrolled proliferation of cells. For solid tumours, as the disease progresses these cells begin to invade surrounding tissues and metastasize to other parts of the body, where they form secondary tumours. Eventually the metabolic load and waste products of these tumours become too great for the body to manage leading to death. Current treatments of many cancers have poor success rates and have severe side-effects including pain, nausea, and organ damage. These drawbacks with current treatments highlight the need for development of new, more effective treatment options.

The eIF4A protein is the most abundant translation initiation factor (Duncan and Hershey, 1983), however in many types of cancers it is often further up-regulated including lung, cervical cancer, and melanoma (Bhat et al., 2015; Eberle et al., 1997). In addition to this, it has been observed that increased expression of eIF4A correlates with poorer prognosis of radiation therapy in cervical cancer (Liang et al., 2014) and increased expression of eIF4A is associated with increased metastasis in some cancers (Chen et al., 2019; Wang et al., 2002). Furthermore, a cellular inhibitor of eIF4A, PDCD4, has been observed to be down-regulated in many cancer types and its expression can be an indicator of poor prognosis (Chen et al., 2003; Wang and Yang, 2019). It is believed that this increased eIF4A abundance helps meet the increased protein requirements of cancer cells as they proliferate. This suggests that inhibition of eIF4A could be an effective therapeutic strategy for cancer therapy to slow proliferation or even induce cell death. Furthermore, in addition to increasing cancer malignancy, activation of translation initiation machinery can also lead to cancer cells acquiring resistance to treatment. Studies investigating therapy resistant metastatic melanoma show increased eIF4F complex formation was a strong determinant of resistance to vemurafenib and inhibiting formation of the complex re-sensitised the cell line (Boussemart et al., 2014). Also of clinical interest, is that certain eIF4A inhibiting compounds are capable of preferentially inhibiting the expression of some mRNAs with a greater need for eIF4A function. As mentioned above, the expression of mRNA transcripts containing a G-quadruplex motif, are preferentially down-regulated when treated with silvestrol. This GC-rich motif has been identified in the 5’ UTR of many mRNAs which drive cancer phenotypes,

reducing the expression of these proteins has the potential of improving patient outcomes (Wolfe et al., 2014).

1.5.1.1. Cancer combination therapies

Multiple studies have investigated the potential of eIF4A inhibition as a therapeutic strategy. A study in 2012 focused on the use of pateamine in combination with radiation therapy. When A549 human lung cancer cells were treated with an analogue of pateamine one hour before irradiation therapy, cell survival was reduced by ~93% when treated with the highest dose of a pateamine analogue compared to a irradiation-only control with some outcomes appearing to be synergistic (Parikh et al., 2012). In addition to being a radiotherapy sensitiser, inhibition of eIF4A has also been shown to sensitise cancer models to chemotherapy. When treated with the DNA damaging drug doxorubicin, mouse Eμ-Myc lymphoma xenograft models showed a significant increase in survival time when treated with hippuristanol (Cencic and Pelletier, 2016).

1.5.2. Cachexia

Cachexia is a muscle wasting disease associated with cancer and other illnesses. Studies have shown that approximately 22% of cancer deaths are linked to the effects of cachexia (Tisdale, 2009). Additionally, the effects of cachexia are associated with poor responses to chemotherapy and decreased survival (Aoyagi et al., 2015). Previous experiments with mice have demonstrated that treatment with pateamine results in a reduction of the effects of cancer-induced cachexia. This effect has been demonstrated at least in part to be the result of pateamine affecting the expression of the inducible nitric oxide Synthase (iNOS) by sequestering iNOS mRNA to stress granules (Di Marco et al., 2012). More recent research has shown this anti-cachexia effect is also seen when treating with hippuristanol (Cramer,2018). Inhibition of eIF4A has been demonstrated to also reduce the expression of the STAT3 transcription factor and prevent downstream expression of IL-6 and other proinflammatory cytokines. This results in the reduction of proinflammatory responses and increasing the expression of MyoD mRNA further attenuating the effects of cachexia (Cramer et al., 2018). To date there is no clinical treatment of the underlying causes of cachexia, and this work reveals that eIF4A inhibition is a new potential therapeutic approach.

1.5.3. Alzheimer's and Huntington's diseases

Alzheimer's disease is the result of aberrant production of the proteins tau and amyloid precursor protein (APP). Accumulation of these two proteins results in large aggregated protein deposits known as plaques to form in the brain. These plaques cause large scale deterioration of the brain and cognitive function, eventually resulting in death. Both tau and APP proteins are known to possess long, highly structured 5' UTRs in their mRNA transcripts requiring eIF4A to unwind. Additionally, these transcripts also contain a form of internal ribosome entry site which requires eIF4A for translation initiation (Beaudoin et al., 2008; Veo and Krushel, 2009). This means that inhibition of eIF4A could be an effective treatment strategy to prevent or decrease the formation of these plaques. This has been demonstrated in some cell types including SH-SY5Y and HeLa cells with the use of hippuristanol. Treatment with hippuristanol resulted in a significant reduction in expression of both tau and APP proteins as determined by western blot (Bottley et al., 2010). It is reasonable to suspect the same effects would be observed with pateamine, potentially with greater responses at lower concentrations due to the clamping effect pateamine induces between eIF4A and structured transcripts.

Huntington's disease is a progressive early onset neurodegenerative disease. Worldwide, Huntington's disease affects 5.8/100,000 people leading to the development of early dementia, dystonia, and Parkinsonism (Green et al., 2016). Huntington's disease is caused by the expansion of a CAG repeat in the protein coding region of the huntingtin gene. This expansion leads to a gain of function of the mRNA strand, the CAG repeats become capable of sequestering RNA-binding proteins and initiating translation at any frame shift through a mechanism known as repeat associated non-AUG (RAN) translation (Banez-Coronel et al., 2015). This unregulated translation leads to a build-up of toxic protein. Recent research has shown that RAN translation initiation still requires much of the same enzymatic machinery needed for canonical cap-dependent initiation, including eIF4A. Using *in vitro* translation experimentation, researchers have shown that inhibiting eIF4A with hippuristanol is capable of preventing RAN-induced translation at concentrations that do not affect the canonical AUG-start translation (Kearse et al., 2016).

1.5.4. Viral infection

There is a growing amount of evidence that host eIF4A is required for replication of many types of viruses. Ebola is a highly contagious viral disease with an average fatality rate of ~50%. Ebola virus mRNAs possess a guanosine cap and significant structure in their 5' UTRs, suggesting that they have a considerable requirement for eIF4A function. Treating Ebola-infected Huh-7 and primary human macrophages with silvestrol at sub-growth inhibiting concentrations, significantly reduced viral proliferation and expression of the viral protein VP40 (Biedenkopf et al., 2017). Influenza is a common viral infection which affects between three to five million people each year of which between 291,000 and 646,000 cases are fatal (CDC, 2017). Of these deaths, the majority occur in young children, the elderly and people with other health issues. Despite the 5' UTRs of influenza mRNA being relatively short and unstructured, research with non-functional eIF4A mutations in HEK293 cells have demonstrated that the influenza virus requires functional eIF4A to proliferate (Yanguez et al., 2011). These effects were also observed when cells were treated with the inhibitor hippuristanol at concentrations that did not affect cell viability (Yanguez et al., 2011). A more recent study has demonstrated that silvestrol and pateamine are also effective at inhibiting influenza proliferation in a reversible and irreversible manner respectively. Pateamine was also shown to be an effective inhibitor of several different strains of influenza virus suggesting having abundant, functional eIf4A is a fundamental requirement for influenza replication (Slaine et al., 2017b). Additionally, inhibition of eIF4AIII with pateamine A has been shown to reduce the nuclear export of human cytomegalovirus mRNAs. This inhibition greatly reduced the accumulation of viral DNA and the virus' ability to proliferate (Ziehr et al., 2016).

1.5.5. Impact of research

Many studies to date which investigate the possible therapeutic benefits of translation initiation inhibition, do so by focusing on specific genes relating to a disease-driving function. However, cap-dependent translation initiation is a fundamental cellular process in which the majority of proteins are produced. This presents a great potential for many unintended and undesirable effects to also result from eIF4A inhibition. Inhibiting such a fundamental pathway is likely to affect the abundance of many different proteins having unexpected consequences. Not only will inhibition of eIF4A influence protein translation directly, it will also have secondary effects. Many mRNAs could be preferentially inhibited by pateamine and if these mRNAs code for transcription factors, as noted for STAT3 above, or proteins associated with protein degradation pathways, expression levels of many other proteins could also be affected, despite pateamine not directly inhibiting their translation. This could cause major changes in the expression profile of the cell as a follow-on effect. Recent studies have utilized polysome profiling to investigate changes in expression as a result of eIF4A inhibition, allowing for the identification of mRNA transcripts directly affected but this approach is less informative when investigating changes in proteostasis and the secondary effects treatment with these drugs may have.

1.6. Research aims

Existing research in the field has highlighted key areas where knowledge needs to be expanded. Overall, the aim of this research is to gain a deeper understanding of the outcomes of reduced eIF4A function, including the follow-on effects of inhibition or reduction in the abundance of functional eIF4A, on the global protein abundance in the cell under conditions that do not significantly affect cell proliferation. To address this aim, this work explores two main approaches:

1. To determine the effects of reducing the abundance of functional eIF4A on the protein landscape in *Saccharomyces cerevisiae*. Analysis of protein abundance will be carried out utilising high throughput confocal microscope analysis of a yeast green fluorescent protein (GFP)-tagged protein library and mass spectrometry. This will be done in combination with eIF4A knock-down mutants to identify changes in protein expression as a result of gene deletion to gain a greater understanding of eIF4A function and the cell wide effects of lost function.

This aim will consist of the following objectives:

Identify methods of determining when translation initiation is reduced

Find genetic methods to reduce translation initiation in yeast

Investigate proteome and pathway changes resulting from reduced functional eIF4A

Identify enriched features in the 5’ UTRs of transcripts differentially affected by a reduction in functional eIF4A

2. To transition this investigation toward a clinical focus by carrying out protein abundance analysis in human cell lines. Protein abundance changes will be assessed with the use of mass spectrometry to identify specific proteins which are disproportionally influenced by low doses of pateamine. This protein list will then be probed to find key aspects of genes which influence the transcript dependent effects of pateamine.

This aim will consist of the following objectives:

Determine preferred cell lines for pateamine investigations

Investigate proteome and pathway changes resulting from pateamine inhibition

Identify enriched features in the 5’ UTRs of transcripts differentially affected by pateamine treatment

Identify enriched features in the 5’ UTR of transcripts differentially affected by a reduction in functional eIF4A

2. Chapter 2 – The Effects Of Reduced eIF4A Abundance In Saccharomyces cerevisiae

2.1. Introduction

The aim of this research is to investigate the effects of inhibition of translation initiation to gain an understanding of the outcomes and follow on effects on biological pathways. In this chapter we use yeast as a model organism to investigate the effects of a reduction in functional cellular eIF4A abundance.

As described in Section 1.4.4, there are currently two suspected models of how pateamine differentially affects the expression of different proteins. The first is that pateamine induces a strong interaction of eIF4A to mRNAs, leading to the being sequestered into stress granules and preventing their expression. The second mechanism is though the depletion of functional eIF4A. Given that expression changes of proteins in cachexia models occur at drug concentrations far below those needed to induce significant cell death (Di Marco et al., 2012), it was suspected that this effect was the result of pateamine inducing this strong binding interaction of eIF4A to certain mRNA transcripts over others. However, subsequent research shows these expression changes are also seen when treating with hippuristanol, a compound that prevents eIF4A from binding RNA, acting as a loss of function mutation (Cramer et al., 2018). This finding casts doubt on the mRNA sequestration model.

Using a yeast model, we attempted to mimic a loss of function model through drug-free reduction in the abundance of eIF4A. This produces a loss of function mutation, without accompanying complications of other effects of a drug treatment. We also used cells that had progressed through multiple generations of condition. We anticipated that this might indicate what the biological response to a long-term treatment with an eIF4A inhibitor may look like if the loss of function effect predominates in cachexia treatment. Through this approach we hope to gain insights in to the effects of translation initiation inhibition on fundamental pathways common to yeast and humans, as a result of reduced abundance of functional eIF4A. Improved understanding of the mechanisms involved could pave the way for development of pharmaceuticals for diseases including cancers, Alzheimer's disease, and cachexia (Bottley et al., 2010; Chan et al., 2019; Cramer et al., 2018; Di Marco et al., 2012). Additionally, this body of research aims to identify the biological pathways altered by reduced

eIF4A activity. This will allow for the improved prediction of the outcomes of eIF4A inhibition and give insights into disease targets of translation initiation inhibition and find potential partner drugs for combination therapies.

The previous chapter gave an overview of the role eIF4A proteins play in translation initiation, described several diseases for which inhibition of eIF4A shows potential to treat and outlined the main aims of our research. The aim of this chapter is to investigate the follow-on effects of a reduction in eIF4A function in a cell wide context. To address this aim we will carry out experimentation using eIF4A knock-down mutants coupled with expression change based analysis to identify key biological pathways affected by a reduction in the amount of functional cellular eIF4A.

2.1.1. Yeast as a model organism

Saccharomyces cerevisiae is a well-established model for investigating eukaryotic systems. It has been used to model a range of human diseases including Alzheimer's disease, mitochondrial diseases, and cancer (Bhatia-Kissova and Camougrand, 2010; Nitiss and Heitman, 2007; Treusch et al., 2011). It is estimated that approximately 3900 human genes have a corresponding yeast ortholog (Laurent et al., 2016) of which 1,000 orthologs have been linked to diseases in humans (Hofer et al., 2018). Additionally, many of these genes have even been shown to function as a substitute for the native gene when expressed in the other organism (Kachroo et al., 2015) demonstrating the comparability between organisms. Deletion of genes is also an effective method for simulating drug effects (Boone et al., 2007).

Yeast is commonly used in biological experimentation due to a number of benefits over alternative systems. When carrying out experimentation which requires genetic manipulation yeast models allow for fast, low-cost protocols including cross mating and homologous recombination techniques and robust selection using antibiotic resistance cassettes (Duina et al., 2014). Additionally, yeast is relatively straightforward to visualise using microscopy and has many established libraries such as GFP-fusion protein and gene deletion arrays which are valuable tools for high throughput analysis (Duina et al., 2014).

However, there is a notable drawback associated with yeast experimentation. Yeast cells are often far more resistant to cytotoxic drugs compared to mammalian cell lines. Although this resistance can be somewhat mitigated with the deletion of the PDR1 and PDR3 genes that

code for the transcription factors that induce the expression of several drug efflux pump portions (Fardeau et al., 2007; Michalkova-Papajova et al., 2000), much higher quantities of drug are required especially when carrying out high throughput experiments.

2.1.2. Yeast libraries

As described above, experimentation with yeast allows for rapid low-cost genetic alteration. This has allowed for the production of several commercially available mutant libraries. Large-scale crosses of these libraries of mutants can be carried out with yeast mating procedures and selections.

2.1.2.1. Yeast knockout collection

The yeast knockout collection is a gene deletion library of yeast strains. Each strain contains a kanamycin resistance gene coupled with a 'molecular barcode' DNA sequence for identification in place of an open reading frame (Winzeler et al., 1999). Production of this deletion library revealed that 80% of yeast genes were not individually essential for normal growth on rich media with the effects of these deletions only becoming apparent under stress conditions. This can be utilized by analysing the strains disproportionately affected by a given stress, giving valuable insight into the pathways a given condition is affecting (Giaever et al., 2002). This deletion strain collection is commercially available.

2.1.2.2. Yeast protein-GFP-fusion tag array

In *Saccharomyces cerevisiae* a protein-GFP-fusion library is now available with each strain possessing a different native protein fused to a GFP label. This commercially available Yeast GFP Clone Collection, consists of 4,159 Mat**a** yeast strains with different open reading frames (ORFs) tagged with GFP each expressed under the control of the endogenous promoter keeping expression at normal biological levels. This collection constitutes 75% of the yeast proteome (Huh et al., 2003). The parent library used in this study has be further modified for the purposes of automation. In order to improve automated cell recognition all clones in the library have been modified to express a constitutive mCherry red fluorescence protein (RFP) (Shaner et al., 2004) that localizes to the cytoplasm and a RedStar2 RFP (Janke et al., 2004) linked to a nuclear localization signal (NLS). These modifications result in a diffuse red fluorescence signal throughout the cytoplasm due to the low intensity, diffuse mCherry RFP and an intense red signal inside the nucleus from the RedStar RFP concentrated there (Figure 11). This clear definition of the cell and nucleus allows for effective automated cell boundary identification and improved measurement of intercellular localization of the library of GFP-fusion proteins and allows for normalization (Bircham et al., 2011).

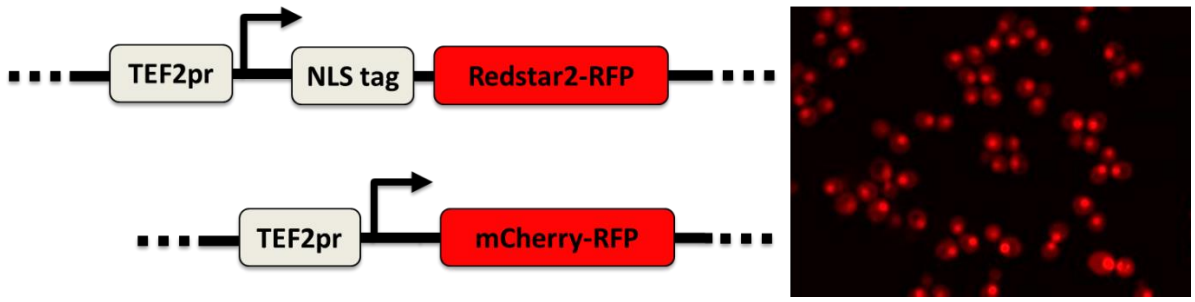

Figure 11. A genetic schematic of the dual RFP labelling method for automated cell recognition. The RedStar2 RFP is tagged with a nuclear localization signal producing an intense red fluorescence in the nucleus. The mCherry RFP is not tagged giving a diffuse signal in the cytoplasm. Both RFPs are placed under the control of the constitutively expressed TEF2 promoter.

2.1.3. Yeast eIF4A

Yeast possesses two genes that produce a homologue of the eIF4A protein involved in translation initiation. These proteins are known as translation initiation factors 1 and 2 (Tif1p & Tif2p). Although the *TIF1* and *TIF2* genes and their promoters are different, Tif1p and Tif2p are indistinguishable, being identical in sequence, structure and function. The proteins from *TIF1* and *2* retain ~66% sequence identity with their mammalian counterparts and function in

much the same way. Expression of either one of these two copies is essential for life, however loss of function of one of these genes has little effect on growth (Venturi, 2012). The closest yeast homologue to eIF4AIII is coded by the gene *FAL1*. Although Fal1p retains ~61% protein sequence identity with eIF4AIII, its role differs from its mammalian homologue and instead it is involved in the biogenesis of the 40S rRNA ribosomal subunit (Kressler et al., 1997). At present there is no strong evidence that pateamine also affects the function of Fal1p, it is possible that pateamine does interact with Fal1p but at far higher concentrations.

2.1.4. GFP microscopy

GFP microscopy often employs a fluorescent *Aequorea victoria* protein attached to a native cellular protein (Heim et al., 1995). With the use of a fluorescence microscope we can make use of this labelling technique to determine the localizations, abundance, and interactions of certain proteins in order to assess how these attributes change with a given stimulus. The production of a GFP-fusion protein involves the use of yeast genomic homologous recombination placing the gene for the GFP from *Aequorea Victoria* downstream from the native gene of interest (Figure 12). Modifying the gene in this way results in the GFP being attached to the C-terminus of the native protein. This allows for quantitation of proteins with accuracy equivalent to that seen in western blot and mass spectrometry analysis (Breker et al., 2013; Newman et al., 2006). As useful as this tool is, there are some limitations and considerations in certain applications. Addition of a GFP protein to the C-terminal end of a cellular protein can influence its dynamics including function, localization, and half-life. Investigation of GFP tagging with essential genes suggests that the majority of proteins retain normal functionality when fused to a GFP protein, with 87% of fused essential gene strains surviving (Goryanin and Goryachev, 2012). Many proteins possess a localization peptide sequence signal at the C-terminal end. In some cases, adding the GFP protein can interfere with the recognition of this signal causing the protein to mis-localise and potentially cause downstream biological effects. However, analysis of the GFP-fusion library has reported 80% agreement with previously reported localizations and more recent analysis of these suggesting this effect may be seen in less than 4% of proteins (Breker et al., 2013; Huh et al., 2003). The use of such GFP-fusion libraries has enabled the ability to visualise many phenotypes not associated with changes in growth rate or morphology (Chong et al., 2012).

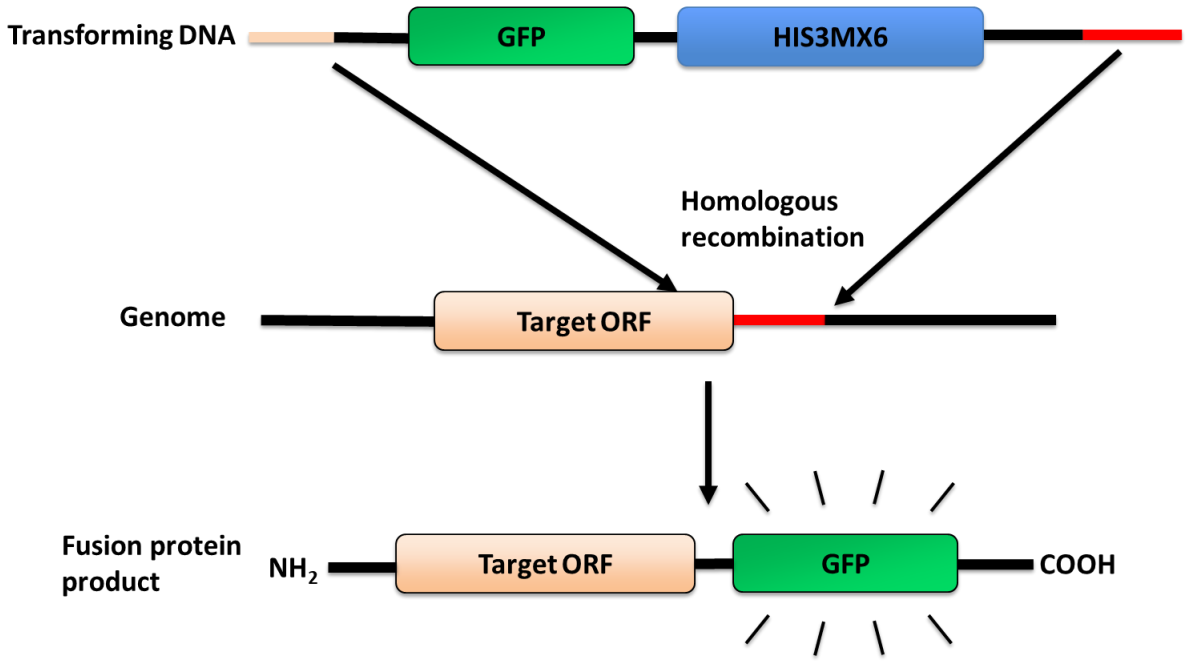

Figure 12. A schematic of the GFP tagging cassette and subsequent fusion protein. A DNA segment containing a GFP and HIS3 selection marker and flanked by sequences homologous to the end of the target ORF and immediately downstream of the target ORF is inserted into the genome using homologous recombination. The protein produced by this modified ORF consists of the native protein fused to the GFP at its C-terminus.

2.1.4.1. High throughput microscopy

Given the large number of GFP clones, to make full use of this powerful tool the library must be coupled with a high-throughput fluorescence microscope, allowing for investigation of cell-wide changes induced by a drug or condition. Automated confocal microscopes are designed for high content, high-throughput screening. Using 488 nm and 561 nm lasers both GFP and RFP respectively can be excited allowing for multiple proteins to be visualized simultaneously and easy definition of cell boundaries. This optical arrangement is combined with a motorized automatic plate holder stage allowing for automated screens of entire plates. The use of this analytical tool has proven effective for investigating the DNA alkylating agent methyl methanesulfonate. Screening of this drug against a GFP fusion protein library identified protein expression changes in a range of processes including DNA repair, chromatin remodelling, and mRNA processing to give insights into cellular responses and the transcription factors involved (Mazumder et al., 2013).

2.1.4.2. Image analysis

The development of higher throughput microscopy has resulted in the massive increases in the amount of data a single experiment can produce. As mentioned earlier, the GFP library consists of 4,159 GFP tagged proteins each of which is imaged multiple times to improve consistency and in multiple planes of focus to ensure the optimal cross section of the cells is taken. When considering this imaging must be carried out in both treated and control, a single simple screening replicate can consist of 74,862 images or more. Analysing this considerable bulk of images is greatly expedited with the use of automated image analysis software.

Previous work at Victoria University Wellington carried out by Peter Bircham with the Acapella software has led to the development of an Acapella script capable of recognising yeast cells and analysing them using multiple metrics (Bircham, 2014). This analytical script functions in a stepwise process, the nucleus of each cell is identified by detecting high intensity RedStar RFP then the cytoplasm is defined using a fainter mCherry RFP and various metrics are used to confirm identification of a cell. The GFP fluorescence can then be analysed for changes in GFP fluorescence intensity and distribution. This measurement is then often normalized against the constitutively expressed RFP (Jonikas et al., 2009). The metrics of treated and control images can then be compared.

Use of the GFP collection coupled with high throughput microscopy can be a useful tool for investigating biological responses to cellular stresses. An example of this is a study published by Breker et al. (2013) that investigated the effects of oxidative stress with H_2O_2, reducing stress with Dithiothreitol (DTT) and nitrogen starvation stress on yeast. This resulted in the identification of a range of protein localization changes and expression changes highlighting key responsive elements to each stress (Breker et al., 2013).

Using these high-throughput, fluorescence-based methods allows for the identification of transient cellular structures such as stress granules and processing bodies (P-bodies) which can be used to determine when translation is being inhibited (Swisher and Parker, 2010).

2.1.5. Stress granules and P-bodies

Stress granules and P-bodies are cytoplasmic granules composed of a mixture of proteins and mRNAs. These cellular structures are transient in nature and serve to store and regulate the expression of mRNA transcripts. Although they carry out similar roles, stress granule, and P-body formation is generally induced as a result of different stimuli and carry out different roles. P-bodies function by uncapping and degrading mRNAs whereas stress granules are suspected to function more as storage for mRNAs, stabilizing transcripts during periods of stalled translation (Bradshaw and Dennis, 2009; Fay and Anderson, 2018). Stress granules have been shown to form in mammalian cells independently of eIF2A phosphorylation-induced translational arrest, as a result of pateamine treatment (Dang et al., 2006). However, as of yet it is unclear whether these effects are also seen in yeast.

A range of conditions for modulating eIF4A function and observing this modulation were evaluated. Using a GFP protein fusion library with a *TIF1* deletion mutation and whole cell proteomic quantitative mass spectrometry on *TIF1* and *2* deletion mutants, we identified a list of proteins with altered expression when altering eIF4A abundance. Analysis of these lists found enrichment in a range of biological processes along the protein production pipeline and homeostasis, ranging beyond translation initiation.

2.2. Methods

2.2.1. Yeast genotypes used

The yeast strains used in this study were originally produced from the S288c S*accharomyces cerevisiae* strain and were maintained in 15% glycerol stocks stored at -80°C. Strains are listed in the table below (Table 1).

Table 1. List of yeast strains used in this study. XXX denotes each gene available in library.

Name	**Description**	**Genotype**
BY4741		Mat**a** *his3*Δ1; *leu2*Δ0; *met15*Δ0; *ura3*Δ0
BY4742		Mat**α**; *his3*Δ1; *leu2*Δ0; *lys2*Δ0; *ura3*Δ0
Mat**a** *tif1*Δ deletion mutant	The *tif1*Δ deletion mutant picked from the Mat**a** yeast knockout collection deletion library with at BY4741 background	Mat**a**; *tif1*Δ::KanR; *his3*Δ1; *leu2*Δ0; *met15*Δ0; *ura3*Δ0
Mat**a** *tif2*Δ deletion mutant	The *tif2*Δ deletion mutant picked from the Mat**a** deletion library with at BY4741 background	Mat**a**; *tif2*Δ::KanR; *his3*Δ1; *leu2*Δ0; *met15*Δ0; *ura3*Δ0
Mat**α** *tif1*Δ deletion mutant	The *tif1*Δ deletion mutant picked from the Mat**α** Open Biosystems yeast knockout collection deletion library with at BY4742 background	Mat**α**; *tif1*Δ::KanR; *his3*Δ1; *leu2*Δ0; *lys2*Δ0; *ura3*Δ0

Mat**α** *tif2*Δ deletion mutant	The BY4742 strain transformed with a *tif2*Δ deletion cassette (Section 2.3.5.2.1)	Mat**α**; *tif2*Δ::KanR; *his3*Δ1; *leu2*Δ0; *lys2*Δ0; *ura3*Δ0
Yeast overexpression empty vector strain	BY4741 transformed with the pBG1805 overexpression plasmid	Mat**a**; *his3*Δ1; *leu2*Δ0; *met15*Δ0; *ura3*Δ0
Yeast WT-*TIF1* overexpression strain	BY4741 transformed with the pBG1805 overexpression plasmid containing the wild type (WT) *TIF1* gene, inserted at the expression site	Mat**a**; *his3*Δ1; *leu2*Δ0; *met15*Δ0; *ura3*Δ0
Yeast P147L-*TIF1* overexpression strain	BY4741 transformed with the pBG1805 overexpression plasmid containing the P147L mutant *TIF1* gene inserted at the expression site	Mat**a**; *his3*Δ1; *leu2*Δ0; *met15*Δ0; *ura3*Δ0
G-quadruplex GFP reporter strain	BY4741 transformed with the G-quadruplex reporter construct (described Section 2.2.9)	Mat**a**; *his3*Δ1; *leu2*Δ0; *met15*Δ0; *ura3*Δ0
Overexpression plasmid transformed GFP-fusion protein strains	The XXX GFP-fusion protein collection (Huh et al., 2003) transformed with the pBG1805 plasmid containing the WT *TIF1* gene, inserted at the expression site	Mat**a**; XXX-GFP-*HIS3*; *his3*Δ1; *leu2*Δ0; *ura3*Δ0; *LYS2*+

Overexpression plasmid transformed GFP-fusion protein strains	The XXX-GFP-fusion protein collection (Huh et al., 2003) transformed with the pBG1805 plasmid containing the P147L mutant *TIF1* gene, inserted at the expression site	Mat**a**; XXX-GFP-*HIS3*; *his3*Δ1; *leu2*Δ0; *ura3*Δ0; *LYS2*+
Overexpression plasmid transformed GFP-fusion protein strains	The XXX-GFP-fusion protein collection (Huh et al., 2003) transformed with the pBG1805 plasmid with no gene inserted at the expression site	Mat**a**; XXX-GFP-*HIS3*; *his3*Δ1; *leu2*Δ0; *ura3*Δ0; *LYS2*+
Yeast RFP + GFP-fusion protein library (Bircham, 2014)	The XXX GFP-fusion protein collection (Huh et al., 2003) crossed with a strain with a nuclear localised RedStar RFP and cytoplasmic localized mCherry RFP	Mat**a**; XXX-GFP-*HIS3*, *can1*Δ::STE2pr-Sp-*URA*; *lyp1*Δ::mCherry-*NAT*; *his3*Δ1; *leu2*Δ0; *ura3*Δ0::NLS-RedStar2-*HPH*; *LYS2*+
Yeast RFP + GFP-fusion protein *TIF1* deletion library	The yeast RFP + GFP-fusion protein library (above) crossed the *tif1*Δ deletion mutant from the Open Biosystems Mat**α** library	Mat**a**; XXX-GFP-*HIS3*, *can1*Δ::STE2pr-Sp-*URA*; *lyp1*Δ::mCherry-*NAT*; *his3*Δ*1*; *leu2*Δ0; *ura3*Δ0::NLS-RedStar2-*HPH*; *LYS2*+; *tif1Δ*::KanR

2.2.2. Plasmids used

For the eIF4A and mutant eIF4A over expression studies the pBG1805-PAR1. The pBG1805-PAR1 was derived from the pRSAB1234 plasmid (Open Biosystems) (Gelperin et al., 2005) and transformed to contain the *TIF1* ORF, expressing either WT eIF4A or eIF4A bearing a P147L pateamine resistance motif under control of the *GAL1* promoter. These plasmids were produced by Dr James Matthews prior to commencement of this study (Matthews, 2010).

In addition to the pBG1805 over expression plasmid, two other plasmids were also used in this study purely as a template for PCR amplification. The pYM44 plasmid was utilized as a template for the GFP gene (Janke et al., 2004) and the pFA6a-kanMX6 plasmid as a template of KanMX6 cassette which contains the KanR gene between the -*TEF* promoter and terminator (Janke et al., 2004).

2.2.3. Growth media

All cultures for experimentation were grown with the media compositions listed below (Tables 2 8) and using procedures stipulated in Amberg (2005). All media components were obtained from Formedium unless otherwise stated. All media was autoclaved at 121°C for 20 min and then allowed to cool to 65 °C before the addition of dextrose solution.

Table 2. Ingredients used to make 1 L YPD media

Ingredient	**Amount**
Yeast extract	10 g
Peptone	20 g
Agar*	20 g
Water	To 950 mL
Dextrose** (Sigma-Aldrich)	50 mL of 40% (w/v)

**Agar only added for solid media*

*** Dextrose added after autoclaving*

Table 3. Ingredients used to make 1 L synthetic media

Ingredient	**Amount**
Yeast nitrogen base without ammonium sulfate	6.7 g
Mono sodium glutamate (MSG) (Sigma-Aldrich)	1 g
"Amino acid mix" (Table 4)	2 g
Agar*	20 g
Water	To 950 mL
Dextrose**	50 mL of 40% (w/v)

**Agar only added for solid media*

*** Dextrose added after autoclaving*

Table 4. Ingredients used to make the "amino acid mix" for yeast synthetic media, consisting of a combination of amino acids and other nutrients. Note: in media for which selections were carried out the corresponding amino acid or nucleobase was omitted

3 g adenine	2 g histidine
2 g uracil (Sigma-Aldrich)	2 g isoleucine
2 g inositol	10 g leucine
0.2 g para-aminobenzoic acid	2 g lysine
2 g alanine	2 g methionine
2 g asparagine	2 g phenylalanine
2 g arginine (Sigma-Aldrich)	2 g proline
2 g aspartic acid	2 g serine
2 g cysteine	2 g threonine
2 g glutamic acid	2 g tyrosine
2 g glutamine	2 g tryptophan (Sigma-Aldrich)
2 g glycine	2 g valine

Table 5. Ingredients used to make 1 L glucose nutrient agar (GNA) pre-Sporulation Media

Ingredient	**Amount**
Yeast extract	8 g
Bacto-peptone	3 g
Agar	2% (w/v)
Water	To 750
Dextrose*	250 mL of 40% (w/v)

** Dextrose added after autoclaving*

Table 6. Ingredients used to make 1 L of enriched sporulation media

Ingredient	**Amount**
Potassium acetate (Sigma-Aldrich)	10 g
Dextrose*	0.5 g
Yeast extract	1 g
Amino acid supplement (histidine, leucine, lysine, uracil)	0.1 g
Agar	20 g

** Dextrose added after autoclaving*

Table 7. Ingredients used to make 1 L of LB media

Ingredient	**Amount**
Tryptone	10 g
Sodium chloride (NaCl)	10 g
Yeast extract	5 g
Agar*	20 g
H_2O	To 1 L

Once dissolved pH was adjusted to 7.0 with 8 M NaOH and dH2O added to 1 L.

**Agar was only added when solid media was required*

Table 8. List of antibiotics used and their final concentrations

Antibiotic	**Concentration**
Geneticin (G418, Invitrogen)	200 µg/mL
Nourseothricin (ClonNat, Werner BioAgents)	100 µg/mL
Canavanine (Carbosythn)	50 µg/mL
Thialysine (Carbosythn)	50 µg/mL
Hygromycin B (HPH, InvivoGen)	200 µg/mL
Ampicillin (Applichem)	100 µg/mL

2.2.4. Yeast genomic extraction

Yeast genomic extractions were carried out using standard procedures outlined in Amberg (2005). Yeast cells were grown overnight in 2 ml liquid YPD media at 30 °C shaking. The culture was palleted by briefly centrifugation at 16,100 *x g*, resuspended in distilled water (dH_2O) and transferred to a micro centrifuge tube where it was re-palleted. The cell pellet was then resuspended in 200 µl of lysis buffer (2% v/v Triton X-100 (Scharlab), 1% sodium dodecyl sulphate (SDS) (Invitrogen), 100 mM NaCl (across organics, 10 mM Tris pH 8 (Sigma-Aldrich) and 1 mM Ethylenediaminetetraacetic acid (EDTA) pH 8 (Applichem). An equal volume of phenol (Sigma-Aldrich) -chloroform (Sigma-Aldrich)-isoamyl alcohol (Fisher chemicals) (25:24:1) mixture was then added and 0.45-0.52 mm acid-washed glass beads added to two thirds of the liquid height. Mixtures were then vortexed for 30 s increments five times with one minute on ice between them. An aliquot of 0.2 mL of TE (10 mM Tris, 1 mM EDTA, pH 8) was then added and briefly mixed and the upper aqueous phase retained. DNA was then precipitated with the addition of 3 volumes of ice-cold 100% ethanol (Carlo Erba) and 0.1 volume of 3 M sodium acetate (Sigma-Aldrich). The tube was mixed and left on ice for 5 min. The DNA was then pelleted by brief centrifugation at 16,100 *x g* at 4˚C for 10 min. Ethanol was removed and the pellet allowed to dry for 5 min in a laminar flow cabinet with the lid off. Finally, the DNA pallet was then dissolved in 50 µl of dH_2O.

2.2.5. PCR reactions

PCR reactions (Saiki, 1988) were carried using Techne Prime thermal cycler (Alphatech) in 25 µL reaction volumes with the following reagents (Table 9). All reagents were added to the reaction tubes with the Ex Taq polymerase added last and mixed immediately prior to loading the tubes into the thermal cycler which was then run at the cycles outlined below (Table 10).

Table 9. Reagents added to a standard PCR reaction

Ingredient	**Concentration**	**Amount**
dNTPs in dH_2O	5 mM	1 µL
Template DNA in dH_2O	100 ng/µL	0.5 µL
Ex Taq PCR buffer 10x (TaKaRa)	10x	2.5 µL
Ex Taq polymerase (TaKaRa)	5 U/µL	0.125 µL
Forward & Reverse primer in dH_2O	100 nM	0.5 µL ea.
dH2O	-	To 25 µL

Table 10. The cycling temperatures and times of a standard PCR protocol

Number of cycles	**PCR step**	**Temperature**	**Duration**
1	Initial melt	98°C	5 min
30	Melt	98°C	30 s
	Annealing	See primer Tables 13 & 12	30 s
	Extension	72°C	1 min 30 s
1	Final extension	72°C	3 min
N/A	Hold	4°C	∞

2.2.6. Procedure for agarose gel electrophoresis

DNA amplicons were separated and visualized using agarose gel electrophoresis analysis (Lee et al., 2012). Agarose gel was produced by combining 0.4 g of agarose powder (Fisher biotech) with 4 mL of 10x TBE buffer (900mM boric acid (Pronalys), 20 mM EDTA disodium dihydrate, 900 mM Tris-Cl, pH 8) buffer and made to 40 mL with dH_20. This was heated in a microwave until the agarose was completely dissolved. The solution was topped up to 40 mL with dH_20 and allowed to cool for 5 min. Prior to pouring, 0.5 µg/ml ethidium bromide (Sigma-Aldrich) was added then the solution was poured into the gel setting chamber with a well comb and left to set. The set gel was transferred into the gel tank and 1x TBE running buffer (90 mM boric acid, 2 mM EDTA disodium dihydrate, 90 mM Tris Base, pH 8) was poured over until the gel was completely immersed. DNA samples and a 1 kb+ ladder were individually mixed with 5x DNA gel loading buffer (glycerol 30% (v/v) (Sigma-Aldrich), bromophenol blue 0.25% (w/v) (Sigma-Aldrich) and deposited into the gel wells. The gel tank was then connected to a power pack and run at a constant voltage of 120 V until the dye front reached the other end of the gel (~40 min). DNA bands were visualized on a UV illuminator at 365 nm and images captured.

2.2.7. Bacterial transformation and extraction

E. coli (DH5α) were utilized to produce usable amounts of plasmids. Bacteria were grown at 37 °C in LB media liquid (Table 7). These cells were then made competent by carrying out the procedure described by Amberg et al. (2005). Competent cells were then frozen at -80 °C until required. When needed competent cells were thawed on ice and transformed with the plasmid of interest by heat shocking the cells at 42°C for 20 s, then outgrown by adding pre-warmed LB to 500 µL and incubated shaking for 1 h at 37 °C. Bacteria containing the plasmid were then selected by spreading on LB agar plates containing ampicillin, once colonies had formed plates were stored at 4 °C until required. When needed, a colony of bacteria was picked from the plate and grown at 37 °C in LB liquid media containing ampicillin. Extraction and purification of plasmids from bacterial growth cultures were carried out with the Zippy™ plasmid miniprep kit (Zymo Research) extraction column kit following the manufacturer's guidelines.

2.2.8. Procedure for yeast transformation

DNA constructs were transformed into the yeast genome by homologous recombination approach as described by Amberg (2005). Yeast were brought to logarithmic growths phase by culturing in liquid YPD media overnight in a shaking incubator at 30 °C. Once the yeast cells reached an OD_{600} between 1 and 2, the cells were palleted via brief centrifugation at 13,000 *x g* and the supernatant removed. Yeast cells were then resuspended in a transformation reaction mixture (Table 11).

Table 11. Reaction mixture for yeast transformation

Reagent	**Concentration**	**Amount**
Polyethylene glycol 3350 (Sigma-Aldrich)	50% (w/v)	240 µL
Lithium acetate (Sigma-Aldrich)	1 M	36 µL
Denatured salmon sperm DNA (Sigma-Aldrich)	2 µg/mL	50 µL
PCR product	-	10 µL
dH_2O	-	24 µL

The cells were subjected to a 40 min heat shock at 42 °C then palleted via brief centrifugation at 13,000 *x g* and the supernatant removed. The cell pellet was then resuspended in YPD liquid media for a 2 h outgrowth at 30 °C. After this outgrowth, the cell suspension was spread across an agar plate containing the appropriate selection criteria and transformed mutants were grown for two days, after which time, successful transformation was assessed via PCR. This procedure was used to produce the Mat**α** tif2Δ strain and the GFP reporter strains (Table 12 – 14).

Table 12. Primer sequences used to produce the TIF2 *deletion transformation contig and their corresponding annealing temperatures. Bold denotes nucleotides that anneal to template during PCR cycles.*

Description	**Sequence**	**Annealing temperature**
Confirmation downstream KanR *TIF2* For.	**CCACCTAAATGGTATTATAATC**	53 °C
Confirmation downstream *TIF2* Rev.	**ATTGCAATTACTATTTATTAGTTTC**	53 °C
Confirmation upstream *TIF2* For.	**ATATTGAGAAACCGACATCT**	52 °C
Confirmation upstream *TIF2* Rev.	**GATTCCATTTTTAATAAGGC**	52 °C
upstream *TIF2* For.	GACTGGTGTGTACAAGAAACTAATAAATAGTAATTGCAAT**AC ATGGAGGCCCAGAATACCCT**	64 °C
upstream *TIF2* Rev.	**CACTTACGACCAGCGATATGAC**AGAGATTCCTCTTCTTTAGGT ATTGATATAATGG	64 °C

2.2.9. Production of GFP UTR reporter strain

A DNA construct was designed containing the GFP gene under the constitutive TEF2 promoter with flanking regions designed to integrate into the yeast genome at the CAN1 site (Figure 14). PCR reactions were carried out to produce each section of the intended construct with flanking regions homologous to their adjoining sections (Figure 13) (Refer to Table 9 & 10 for PCR mixtures and parameters respectively). These sections were then then transformed into the BY4742 strain.

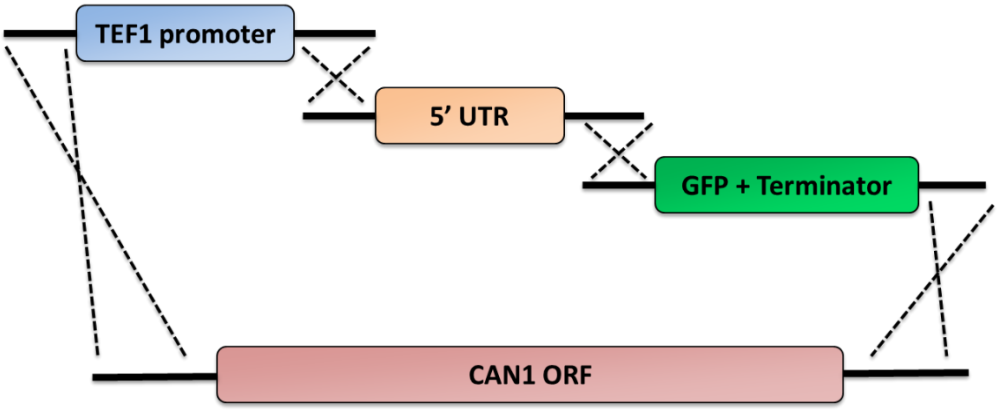

Figure 13. A schematic of the structured 5' UTR GFP reporter construct parts utilizing homologous recombination

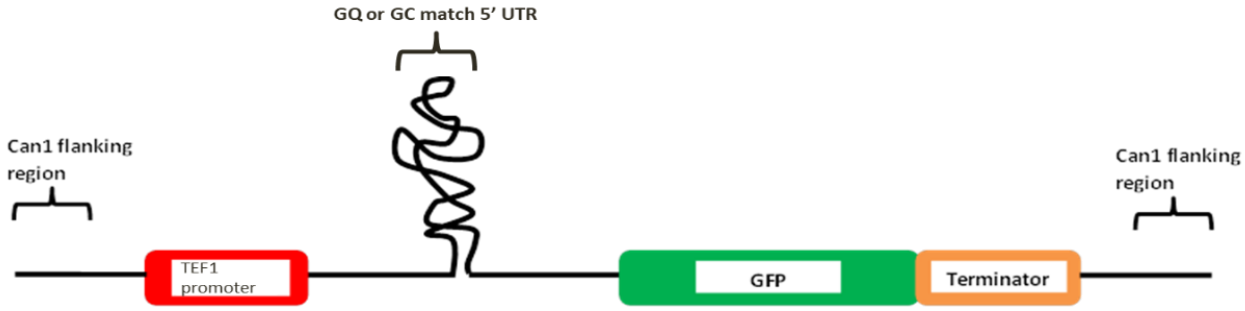

Figure 14. A schematic of the G-quadruplex reporter construct

2.2.9.1. Preparation of G-quadruplex and GC matched sequence

The G-quadruplex and GC matched control sequences containing the sequence of interest flanked by the restriction sites AfeI and SmaI were ordered from Macrogen. These DNA sequences were supplied in a bacterial plasmid. These plasmids were transformed into *E. coli* grown then extracted using a standard yeast transformation method outlined above (Section 2.2.8). Presence of the plasmids was then confirmed using agarose gel electrophoresis as described in Section 2.2.6. The plasmids were then digested using restriction enzymes AfeI and SmaI (New England BioLabs) in the CutSmart buffer (New England BioLabs) using the manufacturer's recommended conditions. An agarose electrophoresis analysis was then carried out on the restriction products and the band relating to the size of the 5' UTR construct was excised from the gel. This gel section was then melted and the DNA was purified with the use of the Geneaid Gene pH low DNA/PCR kit following the manufacturer's recommendations. Extracted 5' UTR sequences were eluted using dH_2O.

Table 13. Primer sequences for amplification of sections of the G-quadruplex reporter

Primer name	**Primer sequence**	**Annealing temp**
TEF1 promoter forward	CTTAACTCCTGTAAAAACAAAAAAAAAAAAAGGCATAGCA**CACAC ACCATAGCTTCAAAA**	58 °C
TEF1 promoter reverse	**TATCGTTAGATTAGATTCAAAATTAATGTT**	58 °C
GFP forward	**ATGTCTAAAGGTGAAGAATTATTCA**	60 °C
GFP + terminator reverse	ATGGCGTGGAAATGTGATCAAAGGTAATAAAACGTCATAT**CTATA CCTGAGAAAGCAACC**	60 °C

Table 14. Sequences of the synthetic construct plasmid 5′ UTR sections. Lower case letters denote flanking nucleotides not present in the final gnomically integrated construct. Bold indicates homologous regions with the TEF1 promoter and start of the GFP gene.

Synthetic construct	**Sequence**
G-quadruplex 5′ UTR	agc**GCTCATTAGAAAGAAAGCATAGCAATCTAATCTAAGTTTTAATTACAA**CT AGGTTGAAAGTACTTTGACGGCGGCGGCGGTCAATCTTACGGCGGCGGCGG ACATAGATACGGCGGCGGCGGTAGAAACTACGGCGGCGGCGGATTAGAAT AGTAAA**ATGTCTAAAGGTGAAGAATTATTCACTGGTGTTGTCCCAATTT**aaat
GC matched 5′ UTR	agc**GCTCATTAGAAAGAAAGCATAGCAATCTAATCTAAGTTTTAATTACAA**CTA GGGCGCACGTACTTCGACAACGTCAGCGTTCAGCGTTCCAACGTCAGCGTACA GCGATCCAACGTCAGCGTTCTGCGCTACAACGTCAGCGTATCCGCGTAGCACA **ATGTCTAAAGGTGAAGAATTATTCACTGGTGTTGTCCCAATTT**aaat

2.2.10. Procedure for P-body and stress granule visualization

Yeast strains containing highly fluorescent GFP-fusion protein markers of P-bodies and stress granule were picked from the GFP-fusion protein + RFP library (Bircham et al., 2011). These were streaked out and grown on synthetic media agar plates with histidine omitted (- HIS) and containing 2% glucose. Several single colonies were then picked from each plate and suspended in liquid synthetic media - HIS, 2% glucose and grown shaking at 30 °C overnight then diluted to a cell density of 1.2 x 10^8 cells/ml. Cells were then pelleted by brief centrifugation at 16,100 *x g* then resuspended in synthetic media – HIS, 2% glucose containing 400 µM pateamine, loaded into a 384-well microscope plate and incubated for 1 h at 30 °C. Additionally, a positive controls containing 100, 50, and 25 µM incednine was prepared and incubated for 1 h shaking at 30 °C. Ten minutes before visualization a second positive control was prepared by pelleting cells and resuspending them in synthetic media – HIS containing no glucose and loaded into the microscope plate. The plate was then visualised on an EvoTec Opera confocal microscope (Perking Elmer) high-throughput spinning disc confocal microscope with a 60x water immersion lens NA 1.2. GFP and RFP were excited using 488 nm and 561 nm lasers with emission fluorescence collected through 520/35 and 600/40 bandpass filters respectively, using a dual camera setup. Images were taken at three locations in each well in three focal planes 1 µm apart with the middle focal plane being 4 µm from the plate bottom. Images were acquired over a 400 ms exposure time and the resulting images were analysed by eye.

2.2.11. P147L overexpression experiments

2.2.11.1. Procedure for spot assay

A single colony was picked from a sample of *S. cerevisiae* BY4741 strain previously streaked on agar, and the colony transformed with the pBG1805 overexpression plasmid (a gift from Dr James Matthews)(Matthews, 2010) either empty or containing the gene for wild-type *TIF1* or P147L mutant *TIF1* and grown overnight in 2 ml liquid SD – URA media shaking at 30 °C. Cells were diluted with SD – URA media to achieve a cell concentration of 1.6 x 10^6 cells per ml. A five-fold serial dilution was then made using SD – URA media. The dilutions were plated in series by depositing 3 µl of each on SD – URA agar plates containing 2, 1, 0.5, 0.25, 0.125 or 0% galactose (w/v) (Carbosynth). Plates were then incubated at 30 °C until colonies were clearly visible (~48 h) images were taken of the plates.

2.2.11.2. Procedure for yeast growth rate assay

A single colony was picked from a sample of *S. cerevisiae* BY4741 strain streaked on agar, and the colony transformed with the pBG1805 overexpression plasmid either empty at the expression site or containing the gene for wild-type *TIF1* or P147L mutant *TIF1* and grown over night in 2 ml liquid SD – URA media shaking at 30 °C. Yeast cells were seeded into a 96-well clear-bottomed plate at a concentration of 1 x 10^5 cells per ml in SD – URA media containing 2, 1, 0.5, 0.25, 0.125 or 0% galactose (w/v). OD_{600} measurements were taken once every hour until the cultures reached saturation with a Wallac EnVision 2102 plate-reader (Perkin-Elmer, Waltham, MA, USA). Data was then exported and trimmed to cover only the logarithmic phase of growth. Regression analysis was then used to find the yeast growth rate per hour.

2.2.12. Production of *tif1*Δ GFP/RFP library

Previous investigations carried out by Peter Bircham resulted in the crossing of a GFP-fusion protein library (Invitrogen) with a strain constitutively expressing a nuclear localized RedStar RFP and cytoplasmic localized mCherry RFP ((Mat**a**; XXX-GFP-*HIS3*, *can1*Δ::STE2pr-Sp-*URA*; *lyp1*Δ::mCherry-Nat; *his3*Δ1; *leu2*Δ0; *ura3*Δ0::NLS-RedStar2-HPH; LYS2+;)) (Bircham et al., 2011). This library was used as the starting strain for crossing with a *tif1*Δ strain (Mat**α**; *tif*Δ::KanR (Open Biosystems)). Yeast crossings were carried out in 384 format with a Singer RoToR High Density Array robot, using standard procedures (Weissman et al., 2010). The two strains were mated together, then prepared for sporulation by growing the diploid cells on

GNA media (Table 5). Strains were then sporulated by growing for one week on sporulation media at room temperature then selected for by adding one selection at a time with outgrowths between (An in-depth protocol can be found in Amberg et al. (2005). This yielded a library of GFP-fusion proteins each with a *TIF1* gene deletion (Mat**a**; XXX-GFP-*HIS3*, *tif1*Δ::KanR, *can1*Δ::STE2pr-Sp-URA; *lyp1*Δ::mCherry-Nat; *his3*Δ1; *leu2*Δ0; *ura3*Δ0::NLS-RedStar2-HPH; *LYS2*+;). Strains were stored on agar at 4°C until required.

2.2.13. Procedure for yeast GFP screen image acquisition

Imaging of GFP-fusion protein libraries were carried out utilizing the method used by Bircham et al. (2011) with some alterations. Libraries were pinned onto synthetic media agar plates deficient in histidine, containing 2% glucose (Table 3) and grown for 16 h at 30 °C. Strains were then transferred to a 384 well clear bottom plate (Perkin Elmer Cell Carrier) containing liquid synthetic media with 2% glucose (Table 3) with selections absent to avoid antibiotic selections affecting the proteome. Strains were allowed to grow for a further 4 h at 30 °C allowing cells to adapt to the new media. Plates were then imaged using an EvoTec Opera (Perkin Elmer) high-throughput spinning disc confocal microscope with a 60x water immersion lens NA 1.2. GFP and RFP were excited using 488 nm and 561 nm lasers with emission fluorescence collected through 520/35 and 600/40 bandpass filters respectively using a dual camera setup. Images were acquired over a 400 ms exposure time at a focal height of 4 μm.

2.2.14. Procedure for image analysis

Automated analysis of yeast images was carried as stated in Bircham et al. (2011). A script in ACAPELLA software v2.0 (PerkingElmer) was used to identify the nucleus (labelled with RedStar) and cytoplasm (labelled with mCherry) of each cell using the RFP channel. From this, several metrics, including the GFP fluorescence intensity of each cell was then measured and a median value for each well was output. GFP fluorescence values were normalized to the constitutively expressed RFP fluorescence signal. Strains were identified as hits if they exhibited a GFP fluorescence fold change greater than 1.4 or less than 0.5 across in 2 or more replications when compared to control.

2.2.15. Preparation of samples for mass spectrometry analysis

2.2.15.1. Procedure for protein extraction

Yeast proteins were extracted using the "non-SDS compatible applications" extraction method described by von der Haar (2007) and upscaled to increase protein yield. Yeast cells were first washed two times with dH_2O then pelleted via brief centrifugation at 16,100 *x g* and the supernatant was removed. The cell pellet was resuspended in the lysis buffer containing 0.1 M NaOH (Sigma-Aldrich), 0.05 M EDTA, 2% SDS (Invitrogen) and 2% β-mercaptoethanol (Sigma-Aldrich) and heated to 90 °C for 10 min. An aliquot of 4 M acetic acid (Sigma-Aldrich) was then added to give a final concentration of 100 mM. The solution was mixed and incubated for a further 10 min at 90 °C. Cellular debris was removed by centrifugation at 13,000 *x g* for 10 min and the supernatant was retained. SDS was then removed from the sample by protein precipitation by first adding four volumes of methanol (Fisher chemicals) followed with one volume of chloroform (Sigma-Aldrich) and finally 3 volumes of dH_2O with mixing between each addition. Proteins were collected by centrifugation at 16,100 *x g* for 10 min at 4 °C, washed with 3 volumes of methanol then spun for a further 5 min at 16,100 *x g* at 4°C. Finally, the supernatant was removed, and the pallet was briefly dried in a laminar flow hood then resuspended in a solution of 8 M urea (Sigma-Aldrich), 100 mM Tris-Cl (pH 8).

2.2.15.2. Procedure for protein quantification

Protein quantification was carried out with the use of the Implen NP80 NanoPhotometer. A 2 µl aliquot was placed in the reader and absorbance was measured at 280 nm wavelength and protein concentration was calculated from the outputs. The samples were then diluted with 8 M urea so that each sample had a concentration of 4 mg/ml of protein.

2.2.15.3. Procedure for protein extract preparation

An aliquot of each of the 8 M urea protein mixtures were diluted 4-fold to give a final urea concentration of 2 M. Samples were reduced by adding DTT (Sigma-Aldrich) to a concentration of 5 mM and incubated at 60 °C for 20 min, then cooled to room temperature. Samples were then alkylated by adding iodoacetamide to a concentration of 10 mM and incubated in the dark at room temperature for 20 min. Sequencing grade trypsin (Roche Diagnostics®) was then added to the samples to give a ratio of 1:50 (trypsin : total protein) which were then incubated overnight at 37 °C. The reaction was quenched with the addition

of 10% formic acid (Merck Millipore) to a concentration of 0.2% and the solution was confirmed as acidic using litmus paper. Peptides were then purified using Sigma-Aldrich Supel-Tips 100 µl C18 micropipette tips. The tips were pre-moistened with 0.2 % formic acid and the peptide solution was passed through the C18 filter 15 times and then washed three times with 0.2% formic acid. Bound peptides were then eluted from the column by passing 0.2% formic acid, 50% acetonitrile (Merck Millipore) through the filter 15 times. This process was then repeated a second time but with a 70% acetonitrile elution solution. The purified peptide samples were then dried at 40 °C in a speed vac and resuspended in 40 µL 0.1% formic acid in High Performance Liquid Chromatography (HPLC) grade water, mixing for 10 min. Samples were then spun at 10,000 x *g* for 5 min and the top 35 µL transferred to glass vials for analysis.

2.2.16. Procedure for mass spectroscopic analysis of protein extracts

Mass spectroscopic analysis was carried out as described by Bosch et al. (2015) with some alterations. Sample vials with glass sample inserts were placed in the refrigerated (10 °C) auto-sampler of a Dionex UltiMate^{TM} 3000 nano liquid chromatography (Nano LC) system feeding into a Linear Trap Quadrupole (LTQ) Orbitrap XL mass spectrometer via a nanospray ion source (Thermo Fisher Scientific, USA). Xcalibur software (Version 2.1.0, Thermo Fisher Scientific, USA) was used for method set up, control of the LC-MS/MS runs, and data acquisition.

Peptides were separated using a flow rate of 0.2 µL/min through a C18 column (Acclaim Pepmap 100 C18, 3 µm, 100 A, 75 µm ID x 15 cm, Dionex, LC Packings, Netherland). A buffer gradient was constructed from 0.1% formic acid (Buffer A) and 0.1% formic acid in 80% acetonitrile (Buffer B): 2% buffer B to start, ramping nonlinearly to 98% B over the course of 360 min, then maintained at 98% buffer B for a further 5 min. The peptides in solution were ionised by electro spray ionisation with a silica tip emitter (360 µm OD x 20 µm ID x 10 µm tip opening, New Objectives, USA), with the voltage potential set at 1.8 kV to produce the most stable spray. Positive ion mode was used with the heated capillary temperature set at 275 °C and tube lens 120 V to permit entry of ions preferentially at 524.30 m/z. Ions with m/z range between 200 - 1850 m/z were analysed during the 360 min acquisition time. Data-dependent MS/MS analysis was carried out on the top 6 intensity ions dynamically selected for helium collision-induced dissociation (CID) fragmentation and detection (1.0 isolation width,

normalised collision energy 35%, activation Q 0.25, activation time 30 ms). The dynamic exclusion settings used were as follows: repeat count 2, repeat duration 30 s; exclusion list size 500; exclusion duration 90 s. A full-scan (500 ms maximum injection time) at a resolution of 30,000 identified. After accumulation of 500,000 ions these were injected into the analyser with a 10 ms maximum injection time. Between each sample run there was a wash with a short gradient from 2% Buffer B to 98% Buffer B across 30 min. A minimum of two technical replicates were carried out on each of the 3 or more biological replicate samples.

2.2.16.1. Procedure for analysis of mass spectroscopic data

The obtained mass spectra files were then analysed with Proteome Discoverer (version 2.1.). The spectra were searched against the *Saccharomyces cerevisiae* Swiss-Prot database consisting of all proteins with evidence (downloaded on 8-4-2015) with the SEQUEST search algorithm and the *Saccharomyces cerevisiae* Swissprot database (downloaded on 8-4-2015) with the MASCOT search algorithm in parallel. A precursor mass range of 350 - 5000 Da was allowed with a precursor mass tolerance of 10 ppm and fragment mass tolerance of 0.6 Da. Trypsin was selected as the digesting enzyme allowing a maximum of 2 missed cleaves. All Peptides ranging in length from 6 to 144 amino acids were analysed. Carbamidomethylation of cysteines was set as a static modification (+57.021 Da) and a dynamic modification of oxidation of methionine residues was allowed (+15.995 Da) with a maximum of 2 dynamic modifications per peptide.

Proteome discoverer output files were then loaded into Scaffold (Proteome Software Inc, Portland, version 4.0) proteomics software for quantification analysis and technical replicates combined using the Mudpit algorithm (Schirmer et al., 2003). Searches were carried out against the *Saccharomyces cerevisiae* Swiss-Prot all evidenced protean database 05-02-15. Protein abundance was quantified using intensity-based absolute quantification (iBAQ) and total ion current (TIC) independently and identified proteins were filtered to require at least 2 unique peptides to be identified. Peptide P-values were then corrected for multiple testing, this was achieved by using an online false discovery rate (FDR) q-value (Storey, 2002). Proteins were filtered with an FDR change-from-control confidence value of 0.10. All proteins with q=0.10 or lower were identified to have changed in abundance. Results from the two quantification methods were then consolidated into two gene lists; significantly increased or decreased.

2.2.16.2. Gene ontology enrichment analysis

Gene ontology enrichment analysis was carried out with the use of the g:Profiler online tool (Raudvere et al., 2019). The proteins identified as changing in abundance were converted into gene names in formats recognized by g:Profiler and were searched using default settings. When analysing the GFP hit list, a custom statistical background was used containing only the genes present in the GFP-fusion library. Searched gene lists consisted of various combinations of lists including, decreased only, increased only, and the two lists combined into one. When investigating the enrichment outputs, ontologies were limited to terms with a total of less than 1000 associated genes to remove top-level ontology terms.

2.2.16.3. Acquisition of 5′ UTR sequences

Sequences used for the 5′ UTR analysis steps were obtained as follows: gene lists were compared against the 5′ UTR sequence data given by Lin et al. (2012). Any 5′ UTRs which were not reported in this list were obtained from the from the yeastgenome.org 5′ UTR data sheet (Yeastgenome.org). When multiple sequences and lengths were available, the most recently published 5′ UTR sequence was taken. For the few transcripts for which no reported 5′ UTR sequence or length, a 150 nucleotide stretch immediately upstream of the start site was taken. When analysing for sequence length these genes were omitted from the analysis.

2.2.16.4. Procedure for 5′ UTR analysis

The MEME web tool suite (Bailey et al., 2009) was used to carry out motif enrichment analysis. The lists of 5′ UTR sequences were analysed by the MEME ungapped motif discovery tool (Bailey. T and Elkan. C, 1994). The 5′ UTR lists were analysed using the following settings; site distribution was set to any number of repeats and number of motifs to find was set to five. In the advanced options the “given strand only” option was selected and motif lengths of 6-30, 6-20, 6-15 and 6-10 were searched individually. In addition to these searches, 3 separate searches for each length constraint and each 5′ UTR list were carried out with the shuffled sequences option enabled to give a measure of the basal statistical background.

2.3. Results

The aim of this body of research is to investigate the effect on the cell that arise from eIF4A inhibition, including changes in cellular pathways. We aimed to utilise a drug-free approach to induce a decrease in eIF4A function avoiding confounding factors associated with drug treatment. An added benefit of this is the reduced use of our limited stocks of pateamine. Our first goal relating to this aim was to find reliable markers of reduced translation initiation. These markers could then be used to determine whether a given condition was inducing a stalling of the initiation complex.

2.3.1. Investigation of markers of inhibition of translation initiation

2.3.1.1. P-bodies and stress granules

Previous research has determined that stress granules form in response to pateamine treatment in mammalian cell lines (Dang et al., 2006). However, it is yet to be established whether this occurs in yeast treated with pateamine. If pateamine does induce stress granule formation in yeast this effect could be a fast way to identify whether eIF4A inhibition is occurring. We planned to utilize this response to screen for methods of mimicking translation inhibition through genetic manipulation. To investigate whether this approach was possible, we selected several P-body and stress granule-associated proteins and selected yeast strains with the corresponding GFP-fusion proteins. When selecting stress granule markers, it was noted that stress granules and P-bodies have a dynamic relationship (Decker and Parker, 2012). This meant it is possible that P-bodies could also form in response to pateamine. As such, a range of P-body markers were also selected.

	Glucose present	Glucose deprived (10 min)
Pap1p-GFP	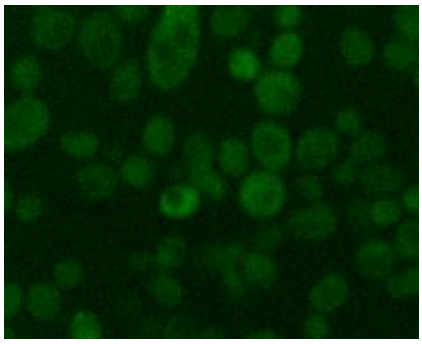	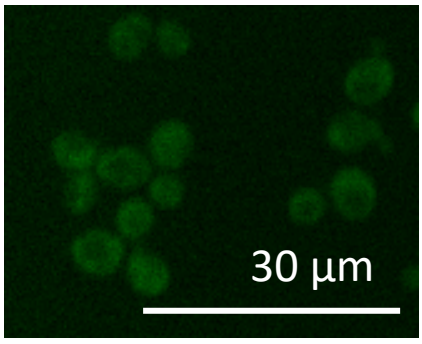
eIF4E-GFP	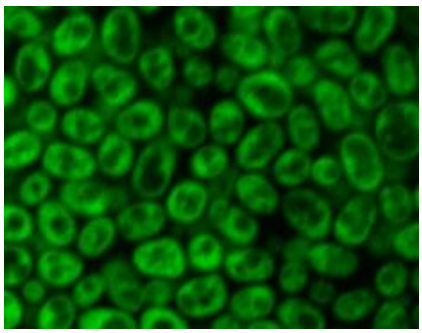	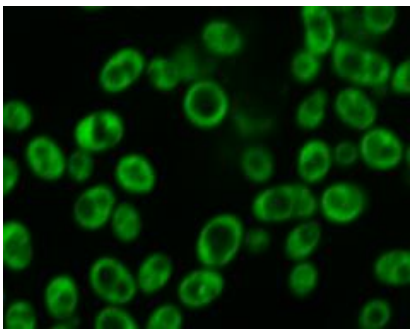
Pbp1p-GFP	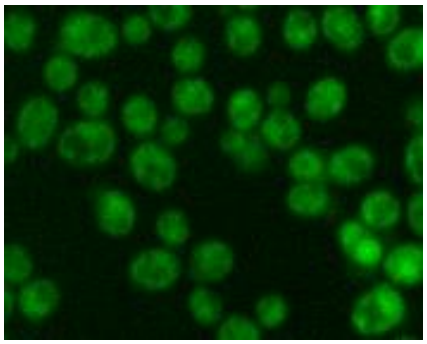	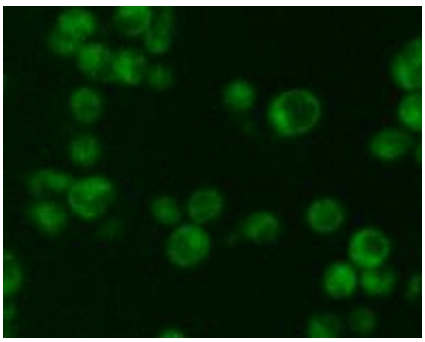
Pub1p-GFP	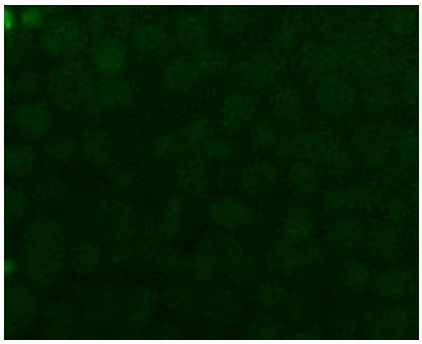	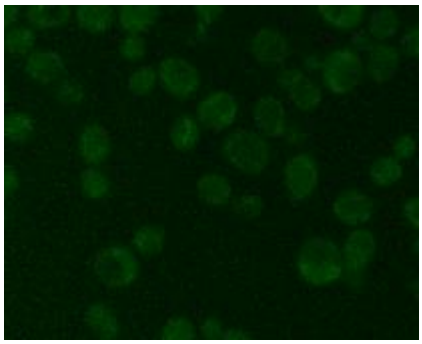
Pbp4p-GFP	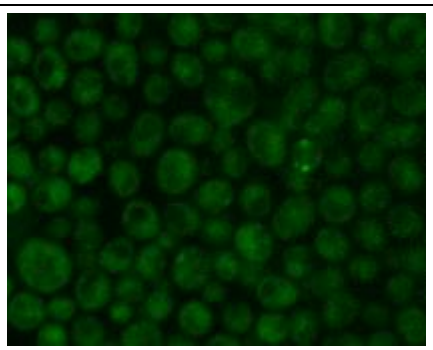	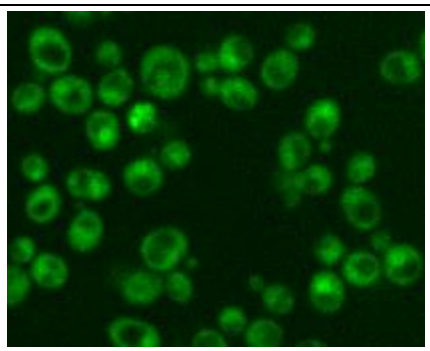

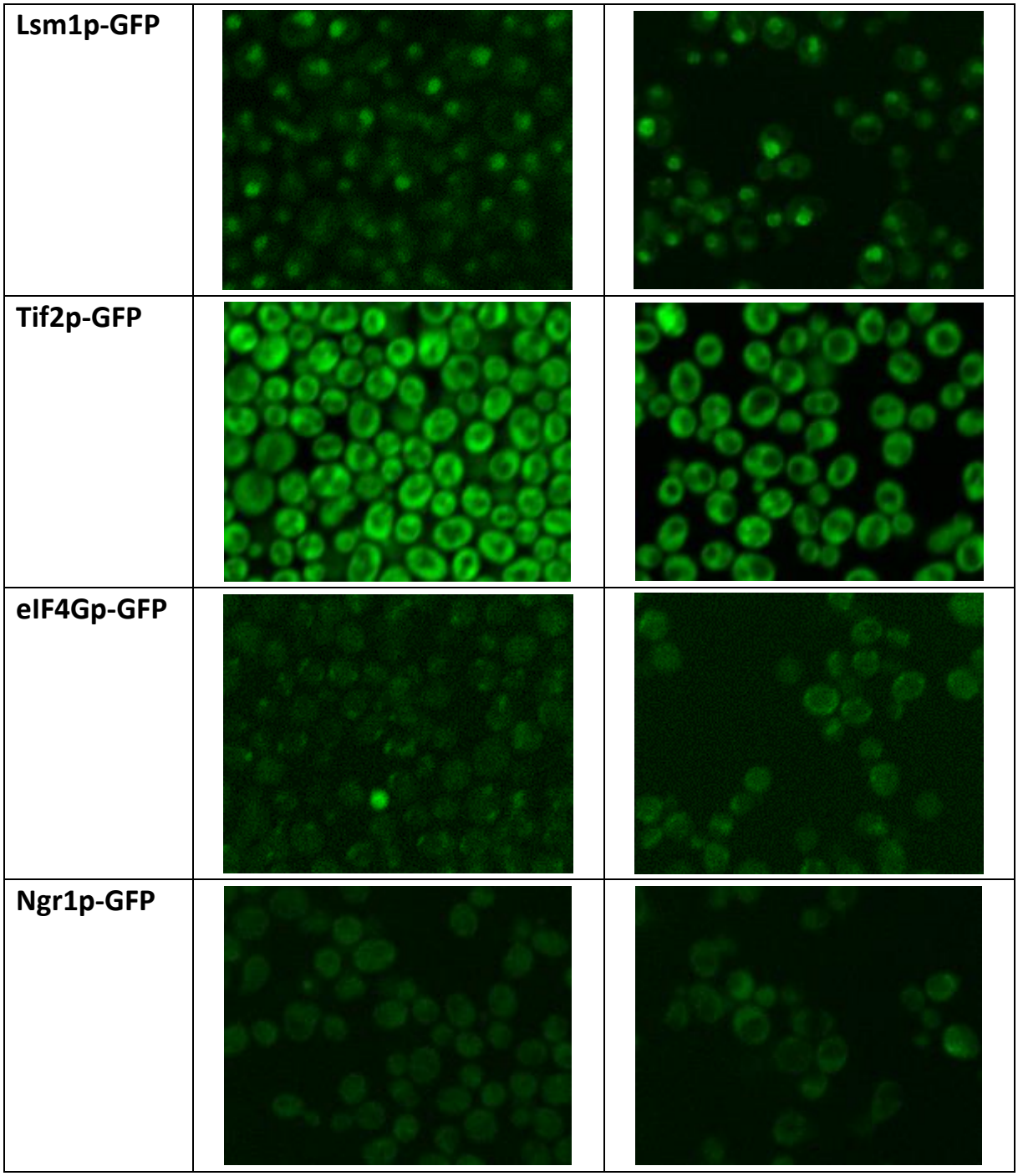

Figure 15. Formation of stress granules could not be visualized. A range of GFP-fusion protein strains were selected from the yeast GFP protein library of proteins known to associate with stress granules. Strains were cultured in glucose-free media for 10 min then visualized on an Opera microscope. All images are at the same scale.

When attempting to visualise GFP-fusion proteins known to localise to stress granules (Figure 15), no punctate phenotype was observed despite glucose deprivation being an established method to induce their formation within 10 minutes (Swisher and Parker, 2010; Yang et al., 2014). It is unclear why we were unable to visualise this effect.

	Glucose present	Glucose deprived (10 min)
Edc3p-GFP	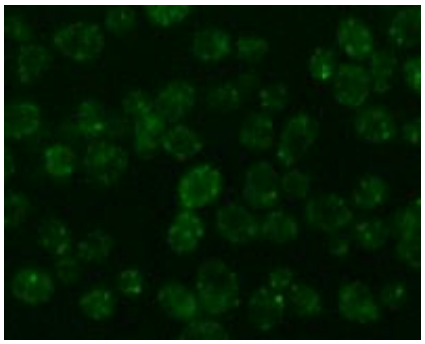	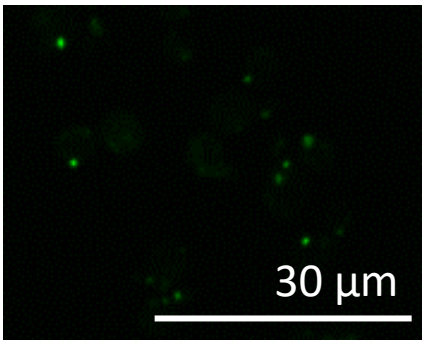
Dhh1p-GFP	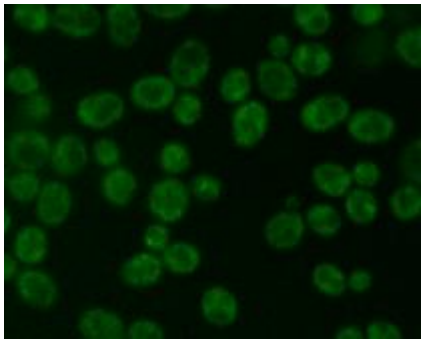	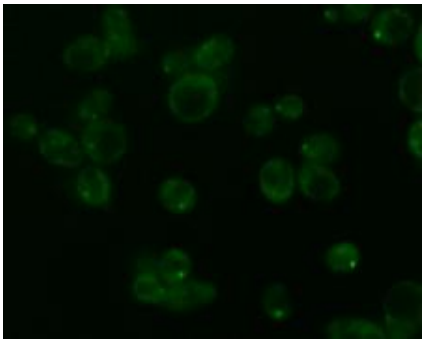
Pat1p-GFP	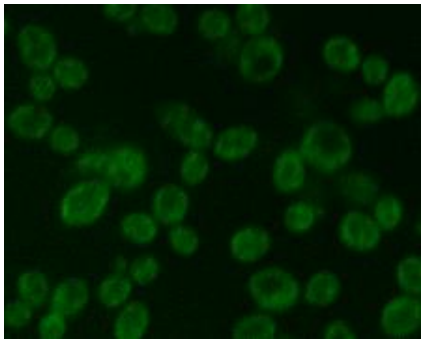	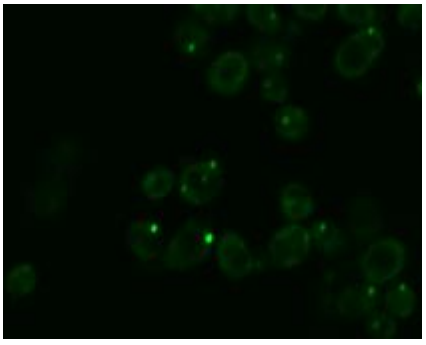
Scd6p-GFP	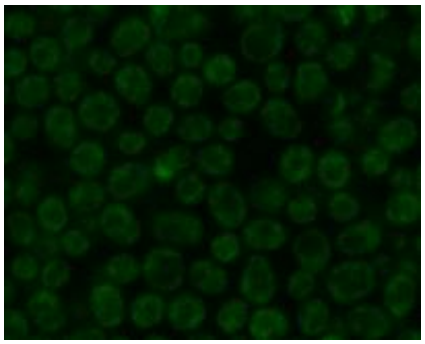	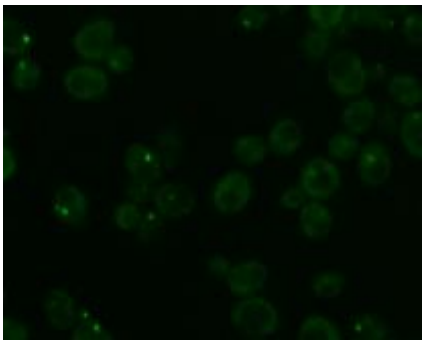
Dcp1p-GFP	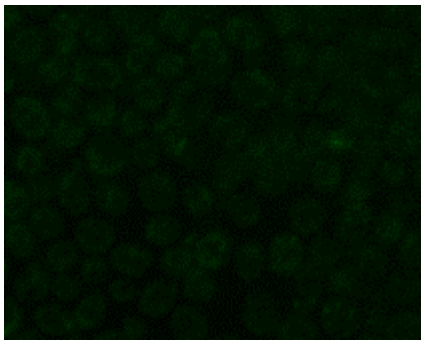	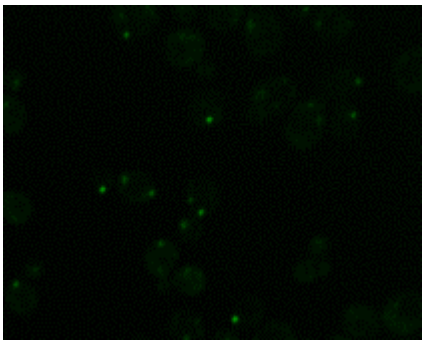

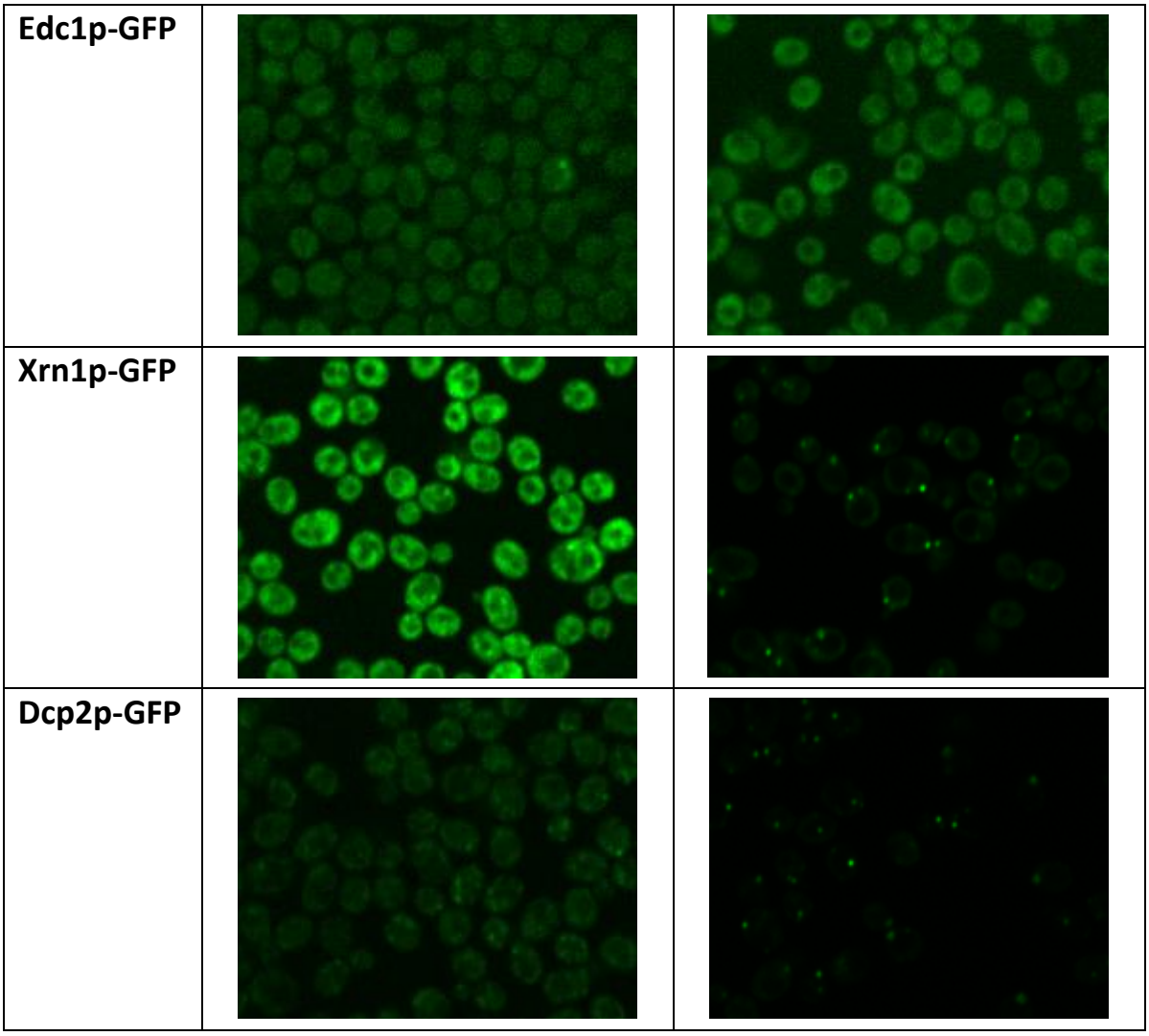

Figure 16. Glucose deprivation induces P-body formation. A range of GFP-fusion protein strains were selected from the yeast GFP protein library of proteins known to associate with P-bodies. Strains were cultured in glucose-free media for 10 min then visualized on an Opera microscope. The bright puncta produced by glucose deprivation are typical of P-bodies. All images are at the same scale. Note: Pat1p is known to localize to both stress granules and p-bodies.

When culturing the yeast strains in media which did not contain glucose, the GFP-fusion proteins known to localise to p-bodies were observed to adopt a punctate phenotype indicating the formation of P-bodies (Figure 16). Interestingly, Edc1p did not exhibit a punctate phenotype, this may mean the GFP tag is interfering with localization.

Having established that we could visualise P-body formation we investigated whether inhibition of eIF4A with pateamine treatment was capable of also inducing these granules.

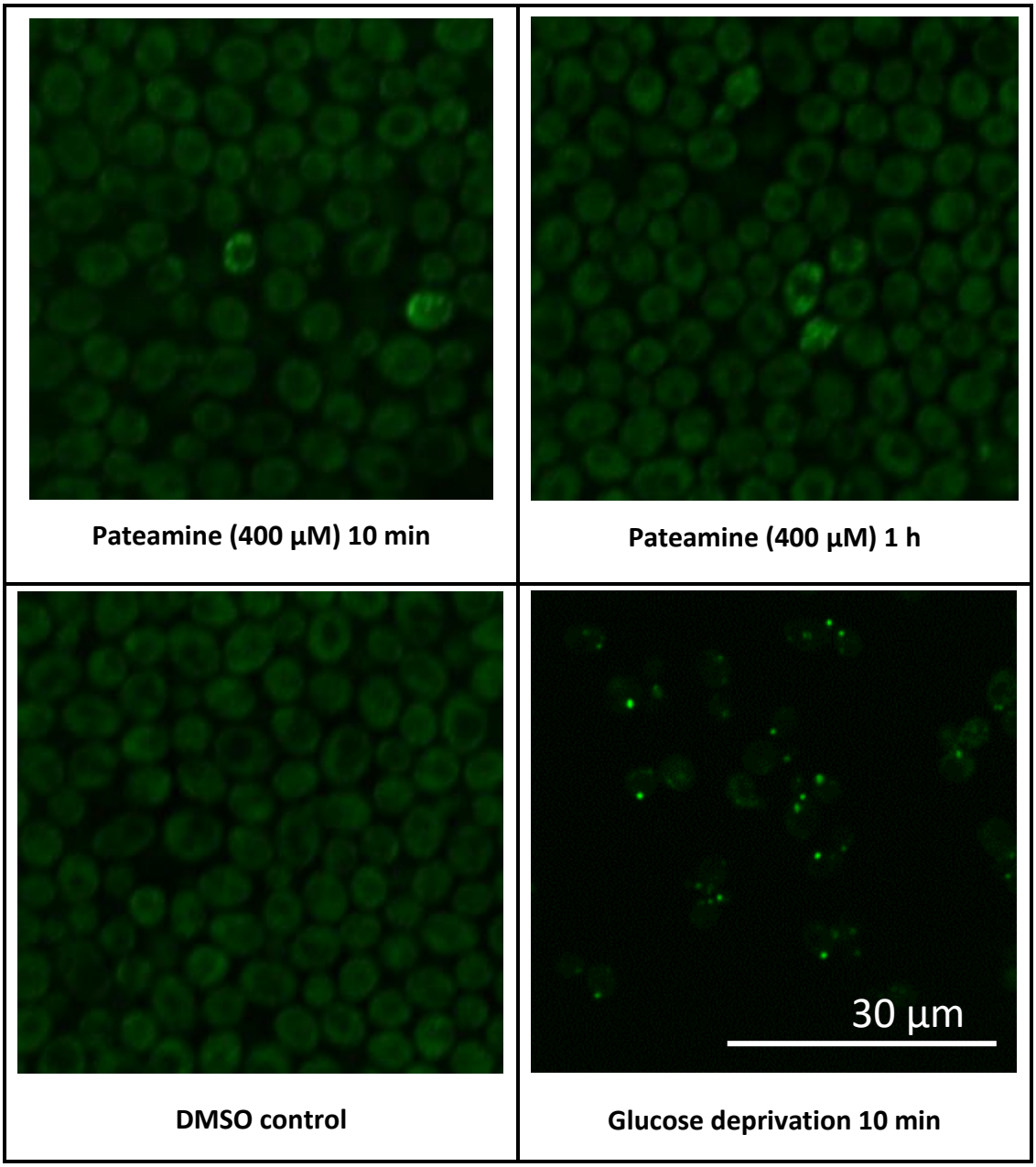

Figure 17. Treatment of yeast with 400 µM pateamine does not induce formation of P-bodies (P-bodies). Edc3p-GFP-fusion strain selected from the yeast GFP protein library and exposed to 400 µM pateamine visualised using an Opera microscope at 10 min increments. All images are at the same scale.

When treating P-body marker GFP strains with high doses of pateamine no punctate phenotype was observed meaning p-bodies were not forming (Figure 17). The initial goal of visualizing this effect was to utilise this observable change as an indication of inhibition of eIF4A activity. Given that stress granules could not be visualized and inhibition of eIF4A with pateamine did not induce P-body formations this approach was abandoned.

2.3.1.2. Production of GFP reporter strain

Having established that stress granule and P-body formation could not be used as an indicator of eIF4A inhibition, it was decided instead to produce a GFP reporter construct. This would be used to test genetic manipulations for altered translation initiation effects. Experiments with the eIF4A inhibitor silvestrol have identified 5′ UTR sequences that are preferentially affected by eIF4A inhibition (Wolfe et al., 2014). When treating with silvestrol, translation of mRNA transcripts with a G-quadruplex forming motif was disproportionately decreased. It was suspected that this effect is the result of this stable structure preventing the formation of the initiation complex when there is insufficient functional eIF4A to resolve the structure. It was decided that this 5′ UTR would be placed upstream of a GFP gene and integrated into the yeast genome. The construction of this strain was carried out by producing a construct consisting of a GFP gene with a spacer and 4 repetitions of the CGG quadruplex motif upstream of the start codon (Figure 13). The GFP gene was controlled by the TEF promoter, a constitutive promoter that controls expression of the TEF1 gene. The promoter was amplified with PCR using genomic DNA as a template and was integrated upstream of the 5′ UTR. The construct sections were integrated into the genome at the *CAN1* gene site together, using homologous recombination. The GFP fluorescence will then act as an indicator, with fluorescence decreasing anticipated as a result of eIF4A inhibition. The segments of this reported construct were first produced with the use of PCR and products were checked to be the correct size with agarose gel electrophoresis (Figure 18 & 20). In addition to the G-quadruplex construct, a reporter construct containing a control 5′ UTR sequence with matched GC content was also designed as a control for general translational repression.

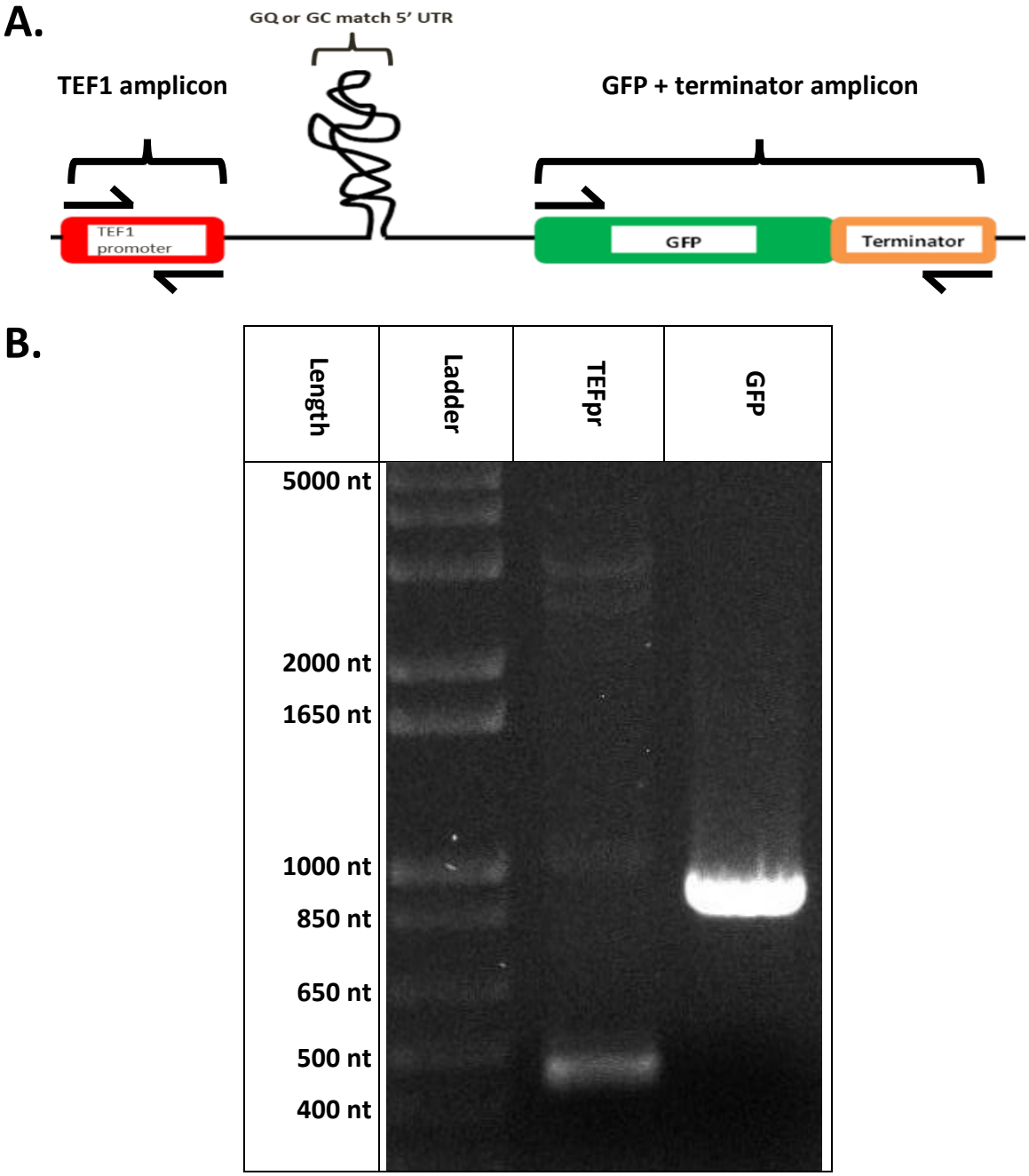

Figure 18. Construct sections of the TEF1 promoter and GFP gene were amplified using primers with flanking sequences homologous to flanking regions in adjoining constructs. ***A.*** *Schematic of the primers used to amplify the TEF1 promoter and GFP gene and terminator.* ***B.*** *The sizes of DNA amplicons were then analysed with agarose gel electrophoresis and visualised using ethidium bromide. PCR amplified sequences of the GFP gene and TEF2 terminator (848 nt) and the TEF promoter (459 nt).*

The G-quadrulplex and GC-match 5' UTRs were excised from their plasmids with restriction digestion and for each of these the three construct sections were combined into a single reaction mixture.

After transformation of yeast with the G-quadruplex reporter construct ~20 colonies grew on the selection agar media, 10 colonies were screened with the Opera confocal microscope. Two of these colonies expressed GFP at detectable levels (Figure 19).

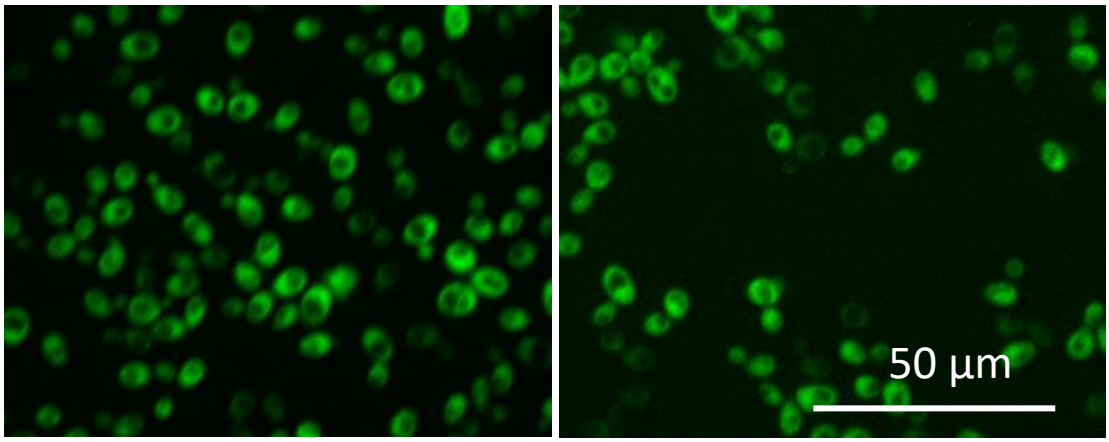

Figure 19. Two G-quadruplex transformants expressed high levels of GFP. This showed the G-quadruplex expression construct had integrated into the genome and was actively transcribed. Transformants were picked from synthetic media -Arg +CAN agar plate and suspended in SD -His then transferred into the Opera confocal microscope for imaging. Excitation at 488 nm and detected at 510 nm for 2000 ms exposure.

Confirmation PCR was then carried out to check that the G-quadruplex construct had correctly integrated into the *CAN1* locus. This confirmed that the reporter construct had correctly integrated giving bands at the expected nucleotide lengths (Figure 20 & 21).

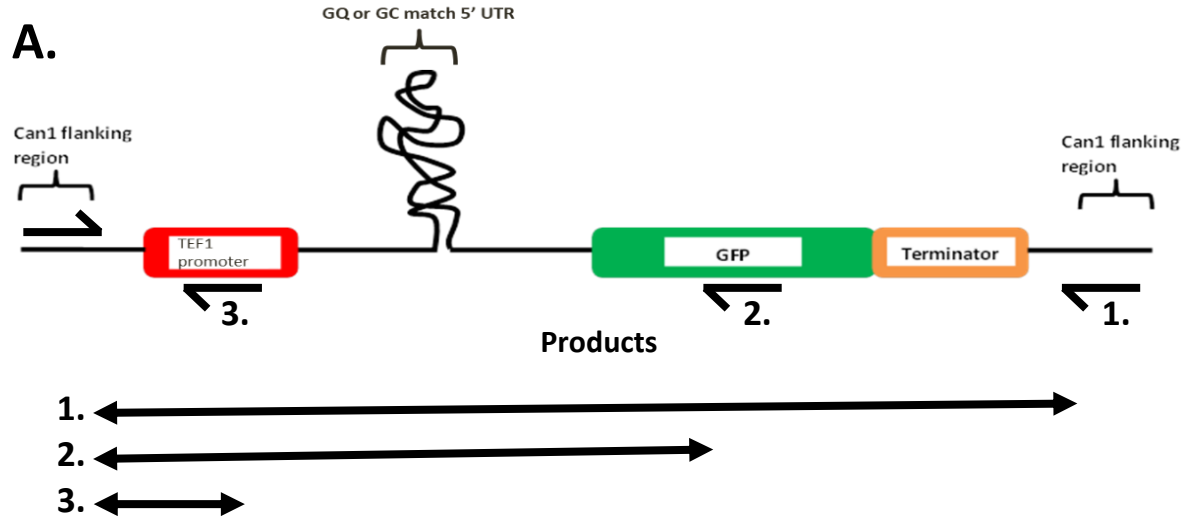

B.

Length	Ladder	GC construct	G-quadruplex construct	Primer locations giving amplification
2000 nt 1650 nt 1000 nt 850 nt 650 nt 500 nt 400 nt	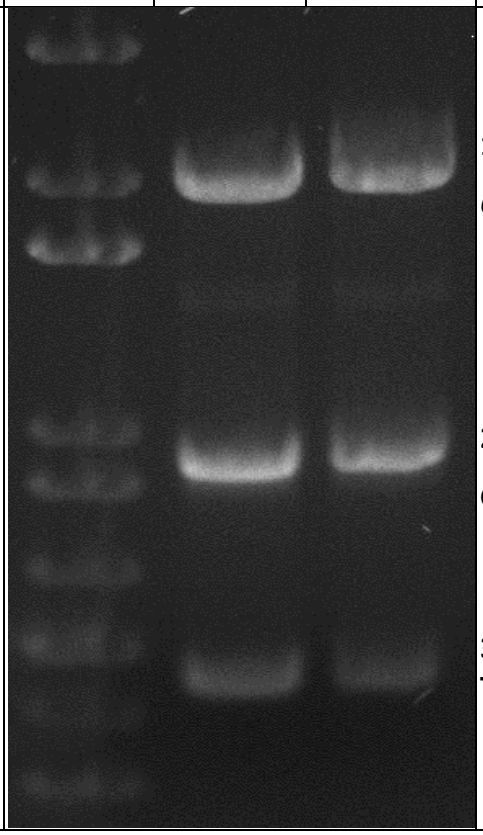			1. *CAN1* upstream - *CAN1* downstream 2. *CAN1* upstream - GFP 3. *CAN1* upstream - TEF promoter

Figure 20. The G-quadruplex construct had integrated into the correct location and was confirmed by PCR with confirmation primers coupled with agarose gel electrophoresis. Genomic DNA was extracted from the transformant and used as a template. ***A.*** *A schematic of the primer combinations to confirm insertion of the reporter construct:* ***1.*** *Primer combinations consisting of a primer upstream of the* CAN1 *locus and a primer downstream of the* CAN1 *locus,* ***2.*** *A primer upstream of* CAN1 *and a primer inset in the GFP gene, and* ***3.*** *a primer upstream of* CAN1 *and a primer inset in the TEF promoter.* ***B.*** *Each amplicon gave a single band at the correct size confirming the construct had integrated correctly.*

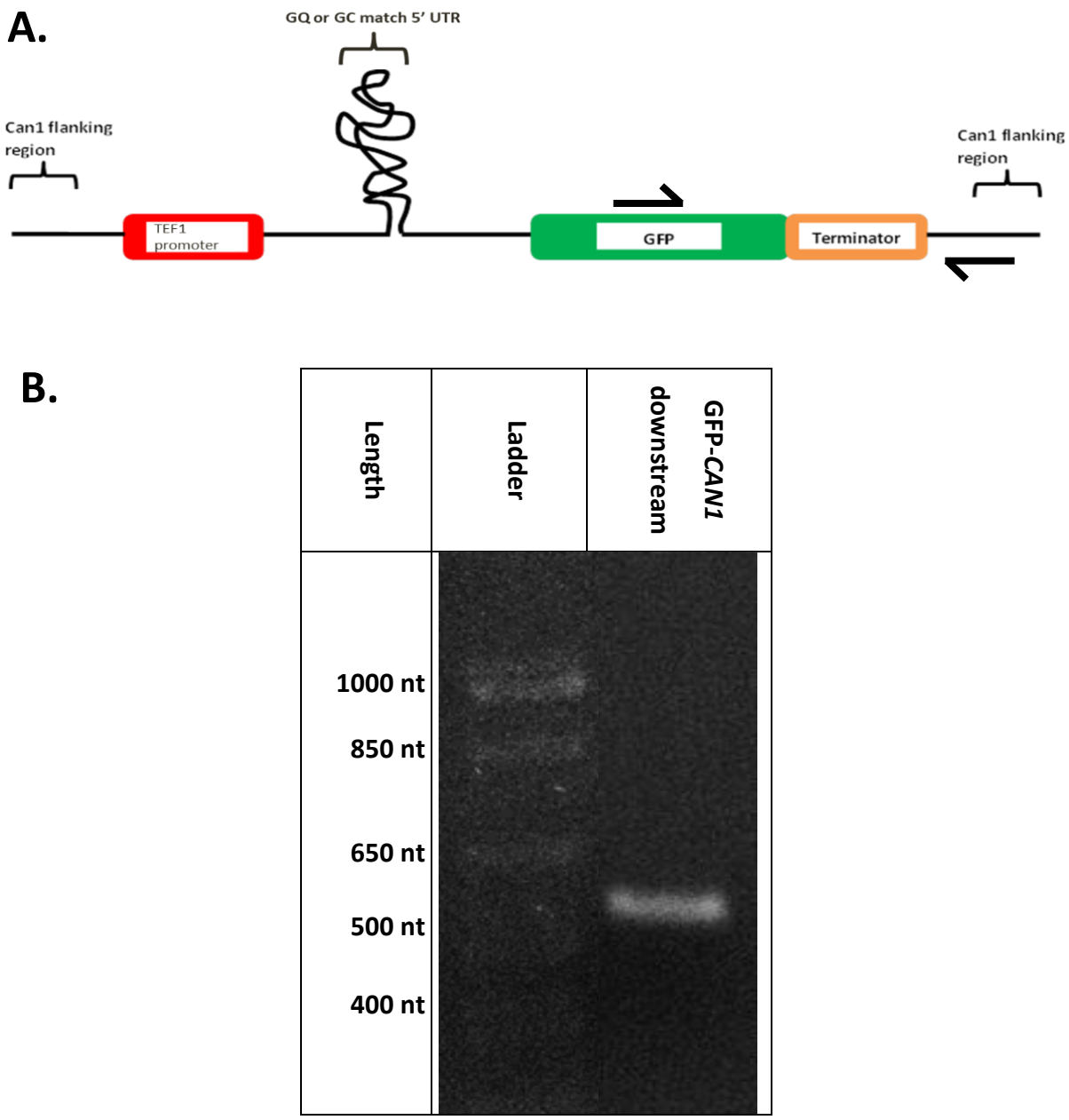

Figure 21. Correct integration of the G-quadruplex construct was further confirmed by PCR coupled with agarose gel electrophoresis confirmed. Genomic DNA was extracted from the transformant and used as a template. ***A.*** *A schematic of the primer combination consisting of a primer inset in the GFP gene and a primer downstream of the* CAN1 *site.* ***B.*** *This gave a single band at the correct size confirming the construct had integrated correctly.*

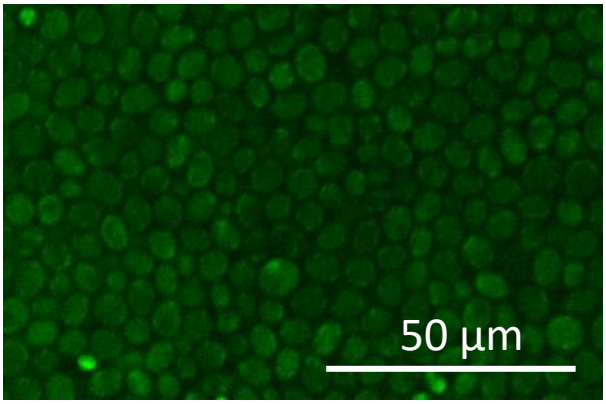

Figure 22. The GC content matched 5' UTR GFP reporter showed extremely low fluorescence values in all transformants. GC matched transformants were picked and suspended in SD -His liquid media then loaded into the Opera fluorescent microscope for analysis. Excitation at 488 nm and detected at 510 nm for 2000 ms exposure.

After transformation of yeast with the GC matched construct 6 colonies grew on the selection plate. When visualized with the fluorescence microscope none of the colonies exhibited any fluorescence signal that was higher than would be expected from auto fluorescence (Figure 22). Despite reattempting this transformation multiple times, a strain containing the control 5' UTR GFP reporter sequence could not be produced. Making it impossible to differentiate eIF4A-specific inhibition from a general downturn in translation using the G-quadruplex construct alone.

2.3.2. Investigation of mimicking eIF4A inhibition

2.3.2.1. Overexpression of P147L

The eIF4A P147L mutation is an amino acid replacement near the mRNA binding portion of the N-terminus of the helicase and was originally identified as conferring resistance to pateamine inhibition (Matthews, 2010). Previous experiments in which P147L has been over expressed lead to a marked decrease in cell growth, suggesting that the mutant eIF4A protein had reduced functionality, possibly a result of weakening the interaction between eIF4A and the RNA transcript (Matthews, 2010). To investigate this, we first investigated the effect of overexpression of P147L-eIF4A on growth. A pBG1805 over-expression plasmid containing the P147L-*TIF1* gene under control of a galactose inducible promoter had previously been produced by James Mathews (2010), this was transformed into the yeast strain BY4741. This overexpression strain was prepared along aside of an empty vector control and WT eIF4A over expression plasmid in BY4741 and serial spot dilutions were laid out on 0, 0.5, 1 and 2% galactose containing synthetic media – URA agar plates (Figure 23).

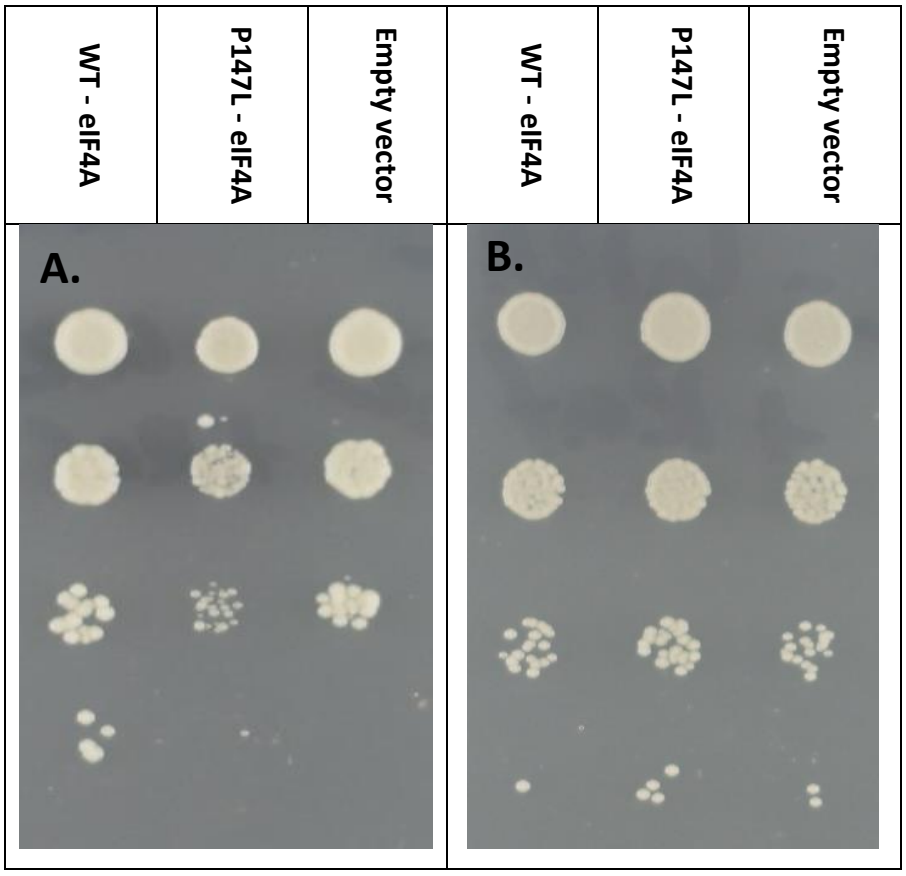

*Figure 23. Overexpression of eIF4A-P147L protein retards growth in yeast on solid media. Vertical spot dilution of BY4741 transform the with the pBG1805 over expression plasmid containing from left to right, WT eIF4A, P147L mutant eIF4A and empty vector on media containing (**A**) 2 % galactose or (**B**) 0 % galactose. Over expression induced by galactose lead to retarded growth for the P147L-eIF4A (best illustrated by third spot down) but normal growth for the WT and empty vector.*

We also investigated this effect in liquid media conditions to measure optical density as a measure of growth rate.

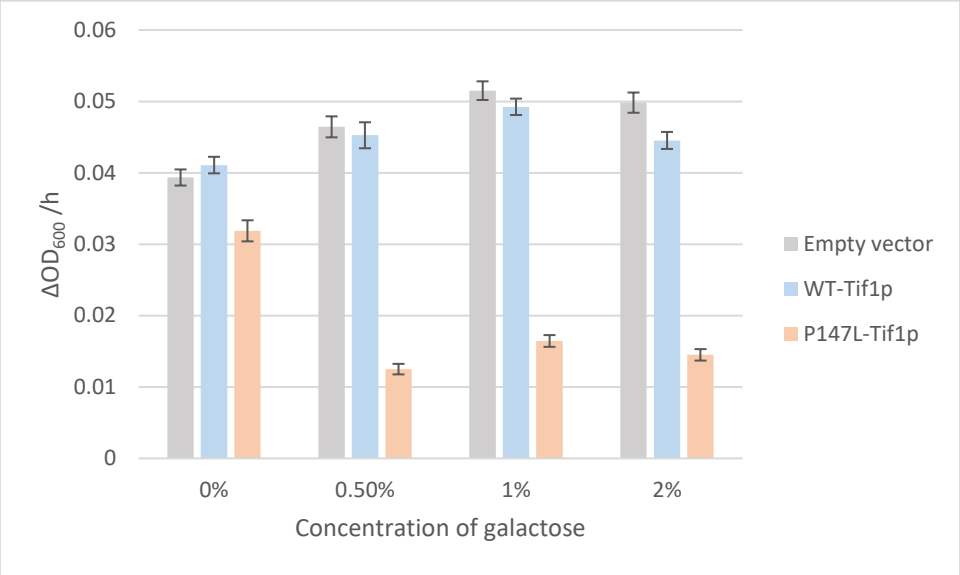

*Figure 24. Overexpression of eIF4A-P147L protein retards growth in yeast in liquid media. BY4741 yeast were transformed with the pBG1805 over expression plasmid either empty or containing WT-*TIF1 *or P147L-*TIF1*. Expression was then induced using a range of galactose concentrations and optical density measured over logarithmic growth phase to obtain a growth rate. Error bars show standard deviation of 4 biological replicates.*

Furthermore, in liquid culture the P147L expressing strain exhibited a marked decrease in growth when induced with galactose compared to the empty vector and WT eIF4A (Figure 24). This demonstrated high amounts of cellular P147L-*TIF1* retarded growth, possibly by inhibiting translation initiation.

2.3.3. P147L eIF4A overexpression as an eIF4A function inhibition mimic

Despite overexpression of P147L eIF4A having a negative effect on growth it was unclear whether this was the result of inhibition of translation initiation or some other mechanism. Given that stress granule formation and the G-quadruplex reporter did not prove to be viable indicators of translation initiation inhibition, it was decided to select a range of genes with varying length 5' UTRs from the GFP-fusion protein library. It has previously been reported that inhibition of eIF4A with silvestrol preferentially affects the translation of mRNAs with longer 5' UTRs (Wolfe et al., 2014). The selected GFP strains (5' UTR length) for this analysis were: YPS (104 nt), DUR1,2 (463 nt), JLP2 (84 nt), SCH9 (455 nt), ERB1 (41 nt), REG1 (514 nt), PPH21 (530 nt) and GPB1 (123 nt).

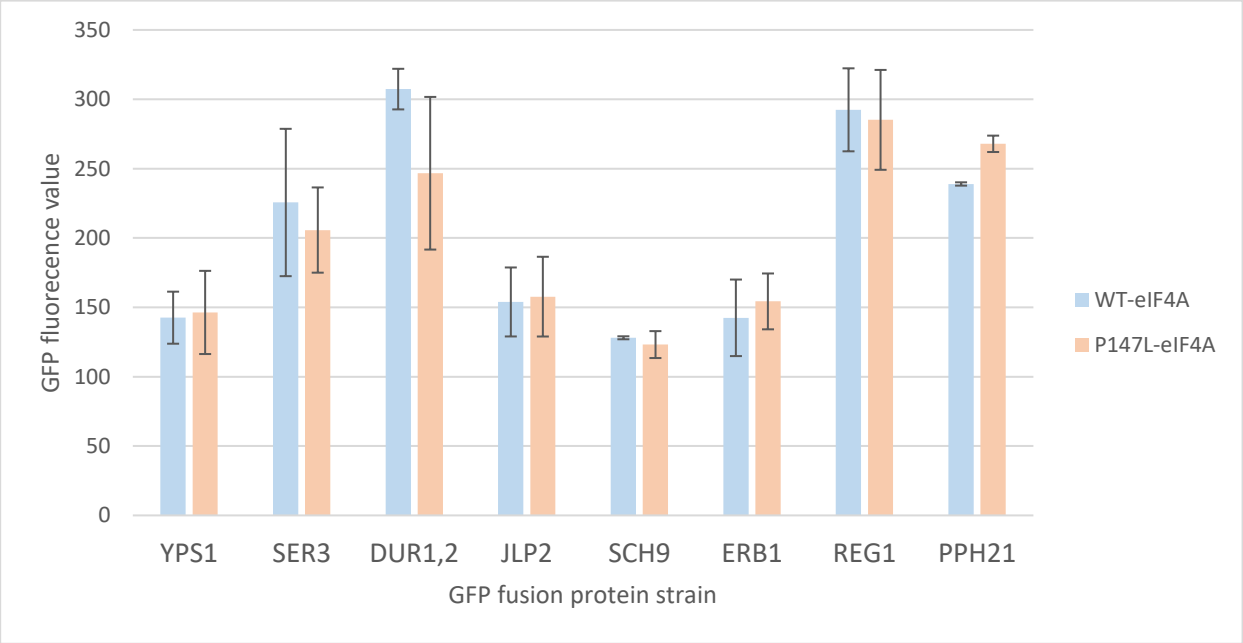

Figure 25. Overexpression of P147L mutant eIF4A does not preferentially decrease the expression of mRNA transcripts with longer 5' UTRs. GFP-fusion protein strains with short, medium or long 5' UTR sequences in the corresponding mRNAs were selected and transformed with the P147L mutant eIF4A overexpression plasmid. Over expression was induced with 2% galactose and fluoresce values measured after 5 h. Error bars show standard deviation of 2 biological replicates. Fluorescence intensity was analysed with an Acepella script that measures the fluorescence intensity of each cell and outputs a median value. Error bars show standard deviation of four replicates.

As shown in Figure 25, GFP expression showed no significant change when P147L was overexpressed compared to WT eIF4A suggesting that overexpression of P147L mutant eIF4A did not inhibit translation based on 5' UTR length. We also decided to investigate whether overexpression of the P147L mutant eIF4A affected the expression of the G-quadruplex reporter.

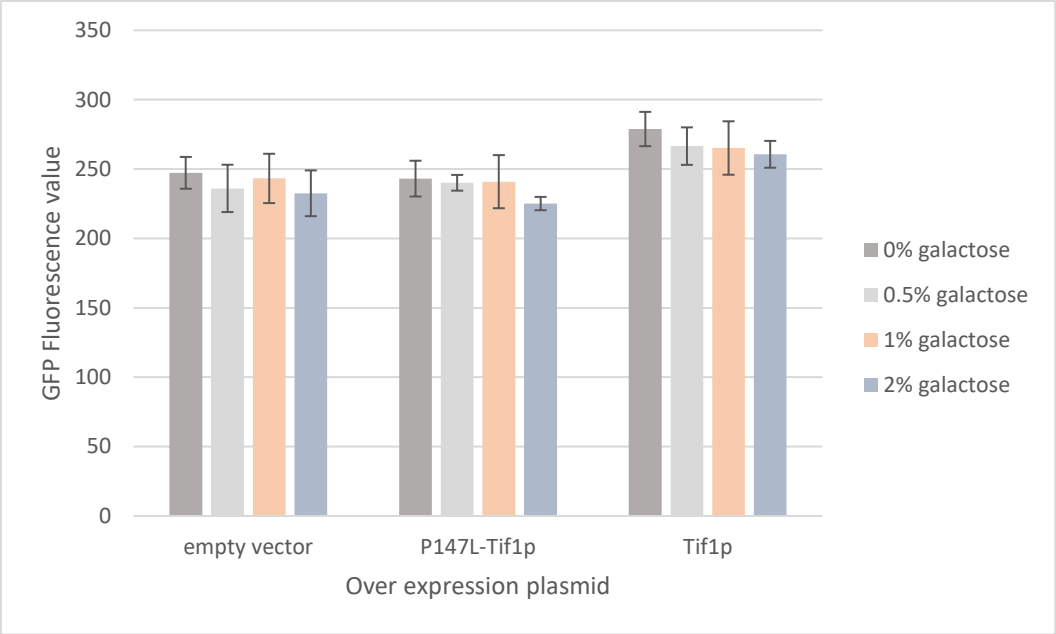

Figure 26. Overexpression of P147L mutant eIF4A does not decrease the expression of the G-quadruplex reporter. The G-quadruplex reporter strain was transformed with the pBG1805 over expression plasmid containing P147L mutant Tif1p, WT-Tif1p or empty vector. Over expression was induced with 0.5, 1 and 2% galactose and fluoresce values measured after 4 h. Fluorescence intensity was analysed with an Acepella script that measures the fluorescence intensity of each cell and outputs a median value. Error bars show standard deviation of four replicates.

As with the long 5' UTR experiment, no change in GFP fluorescence intensity was detected when the over expression of P147L mutant eIF4A protein is induced (Figure 26).

2.3.4. *TIF1* and *TIF2* gene deletion effects on eIF4A protein abundance

Having established that overexpression of the P147L mutant TIF protein mutant was unlikely to cause a readily measurable inhibitory effect on translation initiation as we hoped, we instead opted for a simple method of reducing functional eIF4A protein by deletion of one of the two TIF genes. Although this mutation was likely to have no measurable effect on growth, we could be reasonably confident deletion of one of the TIF loci would result in decreased TIF protein expression. This was confirmed by mass spectrometry with a reduction of 57% in eIF4A protein with a p-value of 0.02 (TIC), when the *TIF1* gene was deleted. When *TIF2* was

deleted instead it was found that the abundance of eIF4A dropped to 64% with a p-value of 0.0032 (TIC) when compared to the wild-type BY4741 control, validating this approach for MS and GFP screening. Due to this mutation having a minor, or no effect on growth it was decided to analyse the outcome from this reduction in functional eIF4A by investigating protein expression changes using sensitive methods for identifying biological changes (fluorescence and mass spectrometry).

2.3.5. GFP expression analysis

2.3.5.1. Expression analysis of tif1Δ *strain*

A *tif1*Δ strain was mated with the GFP-fusion protein library. The progeny of this mating were sporulated and Mat**a** haploids which possessed both mutations were selected, then analysed with a high throughput confocal microscope and eIF4A expression quantified with mass spectrometry. Each strain was normalized to its constitutive RFP fluorescence and compared against the parental GFP library stain. The procedure for plate seeding was optimized. We found that a single basic transfer by the Singer ROTOR robot from a plate incubated for 16 hours did not transfer adequate numbers of yeast cells to the microscope plate. Instead a single pickup and three deposits with mixing was found to maximise the number of wells containing cells at a density that could be analysed after a 4 hour outgrowth. Optimization experiments also found that exposing for a total of 400 ms per image was sufficient to acquire usable data while keeping the screen time manageable. The obtained median GFP fluorescence value per cell was then normalized to the constitutively expressed RFP as is common for this type of analysis (Bircham et al., 2011).

This analysis resulted in the identification of 33 proteins which increased in expression by at least 1.4-fold and 130 proteins which decreased in expression by at least 0.5-fold (Table 15 & Figure 27).

Table 15. List of ORFs which proteins changed in abundance in response to TIF1 *deletion.*

Decreased expression proteins	YMR186W, YDL055C, YDR224C, YDL184C, YGL189C, YLR061W, YGL135W, YBR031W, YDR381W, YGR180C, YPL106C, YML024W, YHR203C, YGL031C, YDR382W, YPR043W, YER043C, YKR057W, YER126C, YJL200C, YJR104C, YOR182C, YDL185W, YMR143W, YMR230W, YLR448W, YLR185W, YLR287C-A, YPR163C, YMR242C, YJR007W, YBR191W, YOR312C, YBR079C, YML073C, YDL182W, YDR234W, YFL036W, YLR175W, YKL180W, YGR162W, YPR041W, YBR011C, YGL120C, YHR087W, YDR346C, YDR129C, YHR141C, YKL060C, YOR303W, YJR109C, YAL047C, YMR260C, YMR314W, YOL140W, YML026C, YKL056C, YNL098C, YGL148W, YFL045C, YML052W, YNR001C, YJR145C, YBR248C, YOR210W, YPR187W, YGR027C, YDL232W, YML106W, YPL081W, YCR018C-A, YIR012W, YBL027W, YER177W, YKL035W, YGR260W, YHR107C, YGR128C, YLR059C, YMR012W, YMR243C, YER003C, YOR206W, YDR300C, YER133W, YAL035W, YGR008C, YDR035W, YKR001C, YML092C, YER074W, YOR340C, YML105C, YHR089C, YKR048C, YER069W, YDR170W-A, YGR218W, YML001W, YDL061C, YDL040C, YCL059C, YMR149W, YGL255W, YKR043C, YPR010C, YOR167C, YFL018C, YJL143W, YLR179C, YGL011C, YMR318C, YBR009C, YGR130C, YLL018C, YLR409C, YKR025W, YDR036C, YOR302W, YLR048W, YCR028C-A, YGR082W, YLR335W, YBR221C, YML070W, YKL016C, YNL189W, YPL243W, YGR207C, YJL088W
Increased expression proteins	YLR204W, YLR362W, YBR098W, YNL031C, YDR437W, YML049C, YIL087C, YDR139C, YDL192W, YMR078C, YLR327C, YHR204W, YBR198C, YAL005C, YML098W, YDR309C, YDR303C, YNL224C, YFL024C, YAL041W, YGR238C, YIL108W, YHR074W, YDR239C, YHR149C, YMR163C, YKL168C, YBL097W, YJL050W, YDL092W, YLR406C, YBR001C, YGR135W

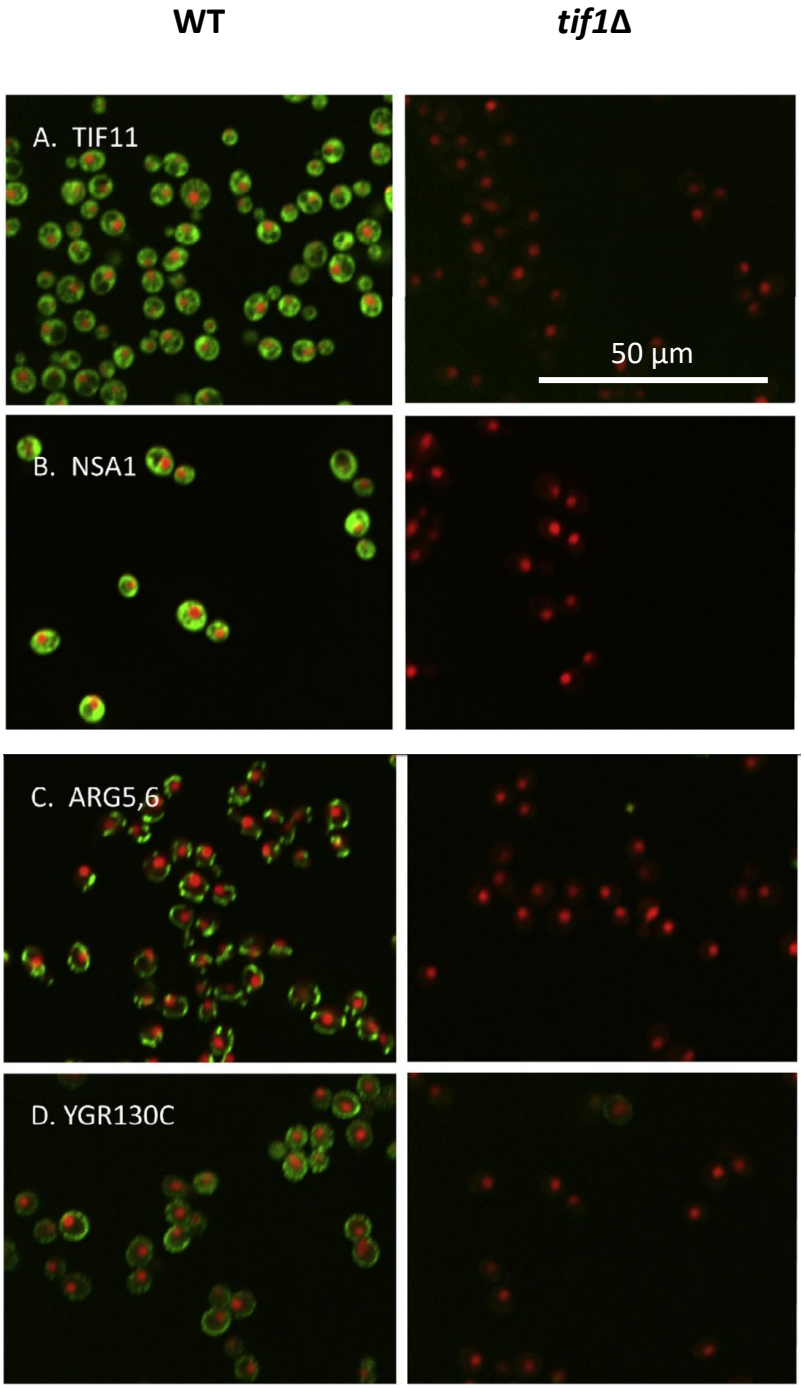

Figure 27. TIF1 *gene deletion causes reduction in expression of GFP in 130 GFP-fusion strains. Strains were grown on SD -His agar for 16 hours then transferred to liquid SD -His media in a 384 well microscope plate and grown for a further 4 hours. Each strain was then visualized with a 400 ms exposure time. Images on the left are of strains from the GFP-fusion protein library with wild-type* TIF1*, images on the right are the same GFP-fusion protein strains crossed with the* tif1Δ *strain from the Open Biosystems Mat**α** gene deletion library resulting in deletion of the* TIF1 *locus. Green represents fluorescence of GFP-fusion protein, intense red denotes a nucleus labelled with NLS-RedStar RFP, faint red denotes cytosolic mCherry RFP. All images are at the same scale.*

In order to confirm that the systems were crossed correctly, the plate location at which the *TIF1* GFP strain was crossed with the *tif1*Δ strain was checked. It was found that no viable colony was produced. This was expected as two selection genes (HIS3 and KanR) needed to be present at the same locus. The P-body fusion proteins Edc3p, Dhh1p Pat1p, Edc1p and Dpc2p also did not exhibit a punctate phenotype suggesting *TIF1* gene deletion does not induce P-body formation or cause a high degree of mRNA degradation. Additionally, the GFP strains selected from P147L-eIF4A overexpression to test effects of 5' UTR length did not exhibit notable expression changes then *TIF1* was deleted.

2.3.5.1.1. tif1Δ *gene ontology analysis*

Having identified a list of proteins which change in abundance as a result of *TIF1* deletion we proceeded to carry out a range of analyses. Firstly, gene ontology was utilized to identify the cellular processes which were disproportionally affected by the deletion of the *TIF1* gene (Table 16).

Table 16. Gene ontology enrichment of tif1Δ *GFP screen down-regulated proteins. Proteins found to be down-regulated in expression in the* tif1Δ *GFP screen were analysed using the g:Profiler enrichment tool (Raudvere et al., 2019) and searched in the biological process, cellular component, Reactome, WikiPathways and KEGG databases with term size limited to 1000. Complete ontological enrichments list is available in supplementary data 1.*

Data source	Term	p-value	Intersecting genes
Biological process	cytoplasmic translation	5.503×10^{-23}	38
	ribonucleoprotein complex biogenesis	4.654×10^{-11}	43
	ribosome biogenesis	6.790×10^{-10}	37
	cytoplasmic translational initiation	1.001×10^{-4}	7
	cellular amino acid biosynthetic process	3.032×10^{-3}	14
	glutamine family amino acid biosynthetic process	4.995×10^{-3}	7
	arginine biosynthetic process	7.647×10^{-3}	5
	GDP-mannose metabolic process	1.192×10^{-2}	3
KEGG	Ribosome	7.690×10^{-11}	32

Gene ontology analysis identified a number of strong enrichments in our dataset, the strongest of which was in translation and translation-related processes including; cytoplasmic translation, ribosome biogenesis, and cytoplasmic translational initiation. The strains found to give an increased GFP signal were also analysed for GO enrichment. However, the list of 33 genes did not return any significant enrichments. Ontologies associated with a combined list of up- and down-regulated proteins were not notably changed from those shown in Table 16.

2.3.5.1.2. tif1Δ *affected 5′ UTR length analysis*

As previously described (Section 1.4.4) inhibition of eIF4A can lead to disproportionately decreased translation of mRNAs with longer 5′ UTRs (Wolfe et al., 2014). We were unsure if this effect would also be seen when the cellular abundance of eIF4A protein was reduced. To investigate the relationship between lengths of the 5′ UTRs and susceptibility to reduced eIF4A abundance we compared the 5′ UTR lengths between the up- and down-regulated protein lists.

Table 17. The average length of the 5′ UTRs for which GFP-fusion proteins changed in abundance then TIF1 *was deleted. These were compared to a control list containing 500 randomly selected 5′ UTRs from Lin et at. (2011) (Supplementary data 10).*

	Mean	Standard deviation	Median	t-test vs control list
Down	106.5806	194.5162	70	0.40
Up	97.3871	90.49957	57	0.27
Control list	109.934	111.261	68	-

A slight trend was seen with the down-regulated transports possessing slightly longer 5′ UTRs than the up-regulated 5′ UTRs and the up-regulated 5′ UTRs being somewhat shorter than the control (Table 17). However, these differences were too small to be significant, suggesting even if this effect is occurring it is very slight.

2.3.5.1.3. tif1Δ *affected 5′ UTR GC content*

GC content is a strong determinant of the stability of 5′ UTR secondary structure and it is suspected that higher GC content 5′ UTRs have a greater need for eIF4A helicase activity to be expressed (Waldron et al., 2019). To investigate whether the GC content in 5′ UTRs is influencing expression when eIF4A abundance is reduced, the GC content for each 5′ UTR sequence was calculated and the average of the up- and down-regulated lists and total genomic GC content (Wood et al., 2002) were compared (Table 18).

Table 18. Averages of the GC content in the 5′ UTRs of the GFP-fusion genes found to change in abundance. These were compared to a control list containing 500 randomly selected 5′ UTRs from Lin et at. (2011). (Supplementary data 10).

	Mean	Standard deviation	Median	t-test vs control
Down	33.3%	6.6	33.5%	0.100
Up	37.2%	7.1	35.2%	0.014
Entire genome average	38.3%	-	-	-
Control list	34.2%	7.6	34.2%	-

When comparing the GC content of the 5′ UTRs in our hits lists, we determined that the average GC content of down-regulated proteins was slightly lower than the up-regulated and genome average. However, this difference was smaller when comparing the median values between the up- and down-regulated lists. This is the opposite trend as would be expected as higher GC content 5′ UTRs have a propensity to form more stable secondary structures meaning they have a greater need for eIF4A helicase activity. An analysis with students t-test found there was a significant difference between the randomly generated 5′ UTR control list and the up-regulated 5′ UTR list but the difference in values between the mean and median indicate this is driven by a small number of high GC content 5′ UTRs. The genome-wide average GC content value (Wood et al., 2002) is higher than any of the of our generated lists, suggesting that yeast 5′ UTRs tend to have lower GC content than the rest of the genome.

2.3.5.1.4. Identification of tif1Δ *affected motifs in the 5′ UTR*

In previous studies inhibiting the function of eIF4A, several sequence motifs in the 5′ UTR have also been identified that are disproportionately affected by eIF4A inhibition (Iwasaki et al., 2016; Iwasaki et al., 2019; Wolfe et al., 2014). To further investigate the effects that the 5′ UTR may be having on the expression of mRNA transcripts when the abundance of eIF4A is reduced, sequence motif analysis was carried out using the MEME search tool (Bailey et al., 2009).

E-value	Number of motif instances	Length of motif	Motif
$7.5x10^{-09}$	**35**	**15**	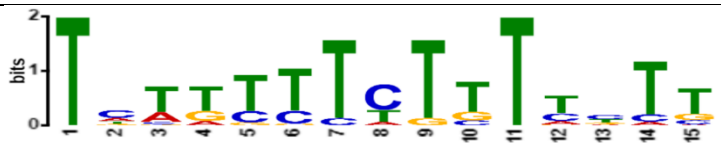
$2.1x10^{-02}$	**35**	**10**	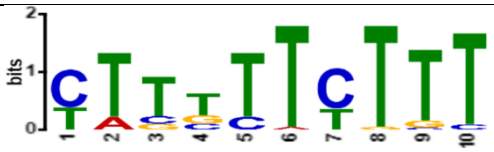

Figure 28. Two significant motifs were identified to be enriched in the down-regulated proteins 5' UTRs. The 5' UTR sequences were searched using the MEME motif search algorithm with the maximum length limited to 30, 20, 15 and 10 nucleotides long.

This 5' UTR motif enrichment analysis yielded only two significant motifs which appear very similar to each other (Figure 28). As the 10 nucleotide long motif was only observed when the maximum motif length was limited to 10 nucleotides this appears to be cropped version of the 15 nucleotide long motif. The 15 nucleotide motif was retained even when the maximum motif setting was increased. A similarly TC-rich motif was also observed in the up-regulated 5' UTR list but did not reach significance. The only polypurine motif similar to the motif identified by Iwasaki et al. (2016) was not significant with an E-value of 1.0 and no motifs identified had the G-quadruplex pattern described by Wolfe et al. (2014).

2.3.5.2. GFP expression analysis of tif2Δ *strain*

2.3.5.2.1. Production the tif2Δ *strain*

Having identified and analysed proteins that change in abundance in response to deletion of the *TIF1* gene, we then planned to carry out the same approach with deletion of the *TIF2* gene. Having a list of proteins which change in response to each gene deletion would allow for greater understanding of the different roles of the two homologues. However, unlike the *tif1*Δ strain, the *tif2*Δ strain was not available in the Mat**α** yeast Open Biosystems gene deletion library. Thus, this strain needed to be produced in-house. PCR primers were produced with flanking regions homologous with regions either side of the genomic *TIF2* locus and designed to express the kanamycin resistance cassette. A homologous recombination approach was then used to integrate the selection cassette into the genome, replacing the *TIF2* locus in the process.

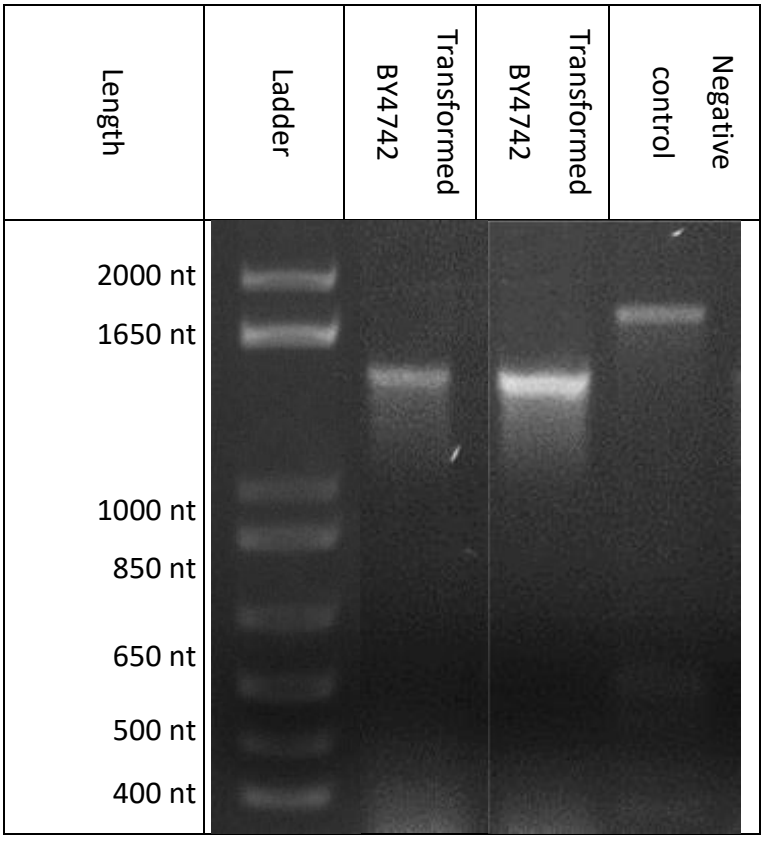

Figure 29. Insertion of the KanMX6 was confirmed. A ~1500 nucleotide long product (1430 expected, 1792 across the TIF2 *locus in the negative control) confirmed insertion at the* TIF2 *locus. Transformed colonies that grew on the geneticin selection plate were picked and genomic DNA extracted and confirmed with the use of flanking primers.*

This approach proved effective resulting in the production of a viable yeast strain that grew on geneticin containing selective media. This strain was then analysed with a confirmation PCR giving the correct size PCR products (Figure 29).

2.3.5.2.2. Production of the tif2Δ *GFP-fusion protein library*

Having produced *tif2*Δ mutant, we then crossed it with the GFP-fusion protein library. The initial cross was successful, producing diploid cells. These cells were then sporulated and haploids selected successfully. However, as selections for each marker were added one at a time, the majority of colonies stopped growing. It was unclear why this was occurring. We theorised that we were not successfully transferring a significant range of different recombinant haploids with the desired mutations. We first attempted to remedy this by increasing the outgrowth period to produce larger colonies allowing for more of each mutant to grow. Additionally, our pinning method was altered by taking multiple pinnings from each colony from different regions to transfer a more varied population of mutants. However, when carrying out selections the same loss of colonies was observed. We then decided that it may be an effect of the specific *tif2*Δ mutant we used in the crossing, so we decided to carry out the crossing with the GFP library again with a different *tif2*Δ transformant. Unfortunately, during the selections a similar loss of colonies was observed. At this point due to significant time and resources spent it was decided to abandon this approach and instead utilise a mass spectrometry approach to quantity protein expression.

2.3.6. Mass spectrometric protein expression analysis in *tif1*Δ and *tif2*Δ strains

With the unsuccessful crossing of the yeast GFP library with a *tif2*Δ mutant, we instead quantified proteins using mass spectrometry. When carrying out the statistical tests on the mass spectrometry data and FDR multiple test correction was carried out. However, doing this test on the *tif1*Δ data resulted in only 4 proteins being deemed significant. To carry out further analysis a p-value cut-off of 0.05 was used instead for this data. When analysing *tif1*Δ strain in the mass spectrometry proteomic experiments, a total of 76 proteins were identified to have changed in abundance when compared to the control (BY4741) ($p \leq 0.05$), with 40 found to decrease in abundance and 36 found to increase in abundance (Table 19). When analysing the *tif2*Δ strain a total of 94 proteins were identified to have changed in abundance when compared to the control (BY4741) (FDR≤0.1), with 53 found to decrease in abundance and 41 found to increase in abundance (Table 20). A complete list of proteins identified to change in abundance with associated statistics is available in Supplementary data, Sections 8 & 9.

Table 19. List of ORFs for which proteins changed in abundance in response to TIF1 *deletion* ($p \leq 0.05$).

Decreased expression proteins	YJR027W, YCR088W, YMR318C, YIL053W, YMR246W, DL131W, YMR038C, YER063W, YDR210C-D, YDR487C, YER165W, YJL138C, YBR078W, YGL105W, YOR323C, YPR041W, YML085C, YPR145W, YER055C, YIL094C, YHR025W, YGR124W, YOR038C, YMR131C, YGL008C, YHR146W, YJL130C, YMR309C, YLR257W, YNL007C, YNL016W, YPR062W, YCL043C, YDR002W, YPR052C, YJR045C, YBR249C, YDR158W, YGL253W
Increased expression proteins	YPL004C, YHL015W, YGL009C, YLR075W, YBR031W, YFL014W, YKR066C, YOR142W, YOR332W, YNL055C, YJR121W, YMR105C, YPR102C, YBL064C, YPR191W, YDL022W, YPL078C, YLR048W, YOR374W, YLR153C, YHR021C, YDL185W, YDR155C, YHL034C, YJL159W, YBL099W, YDR513W, YDR298C, YJR123W, YLL045C, YDR032C, YGL256W, YKL081W, YKL085W, YER117W, YLR304C

Table 20. List of ORFs for which proteins changed in abundance in response to TIF2 *deletion (FDR≤0.1).*

Decreased expression proteins	YBR072W, YFR053C, YCL040W, YFL014W, YDL022W, YDL124W, YJL138C, YMR105C, YMR315W, YER133W, YJL052W, YGL037C, YPL004C, YKL142W, YPL154C, YOR187W, YGR244C, YKL035W, YOR285W, YML100W, YLR438W, YML078W, YNL055C, YLR354C, YMR072W, YKL067W, YDR155C, YER003C, YOR374W, YLL026W, YNL160W, YGL062W, YDL029W, YBL099W, YJR121W, YKL016C, YGR192C, YDL066W, YBR126C, YDR513W, YHR087W, YAR002C-A, YNL134C, YKL085W, YPL231W, YNL015W, YEL060C, YDR032C, YHR104W, YKL103C, YDR533C, YLR300W, YKR066C
Increased expression proteins	YOR335C, YJR016C, YIL053W, YPL106C, YBL076C, YGR034W, YLR432W, YBR121C, YLR447C, YOL154W, YDR071C, YMR309C, YLR344W, YLR060W, YGL234W, YBL072C, YDR385W, YMR108W, YDR429C, YLR249W, YML056C, YNL281W, YDL229W, YGL026C, YHR064C, YHR141C, YPR074C, YOR046C, YLR301W, YBR025C, YNL209W, YPR132W, YGL245W, YLR197W, YDR341C, YDL191W, YEL046C, YIL078W, YER110C, YPL160W, YOR310C

2.3.6.1. GO analysis of mass spectrometry identified genes

As with the GFP screen protein lists, the proteins identified to change in abundance as a result of reduced functional eIF4A abundance were analysed with gene ontology enrichment analysis. This identified the cellular processes and pathways most affected by eIF4A reduction.

2.3.6.1.1. Mass spectrometry: tif1Δ *GO analysis of up-regulated proteins*

Gene ontology analysis identified a number of strong enrichments in the *tif1*Δ up-regulated proteins list with the strongest enrichments relating to protein translation and energy production (Table 21).

Table 21. Ontological enrichments in proteins up-regulated in the tif1Δ *mutant from a total of 36 genes (p<0.05). Proteins found to be up-regulated in expression in the* tif1Δ *mass spectrometry experiment were analysed using the g:Profiler enrichment tool (Raudvere et al., 2019) and searched in the biological process, cellular component, Reactome, WikiPathways and KEGG databases with term size limited to 1000. Complete ontological enrichments list is available in supplementary data 3.*

Source	**GO term**	**p-value**	**Number of intersecting genes**
Biological process	cytoplasmic translation	2.16×10^{-03}	9
	proton transmembrane transport	2.52×10^{-03}	5
	energy coupled proton transport, down electrochemical gradient	9.82×10^{-03}	4
	ATP synthesis coupled proton transport	9.82×10^{-03}	4
	ATP biosynthetic process	9.82×10^{-03}	4
	purine ribonucleoside triphosphate metabolic process	2.30×10^{-02}	4
	purine ribonucleotide biosynthetic process	4.74×10^{-02}	5
KEGG	oxidative phosphorylation	2.87×10^{-04}	7
	ribosome	3.42×10^{-03}	9

2.3.6.1.2. Mass spectrometry: tif1Δ *GO analysis of down-regulated proteins*

Gene ontology analysis identified a number of strong enrichments in the *tif1*Δ down-regulated proteins list with the strongest enrichments relating to amino acid production and a minor enrichment in translation initiation proteins (Table 22).

Table 22. Ontological enrichments in proteins down-regulated in the tif1Δ *mutant from a total of 40 genes (p<0.05). Proteins found to be down-regulated in expression in the* tif1Δ *mass spectrometry experiment were analysed using the g:Profiler enrichment tool (Raudvere et al., 2019) and searched in the biological process, cellular component, Reactome, WikiPathways and KEGG databases with term size limited to 1000. Complete ontological enrichments list is available in supplementary data 2.*

Source	**GO term**	**p-value**	**Number of intersecting genes**
Biological process	cellular amino acid biosynthetic process	8.308×10^{-6}	10
	alpha-amino acid biosynthetic process	7.475×10^{-5}	9
	cellular amino acid metabolic process	4.105×10^{-4}	11
	carboxylic acid metabolic process	3.290×10^{-4}	12
	aspartate family amino acid biosynthetic process	8.645×10^{-4}	6
	translational initiation	4.052×10^{-2}	5
	oxoacid metabolic process	1.385×10^{-2}	12
KEGG	biosynthesis of amino acids	9.182×10^{-5}	9
	lysine biosynthesis	5.950×10^{-3}	3

2.3.6.1.3. Mass spectrometry: tif2Δ *GO analysis of up-regulated proteins*

Gene ontology analysis identified a number of strong enrichments in the *tif2*Δ up-regulated proteins list with the strongest enrichments relating to protein translation and tRNA metabolism (Table 23).

Table 23. Ontological enrichments in proteins up-regulated in the tif2Δ *mutant from a total of 41 genes (FDR<0.1). Proteins found to be up-regulated in expression in the* tif2Δ *mass spectrometry experiment were analysed using the g:Profiler enrichment tool (Raudvere et al., 2019) and searched in the biological process, cellular component, Reactome, WikiPathways and KEGG databases with term size limited to 1000. Complete ontological enrichments list is available in supplementary data 5.*

Source	**GO term**	**p-value**	**Number of intersecting genes**
Biological process	translation	5.98×10^{-11}	22
	peptide metabolic process	3.61×10^{-10}	22
	tRNA aminoacylation for protein translation	2.05×10^{-07}	8
	tRNA aminoacylation	3.94×10^{-07}	8
	ncRNA metabolic process	8.97×10^{-05}	16
	regulation of translational fidelity	9.21×10^{-03}	4
	translational termination	2.06×10^{-02}	4
	'de novo' cotranslational protein folding	1.24×10^{-02}	3
KEGG	aminoacyl-tRNA biosynthesis	9.78×10^{-07}	8
WP	cytoplasmic tRNA Synthetases	1.65×10^{-05}	6

2.3.6.1.4. Mass spectrometry: tif2Δ *GO analysis of down-regulated proteins*

Gene ontology analysis identified a number of strong enrichments in the *tif2*Δ down-regulated proteins list with the strongest enrichments almost solely relating to energy production-related processes (Table 24).

Table 24. Ontological enrichments in proteins down-regulated in the tif2Δ *mutant from a total of 53 genes (FDR<0.1). Proteins found to be down-regulated in expression in the* tif2Δ *mass spectrometry experiment were analysed using the g:Profiler enrichment tool (Raudvere et al., 2019) and searched in the biological process, cellular component, Reactome, WikiPathways and KEGG databases with term size limited to 1000. Complete ontological enrichments list is available in supplementary data 4.*

Source	**GO term**	**p-value**	**Number of intersecting genes**
Biological process	carbohydrate metabolic process	$1.88x10^{-08}$	18
	purine ribonucleotide metabolic process	$5.57x10^{-04}$	9
	oxidation-reduction process	$2.51x10^{-04}$	16
	response to oxidative stress	$1.83x10^{-03}$	9
	response to heat	$6.13x10^{-03}$	7
	glucose metabolic process	$1.56x10^{-02}$	6
KEGG	starch and sucrose metabolism	$5.21x10^{-05}$	7
	glycolysis / gluconeogenesis	$4.76x10^{-03}$	6
	citrate cycle (TCA cycle)	$3.54x10^{-02}$	4
WP	trehalose anabolism	$8.14x10^{-04}$	4
	glycolysis and gluconeogenesis	$3.65x10^{-02}$	5

A second *tif2*Δ GO enrichment analysis was carried out using proteins which changed with a p-value lower than 0.05, as was carried out on the *tif1*Δ data. GO enrichment analysis with this larger dataset, which was not corrected for multiple testing, yielded most of the same enrichments seen in the corrected data (Supplementary data, 6 & 7). Additionally, several other terms were significant which generally related to terms already seen in the multiple test corrected data. This suggests that the enrichments seen in the uncorrected *tif1*Δ data are likely to be meaningful results and are caused by biological effects despite FDR analysis not being carried out.

2.3.6.1.5. Conflicting protein changes

When analysing protein expression, it was noted that 13 proteins found to be down-regulated in the *tif1*Δ mass spectrometry experiment were upregulated in the *tif2*Δ experiment. The reason for this is unclear. When this list of proteins was analysed with gene ontology enrichment, we found 8 proteins were part of the mitochondrion ($p=2.856\times10^{-2}$) and 6 had oxidoreductase activity ($p=3.56\times10^{-2}$) with only 3 genes not being associated with either.

This analysis was also carried out on conflicting genes where the *tif1*Δ upregulated intersected with the *tif2*Δ downregulated and the *tif2*Δ upregulated intersected with the *tif1*Δ downregulated list. However, no relationship in the intersecting lists of these genes was found.

2.3.6.2. Ontological enrichment comparison between experiments

As would be suspected, enrichments in translation-related ontologies are seen throughout our data. Additionally, processes supplementary to translation are also seen such as tRNA, amino acid, and ribosome biogenesis-related processes. Interestingly, we see that in both *tif1*Δ and *tif2*Δ experiments, translation-related proteins are up-regulated whereas specifically translation initiation in the *tif1*Δ experiment is down-regulated. Less expected are the enrichments in proteins involved in energy metabolism, strangely these are seen in the up-regulated *tif1*Δ proteins list and in the down-regulated *tif2*Δ proteins list with the *tif1*Δ proteins being enriched in proton transport and the *tif2*Δ proteins being linked to glycolysis and the TCA cycle.

When the MS and GFP experiments are compared we see both are enriched in translation. However, the enrichments within these intersections somewhat differ. Proteins in the down-regulated GFP list which are linked to translation are weighted toward translation initiation, ribosome assembly and ribosome biogenesis. Whereas the mass spectrometry *tif2*Δ up-regulated proteins linked to translation are weighted toward peptide biosynthetic process, tRNA aminoacylation, regulation of translational fidelity, and translational elongation. On the other hand, the proteins linked to translation in the up-regulated *tif1*Δ mass spectrometry lists more closely resemble the GFP down-regulated list with enrichments in ribosome assembly and ribosome biogenesis.

Also of note, the mass spectrometry and GFP *tif1*Δ down-regulated proteins are both enriched in processes relating to production of amino acids but the *tif2*Δ mass spectrometry up-regulated proteins are enriched in tRNA aminoacylation which are two highly interlinked processes.

When lists were combined and translation, oxidation-reduction and carbohydrate metabolism-related genes are removed, the proteasomal ubiquitin-independent protein catabolic process ontology was enriched with 5 genes ($p=1.206\times10^{-2}$) associated with this term.

2.3.6.3. 5′ UTR length analysis of identified proteins

As with the GFP screen (Section 2.3.5), we analysed the 5′ UTRs of the mRNA transcripts of proteins found to change in abundance. Firstly, the 5′ UTRs were analysed based on length.

Table 25. Mass spectrometry data 5′ UTR lengths of up- and down-regulated transcripts of TIF1 *and* TIF2 *deletion mutants (p≤0.05 and FDR≤0.1 respectively). P-values are reported from a one-tailed t-test. These were compared to a control list containing 500 randomly selected 5′ UTRs from Lin et at. (2011) (Supplementary file 10).*

	Mean	Standard deviation	Median	t-test
*tif1*Δ Up	98.94	70.27	76.00	0.32
*tif1*Δ Down	112.11	102.92	75.50	
*tif2*Δ Up	90.18	70.24	62.00	0.22
*tif2*Δ Down	95.87	65.60	82.00	
Combined Ups	93.91	70.74	69.00	0.21
Combined Downs	102.34	84.04	76.50	
Control list	109.934	111.261	68	-

Analysis of the length of our 5′ UTR lists found a light trend for the transcripts found to be down-regulated to have longer 5′ UTRs (Table 25). However, these trends are small and t-test analysis reported values well above the significance cut off value, making us doubtful this this is a genuine trend.

2.3.6.4. 5′ UTR GC content analysis of identified proteins

GC content is a strong determiner of the stability of 5′ UTR secondary structure and it is suspected that higher GC content 5′ UTRs have a greater need for eIF4A helicase activity to be expressed. To see if this trend is seen in our data the 5′ UTRs of up and down-regulate transcripts were analysed for GC content.

Table 26. GC content analysis of mass spectrometry data 5′ UTR GC content of up- and down-regulated transcripts of tif1Δ and tif2Δ mutants (p≤0.05 and FDR≤0.1 respectively). P-values reported from one-tailed t-test. These were compared to a control list containing 500 randomly selected 5′ UTRs from Lin et at. (2011) (Supplementary file 10).

	Mean	Median	t-test
*tif1*Δ Up	32.8%	32.2%	0.33
*tif1*Δ Down	33.5%	33.4%	
*tif2*Δ Up	32.0%	32.4%	0.24
*tif2*Δ Down	33.1%	33.3%	
Combined Ups	32.4%	32.2%	0.22
Combined Downs	32.9%	33.3%	
Control list	34.2%	34.2%	-
Genome average	38.3%	-	-

Analysis of the GC content of 5′UTRs of up- and down-regulated transcripts found very little difference in GC content between the any of the datasets with a difference of only 1.5% between the highest and lowest values (Table 26). This suggests that the GC content of the 5′ UTR has very little influence on whether expression of a transcript is up or down-regulated when functional eIF4A levels are reduced. Interestingly, our data is about 5% lower than the yeast genome average suggesting 5′ UTRs tend to have lower less GC content than other regions in the genome. This data does not align perfectly with the GC content analysis of the GFP screen (Table 18) that showed the up-regulated 5′ UTRs to have a higher GC content than the down-regulated 5′ UTRs.

2.3.6.5. Analysis of 5′ UTR motif enrichment of identified proteins

As mentioned above (Section 1.4.4), studies investigating inhibitors of eIF4A a identified several sequence motifs in the 5′ UTR that are disproportionately affected by eIF4A inhibition (Iwasaki et al., 2016; Iwasaki et al., 2019; Wolfe et al., 2014). As with the GFP screen, we carried out motif enrichment analysis with the MEME search tool (Bailey et al., 2009) to identify any sequence trends in the 5′ UTRs of transcripts of proteins found to change in abundance in our datasets. Note, motifs are reported as containing thymidine as sequences were reported this way on the data sources for the 5′ UTRs, when in the form of RNA these nucleotides would appear as uracil.

2.3.6.5.1. tif1Δ mass spectrometry: 5′ UTR motif enrichment of down-regulated proteins

E-value	Number of motif instances	Length of motif	Motif
1.7x10^{-02}	**16**	**20**	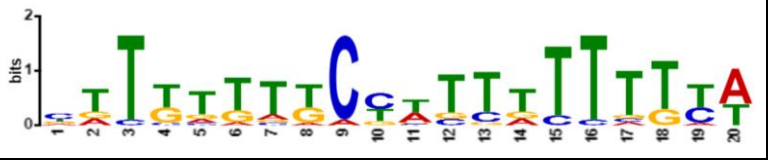

Figure 30. One significant motif was identified to be enriched in the tif1Δ up-regulated proteins 5′ UTRs. The 5′ UTR sequences were searched using the MEME motif search algorithm with the maximum length limited to 30, 20, 15 and 10 nucleotides long. When the sequences were shuffled the lowest E-value achieved was 1.6.

When carrying motif analysis on the *tif1Δ* down-regulated proteins only one statistically enriched motif was identified (Figure 30). This motif had a T-rich sequence somewhat similar to the TC-rich motif identified in the GFP screen.

2.3.6.5.2. tif1Δ *mass spectrometry: 5′ UTR motif enrichment of up-regulated proteins*

E-value	Number of motif instances	Length of motif	Motif
7.1x10^{-03}	**15**	**19**	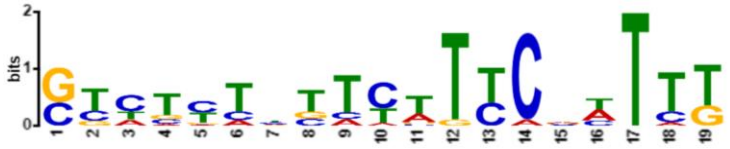
1.2x10^{-02}	**17**	**15**	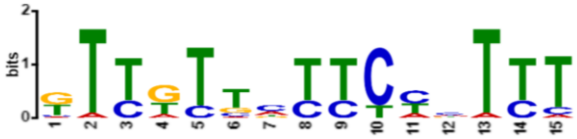

Figure 31. Two significant motifs were identified to be enriched in the tif1Δ down-regulated proteins 5′ UTRs. The 5′ UTR sequences were searched using the MEME motif search algorithm with the maximum length limited to 30, 20, 15 and 10 nucleotides long. When the sequences were shuffled the lowest E-value achieved was 1.2x10^{+1}.

When carrying motif analysis on the *tif1*Δ up-regulated proteins two statistically enriched motifs were identified (Figure 31). These motifs were very similar to the motif found in the down-regulated 5′ UTRs but with slightly higher frequencies of cytosine nucleotides.

2.3.6.5.3. tif2Δ *mass spectrometry: 5′ UTR motif enrichment of down-regulated proteins*

E-value	Number of motif instances	Length of motif	Motif
7.1x10^{-04}	**23**	**14**	
4.3x10^{-03}	**28**	**10**	

Figure 32. Two significant motifs were identified to be enriched in the tif2Δ down-regulated proteins 5′ UTRs. The 5′ UTR sequences were searched using the MEME motif search algorithm with the maximum length limited to 30, 20, 15 and 10 nucleotides long. In these searches the sequences for YOR285W was omitted due so the 5′ UTR sequence being too short for analysis. When the sequences were shuffled the lowest E-value achieved was 1.6.

When carrying motif analysis on the *tif2*Δ down-regulated proteins three statistically enriched motifs were identified (Figure 32). These were all TC-rich appearing to be the result of the same general motif when constrained to different maximum motif lengths.

2.3.6.5.4. tif2Δ *mass spectrometry: 5′ UTR motif enrichment of up-regulated proteins*

When carrying motif analysis on the *tif2*Δ up-regulated proteins no statistically enriched motifs were identified.

2.3.6.5.5. Combined mass spectrometry: 5′ UTR motif enrichment of up-regulated proteins

It was reasoned that the *tif1*Δ and *tif2*Δ mass spectrometry runs being from the same background strain and being the same mating type were similar enough to pool the 5′ UTR sequence lists of the two experiments. This had the potential to better define the motifs already identified and potentially identify any new motifs with more weak enrichments. The 5′ UTR sequences of transcripts found to be up-regulated in either *tif1*Δ or *tif2*Δ conditions in the mass spectrometry experiments were pooled to produce a combined up-regulated list.

E-value	Number of motif instances	Length of motif	Motif
1.5x10^{-05}	**18**	**13**	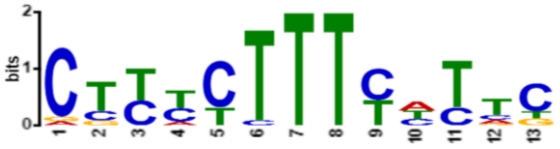

Figure 33. One significant motif was identified to be enriched in the combined up-regulated proteins 5′ UTRs. The 5′ UTR sequences were searched using the MEME motif search algorithm with the maximum length limited to 30, 20, 15 and 10 nucleotides long. When the sequences were shuffled the lowest E-value achieved was 10.

When carrying motif analysis on the combined up-regulated proteins only one statistically enriched motif was identified with the motif following the TC-rich trend seen in previous analyses (Figure 33).

2.3.6.5.6. Combined mass spectrometry: 5' UTR motif enrichment of down-regulated proteins

Combining of the 5' UTR lists of transcripts found in to be down-regulated in either *tif1*Δ or *tif2*Δ conditions in the mass spectrometry experiments was also carried out and analysed for motif enrichments.

E-value	Number of motif instances	Length of motif	Motif
$5.7x10^{-11}$	**28**	**20**	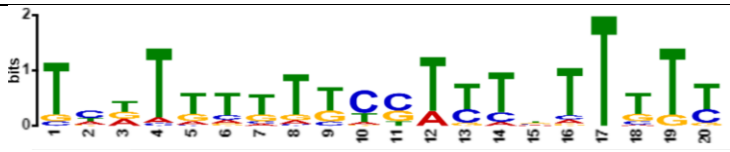
$2.4x10^{-04}$	**30**	**10**	
$1.0x10^{-03}$	**31**	**21**	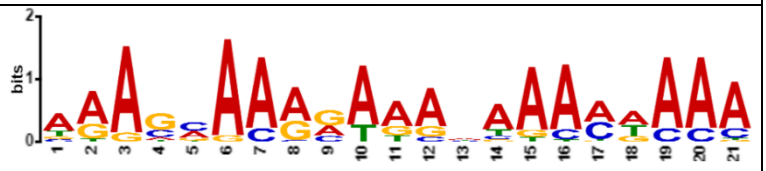

Figure 34. Three significant motifs were identified to be enriched in the combined down-regulated proteins 5' UTRs. The 5' UTR sequences were searched using the MEME motif search algorithm with the maximum length limited to 30, 20, 15 and 10 nucleotides long. In these searches the sequence for YOR285W was omitted due so the 5' UTR sequence being too short for analysis. When the sequences were shuffled the lowest E-value achieved was 2.4.

When carrying motif analysis on the combined down-regulated proteins three statistically enriched motifs were identified (Figure 34). Two of these motifs followed the TC-rich trend seen in previous analyses. However, a third predominantly A-rich motif as also identified with 31 motif sites found in our 5' UTR sequences.

2.4. Discussion

The aim of this study is to gain a deeper understanding of the outcomes of eIF4A inhibition, including direct transcript-specific effects and the follow-on effects of inhibition or reduction of functional eIF4A on the proteome of the cell. Our current understanding of eIF4A inhibition is that inhibitors that induce a strong binding of eIF4A to mRNA, such as pateamine, cause the reduced expression of select mRNA transcripts at concentrations below growth inhibition levels (Di Marco et al., 2012). However, recent studies using hippuristanol, an inhibitor that prevents eIF4A from binding mRNA show similar reductions in select transcripts (Cramer et al., 2018), casting doubt on this working model. In this chapter, we aim to determine the effects of reducing the abundance of functional eIF4A, an outcome the we hypothesise to be similar to hippuristanol inhibition. With genetic alterations, such as deletion of eIF4A-producing genes, we investigate changes in the protein landscape in *Saccharomyces cerevisiae* to gain a greater understanding of the cell-wide effects of reduced eIF4A function. From the analysis carried out, we have identified a range of biological processes and transcript-specific features which are affected as a result of depletion of active eIF4A in yeast.

2.4.1. Methods of translation initiation inhibition detection

2.4.1.1. G-quadruplex GFP reporter for translation initiation inhibition detection

In order to identify a way to produce a genetic method for reducing translation initiation, we needed a way of identifying when translation initiation was being altered. At the onset of our research, a recent study had identified a GC-rich motif consisting of a recurring CGG sequence (Table 14) proposed to form a stable G-quadruplex structure, which was disproportionally affected by the eIF4A inhibitor silvestrol (Wolfe et al., 2014). We reasoned that a fluorescent reporter with this sequence in its 5’ UTR may be an effective method for identifying translation initiation inhibition. To investigate this, we constructed a GFP reporter yeast strain.

2.4.1.1.1. GFP reporter design and considerations

We aimed to create a reporter construct which consisted of the constitutive expressing TEF promoter upstream of a 5' UTR containing the sequence described by Wolfe et al. (2014), linked to the GFP gene. It was decided that this would be integrated into the yeast genome to avoid any effect plasmid of copy number variability.

For the purposes of transformant selection, this GFP reporter was transformed into the *CAN1* gene locus as this would result in successful transformants being resistant to canavanine. However, canavanine resistance can also occur without transformation, meaning screening was required. The *CAN1* gene codes for a membrane permease protein which allows the toxic compound canavanine to enter the cell causing cell death (Suizu et al., 1989). The deletion of the *CAN1* gene prevents canavanine from entering the cell making cells resistant. By disrupting this gene, yeast cells would survive in the presence of canavanine. We utilized this effect as a positive selection when incorporating the G-quadruplex reporter into the genome. However, this is a loss of function transformation selection, meaning random loss of function genetic mutations in the *CAN1* gene will also result in cell survival. This effect means that the selection can result in a large number of false positives. Fortunately, screening the potential transformants could be carried out reasonably quickly and easily as any colony in which the correct genetic construct was incorporated should now express GFP. This screen was carried out using the high throughput microscope and identified two GFP expressing G-quadruplex transformed colonies of the ten screened.

As described in Section 2.3.1.2, a GC content matched 5' UTR GFP reporter yeast strain was produced alongside the G-quadruplex strain. Unfortunately, when transformants containing this control reporter sequence were visualized with the OPERA fluorescent microscope, it was found that the GFP was expressed at very low levels, making them unsuitable to act as an effective control. We suspect that this was caused by the 5' UTR construct possessing a very high GC content inducing stable secondary structure within the strand and preventing translation. A randomly selected control list of 500 yeast 5' UTRs had an average GC content of 34.2% (Supplementary data 10), it is possible that the yeast translation initiation machinery was unable to resolve this structure. However, we would expect this to be an issue for the G-quadruplex forming 5' UTR also as the GC content was the same, although it is possible that a protein other than eIF4A is available to resolve G-quadruplexes in S. cerevisiae.

Although, we failed to produce a control of the reporter construct, this G-quadruplex reporter was one of several tools used to test inhibited translation initiation models.

2.4.1.2. Stress granule and P-body visualization to detect translation initiation inhibition

Stress granules and P-bodies are cellular structures which respectively store and degrade mRNA when cellular translation is stalled or reduced. This effect was of interest to us as it provided a simple and easy method to identify instances of translation initiation inhibition. As described in Section 2.1.5, pateamine is known to induce stress granule formation in mammalian cells (Dang et al., 2006). However, this effect is yet to be characterized in yeast.

A range of GFP-fusion proteins were used to visualise the formation of P-bodies and stress granules. As reported by the literature, short term glucose deprivation is a sufficient condition to induce the formation of both stress granules and P-bodies (Buchan et al., 2008). However, under these conditions no stress granule formation was observed, and we were unable to determine whether this condition was not causing stress granule formation or they could not be visualised. Had this approach been successful, it would have been important to remain tentative about the results. As described earlier (Section 2.1.5) stress granules can form for a variety of reasons in response to different stresses, potentially not in response to translation initiation inhibition but to general cellular stress through eIF2A phosphorylation (Buchan et al., 2008; Buchan et al., 2011). This means that any positive identifications of stress granule formation would require follow-up experiments to confirm translation initiation inhibition was occurring. Although P-body formation was observed under these conditions, this was not replicated following either pateamine treatment or in the *tif1*Δ GFP screen (Figure 17 & Section 2.3.5.1).

Visualizing stress granule and P-body formation could have been a useful tool to identify translation initiation inhibition. However, due to the difficulty we found visualizing stress granules, our finding that treating cells with the eIF4A inhibitor pateamine did not induce P-body formation and that stresses other than initiation inhibition can also cause their formation, we decided to pursue other approaches.

2.4.2. Approaches to inhibit translation initiation

2.4.2.1. Interpretation of P147L overexpression results

We identified overexpression of the P147L-eIF4A mutant protein as a potential approach to inhibit translation initiation in yeast. This mutant eIF4A was first identified for its ability to confer resistance of yeast cells to pateamine. It is suspected that this resistance is achieved by reducing affinity of the eIF4A protein for mRNA transcripts, preventing a strong interaction from forming when treated with pateamine. It was also noted that when this mutant eIF4A was overexpressed the growth rate of yeast cells was substantially reduced. The cause of this effect is not well established but it is suspected that the P147L mutant eIF4A is a less efficient form of eIF4A, leading to slowed translation initiation. We aimed to test whether use of this mutant to inhibit translation initiation could be a useful tool for our research. As reported in Section 2.3.2.1, we were able to reliably inhibit the growth of yeast cells by inducing P147L-eIF4A expression. However, when testing against yeast GFP-fusion proteins with long 5' UTRs and the G-quadruplex 5' UTR GFP reporter (Section 2.3.3) over expression of P147L-eIF4A induced no notable change in expression, suggesting translation initiation was not being significantly affected. These experiments do not rule out that overexpression is causing reduced translation initiation as neither of these test models have been confirmed and pateamine treatment also did not affect the GFP expression of the G-quadruplex reporter. This approach could be further investigated in the future.

Although it had been hoped to use at least two mimics for eIF4A deficiency and multiple approaches to detect the outcomes, substantial time had been invested in these methods without benefit. It was therefore decided to use readily available deletion mutants to mimic eIF4A deficiency and use established high throughput microscopy and proteomic methods to determine outcomes.

2.4.2.2. Effects of TIF1 & TIF2 *gene deletion on eIF4A abundance*

The goal of this screen was to investigate the effects of a reduction of functional eIF4A, achieved through deletion of one of the *TIF1* or *TIF2* genes, on protein expression as revealed by crossing the deletion mutant to the yeast GFP-tagged protein library. This approach relied on the deletion of the *TIF1* gene to have a significant effect on the cellular abundance of the eIF4A protein. The eIF4A protein was identified in both the *tif1*Δ and *tif2*Δ mass spectrometry experiments. When the *TIF1* gene was deleted, eIF4A protein levels were reduced to 57% p= 0.02 (TIC). Similarly, when the *TIF2* gene was deleted, eIF4A protein levels were found to reduce to 64% p=0.0032 (TIC). This result provided us with a reliable approach to reduce the abundance of cellular functional eIF4A and perturb the translation initiation pathway that can be used for GFP and mass spectrometry quantitative analysis. Although the expression levels of eIF4A protein is not directly measured in the GFP screen, it is reasonable to assume a similar reduction is achieved in this experiment with the same *TIF1* gene deletion.

Also of interest, when comparing the *TIF1* and *TIF2* loci, from our mass spec data (Section 2.3.4) we detected a decrease in eIF4A abundance in both *TIF1* and *TIF2* runs. However, neither of which dropped below 50% expression, with *tif1*Δ expression 58% of control and *tif2*Δ expressing 64%. This suggests that the expression of the other gene may be up-regulated in a response to the cellular deficit in eIF4A or that expression has been increased over time as a selective pressure. Given that *TIF1* and *TIF2* possess different regulatory regions, up-regulation of different transcription factors would be required resulting in different expression profile between deletion mutants. This effect has previously been described with yeast paralogue genes. An analysis of 200 GFP-fusion protein strains in which the paralogue of the fusion protein was deleted demonstrated 11% of the strains showed an increase in abundance of the GFP tagged protein with this effect almost exclusively in proteins for which function is required for growth (DeLuna et al., 2010). As eIF4A protein is required for growth, it is not surprising to see this up-regulation.

2.4.3. Interpretation of ontological enrichments

2.4.3.1. tif1Δ *GFP ontological enrichments*

Expression analysis of a *tif1*Δ strain was initially carried out by crossing this deletion mutant with the GFP-fusion protein library. When proteins that were identified to change were analysed for ontological enrichments, unsurprisingly, the strongest enrichment related to cytoplasmic translation with 38 of the identified proteins being associated with this function. Interestingly, this enrichment was seen in the down-regulated proteins, contrary to what would be expected if the cell was attempting to restore flux through the protein synthesis pathway. We suspect that this is due to demand-based effects. With the rate of translation initiation being reduced there will no longer be the same demand for expression of the translation machinery such as parts of the ribosome and amino acid production. This would explain the enrichments in both ribosome biogenesis and cellular amino acid biosynthetic process in the down-regulated proteins.

As described in Section 2.3.5.2.2, integration of a *tif2*Δ deletion into the GFP library proved more difficult than initially expected. As a result, we instead decided to progress our expression analysis with the use of mass spectrometry on *TIF1* and *TIF2* deletion mutants sourced from the Mat**a** gene deletion library.

Although not the focus of our research, when crossing the *tif1*Δ with the GFP-fusion library the *TIF2*-GFP-fusion did not survive the crossing procedure. As mentioned above the eIF4A protein is essential for yeast survival, however, expression of either genetic copy is sufficient for normal growth. Although addition of a GFP fusion protein is generally well tolerated (Goryanin and Goryachev, 2012). This strain being lost in the screen may suggest that fusing the GFP tag to eIF4A produces a non-functioning protein. This would not be especially surprising given the requirement for eIF4A to form a range of intermolecular interactions in order to function in translation initiation

2.4.3.2. tif1Δ *mass spectrometry ontological enrichments*

Expression analysis of *TIF1* gene deletion mutant with mass spectrometry identified 76 proteins in total that changed in abundance. When the 36 up-regulated proteins were analysed two main groups of ontologies were found to be enriched. The most enriched ontology was cytoplasmic translation with 9 proteins associated with this process. Seeing

these proteins being up-regulated suggests that the cell is reacting to a reduction in translation and trying to restore normal flux to this pathway. The second general enrichment relates to oxidative phosphorylation and ATP generation. The reason for this enrichment is less clear and further analysis may be required to understand this response.

Ontological enrichment analysis was also carried out on the 40 down-regulated proteins. Again, two main groups of ontological enrichment were seen in the data. The first consisting of 10 proteins related to amino acid synthesis. As with the *tif1*Δ GFP data we suspect that this is due to the reduced cellular demand for amino acids as a result of reduced translation. The second enrichment, translation initiation, was only just above the significance threshold. This follows the trend seen in the GFP analysis and may be seen due to proteins being down-regulated to maintain stoichiometry or due to reduced demand.

2.4.3.3. tif2Δ *mass spectrometry ontological enrichments*

Expression analysis of *TIF2* gene deletion mutant with mass spectrometry identified 76 proteins in total that changed in abundance. When the 41 proteins found to be up-regulated were analysed for ontological enrichment translation was the most enriched process with several translation-supporting processes also enriched including; tRNA aminoacylation and protein folding. These enrichments follow the general theme of up-regulating various pathways relating to translation likely to restore flux through the pathway. Interestingly, although tRNA aminoacylation is up-regulated in the *tif2*Δ results amino acid production is down-regulated. This may be due to a reduced demand for amino acids leading to reduced production but also causing less tRNAs being primed with amino acids and inducing up-regulation of priming machinery.

Ontological enrichment analysis carried out on the 53 down-regulated proteins resulted in one main group of ontologies relating to energy metabolism with enrichment in the glycolysis pathway. It may be that this is due to reduced demand on glycolysis to provide metabolites for amino acid metabolism but further analysis may be required to elucidate the reasons behind this enrichment.

2.4.3.4. Comparison of experiments

2.4.3.4.1. Comparison of gene ontology enrichments between tif1Δ *experimental approaches*

Interestingly although many of the ontologies and genetic pathways identified through the *tif1*Δ GFP screen were also identified in the *tif1*Δ mass spectrometry analysis there was very little overlap in individual genes with many of the genes identified in the GFP screen not being determined to have changed in the mass spectrometry experiments. Additionally, the most significantly enriched process in the GFP screen was found to be cytoplasmic translation in the down-regulated proteins but this enrichment was seen in the up-regulated genes in the *tif1*Δ mass spectrometry experiment. It is unclear why is disparity between the two experiments exists. One possible point of difference is the background strains used in each of the experiments, the gene deletion strain mated with the GFP library was sourced from the Open Biosystems Mat**α** deletion library whereas the *tif1*Δ strain used in the mass spectrometry analysis was sourced from the Mat**a** gene deletion library. This mating type and evolutionary divergence may at least be somewhat responsible for the discrepancies observed between the GFP and mass spectrometry *tif1*Δ screens, especially as crossing with the eIF4A-replete GFP library may result in some of the evolutionary long-term adaptations being removed by reassortment. Additionally, inherent bias in the two quantitative approaches may also be playing some role in differing gene lists. An analysis of yeast protein quantitative methods that compared nine mass spectrometry and nine GFP based studies has shown that abundance values are more consistent when compared between experiments undertaken using the same quantitative approach. When mass spectrometry and GFP values were compared with like methods an average Pearson correlation coefficient value of 0.75 and 0.70 were seen respectively. In contrast, when different methods were compared this average value dropped to 0.59. This potentially explains some of the differences between the two lists (Ho et al., 2018).

2.4.3.4.2. Comparison of gene ontology enrichments between tif1Δ *and* tif2Δ

When carrying out gene ontology enrichment with the lists of proteins found to change in abundance in repose to TIF gene deletion it was noted that there was very little overlap of specific proteins undergoing changes in abundance between the *tif1*Δ and *tif2*Δ mutants. There were even examples where the same protein appeared with opposing abundance

changes (Section 2.3.6.1.5). However, these results taken together can still provide valuable insights into the biology of *TIF1* and *TIF2*.

As expected, there seems to be specialisation between the *TIF1* and *TIF2* genes, which is consistent with the evolutionary retention of the gene duplicates. This specialisation does not evidence itself in terms of the function of the produced protein, since both genes produce the same eIF4A protein but the sequences in their regulatory regions are very different. Therefore, we anticipated differences relating to the ability to regulate each of the genes in response to specific cellular demands. Although understanding the diverged roles of these two eIF4A-producing loci in *S. cerevisiae* is not an aim of this thesis, it is interesting to compare the consequences of each of the deletions.

From the mass spectrometry data, deletion of the *TIF1* gene primarily led to down-regulation of proteins associated with amino acid metabolism and translation initiation. In contrast, deletion of the *TIF2* gene led to down-regulation of genes associated with carbohydrate metabolism and both heat and oxidative stress. There was also specialisation noted in the up-regulated gene sets, with the *TIF1* deletion leading to energy metabolism, such as oxidative phosphorylation, and some terms relating to transcription and translation. For the *TIF2* deletion, there was up-regulation of a number of processes that support translation, ranging from aminoacyl t-RNA synthesis to protein folding. Thus, as expected, reduction in production of eIF4A achieved through deletion of either the *TIF1* or *TIF2* gene led to increases in processes that support translation, it appears there are genetic links between *TIF1* and amino acid metabolism as these are enriched in both the GFP and mass spectrometry *tif1*Δ data.

The situation relating to energy metabolism is especially interesting and deserving of future investigation. The *TIF1* deletion leads to up-regulation of proteins associated with ATP biosynthesis and oxidative phosphorylation, whereas *TIF2* deletion leads to down-regulation of carbohydrate metabolism, including glycolysis/gluconeogenesis. It is possible that the impact of reduction of eIF4A abundance is read by the cell in a manner equivalent to a starvation response. Amino acid and carbohydrate metabolism are reduced, whereas systems that depend on the more limited outputs of these systems (including amioacyl tRNA production and ATP production) are up-regulated to make the most efficient use of their now-limited substrates.

2.4.4. Interpretation of the effect of 5′ UTR features

As previously described (Section 1.4.4), features of the 5′ UTRs of mRNA transcripts including length, GC content, and specific sequences have been identified to be preferentially affected by inhibition of eIF4A (Iwasaki et al., 2016; Wolfe et al., 2014). These attributes were analysed across the *tif1*Δ GFP, and *tif1*Δ and *tif2*Δ mass spectrometry screens to determine if these or other features were seen in our data.

2.4.4.1. TIF gene deletion effects on 5′ UTR length

As described in Section 2.3.3, previous studies have shown that translation of mRNA transcripts with longer 5′ UTRs is disproportionally inhibited when cells are treated with eIF4A inhibitors (Iwasaki et al., 2016; Wolfe et al., 2014). Additionally, an analysis linking the length of 5′ UTR and protein expression profiles carried out by Lin et al. (2012) negatively correlated 5′ UTR length with protein expression. It would be reasonable to suspect that this effect relates to eIF4A taking longer to unwind longer 5′ UTRs in transcripts, as longer 5′ UTRs have greater potential to form stable secondary structures. From our data (Sections 2.3.5.1.2 & 2.3.6.3), we did not see any significant trend relating expression changes to 5′ UTR length. We had hypothesised that we would see a detectable expression differences based on 5′ UTRs and there are two potential explanations for why we did not. Firstly, it is possible that the correlation between 5′ UTR length described by Lin et al. (2012) is the result of a different mechanism, meaning that this effect is largely eIF4A-independent. Secondly, it is possible that the approximate 40% reduction in eIF4A abundance achieved from deleting either copy of the TIF gene is too small to create a significant impact on the ability to unwind 5′ UTRs. We know that eIF4A protein is expressed at high levels, likely in excess of amounts required for normal protein expression. Deletion of the *TIF1* or *TIF2* loci has little effect on growth rate, also suggesting deletion of either of the *TIF1* or *TIF2* genes likely has only a slight effect on translation initiation (Venturi, 2012). This assumption that there is only minimal disruption to translation is confirmed by our high throughput microscopy study we found only a minority (3.2%) of proteins reduced in abundance relative to the control. This makes the gene deletion model ideal for the purposes of this study, where we are interested in effects seen under conditions where there is minimal disruption of cellular function through use of low concentrations of inhibitors.

2.4.4.2. TIF deletion effects on 5′ UTR GC content

GC content is a strong determiner of the stability of 5′ UTR secondary structure and it is suspected that 5′ UTRs with a higher GC content have a greater need for eIF4A helicase activity to be expressed (Waldron et al., 2019). We therefore wanted to investigate if any 5′ UTR GC content-related trends are seen in our datasets. In general, not much 5′ UTR GC content differences were seen in our data with all but one condition having a value between 32 and 33.5%. The one exception to this is was in the GFP *tif1*Δ experiment up-regulated 5′ UTRs with a value of 37.2%. However, this trend is in the opposite direction, as 5′ UTRs with higher GC content should be expected to be down-regulated as a result of there not being sufficient eIF4A activity to resolve the more stable secondary structures. Given that this result is only seen in one of the three quantitative experiments this result should be viewed sceptically, especially as this result was from the list with the smallest number of proteins, making data more variable. However, further experimentation will be required to confidently rule out GC content as being an influencing factor on expression when active eIF4A protein is reduced in yeast.

2.4.4.3. TIF1 *and* TIF2 *deletion effects on 5′ UTR sequence specific motifs*

Previous studies using eIF4A inhibitors on human cells has led to the identification of two specific 5′ UTR sequence motifs which are disproportionately affected by eIF4A inhibition. As described in Section 2.2.9, one of these sequences consists of a CGG repeat believed to form a stable G-quadruplex structure and the other consisting of a stretch of purine nucleotides. To identify if any sequence-specific effects were occurring in our data, the sequences of 5′ UTRs belonging to proteins which changed in abundance were analysed for motif enrichment. Across all searches of individual conditions, a TC-rich motif was identified (Figure 30). As this motif was seen on both the up- and down-regulated 5′ UTRs at similar frequencies and statistical values, this sequence is not likely to be sensitive to reduced eIF4A protein. Instead, it occurs at high frequencies in yeast 5′ UTRs and is likely involved in some sort of regulatory role. Interestingly, this motif is a long pyrimidine tract much like the vertebrate terminal oligopyrimidine tract (TOP) motif which is involved in regulation of translation of ribosome genes (Caldarola et al., 2004). However, TOPs motifs are found in close proximity to the guanine cap (Kimball, 2017) whereas most of our TC motif instances are not.

When analysing the 5′ UTR sequences it was thought that the statistical analysis may be strengthened if the 5′ UTR sequences of both mass spectrometry experiments were combined. When this combined 5′ UTR sequence list was analysed an additional motif was found to be enriched. This motif was rich in adenosine nucleotides and somewhat resembles the polypurine motif sensitive to rocaglamide A described by Iwasaki et al. (2016) (2019) but with a lower frequency of guanosine. This motif had segments of A-rich sequence and some other regions that were less consistent. Finding a motif in the down-regulated 5′ UTRs with a trend toward purine nucleotides was unexpected as the current model of this motif's rocaglamide sensitively is that the polypurine sequence allows the formation of a rocaglamide binding pocket locking the mRNA to the eIF4A protein (Iwasaki et al., 2019). However, the E-value of the motif we have identified was the weakest of the three motifs found in the combined mass spectrometry down-regulated 5′ UTRs. Although this was the only time the enrichment of this motif was significant, the MEME algorithm did detect other A-rich motifs that did not reach the significance threshold in several of the individual up- and down-regulated 5′ UTR datasets. This result should therefore be viewed sceptically and further analysis with larger datasets will need to be carried out.

No motif resembling the G-quadruplex forming motif reported by Wolfe et al. (2014) was identified in our dataset. Although it is unclear why this motif was not seen as we suspected eIF4A abundance may have been reduced enough for this effect to be detectable in our data, it is consistent with the results of the G-quadruplex reporter where no impact of disruption of eIF4A function was observed. It is possible that *TIF1* or *TIF2* gene deletions alone is not sufficient to reduce functional eIF4A to levels at which mRNA secondary structure effects are seen, or that a different protein is available to resolve RNA G-quadruplexes. It is also possible that yeast do not possess these sequences in their 5′ UTRs and so cannot be detected.

2.4.5. Overview of the effects of eIF4A gene deletion on yeast

We set out to investigate the effects of inhibition of translation initiation to gain an understanding of the outcomes and follow-on effects on biological pathways. This was investigated by carrying out expression experiments on yeast *TIF1* and *TIF2* gene deletion mutants. We hypothesized that two effects would be seen, the first was regulatory expression changes as the cell responds to the eIF4A protein deficiency. The second effect we expected was expression changes of mRNA transcripts with eIF4A-sensitive 5′ UTR features. Systems

tested to model eIF4A disruption included the overexpression of P147L-eIF4A and deletion of each of the two genes responsible for eIF4A production. Three independent approaches were developed to probe the outcome of the reduction in eIF4A; a GFP reporter system, where the fluorescent protein was produced from a transcript with a G-quadruplex producing motif; a GFP-fusion protein based high throughput microscopy; and proteomic analysis. Of these systems, only the gene deletion models linked to GFP and proteomic analysis gave useful outputs.

Despite the conflicting abundance changes between experiment gene lists, general themes still provide insights into the effects of decreased eIF4A expression has on the cell. Deletion of either *TIF1* or *TIF2* genes has far reaching effects resulting in significant abundance changes in proteins which function in many biological processes (Figure 35). Deletion of either of the *TIF1* or *TIF2* genes, as expected, affects translation directly. However, this effect reaches further along the protein production pipeline as it appears that the yeast cell responds to this stress through a coordinated network which covers the full range of protein production from amino acid metabolism to protein folding. These changes suggest that reduced eIF4A protein expression leads to significant changes in demand of cellular resources relating to protein synthesis. In addition to proteins linked to translational functions, proteins relating to energy production through both glycolysis and oxidative phosphorylation are also enriched in our data. It is possible that changes in protein abundance in these pathways suggest a change in the energy requirements of the cell as a result of reduced translation initiation or perhaps linking reduced translation initiation to a starvation response. Although, it is important to note that these energy pathways are also involved in providing starting molecules for producing amino acids, such as α-ketoglutarate for glutamine and oxaloacetate for asparagine, meaning this abundance change may be linked to the changes seen in amino acid biogenesis proteins.

Although the gene deletion models lead to a substantial reduction in the abundance of functional eIF4A (down to approximately 60% of wildtype levels), there was only a minor, non-significant trend in 5’ UTR length and GC content analysis of 5’ UTRs saw a significant difference in only one of three experiments with the trend in the opposite way to expected. There was also no observable effect linked to specific sequence features of the transcript relating to G-quadruplex forming motifs (Wolfe et al., 2014). However, a poly-A stretch similar

to previously seen polypurine stretches (Iwasaki et al., 2016) was detected but only when experimental results were combined and needs further investigation. This was unexpected, as the working model for the role of eIF4A inhibitors in a proposed treatment of cachexia (see Section 2.1) involves a much smaller reduction in abundance of functional eIF4A even when using hippuristanol, an inhibitor equivalent to a loss of function mutation (Cramer et al., 2018; Di Marco et al., 2012).

It could be that the absence of 5' UTR-derived effects in *S. cerevisiae* relates to differences in yeast and mammalian systems. Yeast 5' UTRs are known to have far lower GC content compared to mammalian cells, meaning 5' UTR secondary structure likely has less of a regulatory role for yeast translation initiation. As such, it will be important to probe whether these unexpected findings transfer across to human cell models, where the eIF4A inhibitor pateamine can be applied.

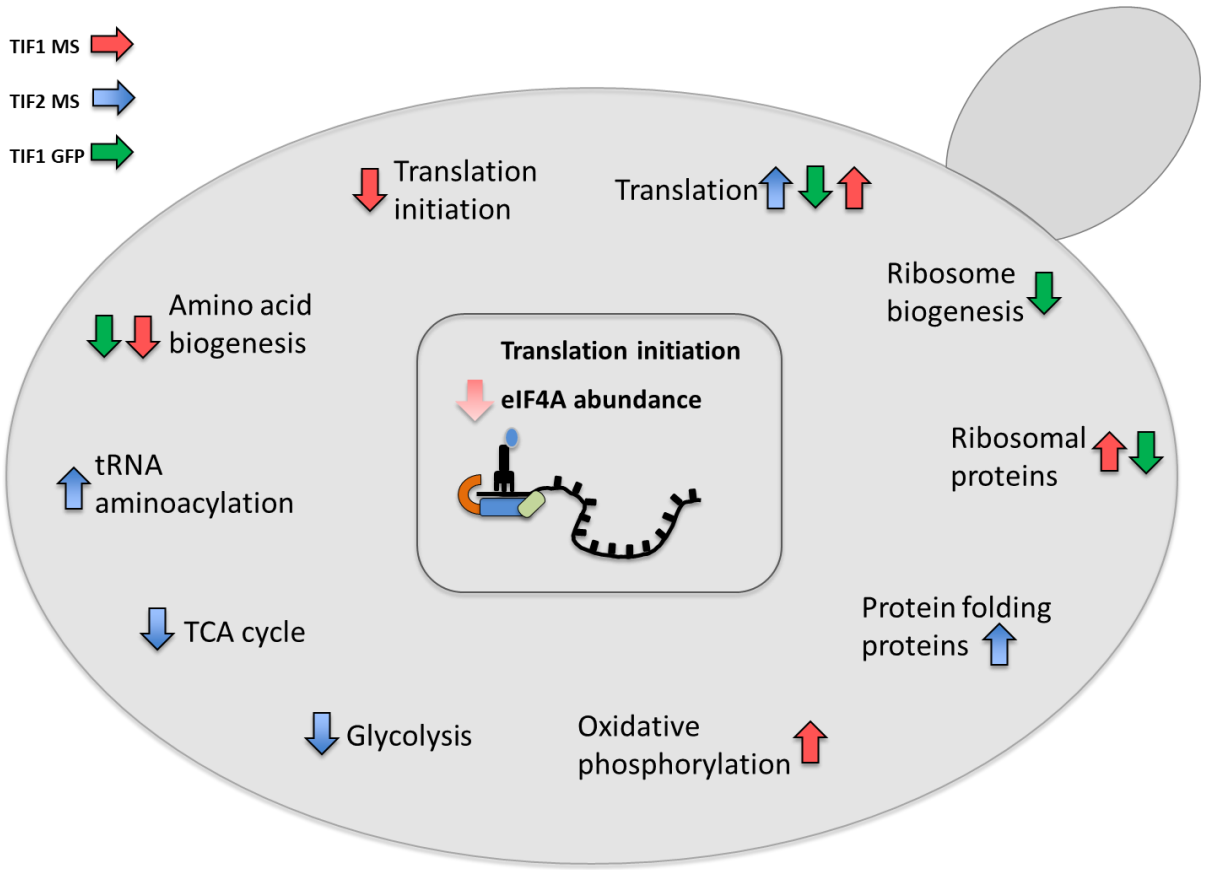

Figure 35. The processes affected by deletion of either the TIF1 *or* TIF2 *genes on Saccharomyces cerevisiae. Direction of arrow denotes whether the enrichment was seen in the up- or down-regulated list and colour denotes the experiment in which the change was seen.*

2.4.6. Limitations

2.4.6.1. P147L over expression testing

A major goal of the research presented in this chapter was to produce a method for mimicking the effects of treating eIF4A with a loss of function inhibitor. We initially planned to achieve this through overexpression of P147L mutant eIF4A. Overexpression of P147L-eIF4A failed to induce any notable change in the models we had available to us but, as previously explained in Section 2.4.2.1, we cannot be certain P147L-eIF4A overexpression does not inhibit growth through translation initiation inhibition.

2.4.6.2. Effect of deletion of TIF1 *or* TIF2 *loci on translation*

The approach we selected to reduce translation inhibition was to delete one of the copies of the genes that produce the eIF4A protein in yeast. The resultant reduction in eIF4A protein was able to be directly measured. The GFP screen shows that this has minimal effect on translation overall, however, it is not clear if this is matched by a lack of change in the rate of translation initiation. As deletion of the *TIF1* or *TIF2* gene alone has little effect on growth rate in nutrient rich media we suspect that the overall effect on translation initiation rate is relatively minor.

As described in the methods section, the *tif1*Δ and *tif2*Δ strains which were mated with the GFP library or used in the mass spectrometry experiments were obtained from the Open Biosystems Inc. gene deletion library. This library has gone through many re-pinning and growth cycles, during production, by the supplier and in our lab to produce working copies. It is important to consider this fact when undertaking an analysis of gene expression. By deleting a gene, a stress is put on the yeast which can affect both growth and metabolism. Should a mutation or expression change occur that mitigates some of these effects, this organism will have a growth advantage over the rest of the population. Over the course of multiple pin and growth cycles the progeny of this mutant will represent a greater portion of the pinned yeast cells. It is reasonable to suspect that some of the gene expression changes identified could be the result of mutations or epigenetic changes resulting in a long-term adaptation to a selection pressure rather than a direct, acute response to reduced active eIF4A. It is possible that the expression changes are the result of these selective effects and this is why we see different proteins changing in abundance in the *tif1*Δ GFP screen and the *tif1*Δ mass spectrometry experiments. These two strains each adapted over time through different

mutations leading to expression changes. Different mutations in each strain that mitigate some of the stresses that the gene deletion induces could lead to different expression profiles making comparing and interpreting results between experiments far more difficult.

The effects of evolutionary selection have the potential to mimic the responses that could arise as a result of longer-term treatment of cachexia in a course of chemo- or radiotherapy spanning a period of weeks or months. Whether the result of regulatory responses or long-term adaptations, these expression changes can provide insight into the biology of eIF4A and its inhibition. This effect would be greater in the mass spectrometry data as the *tif1*Δ GFP strains were the result of a mating cross which would have 'diluted' this effect as the GFP library would not have had this selective stress before mating.

2.4.6.3. GFP screen missing data points

The high throughput GFP screen resulted in missing data points, for example from pinning and transfer failures. This made reliable use of t-test and false discovery calculations difficult. For this reason, data was included for analysis that is anticipated to arise from false positives. This is mitigated by use of gene ontology analysis, where randomly acquired false positive data should have limited impact on the major ontological enrichments observed. This data may influence ontologies at the margins of statistical significance, however care has been taken to avoid extensive interpretation of weaker enrichments.

2.4.6.4. Genetic reassortment during GFP library crossing

Another important factor to consider is that strains used in the *tif1*Δ GFP may carry genetic differences between each GFP strain. As described in the methods section (2.2.12), when producing the *tif1*Δ GFP library a yeast mating approach was utilized. This includes the steps of producing diploid cells and inducing sporulation to produce haploid progeny. This means a reassortment of the genomes of the *tif1*Δ strain and each strains GFP has occurred. The result is that the genomes of each strain in the crossed *tif1*Δ GFP library will have a slightly different combination of the parental strains, adding variability to the analysis. Unfortunately, not much can be done to limit this issue as individual transformations are not feasible for a high throughput analysis but as we are analysing pooled gene lists, analysis should be robust enough for this variability to not have a major impact on analysis.

2.4.6.5. Mass spectrometry analysis

When analysing the mass spectrometry data, we initially planned to perform multiple test correction. The correction resulted in the loss of almost all identified proteins. For this reason, it was chosen not to apply multiple test correction to some experiments greatly increasing the risk of false positives in our data. Due to this we were limited to making interpreting gene list enrichments and could not reliably make inferences on changes of individual proteins. This approach is validated by the congruence of the GFP and mass spectrometry screens, as described in Section 2.4.3.4.

A variable to consider during analysis is that although we selected two different quantitative methods for mass spectrometry analysis to avoid missing relevant protein abundance changes, quantitative values of some proteins were substantially different between methods. Despite many advances in the way mass spectrometry data is analysed, many different approaches are still considered standard. Even though some considerable quantitative differences in some proteins arose when comparing TIC and iBAQ methods, we decided proteins found to change by either method should be kept to avoid missing any ontological or motif enrichments in our data. This does however increase the chance of false positives in our datasets.

2.5. Conclusion

In this chapter we aimed to investigate the biological effects of inhibition of translation initiation in the model organism *Saccharomyces cerevisiae.* We went about this goal by investigating mutant eIF4A overexpression and eIf4A gene deletions as methods to alter the degree of translation initiation being carried out in the cell and attempted to identify markers of translation initiation inhibition. We opted to carry out proteomic expression analysis on yeast strains lacking one of the two eIF4A genes which was effective at reducing the cellular abundance of eIF4A protein. With the use of GFP libraries and quantitative mass spectrometry we identified a total of 305 proteins which changed in abundance as a result of gene deletion in at least one experiment. The 5' UTR sequences of the mRNA transcripts of these proteins were also analysed finding no strong evidence that expression depends on either the sequence or length of these 5' UTRs when active eIF4A is reduced by this method. This result is not consistent with expectations from experiments carried out with eIF4A inhibitors in human cell lines, even though the reduction in available eIF4A is consistent with that anticipated for use of eIF4A inhibitors in the treatment of cachexia. Analysis of the proteins found to change in abundance showed a statistical enrichment of genes related to translation, amino acid biogenesis, protein folding, amino acid loading of tRNA and cellular energy production. These results demonstrate that a range of biological processes are affected by reducing functional eIF4A, including proteins not immediately involved in translation initiation. These changes were seen despite this approach not inducing mRNA sequestration as with pateamine treatment and the gene deletion having no short-term detectable effect on growth rate.

3. Chapter 3 – The effects of pateamine on the proteome of cancer cell lines

3.1. Introduction

The aim of this research is to gain a deeper understanding of the outcomes of eIF4A inhibition, including the follow-on effects of inhibition and reduction of functional eIF4A on the global protein abundance in the cell. As described in Chapter 1, the effects of this inhibition might occur through reducing the availability of functional eIF4A protein in the cell or may result from formation of a complex between eIF4A and its inhibitor that has altered function compared to the non-inhibited protein.

The first aim of this project was to investigate the effects of reducing the abundance of functional eIF4A on the protein landscape in *Saccharomyces cerevisiae.* In Chapter two, we investigated the outcome of reducing the abundance of functional eIF4A by gene deletion of *TIF1* or *TIF2* in the *Saccharomyces cerevisiae* model. This approach identified expression changes of proteins involved in a range of different ontological networks that may be either the result of regulatory responses or of long-term adaptations. These outcomes addressed the first project aim. Our second aim was to transition our research toward a clinical focus by investigating responses to eIF4A inhibition in human cells. In this chapter, we will be addressing this second aim. We will do so by using human cell lines to investigate the direct and potential follow-on effects of treatment with the translation initiation inhibitor pateamine. This will be achieved by treating HL60 cells, a human leukaemia cell line, and HT-29 cells, a human colon adenocarcinoma cell line, with low concentrations of pateamine in order to analyse the subsequent protein expression changes using label-free mass spectrometry and western blot analysis. These expression changes will then be analysed for ontological and sequence motif enrichments that elucidate the underlying responses and mechanisms induced as a result of pateamine treatment.

3.1.1. Pateamine targeting specific transcripts

Identifying the specific attributes which causes the abundance of some proteins to be disproportionately affected by pateamine is of particular interest for our research. Identifying these would allow for a greatly improved understanding of how pateamine functions as a translation initiation inhibitor and could make it possible to predict pateamine's effects on expression of specific proteins. As described in Section 1.4.5, two motif sequences found in the 5' UTRs of some mRNA transcripts had been previously identified to confer greater than average inhibitory effects on translation initiation when treated with rocaglamides. One of these motifs consists of "CGG" repeats (Figure 7) and is suspected to be preferentially affected by silvestrol due to the motif forming a stable G-quadruplex structure (Wolfe et al., 2014) . This motif was identified with the use of ribosome fingerprinting on KOPT-K1 cells with a silvestrol concentration of 25 nM, which is considerably above the IC_{50} of concentration around 10 nM (Wolfe et al., 2014). Altered expression of transcripts containing this motif was then confirmed with synthetic fluorescent expression constructs (Wolfe et al., 2014). This fluorescent construct was also found to be inhibited when treating with pateamine (Wolfe et al., 2014) and is likely the result of there not being sufficient functional eIF4A to resolve the secondary structure.

The second motif was only described after the onset of our experimentation. This motif was found when identifying transcripts with reduced translational efficiency when treating with 30 nM rocaglamide A and consists of a stretch of purines (Figure 8) (Iwasaki et al., 2016). When interacting with eIF4A, this sequence allows the formation of a binding cavity for rocaglamide A clamping eIF4A to the mRNA and preventing translation (Iwasaki et al., 2019). This motif was also identified by using ribosome fingerprinting then confirmed with modelling via X-ray crystallography (Iwasaki et al., 2016; Iwasaki et al., 2019).

3.1.2. Downstream effects of pateamine

Previous studies investigating the effects of pateamine have focused on how expression of a small number of select proteins are affected (Di Marco et al., 2012; Parikh et al., 2012). However, targeting a pathway as broad and integral to the cell as protein synthesis is likely to affect the expression of a large number of genes due to various effects on the protein regulatory pipeline. In particular, there are two major types of proteins to consider for their far-reaching effects. These are transcription factors and enzymes associated with protein degradation. Protein homoeostasis, known as proteostasis (Figure 36), is the concerted result of both production and degradation of cellular proteins with abundance levels of individual proteins being maintained through a balance of these two actors. Some proteins are known to have high transcription rates but also have very short cellular half-lives, whereas other proteins can have low transcription rates whilst having much longer half-lives. This could lead to comparable cellular abundance between the two proteins. Treating with pateamine could have significant effects on this proteostatic equilibrium. Transcription factors are responsible for inducing the transcription and resulting expression of many other genes. Any change in abundance of a transcription factor following pateamine treatment could result in subsequent changes in expression of all the proteins that transcription factor controls. This could cause major changes in the cell's protein landscape as an indirect result of pateamine treatment.

Various regulatory responses could also have a significant effect on proteostasis. Cellular pathways are highly dynamic with numerous feedback loops influencing protein expression. It is possible that pateamine treatment will decrease key proteins in a range of different pathways and expression profiles may change in response. Additionally, very general responses could occur to general cellular stress also altering the proteome. For example, pateamine treatment could also result in the accumulation of some proteins. It is possible that expression of many of the proteins involved in the protein degradation pathway could be inhibited as a result of treatment. Reducing the abundance of the cell's proteolytic machinery will cause a slowing of protein degradation and subsequent accumulation of proteins for which proteolysis is an important contributor to their homeostasis. Finally, cells are expected to elicit a direct biological response to the stress on protein synthesis.

As a result of these processes, effects on the cellular protein landscape are expected to be greater than simple changes in proteins with mRNA transcripts that pateamine inhibits directly. By carrying out a label-free proteomics approach, protein levels can be measured directly to give a clearer view of the resultant expression outcomes from pateamine treatment.

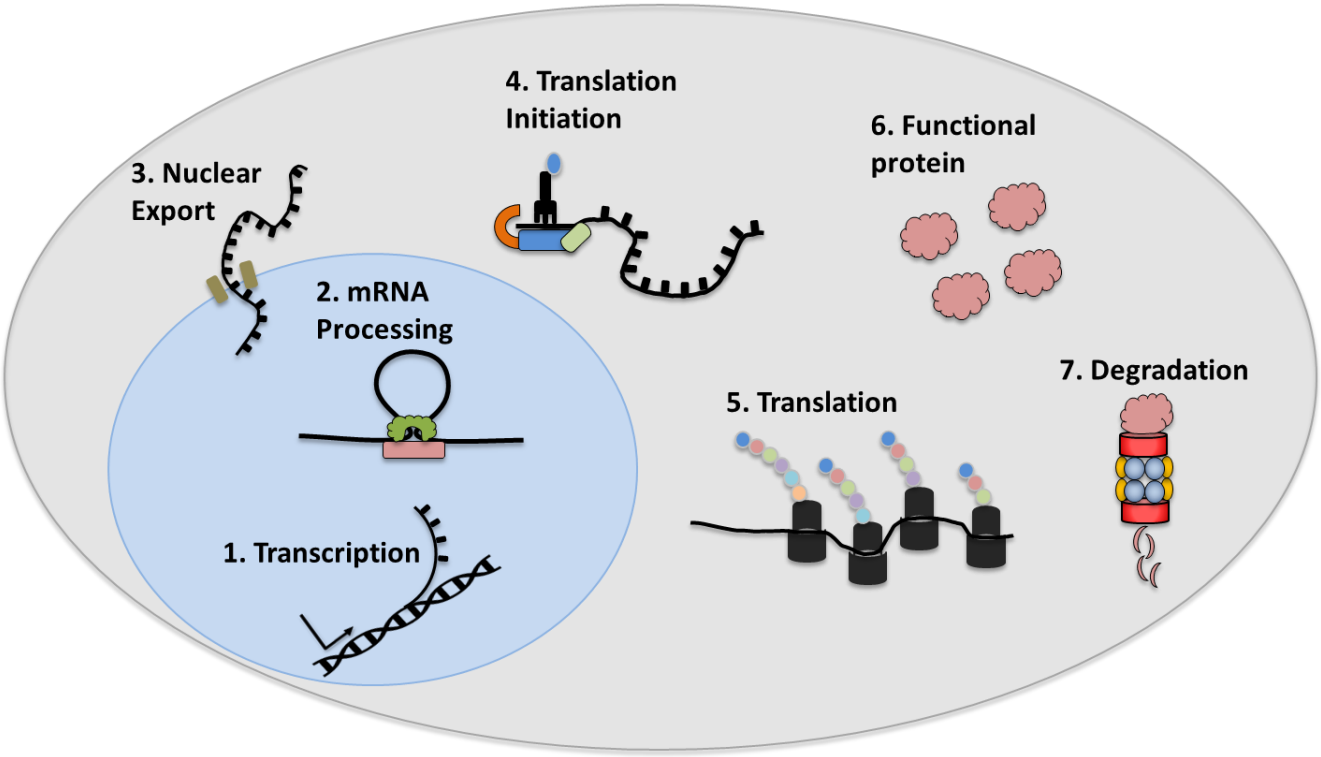

Figure 36. A simplified schematic of the steps involved in protein homeostasis in the cell. ***1.*** *mRNA is transcribed from the genome.* **2.** mRNA is processed and introns removed. ***3.*** *The mRNA is exported from the nucleus via the nuclear pore.* ***4.*** *The transcript is bound by initiation factors forming the initiation complex.* ***5.*** *The protein is produced by the ribosome.* ***6.*** *The completed proteins carry out their functional role in the cell.* ***7.*** *The protein is degraded by the proteasome complex.*

3.1.3. Label-free protein quantification

Proteomic approaches have been successfully used to investigate a range of biological questions. There are two approaches for quantifying protein abundance. Labelled quantitation involves the labelling of proteins from one of the two culture conditions with chemicals such as heavy isotope labelled amino acids and analysing the peptide mixtures in a single mass spectrometry run. This results in two adjacent peaks in the mass spectra which can be compared (Ankney et al., 2018). In contrast, label-free quantitation involves two mass spectrometry runs in which proteins are identified and quantified individually then compared to the other (Zhu et al., 2010). When paired with gene ontology enrichment analysis, label-free proteomics can be a powerful tool for identifying cellular pathways involved in disease. For example, Cheng et al. (2014) used label-free proteomic analysis on hepatocellular carcinoma and compared expression profiles to normal liver tissue. Using this method, they identified 333 proteins which had increased expression in hepatocellular carcinoma. When these genes were analysed with gene ontology enrichment analysis, several pathways, including carboxylic acid metabolism and translation elongation, were found to be up-regulated in the cancer cells giving insights into disease function (Cheng et al., 2014). In our study, we aim to gain a better understanding of cellular responses to a drug-like treatment. One study with a similar goal focused on the treatment of colorectal adenocarcinoma with antiproliferative drug 5-fluorouracil. When treated with 5-fluorouracil label-free proteomic analysis identified increased expression of several members of the peroxiredoxin antioxidant enzyme family, highlighting a possible mechanism of resistance (Bauer, 2012). Thus, given the effectiveness of label-free mass spectrometry in previous studies, we selected this method to directly probe protein expression changes in response to the translation initiation inhibitor pateamine.

There are two commonly adopted approaches to quantify protein and peptide abundance changes through mass spectrometry. These are spectral counting and intensity-based methods, typically using MS2 spectra obtained after fragmentation and MS1 spectra obtained before fragmentation respectively. Early label-free proteomic methods utilized spectral counting to obtain a quantitative value for each protein involving counting each spectrum instance of a given peptide when it is detected. This method performs poorly when quantifying low spectrum-count proteins resulting in high variability in spectrum count

outputs (Lundgren, 2010). Newer and more accurate quantification methods have been developed which utilise more of the information gathered by the mass spectrometer. The most well-established of these newer approaches is the TIC method. This method involves measuring the area under each mass peak belonging to each MS1 parent ion to determine the number of ions that reached the mass detector (Asara et al., 2008). A further variation has been made to this method by utilizing Intensity-based iBAQ which like TIC uses each proteins' total parent ion intensity but divides the values by the number of theoretically detectable tryptic peptides (Krey et al., 2014).

Due to the large number of proteins identified in mass spectrometry experiments, additional statistical analysis is often required to counteract the effects of multiple testing. One such method is using FDR analysis. FDR involves comparing the spread of the p-values associated with each protein in a dataset. A condition that induces a genuine change in a biological system will cause the distribution of p-values to be skewed toward lower values. This distribution can then be used to calculate a q-value for each protein which indicates the expected rate of false discoveries in a group consisting of that protein and all other proteins with lower q-values (Storey and Tibshirani, 2003).

3.1.4. Research outline

As of yet, no study has directly investigated broad expression changes at the protein level in a whole cell context or investigated the overall effects of eIF4A inhibition. Additionally, only the G-quadruplex forming motif described by Wolfe et al. (2014) has been identified to be pateamine-sensitive with no polypurine or other nucleotide sequence yet to be identified. Thirdly, past studies have used concentrations of eIF4A inhibitor at concentrations above IC_{50}, much higher than drug concentrations that would be achieved in a clinical regimen to treat cachexia or Alzheimer's. At these high concentrations the amount of free, functional eIF4A will be extremely limited. This could lead to different effects than would be achieved by lower inhibitor concentrations, where the effect would be expected to be dominated by induction of a strong integration of eIF4A to specific mRNA transcripts, as illustrated in Figure 10. In this study, we aimed to address these three gaps in the literature by directly measuring cellular protein levels and analysing identified proteins for pateamine-specific 5' UTR sequences in their mRNA transcripts.

Using whole cell proteomic mass spectrometry, we identified a range of proteins which change in abundance as a result of pateamine treatment. Analysis of the functions of these proteins showed enrichment in a range of biological processes including, translation, mRNA splicing, nonsense mediated decay, and proteasomal function, demonstrating the far-reaching effect of pateamine on proteostasis in the cell. Furthermore, analysis of the mRNA 5' UTR of these proteins identified an adenosine- and guanidine-rich motif associated with the proteins observed to be down-regulated. This suggests that pateamine has sequence-specific effects at the transcript level. Taken together, these results highlight several effects of pateamine on human cells not previously described, improving understanding of the effects of pateamine inhibition, identifying transcript-specific effects, and providing insights into expected clinical outcomes and side-effects.

3.2. Methods

3.2.1. Procedure for culturing of human cell lines

3.2.1.1. Culturing of HL60 cell line

HL60 cells were maintained in RPMI1640 media (HyClone™) supplemented with 10% foetal calf serum (Life Technologies) and 1% penstrep (Life Technologies). Growth flasks (Falcon) were incubated at 37 °C with 5% CO_2 in a humidified incubator. Cells were maintained in logarithmic phase through passaging every 2 – 3 days by transferring one third of the culture volume containing suspended cells into a new flask and making up to the original volume with fresh media.

3.2.1.2. Culturing of HT-29 cell line

HT-29 cells were maintained in DMEM media (Gibco) supplemented with 10% foetal calf serum and 1% penstrep. Growth flasks were incubated at 37 °C with 5% CO_2 in a humidified incubator. When 80% confluence was reached cells were passaged by partial digesting with TrypLE™ (Gibco), washed with PBS, resuspended in DMEM media with 10% foetal calf serum and 1% penstrep and one third of the cells were transferred to a new flask and made up to the original volume with fresh media.

3.2.2. Procedure for MTT assay

HL60 cell concentration was determined through cell counting using a haemocytometer with the use of trypan blue for the exclusion of inviable cells. Cell were diluted in media to $2x10^5$ cells/mL and 50 µL aliquots were added to a 96-well tissue culture place (Falcon). A two-fold serial dilution of pateamine was made in dimethyl sulfoxide (DMSO) and added to media to give a concentration of 0.2% DMSO (Sigma-Aldrich) and a top concentration of 40 nM pateamine. Aliquots of 50 µL of these drug dilutions in media were then added to the cells arrayed in a 96-well plate to give final concentrations of 0.1% and 20 nM (top concentration) of DMSO and pateamine respectively. Plates were then incubated for 72 hours at 37 °C with 5% CO_2. After drug treatment incubation plates were removed from the incubator and 20 µL of 5 mg/ml 3-(4,5-dimethylthiazol-2-yl)-2,5-diphenyltetrazolium bromide (MTT) (Sigma-Aldrich) in water was added to each well to assess cell viability (Mosmann, 1983). Plates were then returned to the incubator for a further 2 h after which cells were lysed and MTT solubilized with the addition of 100 µl of a solution containing 10% SDS (w/v) and 45% dimethylformamide (w/v) (Sigma-Aldrich). Plates were left overnight at 37 °C in a humidified

incubator, before being read on a Perkin Elmer EnSpire™ 2300 multi label plate reader measuring absorbance at 570 nm. Absorbance values were normalized to a DMSO control.

MTT analysis on adhesive cell lines were carried out as described above with an alteration to the plate cell seeding step. An $8x10^4$ cell/mL suspension in media was made. A 100 µL aliquot was then added to each well and cells were left to attach for 24 h at 37 °C. Following attachment 50 µL of media was removed from each well and replaced with a 50 µL aliquot of 2x drug in media. Subsequent steps were carried out as described for suspension cells.

3.2.3. Proteomic analysis of treated cells

3.2.3.1. Procedure for cell growth and harvesting

Flasks were seeded at a cell concentration of $1x10^5$ cells/mL. An aliquot of pateamine in DMSO was added to give a final concentration corresponding to IC_{20} or IC_0 the highest sub-inhibitory concentration of pateamine and 0.1% DMSO in each sample. Following drug treatments, cells were incubated at 37 °C with 5% CO_2 for 72 h, then harvested. Cell pellets were washed 3 times with ice cold phosphate buffered saline (made with Sigma-Aldrich PBS tablets + pH 7.4). On the final wash one quarter of the cell suspension solution was removed and pellets were stored frozen at -80 °C to be available for subsequent analysis if required. The remaining cells were pelleted and resuspended in RIPA buffer at a concentration of 5×10^6 cells/mL containing a protease inhibitor cocktail (Roche) and left shaking at 4 °C for 30 min. Lysate was then spun to remove cellular debris for 10 min at 16,100 *x g* in a 4 °C refrigerated centrifuge. Proteins were then precipitated from the lysed samples as described below.

When carrying out this protein extraction method the on adherent cell line, the procedure was carried as above with some modifications. Before the first wash step the cells were first treated with TrypLE™ to release them from the bottom of the culture flask. The extraction procedure was then carried out at above.

3.2.3.2. Procedure for protein precipitation

An equal volume of 100% weight/volume solution of ice-cold trichloroacetic acid in acetone was mixed with prepared cell lysates and incubated on ice for 5 min. Precipitated proteins were then pelleted by centrifuging at 16,100 *x g* for 30 min at 4 °C. Supernatant was removed and pellet was washed by adding 500 µL ice cold 70% ethanol and centrifuged for a further 5 min. The ethanol wash solution was then removed, and pellets dried with the lid off in a

laminar flow then redissolved in 8 M urea, 100 mM Tris-HCl (pH 8), agitated with a pipette, then shaken at 37 °C for 30 min.

3.2.3.3. Procedure for protein quantification

Protein quantification was carried out with the use of the Implen NP80 NanoPhotometer following the method described in Section 2.2.15.2.

3.2.3.4. Procedure for protein extract preparation

Protein extracts were prepared for mass spectroscopic analysis following the method described in Section 2.2.15.3.

3.2.3.5. Procedure for mass spectroscopic analysis of protein extracts

Sample vials with glass inserts were placed in the refrigerated (10 °C) auto-sampler of a Dionex UltiMate^{TM} 3000 Nano LC system feeding into an LTQ Orbitrap XL mass spectrometer via a nanospray ion source (Thermo Fisher Scientific, USA). Xcalibur software (Version 2.1.0, Thermo Fisher Scientific, USA) was used for method set up, control of the LC-MS/MS runs, and data acquisition. A buffer gradient was constructed from 0.1% formic acid (buffer A) and 0.1% formic acid in 80% acetonitrile (buffer B): 2% buffer B to start, ramping nonlinearly to 98% B over the course of 360 min, then maintained 98% buffer B for a further 5 min, with the gradient at a rate determined by the gradient optimization analysis tool (GOAT) (Trudgian et al., 2014). Data was obtained with the settings described in Section 2.2.16. A minimum of two technical replicates were carried out on each of the 3 or more biological replicate samples.

3.2.3.6. Procedure for analysis of mass spectroscopic data

The obtained mass spectra files were analysed with Proteome Discoverer (ThermoFisher, version 2.1). The spectra were searched against the Swiss-Prot human proteome database consisting of all proteins with evidence (downloaded on 8-4-2015). A precursor mass range of 350 Da min to 5000 Da max was allowed with a precursor mass tolerance of 10 ppm and fragment mass tolerance of 0.6 Da. Trypsin was selected as the digesting enzyme allowing a maximum of 2 missed cleavages. All Peptides ranging in length from 6 to 144 amino acids were analysed. Carbamidomethylation of cysteines was set as a static modification (+57.021 Da) and modification of methionine residues by oxidation (+15.995 Da) was allowed as a dynamic modification, with a maximum of 2 dynamic modifications per peptide.

Proteome Discoverer output files were then loaded into Scaffold (Proteome Software Inc, Portland, version 4.0) proteomics software for quantification analysis and technical replicates combined using the Mudpit algorithm (Schirmer et al., 2003). Searches were carried out against the Swiss-Prot human all evidence proteomic database 05-02-15. Protein abundance was quantified using iBAQ and TIC independently and identified proteins were filtered to require at least 2 unique peptides to be identified. Peptide P-values were then corrected for multiple testing, this was achieved by using an online FDR q-value tool (Storey, 2002). Proteins were filtered with an FDR change-from-control confidence value of 0.10. All proteins with had a q-value of 0.1 or lower were identified to have significantly changed in abundance. Results from the two quantification methods were then consolidated into two gene lists: significantly increased or decreased.

3.2.4. Downstream analysis of gene lists

3.2.4.1. Procedure for gene ontology enrichment

Gene ontology enrichment analysis was carried out with the use of the g:Profiler online tool (Raudvere et al., 2019). Gene names were converted into formats recognized by g:Profiler and were searched. The organism type was set to *Homo sapiens* and searches were conducted using lists of proteins that decreased only, increased only and all proteins that changed in abundance (the first two lists combined into one). This was done for each cell type and condition and for all cell types and conditions combined with duplicates removed. When investigating the enrichment outputs, ontologies were limited to terms with a total of less than 1000 associated genes to remove top-level ontology terms. The following terms identified from the databases were searched: Biological process, Reactome, WikiPathways and Cell component. The default background was used in all searches.

3.2.4.2. Procedure for 5' UTR motif enrichment analysis

The 5' UTR regions of identified hit genes were downloaded from the UTRDB database (Grillo et al., 2010) and arranged into FASTA format. With validated and longer sequences selected when multiple 5' UTR sequences were available. Additionally, the H4 protein in the mass spectrometry data was removed as it is the product of multiple genes with differing 5' UTRs. The 5' UTR sequences were then analysed for enrichment for de novo motif enrichments through the use of the MEME-suite online tool (Bailey et al., 2009; Bailey. T and Elkan. C, 1994). The search tool was set to identify any number of motifs on each sequence, to identify

a total of 6 possible motifs and to only use the given RNA stand. The maximum motif length was systematically varied between searches, constraining the motif lengths values to 6 - 20, 15 and 10 motif length ranges, and exact nucleotide lengths of 6, 7, and 8. All other parameters were left at default settings and values. In addition to these searches, the same searches were carried out multiple times with shuffled input UTR sequences allowing determination of a significance cut off E-value and number of sites found.

3.2.5. Procedure for western blot analysis

Gel protein separation was carried out using a standard SDS-PAGE method (Smith, 1984). A 10% 1.5 mm SDS-PAGE gel was prepared by producing 20 mL of separating gel containing (375 mM Tris-HCl (pH 8.8), 1% (w/v) SDS, 10% acrylamide (BioRad), 1% bis-acrylamide (BioRad), 10 µL tetramethylethylenediamine (TEMED), 100 µL 10% ammonium persulfate (APS)) and 9 mL of stacking gel (100 mM Tris-HCl (pH 6.8), 0.1% (w/v) SDS, 4.4.% acrylamide, 0.5% bis-acrylamide, 10 µL TEMED, 50 µL 10% APS) with ten wells. Frozen protein samples in 8 M urea were thawed on ice and mixed. An aliquot of protein solution to give a total protein amount of xx was then removed and mixed with the appropriate amount 4x SDS loading buffer (200 mM Tris-HCl (pH 6.5), 8% SDS (w/v), 5% (w/v) β-mercaptoethanol, 0.2% (w/v) bromophenol blue). Samples were heated to 90 °C for 10 min then allowed to cool to room temperature. An electrophoresis tank was prepared and a running buffer (25 mM Tris pH 8.3, 192 mM glycine (Sigma-Aldrich), 0.1% SDS), poured in. Protein solutions were then loaded into the SDS gel along with a pre-stained molecular weight marker ladder (PageRuler™ ThermoFisher). Electrophoresis was then carried out at 180 V until the dye front reached the bottom of the gel (~80 min). The gel was then removed from the glass casement and positioned on a pre-wet sheet of nitrocellulose membrane and placed inside a transfer chamber containing transfer buffer (25 mM Tris pH 8.3, 192 mM glycine, 20% methanol). Proteins were transferred to the nitrocellulose membrane at 20 V overnight at 4 °C.

Proteins for analysis were stained for detection using primary polyclonal rabbit antibodies sourced from abcam and the ThermoFisher Fast Western ECL kit as per manufacturer's guidelines. The nitrocellulose membrane was removed from the transfer chamber and washed with the Fast Western™ wash buffer. The primary antibodies in the antibody diluent solution were then applied to the membrane and incubated for 30 min with rocking at room temperature. The membrane was then transferred to a fresh container and the ECL detection

solution containing the secondary antibody, was added and incubated for 15 min with rocking at room temperature. The membrane was then washed 4 times for 5 min each with the Fast Western™ wash buffer in a fresh container. Once washed, the fast western ECL substrate mix was added and allowed to react for 5 min at which point the membrane was removed from the solution and placed in a ChemiDoc Amersham Imager 600 (General Electric) for imaging with varying exposures depending on signal strength. Band intensities were determined using the analysis software supplied with the imager.

3.3. Results

3.3.1. Growth inhibition by pateamine

The proposed use of pateamine in treatment of cachexia is at concentrations well below those that cause significant cytotoxicity (Di Marco et al., 2012). To understand the proteomic changes under these conditions, the concentrations of pateamine that lead to a slight reduction in cell proliferation (IC_{20}) and the maximum sub-inhibitory concentration were found. The IC_{50} was also determined, as this indicates whether a batch of pateamine retains full activity or has degraded. MTT analysis (Mosmann, 1983) was used to determine pateamine concentrations to use for proteomic analysis. To determine the correct treatment concentrations when producing the protein extracts for mass spectrometry analysis, the cell lines were treated with pateamine or cycloheximide for 72 hours. The relative amount of metabolically active drug-treated cells was then determined by the colour change of tetrazolium dye when reduced by respiring cells as described in Section 3.2.2.

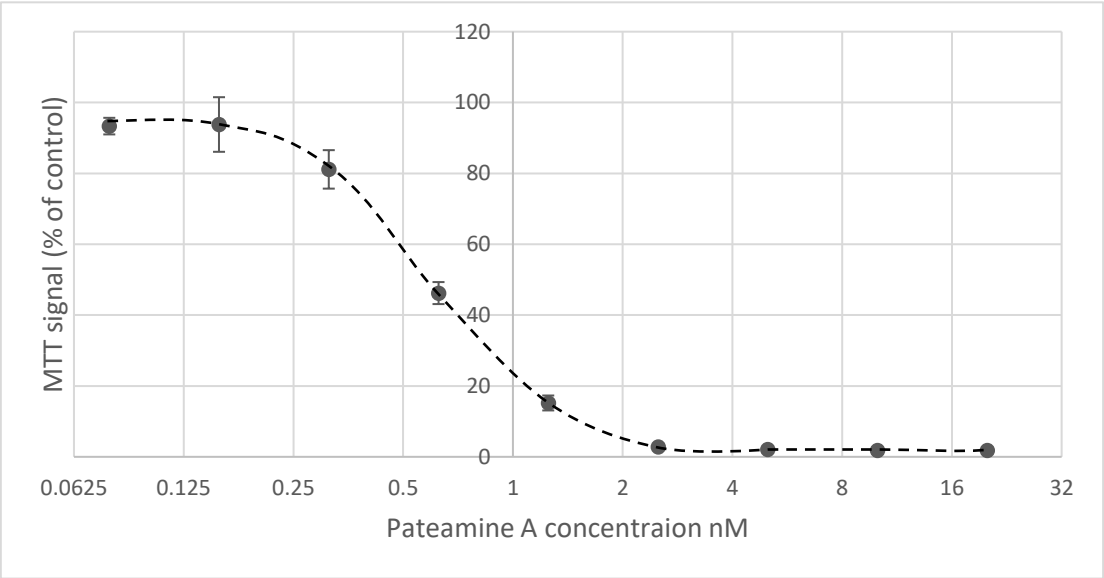

Figure 37. Inhibitory effects of pateamine on HL60 cells can be seen at concentrations above 0.125 nM. HL60 cells were treated with a 2-fold serial dilution of pateamine for 72 hours then tested for metabolic activity using MTT. A blank was subtracted from each absorbance value and normalized to a DMSO only control. Error bars show standard deviation. Data was obtained from at 3 replicates repeated 3 times.

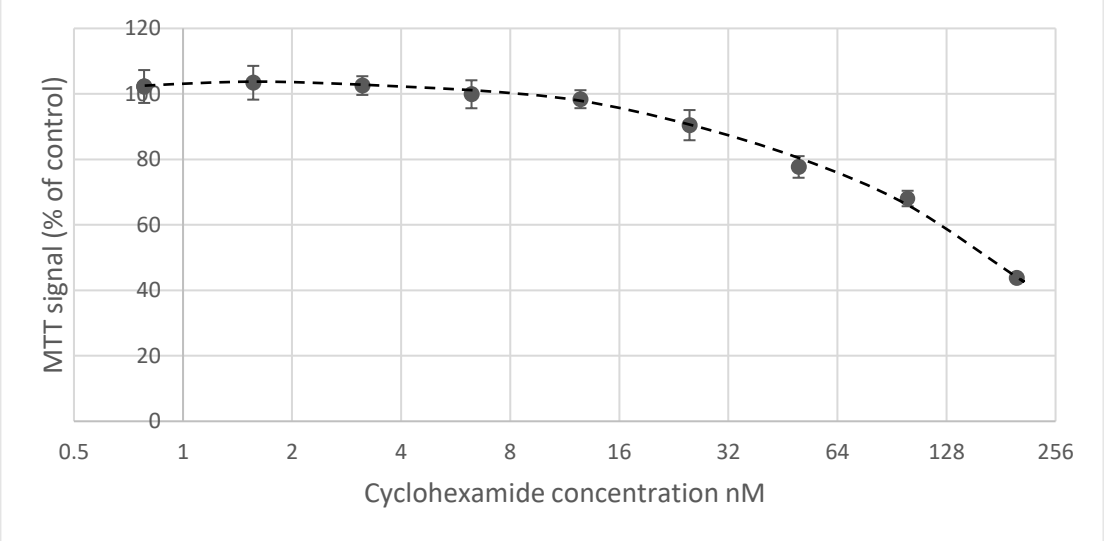

Figure 38. Inhibitory effects of cycloheximide on HL60 cells can be seen at concentrations above 12.5 nM. HL60 cells were treated with a 2-fold serial dilution of cycloheximide for 72 hours then tested for metabolic activity using MTT. A blank was subtracted from each absorbance value and normalized to a DMSO only control. Error bars show standard deviation. Data was obtained from at least 3 replicates repeated 2 times.

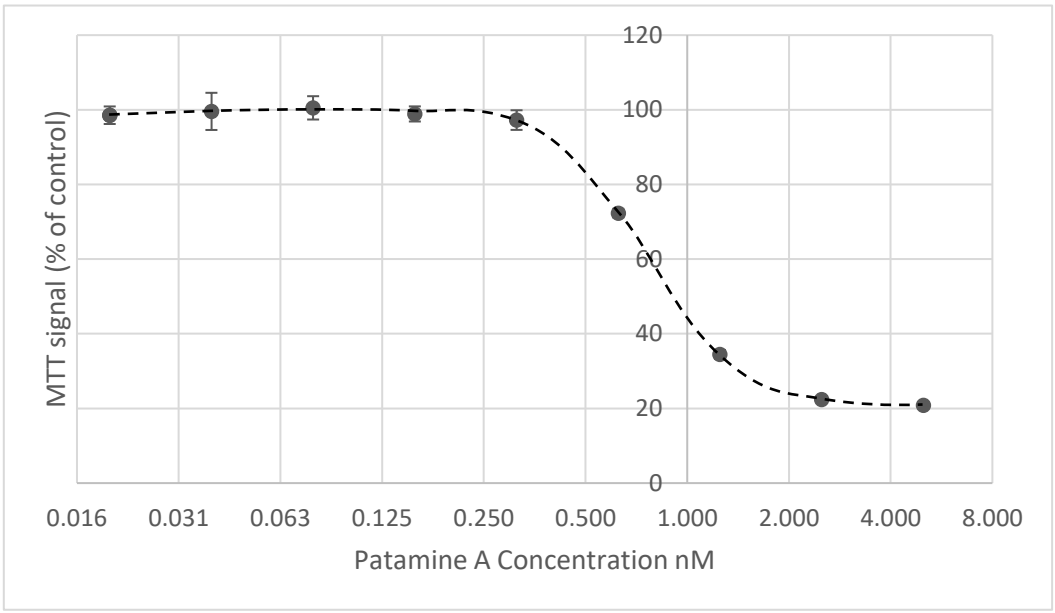

Figure 39. Inhibitory effects of pateamine on HT-29 cells can be seen at concentrations above 0.3 nM. HT-29 cells were treated with a 2-fold serial dilution of pateamine for 72 hours then tested for metabolic activity using MTT. A blank was subtracted from each absorbance value and normalized to a DMSO only control. Error bars show standard deviation. Data was obtained from at least 3 replicates repeated 3 times.

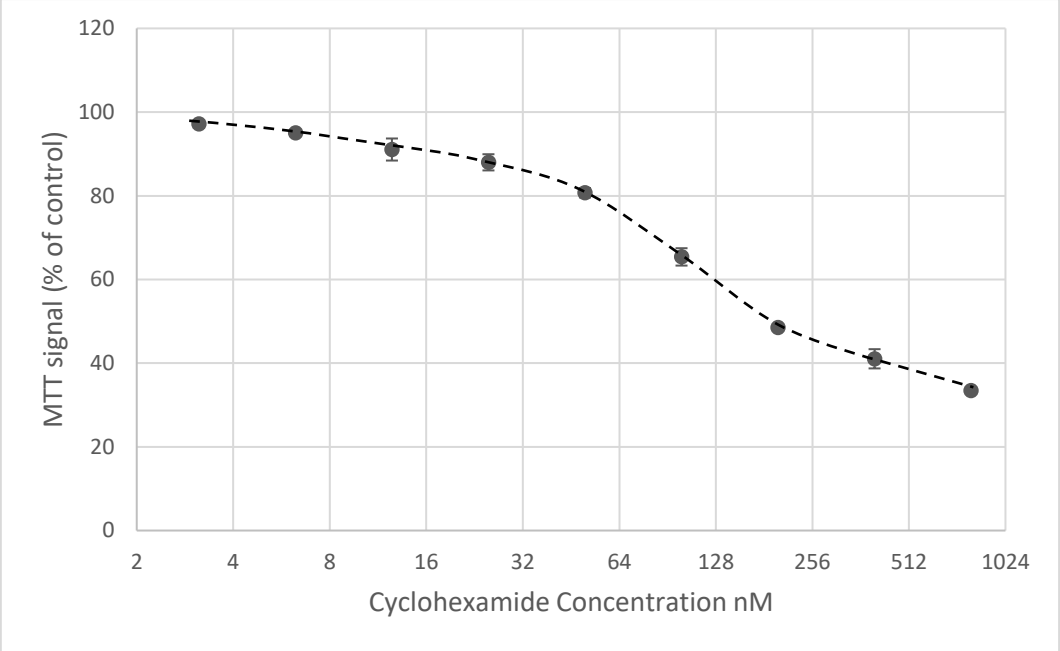

Figure 40. Inhibitory effects of cycloheximide on HT-29 cells can be seen at concentrations above 12.5 nM. HT-29 cells were treated with a 2-fold serial dilution of cycloheximide for 72 hours then tested for metabolic activity using MTT. A blank was subtracted from each absorbance value and normalized to a DMSO only control. Error bars show standard deviation. Data was obtained from at least 3 replicates repeated 2 times.

From the data presented (Figure 37 - 40), we were able to determine the maximum concentration of pateamine which does not induce a detectable inhibitory effect on growth and the concentration to treat cells at to achieve a 20% growth inhibition. From the results we selected a concentration of pateamine of 0.125 nM to achieve a maximal sub-inhibitory treatment and 0.33 nM to achieve an IC_{20} treatment in HL60 cells. HT-29 cells proved to be slightly more resistant to pateamine and a concentration of 0.25 nM was selected for a maximal sub-inhibitory concentration and 0.5 nM to achieve an IC_{20} inhibition. Alongside the pateamine treatments, treatments of cycloheximide were also carried out in order to determine treatment concentrations of an indiscriminate protein synthesis inhibitor control. A cycloheximide concentration of 8 nM was selected for a maximal sub-inhibitory treatment and a concentration 50 nM to achieve an IC_{20} treatment in HL60 cells. For the HT -29 cells concentration of 4 nM for a maximal sub-inhibitory treatment and a concentration 50 nM to achieve an IC_{20} treatment was selected. As we were only aiming to identify a maximum sub-inhibitory and IC_{20} treatment concentration, a complete inhibition curve for cycloheximide was not required. These treatment concentration values were then used when carrying out the mass spectrometry protein expression analysis.

3.3.2. Whole cell mass spectrometry optimizations

Once pateamine and cycloheximide treatment conditions and concentrations had been established these treatments were carried out in 10 mL volumes. Treated cells were then lysed, proteins purified and prepared for quantitative mass spectrometry.

Initial results from the mass spectrometry runs proved to be fairly poor with an average of 690 proteins being identified in any single given run. When inspecting the resultant chromatogram of the first mass spectrometry runs it was noticed that many peaks were overlapping at lower retention times. This suggested multiple peptides were entering the mass spectrometer at the same time likely decreasing the number of peptides which were selected for collision-induced dissociation analysis. To remedy this, we manually increased the gradient length and altered the chromatography gradient making it shallower at the start where peaks were seen overlapping in the MS1 chromatogram and making the gradient steeper later in the run when peaks were more sparse. This led to improved peptide identification and a higher average of 776 proteins.

Despite improving the number of proteins detected after making the chromatography gradient more shallow, peptide mass peaks were still observed to overlap in some regions of the gradient. To further tailor the gradient to the peptide peak profile the computational tool GOAT was utilized (Trudgian et al., 2014). GOAT functions by comparing the separation of the chromatographic peaks to the liquid chromatography buffer gradient and suggests alterations to the gradient to enhance ion peak separation (Trudgian et al., 2014). Implementing the GOAT optimized gradient yielded further improvement, leading to the identification of an average of 884 proteins.

Comparative studies investigating different mass spectrometry search algorithms have shown that when searching the same MS data, the majority of protein identifications between MASCOT and SEQUEST algorithms overlap. However, each search still yields a small number of unique protein identifications (Tu et al., 2015). As a result, combining the analytical outputs of these two algorithms has the potential to improve the number of overall protein identifications (Paulo, 2013). For this reason, it was decided to add the MASCOT algorithm to our search workflow alongside the SEQUEST HT algorithm. This led to a small increase about 15 proteins more per run.

3.3.3. Protein expression analysis

Having established an optimized liquid chromatography gradient and the approach for protein identification, the pateamine and cycloheximide treated protein extracts were then analysed. Both TIC and iBAQ quantitative approaches were carried out separately. The resultant protein change p-values were then analysed using false discovery analysis with a cut-off of 10% and significant proteins from each quantitative approach combined.

3.3.3.1. Protein expression analysis of pateamine treated cells

Table 27. Numbers of proteins found in at least one replicate from each condition and cell type when treated with pateamine. Note analyses were combined, leading to the same total number of proteins identified in both conditions but each quantitative expression analysis between condition and control was carried out separately.

	HL60		**HT-29**	
Condition	**Maximal subinhibitory**	**IC_{20}**	**Maximal subinhibitory**	**IC_{20}**
Total proteins identified	948	1439	834	834
Proteins that changed p<0.05	47	285	183	145
Proteins that changed after FDR correction	0	214	29	60
Proteins with increased expression after FDR	0	124	27	19
Proteins with decreased expression after FDR	0	90	2	47

In the sub-inhibitory pateamine concentration treatment with HL60 cells although a total of 948 proteins were identified (Table 27). When analysed for expression changes only 47 proteins in this list had a t-test value lower than 0.05. Once multiple test correction was carried out no proteins passed the 10% FDR cut-off requirement. This condition is not discussed further as no gene list was produced for further analysis.

3.3.3.1.1. Discrepancy between conditions

A small number of proteins were identified to increase in expression in one cell type, or pateamine concentration, and decrease in another. These are listed in Table 28.

Table 28. A list of proteins identified to have increased in expression in one condition and decreased in another.

Protein	Disparity
CAPG	Down in **Sub-inhibitory HT-29**, up in **IC_{20} HT-29**
HNRNPA1	Down in **Sub-inhibitory HT-29** and **IC_{20} HL60**, up in **IC_{20} HT-29**
HNRNPA3	Down in **Sub-inhibitory HT-29**, up in **IC_{20} HT-29**
TNKS1BP1	Down in **Sub-inhibitory HT-29**, up in **IC_{20} HT-29**
MISP	Down in **Sub-inhibitory HT-29**, up in **IC_{20} HT-29**
RCC1	Down in **Sub-inhibitory HT-29**, up in **IC_{20} HL60**
FBL	Down in **Sub-inhibitory HT-29**, up in **IC_{20} HL60**
HMGB1	Down in **IC_{20} HL60**, up in **Sub-inhibitory HT-29**
ANP32A	Down in **IC_{20} HL60**, up in **Sub-inhibitory HT-29**
ANP32B	Down in **IC_{20} HL60**, up in **Sub-inhibitory HT-29**

It is possible that some of the protein differences between HL60 and HT-29 cells in Table 28 are the result of cell type specific effects. When the proteins that vary in response between HL60 and HT-29 cells are analysed with g:Profiler (Raudvere et al., 2019), the lowest p-values relate to tissue specific expression showing that expression of these proteins vary considerably depending on cell type. Although this effect alone does not apply to all the proteins listed above, these cell type-specific expression differences may go some way to explain why some of these discrepancies are seen.

Interestingly, when results from different experimental conditions were compared there was very little overlap in the proteins found to change in abundance with no overlap being observed between the two HL60 experimental conditions and only 8 proteins overlapping between the HT-29 experiments (Figure 41)

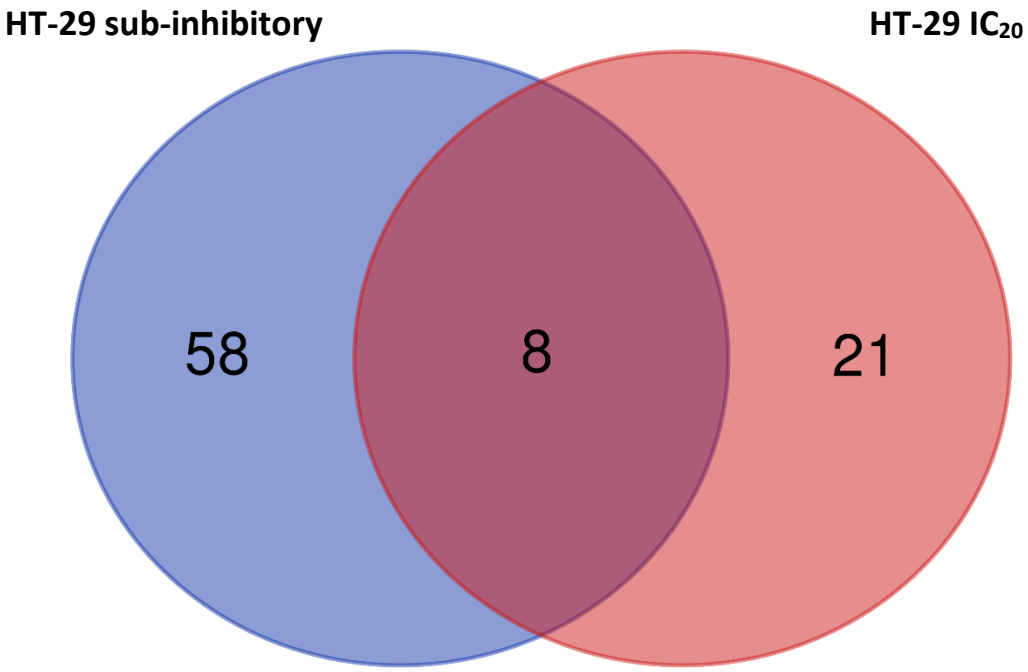

Figure 41. Only 8 genes found to change in both the IC_{20} and the sub-inhibitory HT-29 cell line experiment. The total number of proteins identified to change in abundance in each condition was tallied in the sub-inhibitory pateamine treatment (Left) containing a total of 66 proteins and the IC_{20} pateamine treatment (Right) containing a total of 29 proteins. Intersection of these two lists found only 8 proteins that changed in abundance in both conditions.

3.3.3.2. Protein expression analysis of cycloheximide treated cells

As described in the methods (Section 3.2.3.1) alongside the pateamine treatments, the same experiment was carried out with cycloheximide to give a control for nonspecific translation inhibition and individually compared against a DMSO control. The numbers of proteins identified in this experiment are as follows.

Table 29. Numbers of proteins found in at least one replicate from each condition and cell type when treated with cycloheximide. Note analyses were combined, leading to the same total number of proteins identified in both conditions but each quantitative expression analysis between condition and control was carried out separately.

	HL60		**HT-29**	
Condition	**Maximal subinhibitory**	**IC_{20}**	**Maximal subinhibitory**	**IC_{20}**
Total proteins identified	521	521	734	734
Proteins that changed p<0.05	14	14	38	35

Analysis of the cycloheximide expression experiment found that once the data was subjected to multiple test correction not a single protein was found to be significantly changed in abundance (Table 29). This, when compared with the pateamine results, may suggest that the proteins observed to change in the pateamine treatment analysis are the result of pateamine-specific effects and not the result of a general reduction in protein synthesis rate.

From the numbers of proteins identified in each mass spectrometry experiment it was noticed that the proteins numbers for both cycloheximide treatments were lower than numbers seen in the pateamine treatment experiments. It is unclear why this occurred although the mass spectrometer did have some mechanical issues at some stages which may have contributed. However, the numbers of proteins in these experiments are still large enough that a reasonable amount would be identified to change if a biological response was occurring. Having obtained several lists of genes whose proteins change in abundance in response to pateamine treatment, it was now possible to carry out further analysis.

3.3.4. Gene ontology enrichment analysis of identified hits

3.3.4.1. Ontological enrichment of HL60 cell line

In the future, should pateamine be used as a therapeutic for cachexia, cancer, viral infection, or Alzheimer's disease it will be of great value to know the molecular pathways likely to be affected. This will allow for a better understanding of how this drug elicits its therapeutic effects as well as has the potential for identification of possible side effects and drug interactions. To identify these pathways gene ontology enrichment was utilized.

When proteins identified to increase in expression in response to pateamine at IC_{20} concentrations in HL60 were analysed for ontological enrichments (Table 30), a range of themes emerged. Ontologies relating to mRNA such mRNA metabolic process and nonsense mediated decay, and ontologies relating to protein production and downstream processes such as translation and protein folding were significantly enriched.

Table 30.The statistically enriched ontological terms from the list of proteins up-regulated when HL60 cells are treated with an IC_{20} pateamine concentration. A list consisting of 124 proteins was submitted into the g:Profiler web tool (Raudvere et al., 2019) and results limited to ontologies consisting of fewer than 1000 genes. Results were limited to enrichments found in the biological process, reactome, wikipathways and cellular component ontological databases with the default background. Table has been abridged, a complete g:Profiler output table can be found in supplementary file 15.

Ontology type	Ontology	p-value	Number of contributing genes from hits list
Biological process	protein folding	7.854×10^{-13}	19
	translation	1.278×10^{-12}	30
	translational initiation	1.034×10^{-9}	16
	mRNA metabolic process	2.606×10^{-7}	25
	nuclear-transcribed mRNA catabolic process, nonsense-mediated decay	5.053×10^{-9}	13
	viral process	7.966×10^{-7}	23
	RNA localization	1.175×10^{-3}	11
	cellular protein localization	$1.6099\text{x}10^{-3}$	32
	regulation of cellular response to stress	3.886×10^{-4}	19
	purine-containing compound metabolic process	9.892×10^{-3}	15
	telomere maintenance	2.930×10^{-3}	9
	drug metabolic process	4.479×10^{-2}	17
Reactome	translation	1.104×10^{-14}	26
	cap-dependent translation initiation	7.355×10^{-10}	15
	metabolism of RNA	6.209×10^{-11}	32
	regulation of expression of SLITs and ROBOs	7.814×10^{-11}	18
	nonsense mediated decay (NMD) enhanced by the exon junction complex (EJC)	1.259×10^{-6}	12
	host Interactions of HIV factors	2.897×10^{-4}	10
	influenza viral RNA transcription and replication	5.159×10^{-4}	10
Cellular compartment	extracellular exosome	1.087×10^{-28}	67
	cytosol	1.931×10^{-14}	78
WikiPathways	proteasome Degradation	2.184×10^{-2}	6

When proteins identified to decrease in expression in response to pateamine at IC_{20} concentrations in HL60 cells were analysed for ontological enrichments (Table 31), some similar themes were seen. As with the increased expression protein list, ontologies relating to mRNA such RNA splicing and mRNA transport were significantly enriched. The term ”aromatic compound catabolic process” also relates to mRNA, with almost all proteins associated with that ontology also associated with its granddaughter term “mRNA catabolic process”. However, unlike the increasing proteins list no protein production-related ontologies reach a $p < 0.05$ threshold.

Table 31. The statistically enriched ontological terms from the list of proteins down-regulated when HL60 cells are treated with an IC_{20} pateamine concentration. A list consisting of 90 proteins was submitted into the g:Profiler web tool (Raudvere et al., 2019) and results limited to ontologies consisting of fewer than 1000 genes. Results were limited to enrichments found in the biological process, reactome, wikipathways and cellular component ontological databases with the default background. Table has been abridged, a complete g:Profiler output table can be found in supplementary file 14.

Ontology type	Ontology	p-value	Number of genes
Biological process	aromatic compound catabolic process	2.415×10^{-12}	24
	nuclear export	6.671×10^{-6}	11
	protein export from nucleus	4.251×10^{-5}	10
	positive regulation of organelle organization	2.483×10^{-3}	14
	mRNA transport	1.644×10^{-2}	7
	RNA splicing	1.956×10^{-3}	12
	regulation of endopeptidase activity	1.183×10^{-2}	11
	small molecule biosynthetic process	4.932×10^{-3}	15
	response to organic cyclic compound	1.842×10^{-2}	16
Reactome	metabolism of RNA	6.965×10^{-9}	23
	mRNA Splicing - major pathway	1.020×10^{-4}	10
	signalling by ROBO receptors	5.991×10^{-4}	10
	infectious disease	1.939×10^{-3}	12
	influenza Infection	2.724×10^{-3}	8
	nonsense mediated decay (NMD)	4.510×10^{-2}	6
Cellular compartment	extracellular exosome	4.021×10^{-14}	41
	cytosol	1.489×10^{-12}	59

As described in Section 3.3.3.1 no genes in the HL60 cell maximal sub-inhibitory treatment were significant after a 10 % FDR was applied to the data and as such ontological enrichment analysis could not be carried out on this experiment.

3.3.4.2. Ontological enrichment of HT-29 cell line

When proteins identified to increase in expression in response to pateamine IC_{20} concentrations in HT-29 cells were analysed for ontological enrichments (Table 32), mRNA processing-related ontologies were again found to be enriched. Interestingly, as with the HL60 increased expression list, telomere maintenance-related processes are also enriched.

Table 32. The statistically enriched ontological terms from the list of proteins up-regulated when HT-29 cells are treated with an IC_{20} pateamine concentration. A list consisting of 27 proteins was submitted into the g:Profiler web tool (Raudvere et al., 2019) and results limited to ontologies consisting of fewer than 1000 genes. Results were limited to enrichments found in the biological process, reactome, wikipathways and cellular component ontological databases with the default background. Table has been abridged, a complete g:Profiler output table can be found in supplementary data 16.

Ontology type	Ontology	p-value	Number of genes
Biological process	mRNA metabolic process	1.693×10^{-7}	12
	mRNA processing	3.682×10^{-4}	8
	RNA transport	9.944×10^{-3}	5
	telomere maintenance via telomerase	4.479×10^{-3}	4
	RNA splicing	3.146×10^{-2}	6
	positive regulation of tau-protein kinase activity	4.922×10^{-2}	2
Reactome	uptake and function of diphtheria toxin	3.135×10^{-5}	3
	mRNA Splicing - major pathway	1.921×10^{-4}	6
	metabolism of RNA	3.548×10^{-4}	9

As described in Section 3.3.3.1, only two proteins were found to significantly change in the HT-29 IC_{20} decreased expression list. This number of proteins is insufficient to carry out a meaningful ontological enrichment analysis and as such no table of enrichments is reported.

When proteins identified to increase in expression in response to maximal sub-inhibitory concentrations of pateamine in HT-29 cells were analysed for ontological enrichments (Table 33), far fewer enrichments were seen. This is likely due to a low number of proteins in this list

(19 proteins). Despite this small list, ontologies relating to the end of the protein production pipeline (protein localization and protein folding) are significantly enriched.

Table 33. The statistically enriched ontological terms from the list of proteins up-regulated when HT-29 cells are treated with a sub-inhibitory pateamine concentration. A list consisting of 19 proteins was submitted into the g:Profiler web tool (Raudvere et al., 2019) and results limited to ontologies consisting of fewer than 1000 genes. Results were limited to enrichments found in the biological process, reactome, wikipathways and cellular component ontological databases with the default background. Table has been abridged, a complete g:Profiler output table can be found in supplementary file 17.

Ontology type	Ontology	p-value	Number of genes
Biological process	regulation of protein localization	$3.502x10^{-3}$	8
	positive regulation of cellular protein localization	$1.960x10^{-2}$	5
	interleukin-12-mediated signalling pathway	$2.351×10^{-2}$	3
Reactome	interleukin-12 signalling	$1.230×10^{-2}$	3

When proteins identified to decrease in expression in response to maximal sub-inhibitory concentrations of pateamine in HT-29 cells were analysed for ontological enrichments (Table 34), a similar trend was seen compared to previous enrichment analyses. Ontologies relating to the protein production pipeline including translation and mRNA metabolism are significantly enriched. Interestingly, only in this experiment were proteins relating to translation significantly enriched in the list of down-regulated proteins.

Table 34. The statistically enriched ontological terms from the list of proteins down-regulated when HT-29 cells are treated with a sub-inhibitory pateamine concentration. A list consisting of 47 proteins was submitted into the g:Profiler web tool (Raudvere et al., 2019) and results limited to ontologies consisting of fewer than 1000 genes. Results were limited to enrichments found in the biological process, reactome, wikipathways and cellular component ontological databases with the default background. Table has been abridged, a complete g:Profiler output table can be found in supplementary file 18.

Ontology type	Ontology	p-value	Number of genes
Biological process	mRNA metabolic process	1.501×10^{-8}	17
	RNA splicing	2.274×10^{-5}	11
	translation	4.725×10^{-4}	12
	translation initiation	1.036×10^{-4}	8
	posttranscriptional regulation of gene expression	5.582×10^{-4}	12
	nucleobase-containing compound catabolic process	3.377×10^{-3}	10
	nuclear-transcribed mRNA catabolic process, nonsense-mediated decay	3.871×10^{-2}	5
	eukaryotic translation initiation factor 4F complex assembly	4.533×10^{-2}	2
Reactome	metabolism of RNA	1.451×10^{-8}	17
	L13a-mediated translational silencing of ceruloplasmin expression	4.971×10^{-5}	7
	mRNA splicing - major pathway	7.884×10^{-5}	8
	eukaryotic translation initiation & cap-dependent translation initiation	7.989×10^{-5}	7
	FGFR2 alternative splicing	7.499×10^{-4}	4
	nonsense mediated decay (NMD)	2.111×10^{-2}	5

3.3.4.3. Ontological enrichment of combined conditions

Analysis of these gene lists have identified key cellular processes with are affected by pateamine treatment. However, there may be other more, subtle changes or trends without sufficient statistical power to be identified in lists of this size. It was also noticed that many processes are enriched in both the up and down-regulated protein lists suggesting the cellular responses to pateamine were more complex than complete up or down-regulation of a given process. To investigate this further, protein lists used in the above analyses were combined to produce lists containing all up-regulated proteins, all down-regulated proteins and a list containing all proteins seen to change across the expression experiments. These combined lists were used for gene ontology enrichment analysis and other subsequent analyses.

Combining the lists resulted in stronger enrichments in most terms already identified in the individual condition lists. In the down-regulated protein lists these terms included mRNA metabolic process, nuclear export, and translation-related ontologies (Table 35). A much greater number of ontological terms were also identified to be significantly enriched than in the individual searches. Many of these new enrichments fall under broader terms already identified previously (Supplementary data 19).

Table 35. The statistically enriched ontological terms from the list of all proteins identified to decrease in expression upon pateamine treatment. A list consisting of 136 proteins was submitted into the g:Profiler web tool (Raudvere et al., 2019) and results limited to ontologies consisting of fewer than 1000 genes. Results were limited to enrichments searched in the biological process, reactome, wikipathways and cellular component ontological databases with the default background. Table has been abridged, a complete g:Profiler output table can be found in supplementary file 19.

Ontology type	Ontology	p-value	Number of genes
Biological process	mRNA metabolic process	3.623×10^{-18}	40
	mRNA catabolic process	8.203×10^{-13}	24
	RNA splicing	2.261×10^{-8}	21
	peptide metabolic process	1.502×10^{-7}	28
	translational initiation	4.369×10^{-7}	14
	nuclear export	5.235×10^{-6}	13
	translation	8.290×10^{-6}	23
	protein localization to organelle	5.770×10^{-5}	25
	monosaccharide catabolic process	7.514×10^{-5}	8
	RNA localization	2.660×10^{-3}	11
	carbohydrate catabolic process	3.871×10^{-2}	8
	mRNA transport	3.182×10^{-3}	9
Reactome	metabolism of RNA	6.771×10^{-17}	38
	cap-dependent translation initiation	8.191×10^{-8}	13
	processing of capped Intron-Containing Pre-mRNA	8.786×10^{-8}	17
	mRNA Splicing	2.123×10^{-8}	16
	influenza Life Cycle	7.428×10^{-6}	12
	nonsense mediated decay (NMD)	9.073×10^{-6}	11
	influenza life cycle	1.191×10^{-5}	12
	translation	5.509×10^{-4}	14
	translation initiation complex formation	8.134×10^{-4}	7
	rRNA processing	2.549×10^{-3}	11
	glycolysis	2.323×10^{-2}	6

As with the combined down-regulated proteins list, stronger enrichments were also seen when the combined up-regulated protein list was analysed. These enrichments include mRNA metabolic process, protein folding, translation, nonsense mediated decay and telomere maintenance-related ontologies (Table 36). Like the combined protein list, a greater number of lower order enrichments were also identified many of which fall under more broad terms previously identified in the individual list searches (Supplementary data 20).

Table 36. The statistically enriched ontological terms from the list of all proteins identified to increase in expression upon pateamine treatment. A list consisting of 160 proteins was submitted into the g:Profiler web tool (Raudvere et al., 2019) and results limited to ontologies consisting of fewer than 1000 genes. Results were limited to enrichments searched in the biological process, reactome, wikipathways and cellular component ontological databases with the default background. Table has been abridged, a complete g:Profiler output table can be found in supplementary data 20.

Ontology type	Ontology	p-value	Number of genes
Biological process	mRNA metabolic process	1.904×10^{-19}	45
	protein folding	4.273×10^{-14}	22
	viral process	7.484×10^{-14}	38
	translation	2.597×10^{-12}	34
	translational initiation	2.412×10^{-11}	19
	nuclear-transcribed mRNA catabolic process, nonsense-mediated decay	2.789×10^{-11}	16
	chaperone-mediated protein folding	6.548×10^{-9}	11
	protein localization to organelle	2.405×10^{-6}	30
	RNA localization	5.568×10^{-6}	15
	telomere maintenance via telomerase	2.107×10^{-5}	9
	mRNA splicing, via spliceosome	6.049×10^{-3}	14
Reactome	translation	3.877×10^{-17}	31
	metabolism of RNA	1.456×10^{-15}	42
	cap-dependent translation initiation	8.225×10^{-12}	18
	nonsense mediated decay (NMD)	1.248×10^{-8}	15
	influenza life cycle	2.312×10^{-7}	15
	mRNA splicing	7.387×10^{-5}	14
	rRNA processing	6.656×10^{-3}	12
Cellular component	proteasome complex	5.443×10^{-4}	7

When all proteins found to change were analysed together the same enrichments as pervious were identified. Terms relating to mRNA metabolic processes, translation, protein folding, RNA localization, nonsense mediated decay, and the proteasome complex were more enriched than in previous searches (Table 37). This increased enrichment when the up- and down-regulated protein lists are combined shows that the response to pateamine is complex with abundance changes of many proteins in both directions.

Table 37 The statistically enriched ontological terms from the list of all proteins identified to either increase or decrease in expression upon pateamine treatment. A list consisting of 288 proteins was submitted into the g:Profiler web tool (Raudvere et al., 2019) and results limited to ontologies consisting of fewer than 1000 genes. Results were limited to enrichments searched in the biological process, reactome, wikipathways and cellular component ontological databases with the default background. Table has been abridged, a complete g:Profiler output table can be found in supplementary file 21.

Ontology type	Ontology	p-value	Number of genes
Biological process	mRNA metabolic process	2.287×10^{-37}	81
	viral process	8.868×10^{-22}	62
	translational initiation	3.933×10^{-21}	33
	translation	1.015×10^{-20}	57
	protein localization to organelle	6.807×10^{-14}	55
	protein folding	1.404×10^{-13}	27
	RNA splicing	4.301×10^{-11}	34
	RNA localization	6.588×10^{-9}	23
	nuclear export	1.381×10^{-8}	21
	telomere maintenance	1.628×10^{-5}	16
	cellular response to oxidative stress	1.819×10^{-4}	20
Reactome	metabolism of RNA	1.587×10^{-30}	75
	translation	1.626×10^{-22}	45
	cap-dependent translation initiation	6.676×10^{-22}	31
	signalling by ROBO receptors	1.143×10^{-18}	36
	nonsense mediated decay (NMD)	2.163×10^{-16}	26
	influenza life cycle	4.032×10^{-15}	27
Cellular component	proteasome complex	1.464×10^{-6}	11

3.3.5. String analysis of combined proteomic hits lists

To visualise the large protein lists in a more visually understandable way, we produced a graphic of our proteomic results with the String bioinformatic software (Szklarczyk et al., 2019a). Gene lists identified through the mass spectrometry expression analysis were combined together to produce 3 gene lists consisting of all up-regulated proteins in all experiments (Figure 42), all down-regulated proteins in all experiments (Figure 43) and a combined up- and down-regulated list consisting of all proteins found to change in abundance (Figure 44). These lists were then uploaded individually on to the String analysis server.

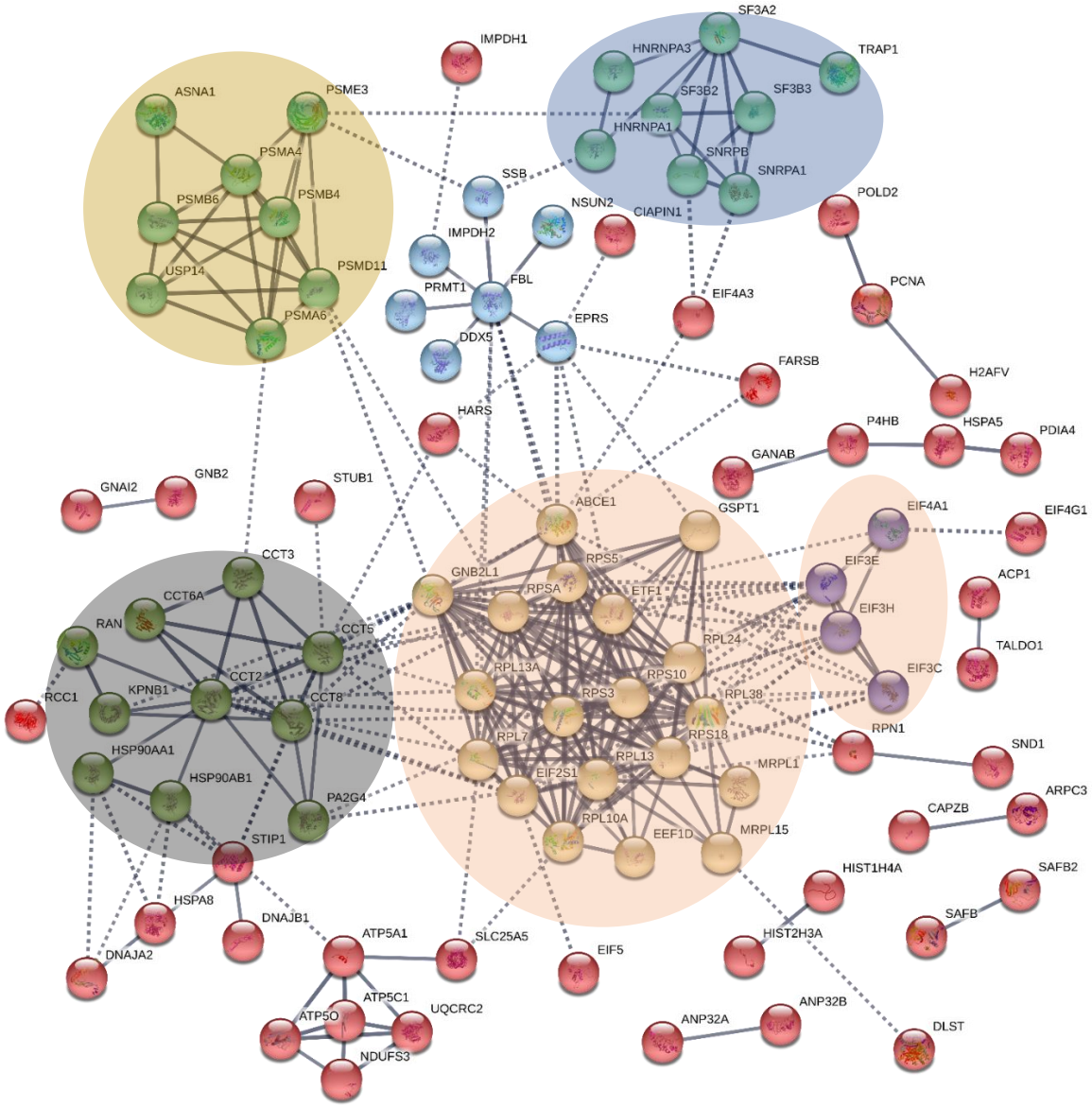

Figure 42. String analysis of all up-regulated proteins reveals protein groups involved in translation , tRNA metabolism , proteasome activity and mRNA splicing . The combined up-regulated proteins list was analysed with the String network analysis tool (Szklarczyk et al., 2019a). Parameters were set as follows: edges set to confidence, disconnected nodes hidden, interactions used: co-expression, experiments and gene fusion. 0.8 confidence. Kmeans clustering, 7 clusters.

String analysis of the combined up-regulated proteins showed a similar trend as the ontological enrichment analysis. Analysis found proteins being clustered into four main processes relating to translation , tRNA metabolism , proteasome activity, and mRNA splicing (Figure 42).

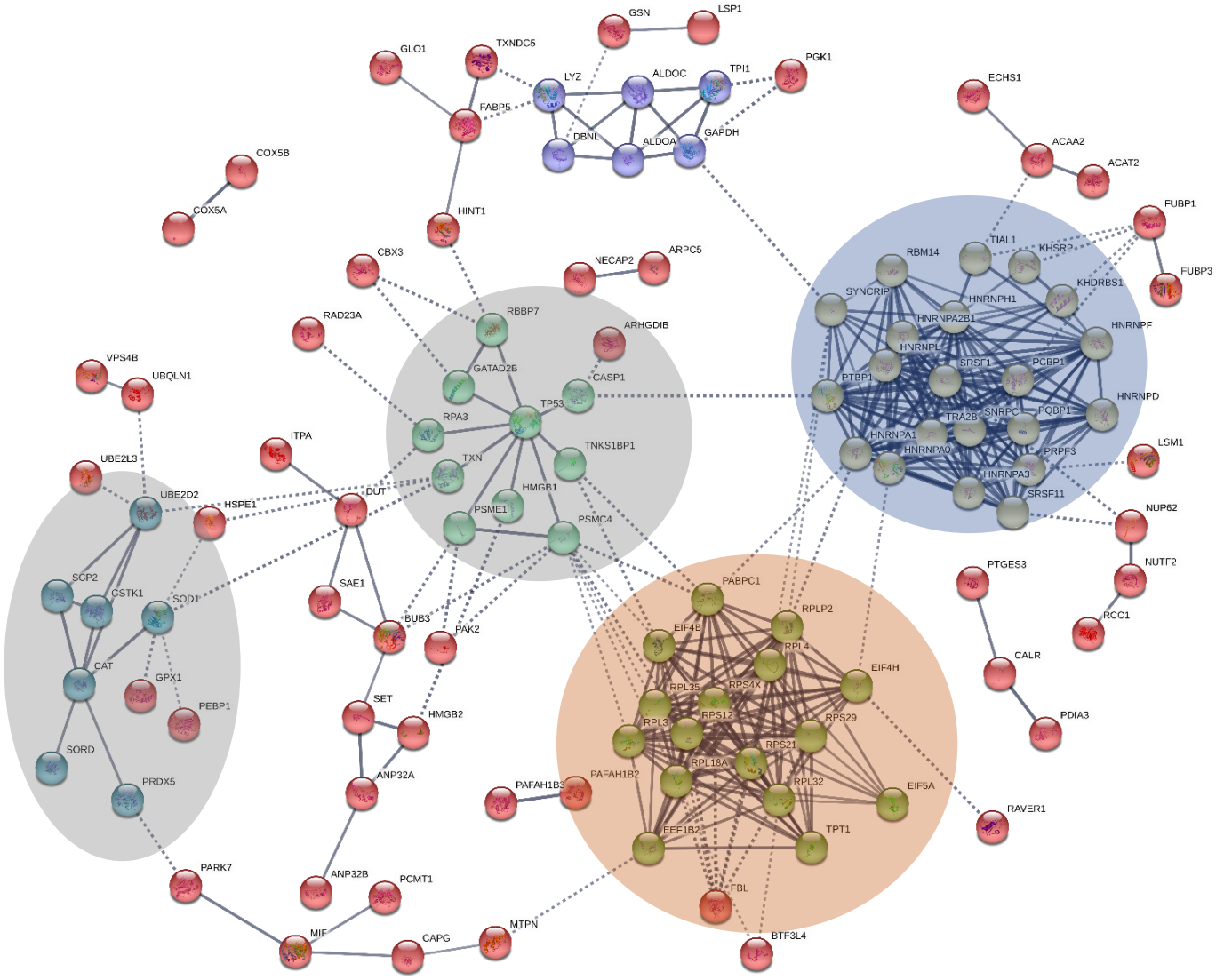

Figure 43. String analysis of all down-regulated proteins identified protein groups relating to translation , mRNA splicing , P53 regulation and oxidation-reduction The combined down-regulated proteins list was analysed with the String network analysis tool (Szklarczyk et al., 2019b). Parameters were set as follows: edges denote confidence, disconnected nodes hidden. Interactions shown: experiments, databases, co-expression and gene fusion. High confidence (0.7). Kmeans clustering, 6 clusters.

String analysis of the combined down-regulated proteins also showed a similar trend as the ontological enrichment analysis, with clusters forming that related to translation, mRNA splicing, and oxidation-reduction. Additionally, a cluster relating to P53 regulation was also found that had not previously been identified (Figure 43).

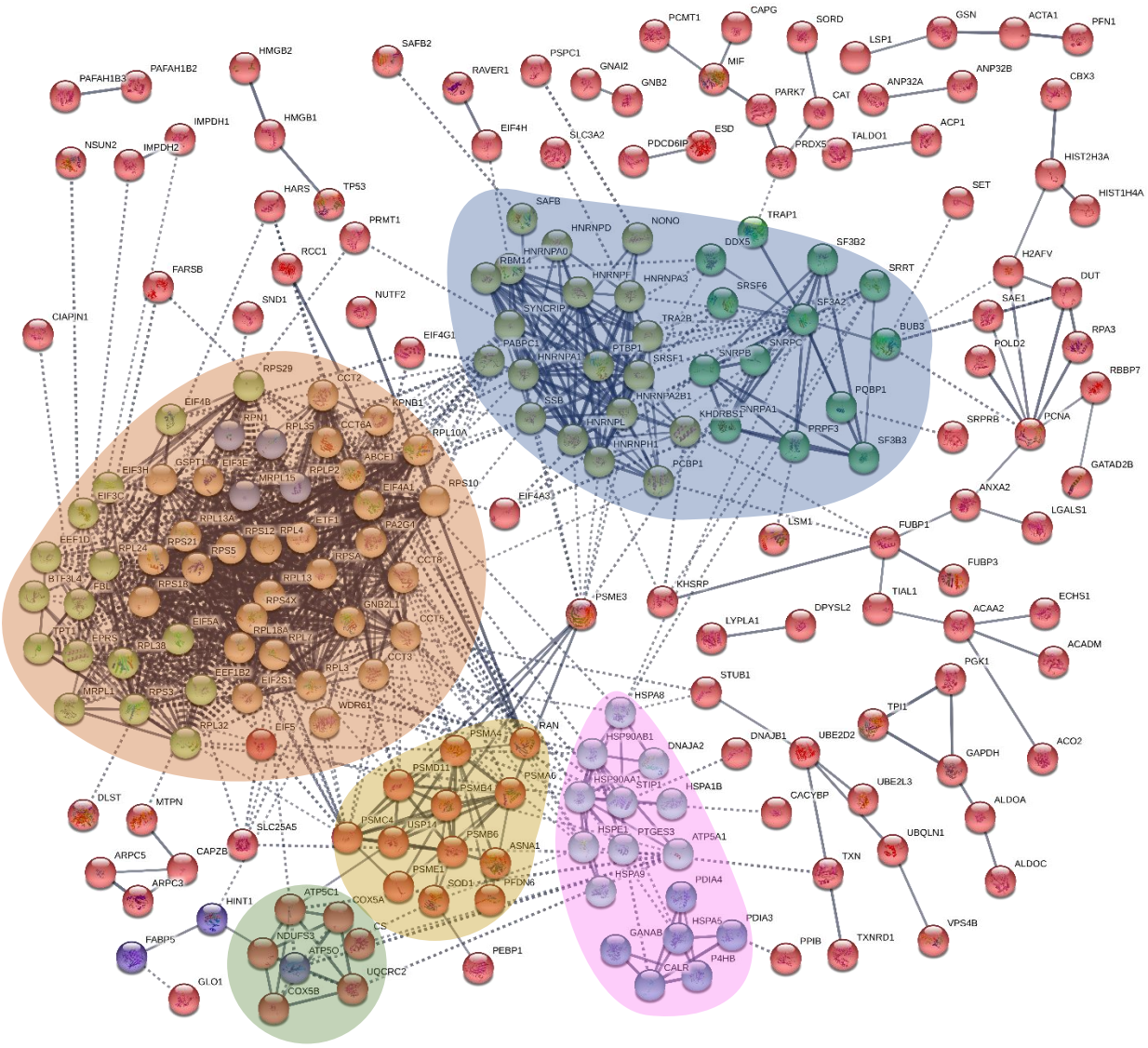

Figure 44. String analysis of all up- and down-regulated proteins identified protein groups relating to translation , mRNA metabolism , the proteasome , mitochondria and protein folding . The combined up- and down-regulated proteins list was analysed with the String network analysis tool (Szklarczyk et al., 2019a). Parameters were set as follows: edges denote confidence. High confidence interactions (0.7). Interactions shown: experiments, co-expression and gene fusion. disconnected nodes hidden. Kmeans clustering, 9 clusters.

String analysis of all proteins found to change found 5 main clusters. These clusters related to translation, mRNA metabolism, the proteasome, mitochondria, and protein folding (Figure 44).

Overall, String analysis produced clusters relating to many of the same gene ontology terms identified in the gene ontology analysis above (Section 3.3.4). Translation-related proteins produced the largest clusters in all three gene lists as well as identifying a range of other gene groups relating to tRNA metabolism, proteasome activity and mRNA splicing mirroring the ontological enrichments seen with g:Profiler.

3.3.6. Analysis of characteristics of mRNA of up- and down-regulated proteins

From the ontological enrichment analysis above we see that a lot of the proteins identified to change in abundance are linked to ontologies that are likely to be affected by pateamine treatment. However, of the 288 proteins found to change in response to pateamine treatment at any concentration, only 177 of those proteins are associated with the major ontological enrichments that are associated with the biological response to pateamine treatment. As described in Section 1.4.4, other eIF4A inhibitors have been shown to disproportionately affect some proteins over others based on features of the mRNA 5' UTR. We suspected that some of the expression changes seen in our data may be caused by these or other mRNA features. We could not guarantee that all the proteins linked to an enriched ontology were solely the result of a cellular response and were not mRNA future independent. Furthermore, we did not preclude the idea that the mRNA of the biological responders may have these features specifically to enable their response to a stress on translation initiation. For this reason, we chose to carry out analysis of the 5' UTRs of all gene transcripts in our list.

3.3.6.1. UTR length analysis

As described in Chapter 1 (Section 1.2), it is well established that pateamine elicits its translation inhibitory effects by interacting with the translation initiation factor eIF4A. This enzyme functions by unwinding the secondary structure of the mRNA 5' UTR allowing the ribosome to bind the transcript. It was theorised that translation initiation would stall on longer 5' UTRs more often and induce a greater down-regulation of their corresponding proteins. The reverse may also elicit an effect, as a shorter 5' UTR would have fewer positions for the preinitiation complex to bind and stall, and greater access to ribosomes that become available as they are not processing stalled transcripts. This would lead to an increase in protein abundance of these shorter transcripts when total protein is normalised. As we were treating with relatively low concentrations of pateamine, we did not expect this effect to be present in our data as there should still be a significant amount uninhibited eIF4A present in the cell. To probe this, the 5' UTR length of all transcripts of proteins that were identified to have changed in abundance and lengths of up- and down-regulated 5' UTRs compared. It was found that the average mean 5' UTR length of the down-regulated genes was 211 nucleotides long whereas the average length of the up-regulated 5' UTRs was 180 nucleotides long, a difference of 31 nucleotides. However, on closer inspection of the data it was determined

that this difference was mainly the result of 3 very long 5’ UTR influencing the mean. When the median was taken the difference between the two data sets largely disappeared with the downs having a median 5’ UTR length of 146.5 nucleotides long and the ups having a median 5’ UTR length of 142 a difference of only 4.5 nucleotides.

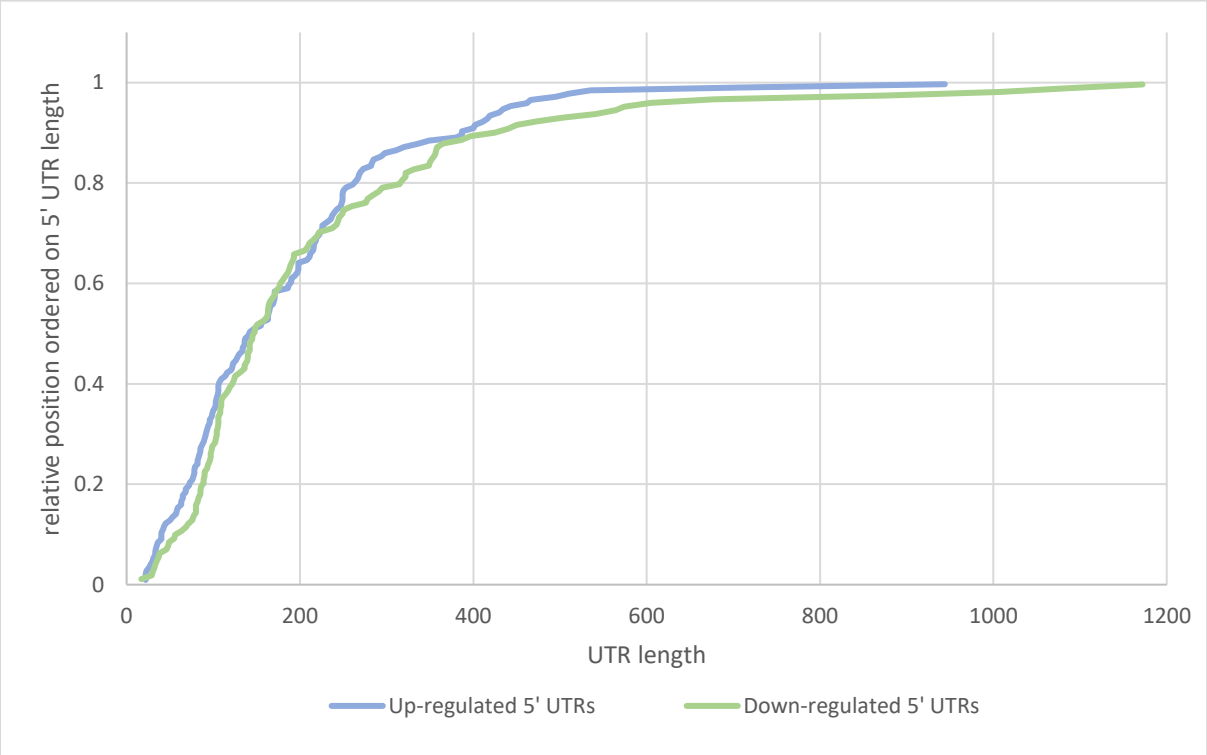

Figure 45. No strong difference in length of the 5’ UTRs of transcripts was detected when comparing the up- and down-regulated transcript 5’ UTR length. Asymptote graph was produced by ordering all up or down-regulated 5’ UTRs based on length, then plotting the 5’ UTR length against relative position in list. Data is accumulated from 160 5’ UTRs from the up-regulated gene list and 136 in the down-regulated gene list.

When the 5’ UTRs are ordered and the relative position plotted against 5’ UTR length we see a relatively similar profile between the up-regulated and down-regulated protein lists (Figure 45). There is a slight trend of the longest 20% of down-regulated 5’ UTRs to be longer than those of the up-regulated 5’ UTRs but this trend is not large enough to be considered important.

3.3.6.2. uORF analysis

When investigating the effects of rocaglamide A, Iwasaki et al. (2016) determined that the transcripts they identified to have reduced translational efficiency when treated with rocaglamide were more likely to possess an upstream open reading frame (uORF) in their 5' UTRs (Iwasaki et al., 2016). To determine whether pateamine at concentrations leading to low levels of eIF4A inhibition also disproportionately reduces the translation of transcripts which possess a uORF, our gene lists were checked against a dataset of known uORFs (Lee et al., 2012b).

Table 38. Frequencies of uORFs found in the combined up- and down-regulated proteins list

	All up-regulated	All down-regulated
Fraction of transcripts	84/160	92/136
Percentage	54%	67%

When checked against this dataset, 67% of the down-regulated proteins were found to possess at least one uORF in their 5' UTRs, only slightly more than that of the combined up-regulated proteins at 54% (Table 38). This difference is reasonably small suggesting that if uORFs are affecting translation inhibition by pateamine, the effect is also relatively small. However, as discussed previously the protein expression changes measured are the culmination of many different factors including cellular responses, feedback loops, and possibly other direct transcript-specific effects of pateamine. So, it is possible uORFs are having a minor impact and this 13% difference is a genuine but small effect.

3.3.6.3. GC content analysis

It has previously been reported that an RNA transcript's requirement for functional eIF4A to be expressed is highly dependent of the amount of structure in the transcript's 5' UTR (Leppek et al., 2018). A major contributor to this structure is the percentage on guanidine and cytosine bases within the 5' UTR (Babendure et al., 2006). The GC content in the 5' UTRs of both the up- and down-regulated transcripts was determined. It was found that the up-regulated transcripts had an average GC content of 65.1%, compared to 65.7% for the down-regulated transcripts. Given how close these two values are, it was determined that the GC content did not appear to a strong have an influence on expression at these treatment concentrations. As with the 5' UTR length, we did not expect much difference between these values due to the low pateamine concentrations not significantly reducing the abundance of functional eIF4A.

3.3.6.4. Internal ribosome entry site analysis

As described in Section 1.4.4, when investigating the translation initiation inhibitory effects of silvestrol Wolfe et al. found that transcripts with increased translational efficiency were more likely to possess an IRES sequence in their 5' UTRs (Wolfe et al., 2014). To determine whether IRESes had an influence on the genes identified through our approach, our 5' UTRs sequence lists were scanned with the IRESite web site tool (Mokrejs et al., 2010). In the 5' UTRs of the combined up-regulated genes, IRESite found 31/160 (19.4%) UTRs with an IRES probability e-value of less than 0.05. For the combined down-regulated genes, this figure was 28/136 (20.6%). Given that the proportions of potential IRES sites found in both the up and down gene lists were so similar, we concluded that it was not likely that IRESes were contributing to the observed expression changes.

3.3.6.5. Motif analysis of 5' UTR

As described in both Wolfe et al. and Iwasaki et al., certain mRNA transcripts are more greatly affected by eIF4A inhibition than others. This effect, at least in part, appears to be the result of particular nucleotide sequence motifs located in the 5' UTR of the transcripts (Iwasaki et al., 2016; Wolfe et al., 2014). To investigate whether the changes in expression we observed were also a result of a 5' UTR sequence motif, we employed a search method similar to that used by Wolfe et al. The 5' UTR sequences of all up- and down-regulated protein lists were analysed with the MEME search algorithm (Bailey et al., 2009) as described in Section 3.2.4.2. The MEME algorithm uses a statistical E-value which is an estimate of the expected number of random alignments that would exhibit an entropy score that is at least as high as the motif identified (Nagarajan et al., 2006). To avoid false identifications the default E-value cut-off of 0.05 was used. To avoid impacts of length bias, individual searches were carried out with the maximum motif length constrained to values of 20 (Figure 46, 48, & 51), 15 (Figure 49 & 52) and 10 (Figure 47, 50, 53, & 54). Additionally, the default site distribution option was changed to any number of repeats and the "use given strand only" option was selected. Also, of importance to note; the UTRdb web site reports sequences as DNA, for this reason thymidine is reported instead of uracil as it would appear as RNA.

3.3.6.5.1. Individual condition motif analysis

The 5' UTR sequences from the mRNA of proteins found to be up or down-regulated were compiled into lists for each condition. These lists were then analysed with the MEME motif enrichment search algorithm (Bailey et al., 2009).

3.3.6.5.1.1. HL60 20% inhibition down-regulated motif analysis

When searching the 5' UTRs of the HL60 IC_{20} pateamine treated down-regulated proteins (Figure 46 & 47) four themes of enriched motifs were identified across the length constrained searches. One rich in Ts and Cs, one rich in As and Gs similar to the motif reported by Iwasaki et al. (2016); (2019) sometimes with either As or Gs predominating, one with some bias toward As and Ts and one consisting of Gs and Cs similar to the G-quadruplex forming motif reported by Wolfe et al. (2014).

E-value	Number of motif instances	Length of motif	Motif
$6.4x10^{-21}$	**52**	**15**	
$1.3x10^{-19}$	**46**	**15**	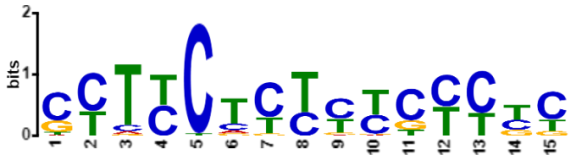
$6.2x10^{-08}$	**15**	**20**	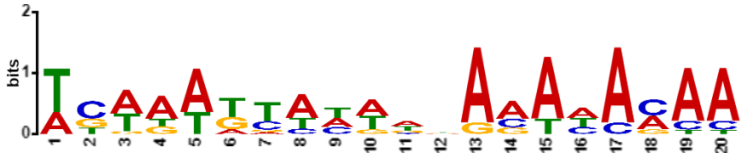
$4.4x10^{-3}$	**35**	**15**	

Figure 46. The HL60 IC_{20} down-regulated 5' UTR list constrained to 6 - 20 nucleotides yielded four significant motifs. A total of 90 5' UTR sequences from the HL60 IC_{20} pateamine treatment down-regulated list were submitted into the MEME search algorithm constrained to motif lengths between 6 and 20 nucleotides long. None of the shuffled sequences with these parameters reached the standard 0.05 significance cut-off.

The 6-15 nucleotide search did not show any significant motifs which are not already present in the 6-20 nucleotide table and so is omitted.

E-value	Number of motif instances	Length of motif	Motif
$1.3x10^{-11}$	39	10	
$5.7x10^{-11}$	70	10	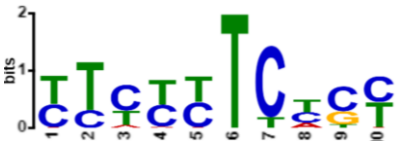
$1.5x10^{-3}$	36	10	

Figure 47. The HL60 IC_{20} down-regulated 5′ UTR list constrained to 6 and 10 nucleotides yielded three significant motifs. A total of 90 5′ UTR sequences from the HL60 IC_{20} pateamine treatment down-regulated list were submitted into the MEME search algorithm constrained to motif lengths between 6 and 10 nucleotides long. None of the shuffled sequences with these parameters reached the standard 0.05 significance cut-off.

3.3.6.5.1.2. HL60 20% inhibition up-regulated motif analysis

When searching the 5' UTRs of the HL60 IC_{20} pateamine treated up-regulated proteins (Figure 48, 49, & 50) three themes of enriched motifs were identified across the length constrained searches. One rich in Ts and Cs, one rich in Gs and Cs showing some similarity to the motif reported by Wolfe et al. (2014) and one with some weak trend toward As and Gs. The most notable changes from the up- to the down-regulated HL60 list is that the GA and GC motifs appear less defined and the E-value of the GA motif in the down-regulated list is much lower than in the up-regulated list ($6.4x10^{-21}$ and $3.10x10^{-07}$ respectively) as well as the number of motif instances (52 and 12 respectively). However, although being less well defined the GC-rich motif is seen with a lower E-value in the up-regulated list the opposite of what would be expected given the findings of Wolfe et al. (2014) The AT-rich motif is also not observed.

When 5' UTR sequences from HL60 IC_{20} up-regulated list was limited to a maximum length of 20 nucleotides, three significant motifs were identified consisting of a TC- rich motif, and GC-rich motif and a A-rich motif with a trend also toward As and Gs (Figure 48).

E-value	Number of motif instances	Length of motif	Motif
$3.70x10^{-14}$	**56**	**11**	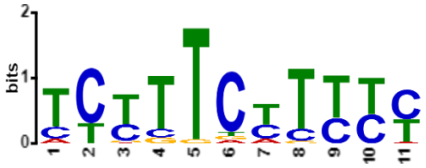
$1.30x10^{-12}$	**56**	**15**	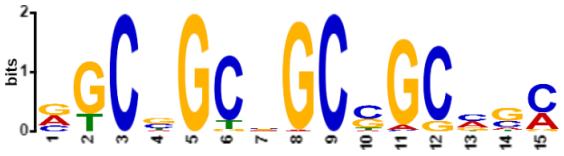
$3.10x10^{-07}$	**12**	**19**	

Figure 48. The HL60 IC_{20} up-regulated 5' UTR list constrained to 6 and 20 nucleotides yielded three significant motifs. A total of 122 5' UTR sequences from the HL60 IC_{20} pateamine treatment up-regulated list were submitted into the MEME search algorithm constrained to motif lengths between 6 and 20 nucleotides long. None of the shuffled sequences with these parameters reached the standard 0.05 significance cut-off.

When the motif analysis of the same HL60 IC_{20} up-regulated 5' UTR list was limited to a maximum length of 15 nucleotides, the same TC- and GC-rich motifs were identified (omitted from figure), additionally, a slightly shorter A-rich motif was found (Figure 49).

E-value	Number of motif instances	Length of motif	Motif
3.80×10^{-04}	**20**	**15**	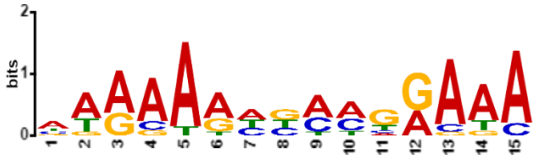

Figure 49. The HL60 IC_{20} up-regulated 5' UTR list constrained to 6 and 15 nucleotides yielded three significant motifs two of which were identical to the 6 – 20 nt search. A total of 122 5' UTRs from the HL60 IC_{20} pateamine treatment up-regulated list were submitted into the MEME search algorithm constrained to motif lengths between 6 and 15 nucleotides long. None of the shuffled sequences with these parameters reached the standard 0.05 significance cut-off.

When the motif analysis of the same HL60 IC_{20} up-regulated 5' UTR list was limited to a maximum length of 10 nucleotides, only two motifs were identified a CT-rich motif and a GC-rich motif that appears to have a CGG repeat sequence (Figure 50).

E-value	Number of motif instances	Length of motif	Motif
9.40×10^{-17}	**51**	**10**	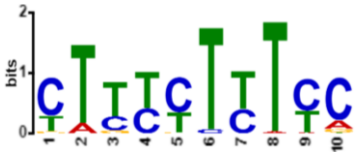
8.90×10^{-03}	**23**	**10**	

Figure 50. The HL60 IC_{20} up-regulated 5' UTR list constrained to 6 and 10 nucleotides yielded two significant motifs. A total of 122 5' UTRs from the HL60 IC_{20} pateamine treatment up-regulated list were submitted into the MEME search algorithm constrained to motif lengths between 6 and 10 nucleotides long. None of the shuffled sequences with these parameters reached the standard 0.05 significance cut-off.

3.3.6.5.1.3. HT-29 maximal sub-inhibitory down-regulated motif analysis

When the HT-29 maximal sub-inhibitory down-regulated 5' UTRs were analysed for motif enrichment (Figure 51, 52, & 53), four themes of motif emerge. As with the HL60 IC_{20} down-regulated analysis, the most enriched is an A-rich motif followed closely by a GC-rich motif with CGG repeats similar to the motif identified by Wolfe et al. (2014) are seen. Additionally, we see a motif rich in Ts staring with a single A or C and a motif rich in Cs with some trend toward GCC repeats.

Analysis of the HT-29 maximal sub-inhibitory down-regulated 5' UTR list when limited to a maximum length of 20 nucleotides, identified four significant motifs. The most significant of which was an A-rich motif followed by a GC-rich motif with a CGG repeat, a C-rich motif and a T-rich motif starting with an A or C (Figure 51).

E-value	Number of motif instances	Length of motif	Motif
$3.30x10^{-15}$	**14**	**19**	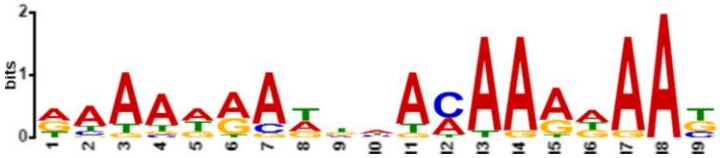
$3.50x10^{-14}$	**18**	**15**	
$6.40x10^{-09}$	**39**	**20**	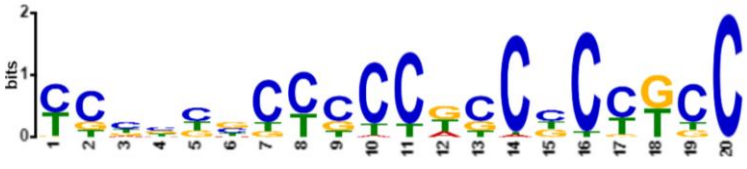
$1.60x10^{-03}$	**11**	**14**	

Figure 51. The HT-29 maximal sub-inhibitory down-regulated 5' UTR list constrained to 6 and 20 nucleotides yielded four significant motifs. A total of 47 5' UTRs from the HT-29 maximal sub-inhibitory pateamine treatment down-regulated list were submitted into the MEME search algorithm constrained to motif lengths between 6 and 20 nucleotides long. None of the shuffled sequences with these parameters reached the standard 0.05 significance cut-off.

When the motif search was limited to a maximum length of 15 nucleotides two new motifs resembling the A-rich and C-rich motifs above but shorter were found (Figure 52). A T-rich and a GC-rich motif were found but omitted as they were identical to the motifs identified in Figure 51.

E-value	Number of motif instances	Length of motif	Motif
$1.30x10^{-13}$	17	15	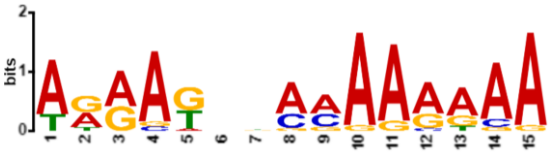
$8.80x10^{-07}$	34	15	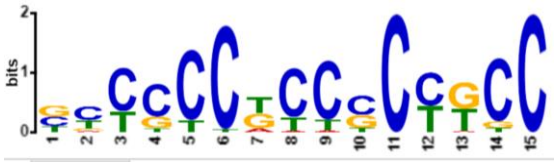

Figure 52. The HT-29 maximal sub-inhibitory down-regulated 5' UTR list constrained to 6 and 15 nucleotides yielded two new significant motifs. A total of 47 5' UTRs from the HT-29 maximal sub-inhibitory pateamine treatment down-regulated list were submitted into the MEME search algorithm constrained to motif lengths between 6 and 15 nucleotides long. None of the shuffled sequences with these parameters reached the standard 0.05 significance cut-off.

When the motif search was limited to a length of 10 nucleotides three motifs similar to the A-rich the GC-rich the CT-rich motifs found above. The C-rich motif, however, was absent (Figure 53).

E-value	Number of motif instances	Length of motif	Motif
$2.30x10^{-10}$	29	8	
$7.20x10^{-05}$	26	10	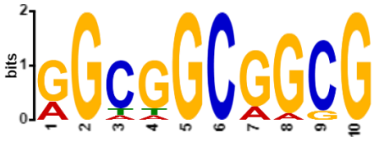
$5.60x10^{-03}$	37	10	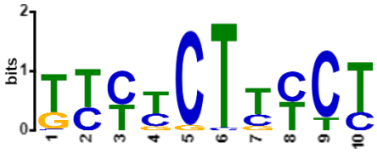

Figure 53. The HT-29 maximal sub-inhibitory down-regulated 5' UTR list constrained to 6 - 10 nucleotides yielded three significant motifs. A total of 47 5' UTRs from the HT-29 maximal sub-inhibitory pateamine treatment down-regulated list were submitted into the MEME search algorithm constrained to motif lengths between 6 and 10 nucleotides long. None of the shuffled sequences with these parameters reached the standard 0.05 significance cut-off.

3.3.6.5.1.4. HT-29 maximal sub-inhibitory up-regulated motif analysis

When carrying out motif enrichment searches on the 5' UTRs of the HT-29 sub-inhibitory pateamine up-regulated protein list (Figure 54), only one statistically significant motif was found. This motif was only just above the significance threshold. We suspect that so few motifs were found due to there being only 19 5' UTR sequences in this list.

E-value	Number of motif instances	Length of motif	Motif
3.20×10^{-02}	**6**	**10**	

Figure 54. The HT-29 maximal sub-inhibitory up-regulated 5' UTR list when constrained to 6 - 10 nucleotides yielded one significant motif. A total of 19 5' UTRs from the HT-29 maximal sub-inhibitory pateamine treatment up-regulated list were submitted into the MEME search algorithm constrained to motif lengths between 6 and 10 nucleotides long. None of the shuffled sequences with these parameters reached the standard 0.05 significance cut-off.

3.3.6.5.1.5. HT-29 IC_{20} inhibition down-regulated motif analysis

As stated in Section 3.3.3.1, only two genes were found to have significantly decreased in expression in this pateamine treatment condition. As a result, motif analysis was not be carried out on this data.

3.3.6.5.1.6. HT-29 IC_{20} inhibition up-regulated motif analysis

When carrying out motif enrichment searches on the 5' UTRs of the HT-29 IC_{20} pateamine up-regulated protein list, no statistically significant motif was found. However, several motifs which did not reach significance were seen with similar trends to motifs found in earlier analysis.

3.3.6.5.2. Combined 5' UTR list motif searches

The analysis above identifies potential 5' UTR sequence motifs associated with individual cell types and pateamine concentration treatments. However, it is reasonable to assume that where a sequence motif leads to pateamine sensitivity it should do so in any human cell line. Additionally, given the two pateamine concentrations used in these experiments are relatively similar, it is reasonable to assume that the pateamine-sensitising sequence motifs should also be broadly similar. These two assumptions are supported by the relative similarity of the motifs obtained from analysing the individual treatment conditions. Therefore, to obtain a more robust analysis, it was decided to repeat the MEME sequence analysis using pooled data as was done with the ontological enrichment analysis above, representing all down-regulated or all up-regulated genes across both cell types and pateamine concentrations.

3.3.6.5.2.1. Combined down-regulated 5' UTR motif analysis

When combining the 5' UTRs of all down-regulated proteins a list of 136 5' UTR sequences was produced. These were analysed with the MEME algorithm. In these combined lists in addition to the range of motif lengths stated above, additional searches were undertaken, constrained to exactly six, seven and eight nucleotides to probe for motifs of similar length to the motif identified by Iwasaki et al. (2016) for both down-regulated and up-regulated proteins (Figure 55 & 59).

As a result of combining the down-regulated protein list to produce a larger 5' UTR sequence pool for analysis, the motifs found were more well defined and had lower E-values (Figure 58 - 56). The motifs identified are the same as seen in previous motif enrichment searches. These consist of a CT-rich motif, a motif with CGG repeats, a motif with GCC repeats, a motif reasonably rich in As and Ts and a GA-rich or polypurine motif. Generally, a polypurine rich motif showed the greatest enrichment in all searches.

When all down-regulated 5' UTR sequences were constrained to seven nucleotides in length, 168 polypurine motifs (Figure 55) were identified in the submitted 5' UTR sequences of down-regulated transcripts belonging to 78 unique gene IDs. When constrained to six nucleotides 98 sites were identified belonging to 47 gene IDs, three of which were not identified in the 7-nucleotide list (CHTF8, RPL32, RCC1). The 8-nucleotide motif did not belong to any new genes not already identified in the 6 and 7 nucleotide long searches.

E-value	Number of motif instances	Length of motif	Motif
$1.30x10^{-19}$	98	6	
$1.90x10^{-19}$	168	7	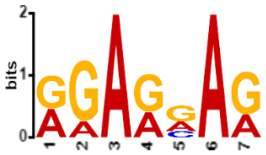
$5.8x10^{-8}$	49	7	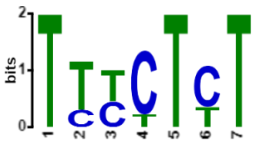
$3.40x10^{-16}$	48	8	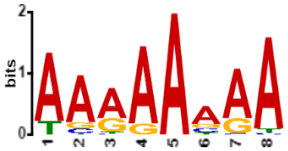
$4.00x10^{-08}$	44	8	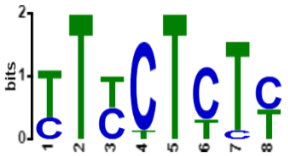
$2.20x10^{-04}$	35	8	

Figure 55. The combined down-regulated protein 5' UTR list constrained to a 6, 7 or 8 nucleotide motif length yielded two significant motifs. A total of 136 5' UTRs compiled from all proteins which were down-regulated in response to pateamine treatment were submitted into the MEME search algorithm constrained to motif lengths of 6, 7 and 8 nucleotides long independently. None of the shuffled sequences with these parameters reached the standard 0.05 significance cut-off.

When the 5' UTRs of all down-regulated proteins were analysed for motif enrichment with the maximum motif length limited to 20 nucleotides, five significant motifs were found. Some of these motifs followed the same trends as seen above with an A-rich and TC-rich motif, A GC-rich motif with a CGG repeat. Additionally, a GC-rich motif with a much stronger trend toward a GCC repeat than previously identified was found and a motif mainly consisting of purines (Figure 56).

E-value	Number of motif instances	Length of motif	Motif
9.00×10^{-43}	37	20	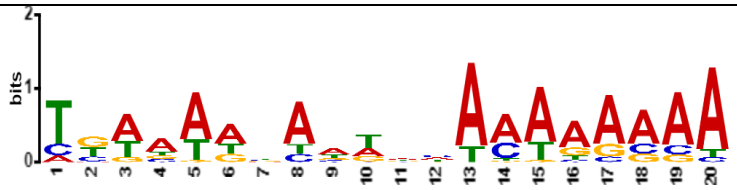
5.60×10^{-36}	79	20	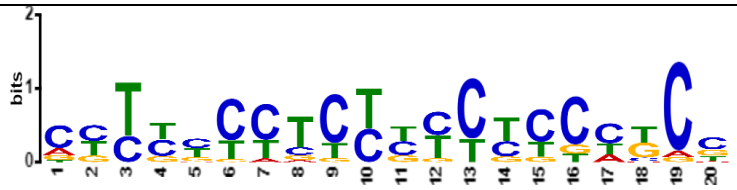
3.20×10^{-25}	49	20	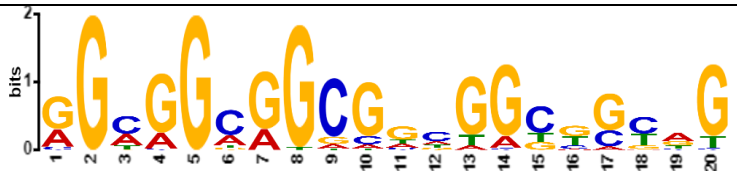
4.00×10^{-11}	25	15	
3.40×10^{-10}	51	20	

Figure 56. The combined down-regulated protein 5' UTR list constrained to a 6 - 20 nucleotide motif length yields a less well-defined GA-rich motif with a much lower e-value. A total of 136 5' UTRs compiled from all proteins which were down-regulated in response to pateamine treatment were submitted into the MEME search algorithm constrained to motif lengths between 6 and 20 nucleotides long. None of the shuffled sequences with these parameters reached the standard 0.05 significance cut-off.

When the motif enrichment analysis was limited to a maximum length of 15 nucleotides long the general trend of the motifs stayed the same. However, the GA-rich poly purine motif was much more significantly enriched with an E-value of 3.20×10^{-36}, with 75 instances found in the dataset and very low C and T frequencies (Figure 57).

E-value	Number of motif instances	Length of motif	Motif
$3.20x10^{-36}$	75	15	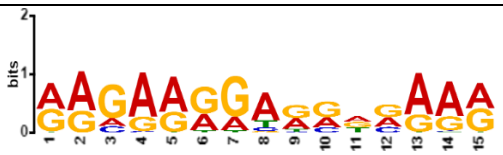
$2.60x10^{-35}$	74	15	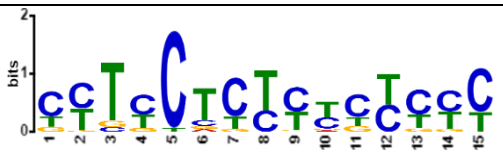
$2.50x10^{-20}$	37	15	
$7.40x10^{-08}$	30	15	
$5.10x10^{-08}$	18	15	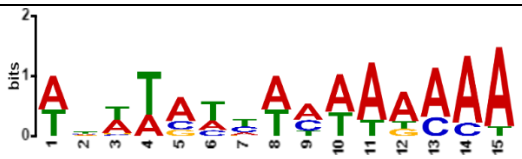

Figure 57. The combined down-regulated protein 5' UTR list constrained to a 6 - 15 nucleotide motif length yielded five significant motifs. A total of 136 5' UTRs compiled from all proteins which were down-regulated in response to pateamine treatment were submitted into the MEME search algorithm constrained to motif lengths between 6 and 15 nucleotides long. None of the shuffled sequences with these parameters reached the standard 0.05 significance cut-off.

When the motif enrichment analysis was limited to a maximum length of 10 nucleotides long four significant motifs were found. These were an AG-rich motif, a CT-rich motif, a GC-rich motif with CGG repeat, and an AT-rich motif (Figure 58).

E-value	Number of motif instances	Length of motif	Motif
$1.30x10^{-19}$	98	6	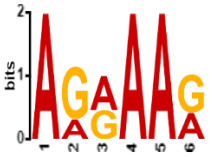
$4.00x10^{-17}$	79	10	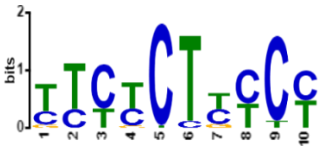
$9.40x10^{-10}$	48	10	
3.30x10^{-02}	***19***	***10***	

Figure 58. The combined down-regulated protein 5' UTR list constrained to a 6 - 10 nucleotide motif length yielded four significant motifs. A total of 136 5' UTRs compiled from all proteins which were down-regulated in response to pateamine treatment were submitted into the MEME search algorithm constrained to motif lengths between 6 and 10 nucleotides long. None of the shuffled sequences with these parameters reached the standard 0.05 significance cut-off.

3.3.6.5.2.2. Combined up-regulated 5’ UTR motif analysis

As with the 5’ UTRs of the down-regulated proteins, a combined list was made consisting of all up-regulated proteins. This list consisted of 160 5’ UTR sequences which were then used for motif enrichment analysis (Figure 60 - 62)

When searching the combined up-regulated protein 5’ UTR list constrained to exactly 6, 7 or 8 nucleotides long (Figure 59) the only motif found to be enriched was the TC-rich motif. This contrasted with the results seen from the down-regulated protein 5’ UTR list (Figure 55) which was enriched for some TC-rich motifs but also a GA-rich motif.

E-value	Number of motif instances	Length of motif	Motif
4.00×10^{-06}	**91**	**6**	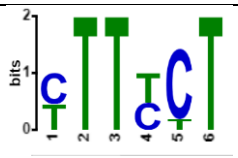
4.1×10^{-07}	**71**	**7**	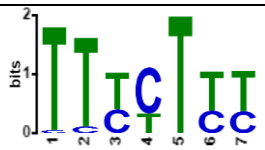
4.0×10^{-17}	**85**	**8**	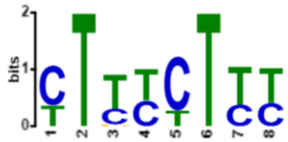

Figure 59. The combined up-regulated protein 5’ UTR list constrained to a 6, 7 or 8 nucleotide motif length showed only TC-rich motifs were significant. A total of 160 5’ UTRs compiled from all proteins which were up-regulated in response to pateamine treatment were submitted into the MEME search algorithm constrained to motif lengths of 6, 7 and 8 nucleotides long independently. None of the shuffled sequences with these parameters reached the standard 0.05 significance cut-off.

When the 5′ UTRs of all up-regulated proteins were analysed for motif enrichment with the maximum motif length limited to 20 nucleotides four significant motifs were found (Figure 60). As with the down-regulated 5′ UTR analysis a GC-rich CGG repeat motif and CT-rich motif and a GC-rich GCC repeat motif were found. A motif with A's found in select positions was also found.

E-value	Number of motif instances	Length of motif	Motif
$2.0x10^{-18}$	28	20	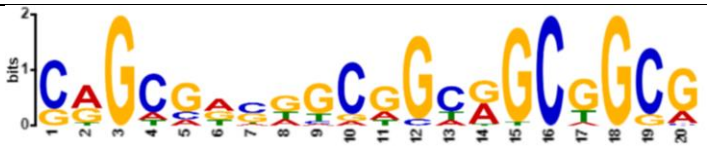
$4.0x10^{-17}$	85	8	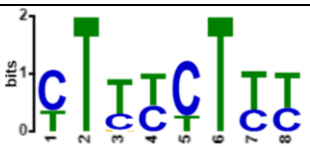
$6.8x10^{-13}$	21	15	
$2.4x10_{-09}$	33	20	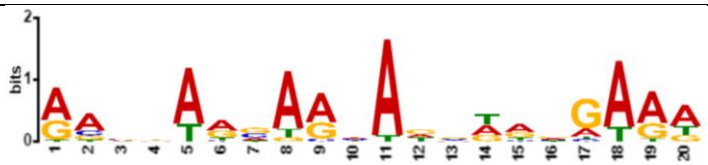

Figure 60. The combined up-regulated list constrained to a 6-20 nucleotide motif length yielded four statistically significant motifs. A total of 160 5′ UTRs compiled from all proteins which were up-regulated in response to pateamine treatment were submitted into the MEME search algorithm constrained to motif lengths between 6 and 20 nucleotides long. None of the shuffled sequences with these parameters reached the standard 0.05 significance cut-off.

When the 5′ UTRs of all up-regulated proteins were analysed for motif enrichment with the maximum motif length limited to 15 nucleotides four significant motifs were found. These motifs followed the trends seen in the 6-20 nucleotide long search with a TC-rich, a GC-rich and two motifs with A's in select positions (Figure 61).

E-value	Number of motif instances	Length of motif	Motif
$4.00x10^{-17}$	85	8	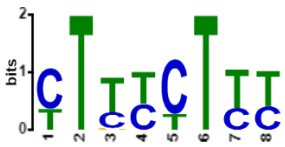
$2.00x10^{-17}$	41	14	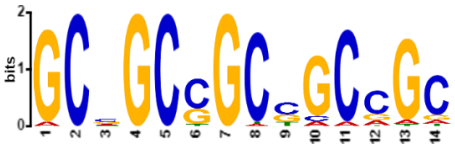
$2.90x10^{-12}$	35	15	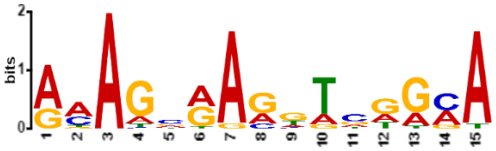
$1.0x10^{-2}$	15	15	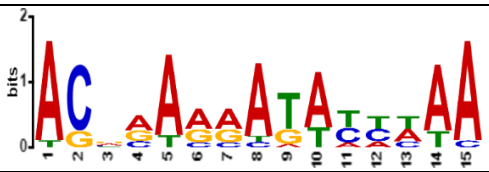

Figure 61. The combined up-regulated list constrained to 6-15 a nucleotide motif length yielded four statistically significant motifs. A total of 160 5' UTRs compiled from all proteins which were up-regulated in response to pateamine treatment were submitted into the MEME search algorithm constrained to motif lengths between 6 and 15 nucleotides long. None of the shuffled sequences with these parameters reached the standard 0.05 significance cut-off.

When the 5' UTRs of all up-regulated proteins were analysed for motif enrichment with the maximum motif length limited to 15 nucleotides only two significant motifs remained: a TC-rich motif and a GC-rich motif (Figure 62).

E-value	Number of motif instances	Length of motif	Motif
$2.40x10^{-17}$	71	10	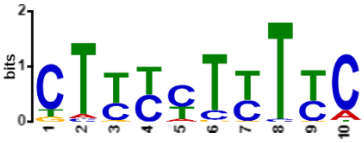
$1.20x10^{-09}$	57	10	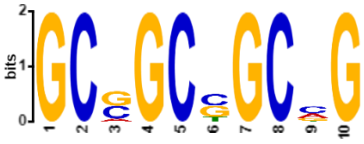

Figure 62. The combined up-regulated list constrained to a 6-10 nucleotide motif length yielded two statistically significant motifs. A total of 160 5' UTRs compiled from all proteins which were up-regulated in response to pateamine treatment were submitted into the MEME search algorithm constrained to motif lengths between 6 and 10 nucleotides long. None of the shuffled sequences with these parameters reached the standard 0.05 significance cut-off.

3.3.6.5.3. Control 5' UTR motif analysis

In order to further check the validity of the polypurine motif we had identified, we produced a randomly selected 5' UTR list obtained from the UTRdb website (Grillo et al., 2010). This list contained the same number of sequences as the combined down-regulated 5' UTR list (136) and was searched with the MEME algorithm using the same parameters (Supplementary data 23). Searches with this negative control data set showed a strong, statistically significant enrichment of a TC-rich and a GC-rich nucleotide motif. Other motifs were also found including an AG-rich motif similar to our proposed pateamine-sensitive polypurine motif. However, the motif identified did not have as consistent nucleotide frequencies, as low an E-value or have as many motif instances as were found in our combined down-regulated 5' UTR dataset.

3.3.6.5.4. Summary of the 5' UTR motif analysis

From the results from the motif analysis obtained from both the individual and the combined conditions gene lists we see five major motifs identified. Firstly, a cytosine and thymidine-rich motif was observed in both up and down gene lists. Secondly, a guanidine and cytosine-rich motif found in both up- and down-regulated transcripts, which appears to follow a sequence similar to the G-quadruplex forming sequence identified by Wolfe et al. (2014). Thirdly, a GC-rich motif with a GCC repeat similar but opposite to the G-quadruplex forming motif. Fourth, a motif consisting of predominantly adenosine and thymidine. Fifth, a GA-rich, polypurine motif. Some of these motifs appeared in both up-regulated and down-regulated gene lists with low E-values suggesting that these identifications were not identified as a result of inhibition of eIF4A with pateamine but a result of the sequences being very commonly found in mRNA 5' UTRs. However, the GA-rich polypurine motif (Figure 57) appears to be much more well defined with very low T and C frequencies, has much lower E-values and a greater number of instances in the down-regulated 5' UTR sets than GA-rich motifs identified from the up-regulated 5' UTR sets (Figure 60).

Interestingly, in some of the MEME motif identifications two purine-rich motifs are found; one with predominantly guanine nucleotides and one with predominantly adenosine. In some searches both of these motifs were determined as significant. With this considered, it is possible the inhibitory effects by pateamine are functioning similarly to RocA and inhibiting transcripts with polypurine tracts indiscriminately of whether it contains guanine or

adenosine (Iwasaki et al., 2019). If so, these two identified motifs could be considered equivalent and if combined, would possess a much lower E-value. From these results, we suspected that the GA-rich polypurine motif identified may be responsible for the decrease in expression of some of these proteins identified.

When this motif was searched for in the up-regulated 5' UTR sentences using the MEME suite FIMO algorithm (Grant et al., 2011), only 19 instances belonging to 12 unique genes were identified. This made up only 7.5% of the 160 up-regulated 5' UTRs considerably contrasting the 25.7% proportion of the 136 down-regulated 5' UTRs.

3.3.6.5.5. Investigation of the polypurine stretches

When searching for stretches of purines in the 5' UTR sequences it was noticed that many up-regulated transcripts also possessed some stretches of purines. To investigate whether longer polypurine stretches are more greatly represented in the down-regulated 5' UTRs than the up-regulated 5' UTRs all polypurine stretches in each list were identified and the length recorded. The results of both lists were then compared.

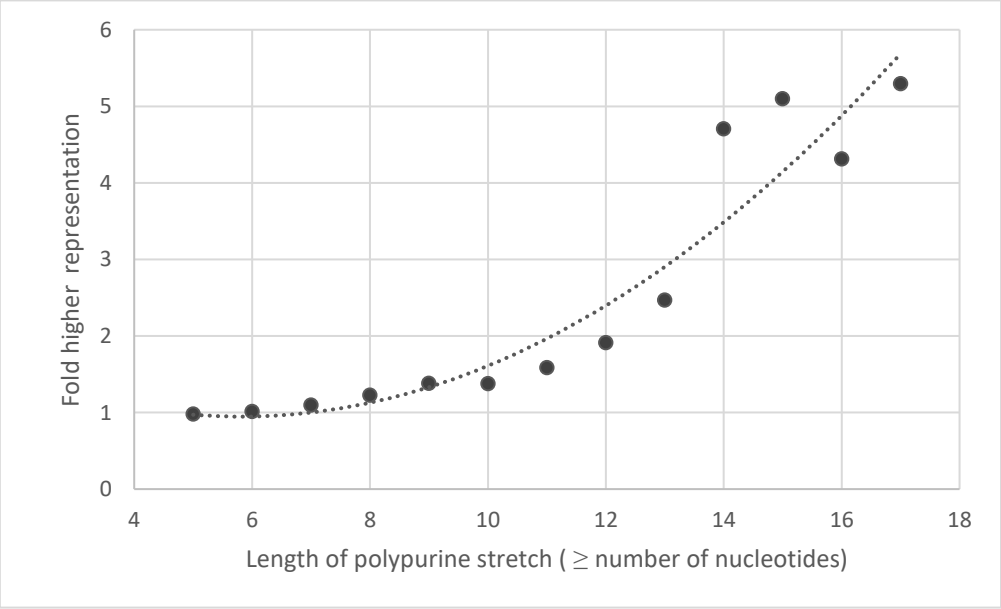

Figure 63. Longer polypurine stretches are more greatly represented in the 5' UTRs of down-regulated genes compared to up-regulated genes. The number of poly-purine stretches in the 5' UTR sequences of each length was tallied in the up and down protein lists. The number of polypurine stretches longer than a specified length in the combined down-regulated list was then divided by the corresponding number of polypurine stretches in the combined up-regulated list.

This comparative analysis showed that there were considerably more long polypurine stretches in the 5' UTRs of the down-regulated proteins compared to those of the up-regulated proteins (Figure 63). It is important to consider quite low numbers of purine

stretches are seen in both 5’ UTR lists once the stretch length is as high as 16, making the analysis of the uppermost lengths prone to variability. It is particularly noticeable that there are few polypurine motifs of length 14 or above in the up-regulated genes. This causes a steep increase in the ratio at this length and a subsequent plateau.

3.3.6.5.5.1. Polypurine distribution on the 5’ UTR

Previous reports on the inhibition of eIF4A with silvestrol indicate that the inhibition-associated motif so biases in positioning along the 5’ UTR (Wolfe et al., 2014). To investigate whether our motif data also showed a trend we took the position of each identified motif from our 7 nucleotide output from the compiled list of down-regulated genes and divided this value by the complete length of its corresponding 5’ UTR. This gave a decimal value for each motif which was then averaged, giving a value of 0.48, showing that the average position of the motif very close to the centre of the transcript. This is where the average position would be expected to be if the positioning of the motif was relatively random. This indicates that any inhibitory effects of the 7 nucleotide motif are likely to be independent of its location. To investigate this further, the 5’ UTRs were segmented into tenths and the positions of each motif was tallied and graphed (Figure 64). Although some variation between the number of motifs in each segment was seen this graph, the values are reasonably consistent with what would be expected from a random distribution.

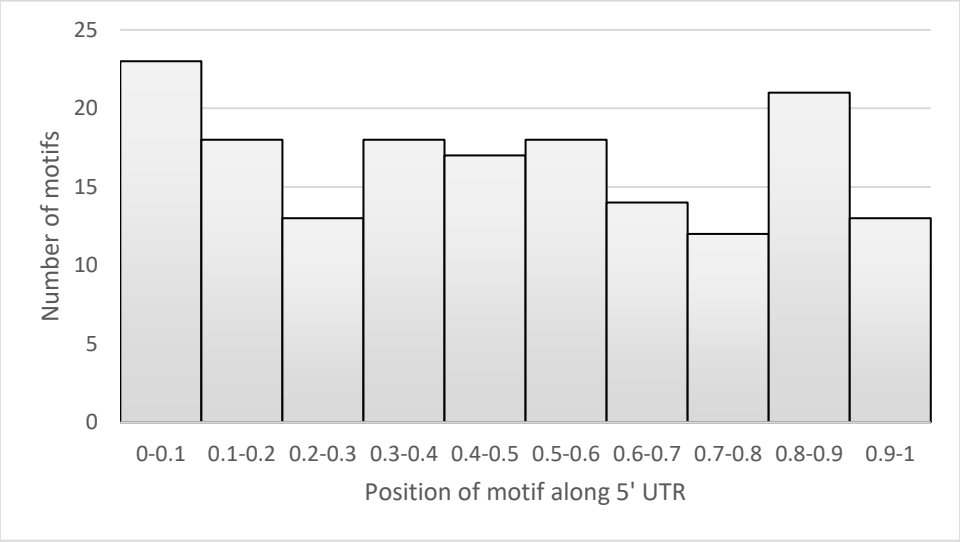

Figure 64. The distribution of identified 7 nucleotide polypurine motif identified from the combined down-regulated proteins list on the corresponding 5’ UTR. Each 5’ UTR was divided evenly into 10 sections and the number of motifs beginning in each section counted. A location value of 0 denotes the most distal position from the start codon, whereas a value of 1 denotes a position immediately prior to the start codon.

The same analysis was carried out for the 15-nucleotide long motif identified in the combined down-regulated proteins list (Figure 65). When analysing the position of the 15-nucleotide motif, along its corresponding 5' UTR the average position was found to be 0.44 suggesting a potential slight bias toward the guanine-cap.

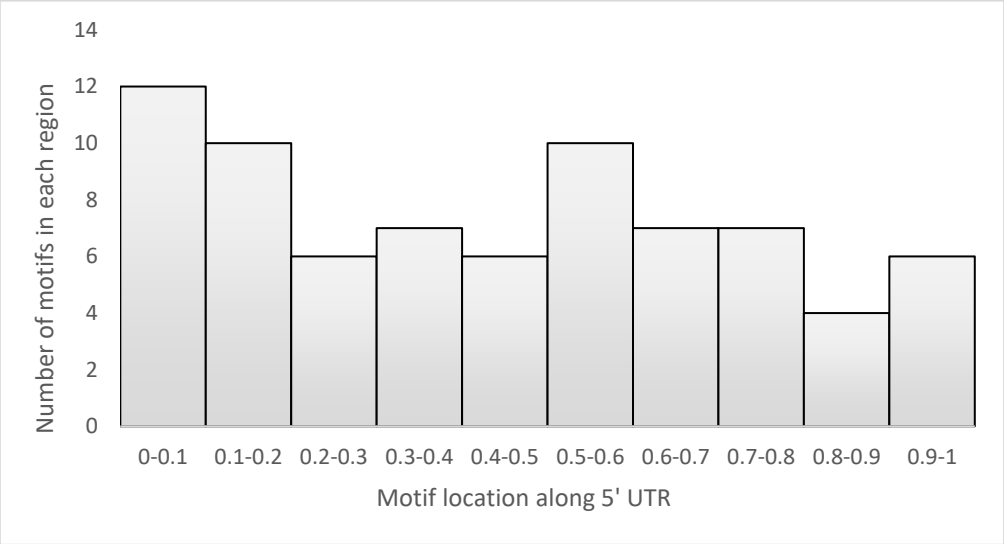

Figure 65. The distribution of identified 15 nucleotide polypurine motif from the combined down-regulated proteins list on its corresponding 5' UTR. Each 5' UTR was divided evenly into 10 sections and the number of motifs beginning in each section counted. A location value of 0 denotes the most distal position from the start codon, whereas a value of 1 denotes a position immediately prior to the start codon.

When the distributions of the 15 nucleotide motif on the 5' UTR was graphed and the 5' UTR position was binned to 0.2, this weak trend could be seen (Figure 66), suggesting there may be some bias for the motif to appear closer to the guanine-cap.

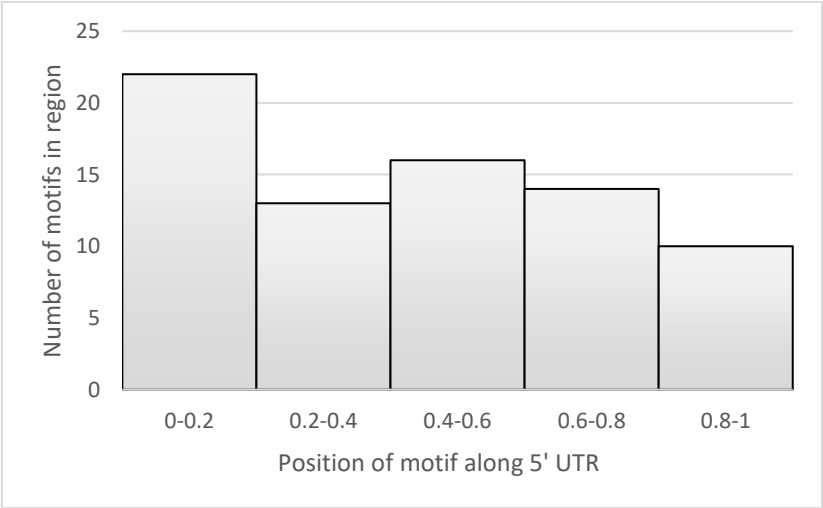

Figure 66. The 15 nucleotide polypurine motif to tends closer to guanine-cap. Binning the motif position to a range of 0.2 give a weak trend positional trend. Each 5' UTR in which MEME-identified a 15 nucleotide long polypurine motif was divided evenly into 5 sections and the number of motifs beginning in each section counted. A location value of 0 denotes the most distal position from the start codon, whereas a value of 1 denotes a position immediately prior to the start codon.

To investigate the positioning trends of the 7 and 15 nucleotide long motifs further, we graphed the relative position of each motif instance. This was done by ordering both lists based on the distance each motif instance was along the 5' UTR. Each entry in the list was assigned a number between one and zero based on its position in the list with zero representing the 5' UTR with the motif closest to the methylguanine-cap. These assigned values were then plotted against the actual distance of the motif instance from the methylguanine-cap (a number between zero and one). This analysis found a general slight trend for the 15 nucleotide long polypurine motif to be closer to the methylguanine-cap (below the average line) (Figure 67).

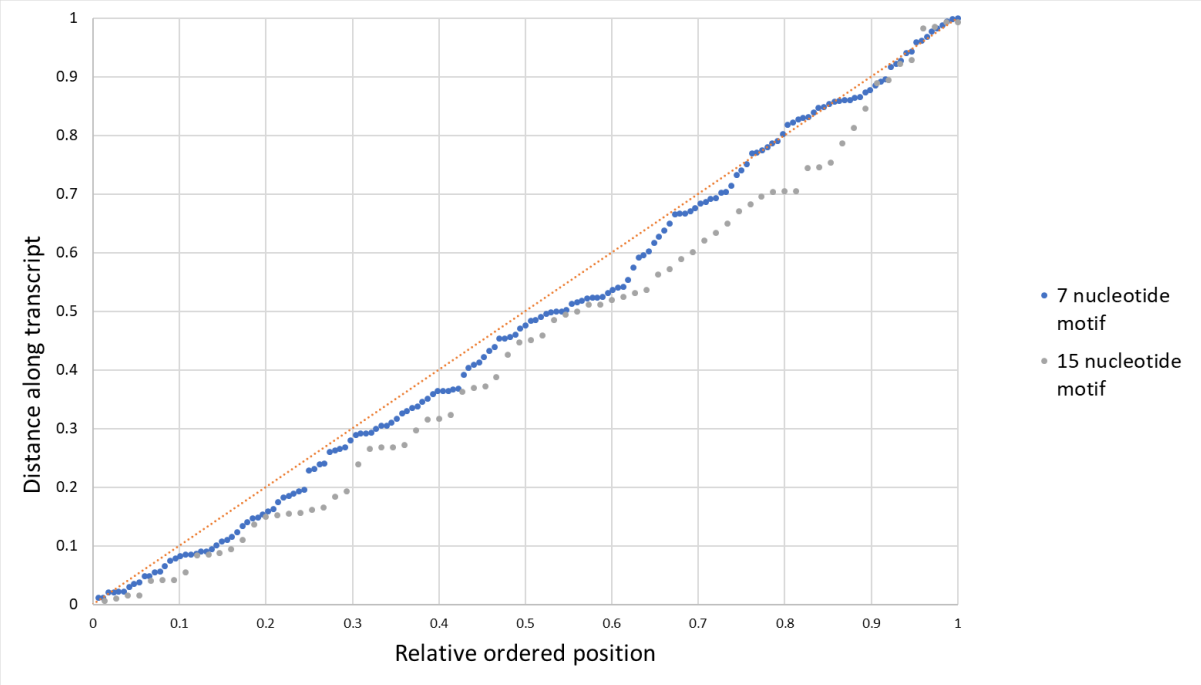

Figure 67. The 15 nucleotide motif shows a slight trend to be closer to the guanine-cap. The 7 and 15 nucleotide motif lists were ordered based on each motif's relative location along the 5' UTR and numbered between 0 and 1 based on the position in the list. The distance along the transcript was then graphed against the position in the list. A distance value of 0 denotes the most distal position from the start codon, whereas a value of 1 denotes a position immediately prior to the start codon. The red line indicates the line expected if all motifs were perfectly evenly spaced along the 5' UTR.

3.3.7. Protein half-life comparison

Maintenance of proteostasis is a balance between protein production and degradation. A protein with high production rate but also a high degradation rate may have a similar cellular abundance as one with a much slower production and degradation. For this reason, it was theorised that inhibition with pateamine may have a greater effect on the abundance of some proteins over others by changing this balance. To investigate this, published data on the half-lives of proteins from breast epithelial cells were used (Ly et al., 2018) and the half-lives of the up-regulated proteins was compared to those of the down-regulated proteins (Table 39).

To put these half-life values into context, this analysis was also performed on proteins shown to change in abundance in response to the proteasome inhibitor bortezomib (Uttenweiler-Joseph et al., 2013). When these two conditions are compared, we see a clear trend in the bortezomib data, with proteins which increase in abundance when the proteasome is inhibited having shorter half-lives. Following proteasome inhibition, these proteins are not so rapidly degraded and so increase in abundance. If pateamine was affecting proteostasis via protein production, the opposite trend would be expected. However, we do not see any notable difference between the average half-lives of the up- and down-regulated proteins.

Table 39. Average half-lives of the combined list of proteins up- and down-regulated in response to pateamine compared to bortezomib. *Protein half-lives (presented in hours) were obtained from Ly et al. (2018) of which 119/136 of our down-regulated proteins and 119/160 of our up-regulated proteins were present in the data and in the bortezomib data 31/101 of the up-regulated and 21/50 of the down-regulated proteins were present in the data.*

	Downs	Ups
Pateamine mean basal	15.37364546	15.61179
Pateamine median basal	14.2538	14.8812
Bortezomib mean basal	14.8123	11.6857
Bortezomib median basal	16.3517	10.7833

3.3.8. Western blot analysis of transcription factors

3.3.8.1. Protein detection confirmations

Protein extracts were probed using western blot analysis (Towbin et al., 1979) to quantify the expression of select proteins of interest not observed in the mass spectrometry analysis. The iNOS protein was selected for analysis as its expression has previously been shown to drop as a result of pateamine treatment (Di Marco et al., 2012). In addition to iNOS the NF-κB p65 and NF-κB p105 proteins were also investigated for their involvement in cachexia. NF-κB p105 possesses a poly-purine stretch in its 5' UTR, whereas NF-κB p65 does not. This allowed us to have a negative control to poly-purine inhibitory effects and separate them from general NK-κB system expression changes. Finally, SOX6 and GATA3 proteins were also chosen for analysis as they also possessed purine-rich stretches in their 5' UTRs.

Due to limited amounts of protein extract obtained from some pateamine treatments it was decided in some instances to treat each blot with three primary antibodies, one for the HPRT loading control and two for our proteins of interest with non-overlapping masses. In order to assess whether this was a viable strategy we needed to ensure there was no cross-reactivity of each antibody in mass regions close to another protein. To test this, an extract was run on multiple lanes of an SDS-PAGE gel and transferred to a nitrocellulose membrane. This membrane was then cut and each lane treated with a different primary antibody (Figure 68 & 69). These results confirmed that a combination of primary antibodies could be used on the same blot without interference.

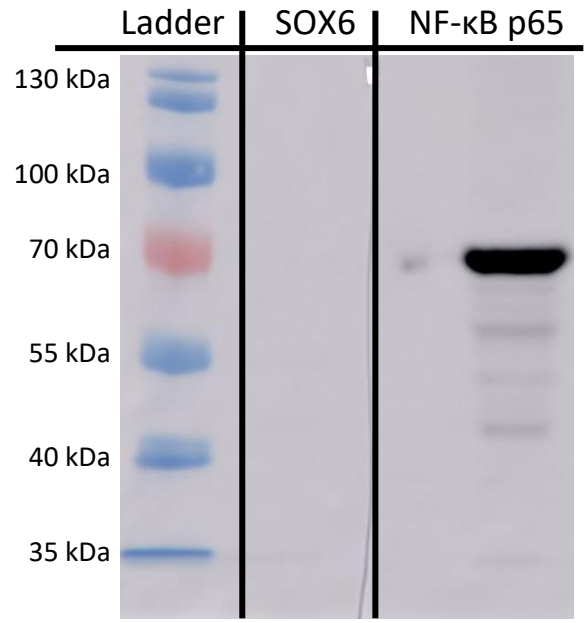

Figure 68. Primary antibodies to SOX6 and NF-κB p65 were tested against HL60 protein extracts using western blot analysis. The SOX6 primary antibody did not produce any detectable band even at longer exposures. The NF-κB p65 primary antibody produces one high intensity band at the expected size (65 kDa) and some faint smaller molecular weight bands. Whole cell protein extracts from HL60 cells were run on an SDS-PAGE gel and transferred to a nitrocellulose membrane. Lanes were then separated then blotted with anti-Sox6 or anti-NF-κB p65 antibody. Blot was exposed for 10 s.

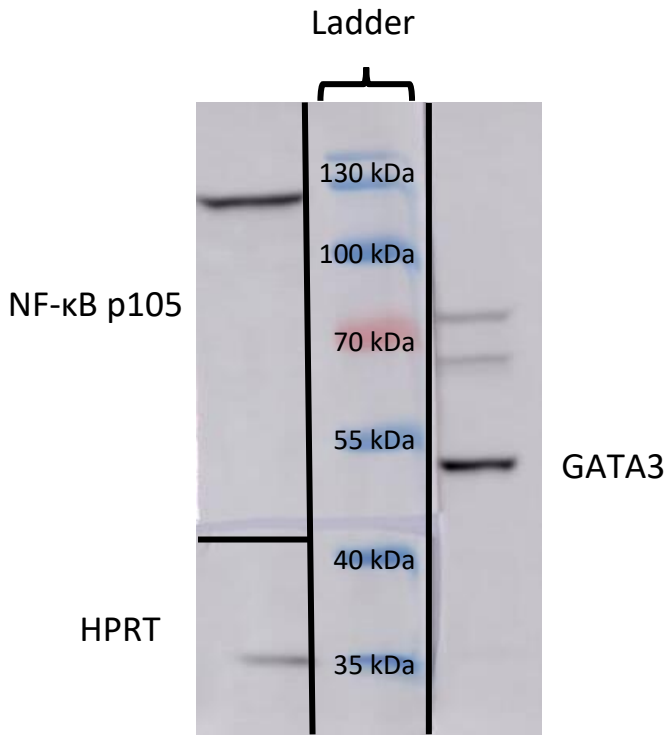

Figure 69. Primary antibodies to NF-κB p105, GATA3 and HPRT were tested against HL60 protein extracts using western blot analysis. The NF-κB p105 primary antibody (left) produced a single band at the expected molecular weight (105 kDa). The GATA3 primary antibody produced a high intensity band at the expected molecular weight (47 kDa) and two moderate intensity bands at higher masses (right). HPRT (bottom left) produced a single band at the protein front presenting as a higher mass than 20 kDa. Whole cell protein extracts from HL60 cells were run on an SDS-PAGE gel and transferred to a nitrocellulose membrane. Lanes were then separated then blotted with anti-GATA3, anti-NF-κB p105 or anti-HPRT antibodies. Blot was exposed for 1 min.

3.3.8.2. Western blot expression analysis

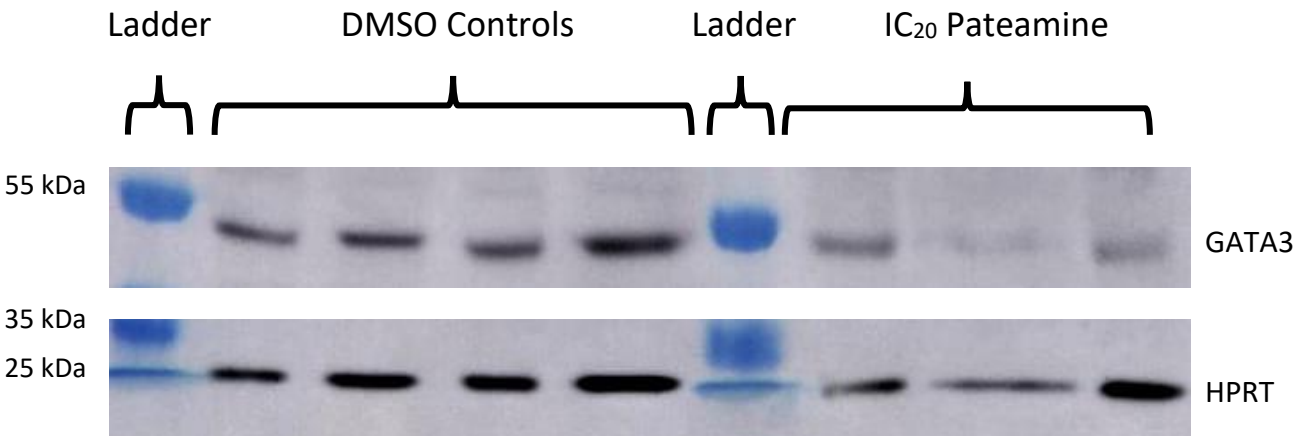

Figure 70. The first western blot analysis suggested GATA3 may be reducing in expression when treated with pateamine. DMSO control treated (left) and pateamine treated (right) cell protein extracts were analysed with SDS-PAGE and immunoblotted against GATA3.The pateamine treated extracts showed fainter bands suggesting an expression change may have occurred but showed some irregular migration and spreading in GATA3 and the HPRT loading control protein bands. Because of these migration errors GATA3 needed to be analysed with a second western blot. The blot was exposed for 20 min.

Initial western blot analysis of the GATA3 protein suggested that treatment with pateamine may be reducing its expression (Figure 70). However, the bands associated with the pateamine treated extract appeared to have spread out during migration (middle pateamine treatment band).

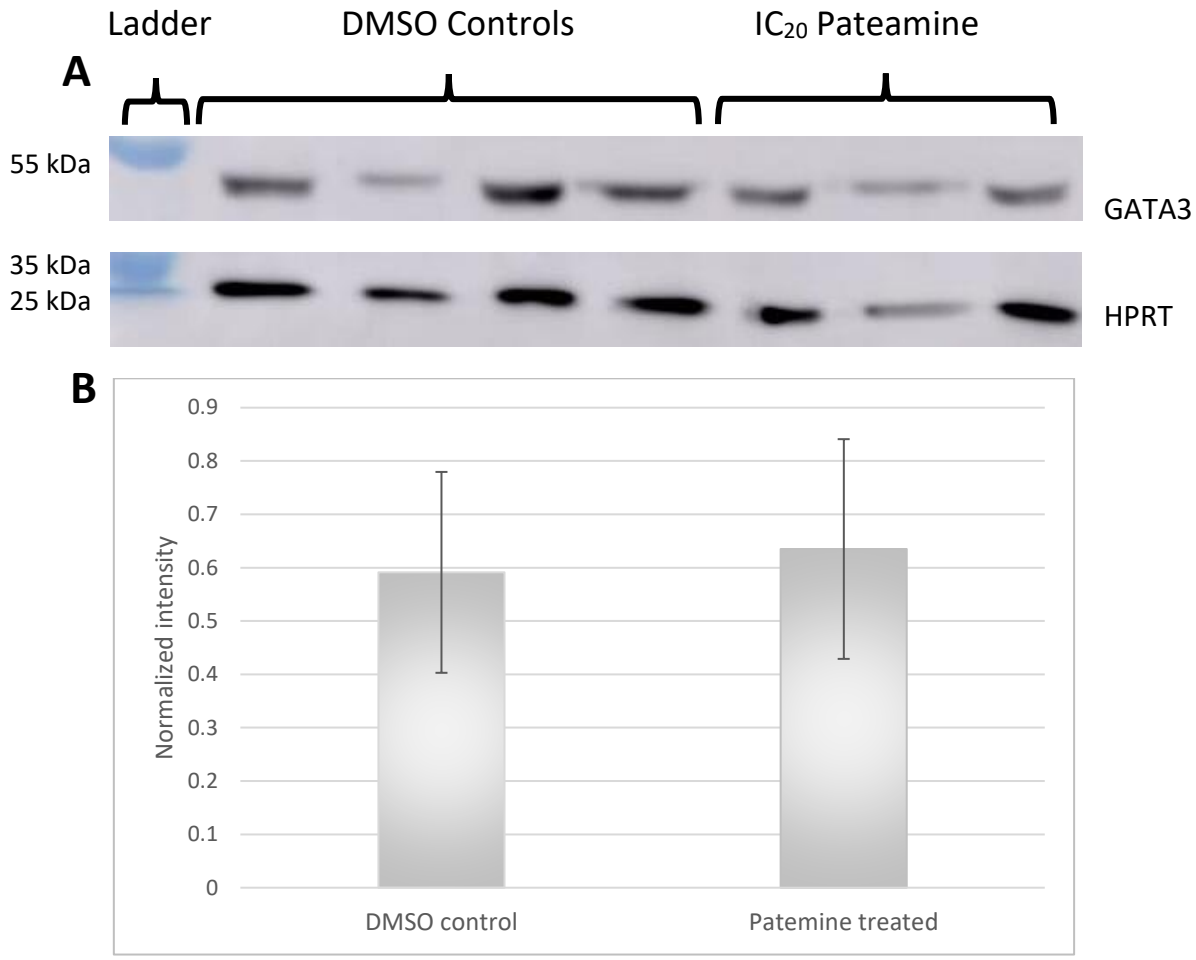

Figure 71. A second western blot showed no reduction of GATA3 when normalized to the loading control. Upper panel: DMSO control treated (left) and pateamine treated (right) cells. Cell protein extracts were separated with SDS-PAGE and immunoblotted against GATA3. The gel scan was analysed. Lower panel: when normalized against the HPRT loading control no detectable difference in expression of GATA3 was observed, suggesting the variation seen in the previous western analysis (Figure 70) was the result of migration error. Blot was exposed for 20 min. The bar graph in the lower panel was compiled from the three biological replicates and error bars denote standard deviation.

When a follow-up western blot analysis of the GATA3 protein was carried out, it was confirmed that GATA3 expression was not changing in response to pateamine treatment (Figure 71).

3.3.8.3. MTT analysis of pateamine against cells treated with PMA and LPS

Blots carried out investigating the expression of the iNOS protein gave no detectable signal. It became apparent that iNOS is expressed at low levels and was unlikely to be detected by western blot without induction. It has been previously reported that nitric oxide production can be induced in HL60 cells by treating with a combination of lipopolysaccharide (LPS) and para-methoxyamphetamine (PMA) (Rockett et al., 1998). To achieve measurable levels of expression of iNOS it was decided to carryout pateamine treatments of HL60 cells under these induction conditions for western blot analysis. However, we needed to confirm that this additional treatment did not affect the susceptibility of the cells to pateamine. For this reason, an MTT analysis was carried out with pateamine under these new conditions, revealing that the IC_{20} did not change in response to the LPS and PMA inducing conditions (Figure 72).

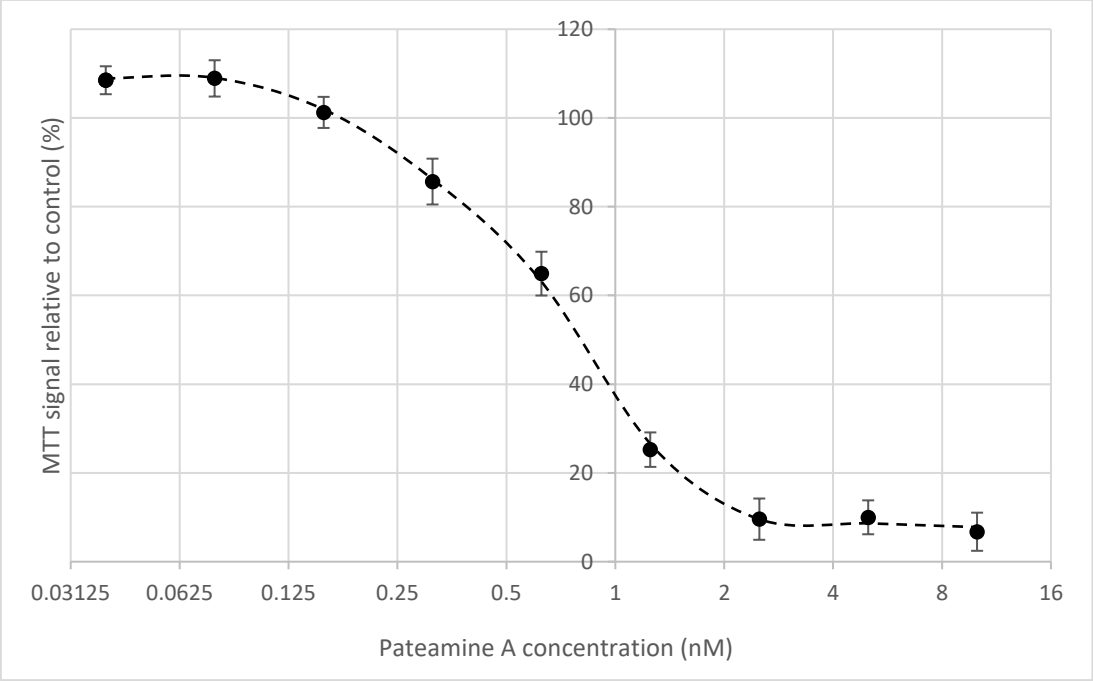

Figure 72. PMA and LPS stimulation of HL60 cells did not change the inhibitory effects of pateamine. HL60 cells were treated PMS and LPS and also with a 2-fold serial dilution of pateamine for 72 hours then tested for metabolic activity using MTT. A blank was subtracted from each absorbance value and normalized to a DMSO only control. Error bars show standard deviation. Data was obtained from at least 3 replicates repeated 2 times.

Additionally, upon treatment of the HL60 cells with PMA and LPS, the cells' morphology changed, and they became adherent appearing to have differentiated into macrophages, suggesting some protein expression changes had occurred. Having established the pateamine concentration to achieve an IC_{20} growth inhibition on the LPS and PMA induced cells, we could now carry out expression analysis on these conditions.

3.3.8.4. Western blot analysis of LPS & PMA treated cells

Under the PMA and LPS induction conditions, iNOS expression was increased to detectable levels. As shown in Figure 73, despite a slight trend of the pateamine treated samples being lower in abundance of iNOS, the difference is not large or consistent enough to suggest a genuine change in expression. It is possible that this is a genuine effect but treatment at these concentrations does not elicit a large enough response.

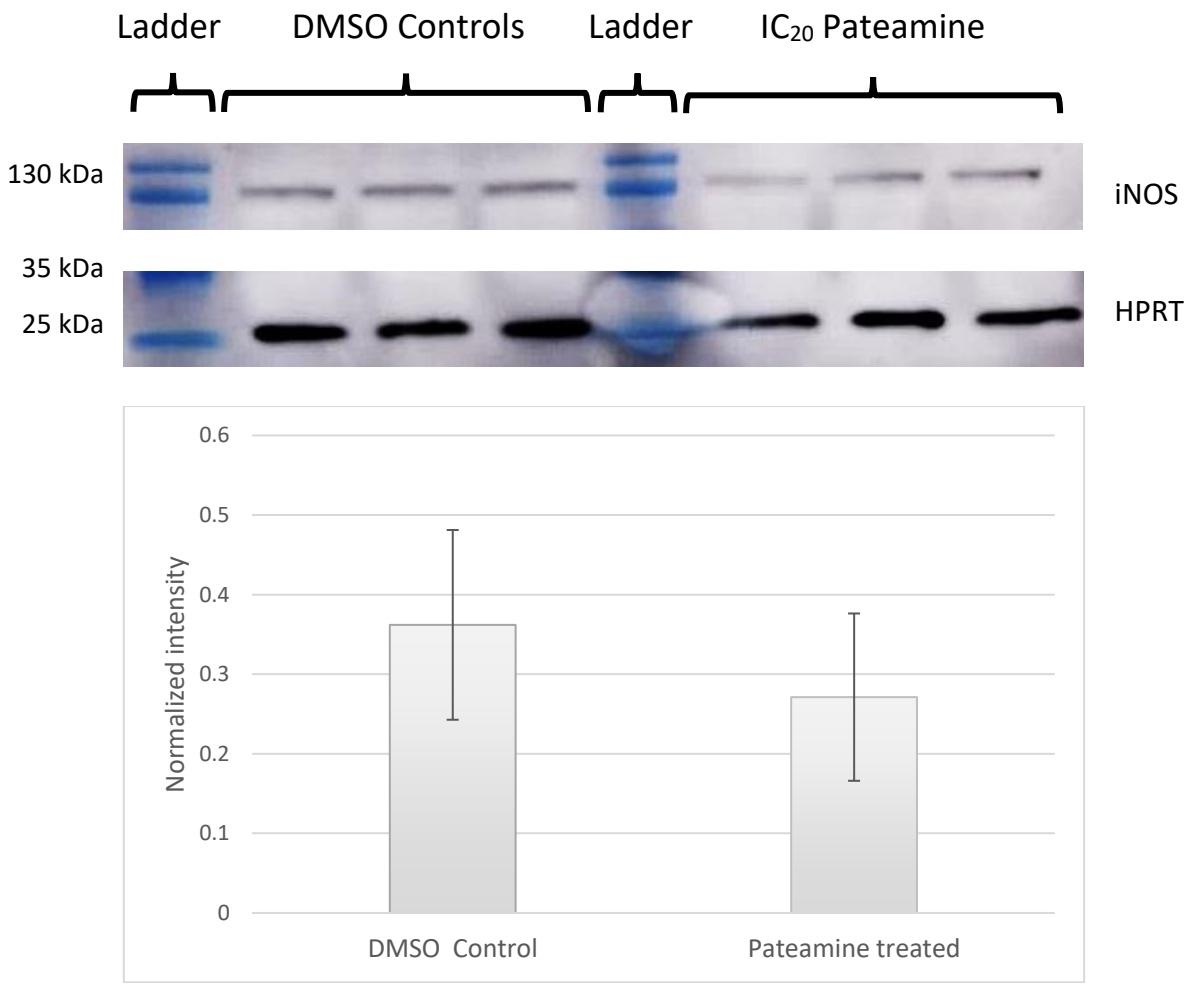

Figure 73. Pateamine treatment at IC_{20} concentrations in HL60 cells does not inhibit the expression of iNOS. Upper panel: DMSO control treated (left) and pateamine treated (right) cells were incubated with PMA and LPS to stimulate iNOS expression. Protein extracts were separated using SDS-PAGE then immunoblotted against iNOS and HPRT protein. Blot was exposed for 20 mins. Lower panel: detected iNOS bands were normalized against the HPRT housekeeping loading control. The bar graph in the lower panel was compiled from the three biological replicates and error bars denote standard deviation.

Due to a scarcity of protein extract, the expression of NF-κB in response to pateamine was also analysed with protein extracts from the PMA + LPS treated HL60 cells. We rationalised that although these induction conditions might change the global abundance of NF-κB, they would not change the tendency of pateamine to directly modulate expression through features of the transcript. Pateamine did not appear to have an effect on NF-κB p105 expression (Figure 74).

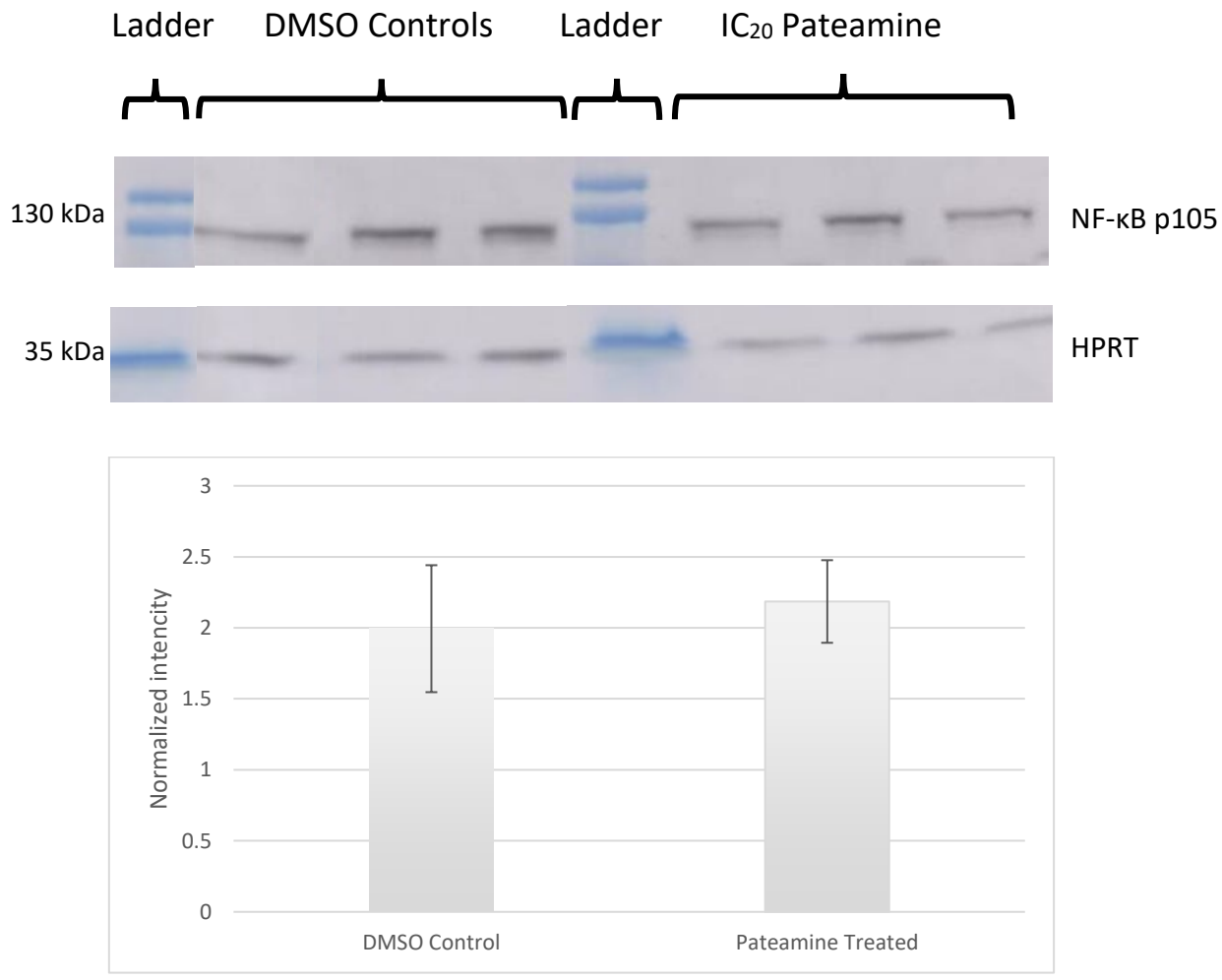

Figure 74. Expression of NF-κB p105 did not change in response to treating with pateamine. Upper panels: DMSO control treated (left) and pateamine treated (right) cell protein extracts from LPS and PMA stimulated HL60 cells were analysed with SDS-PAGE and immunoblotted against NF-κB p65, NF-κB p105 and HPRT. Blot was exposed for 1 min. Lower panel: when normalized against the HPRT loading control NF-κB p105 was found not to change in expression in the pateamine treated samples. The bar graph in the lower panel was compiled from the three biological replicates and error bars denote standard deviation.

Unexpectedly, given that pateamine is an inhibitor of translation, abundance of NF-κB p65 was higher in the pateamine treated samples. In order to confirm the expression change of NF-κB p65, a second western analysis of the protein extracts was carried out (Figure 75). This second western analysis showed a similar difference in expression as the first blot, confirming that expression of NF-kB p65 was increasing in response to pateamine treatment.

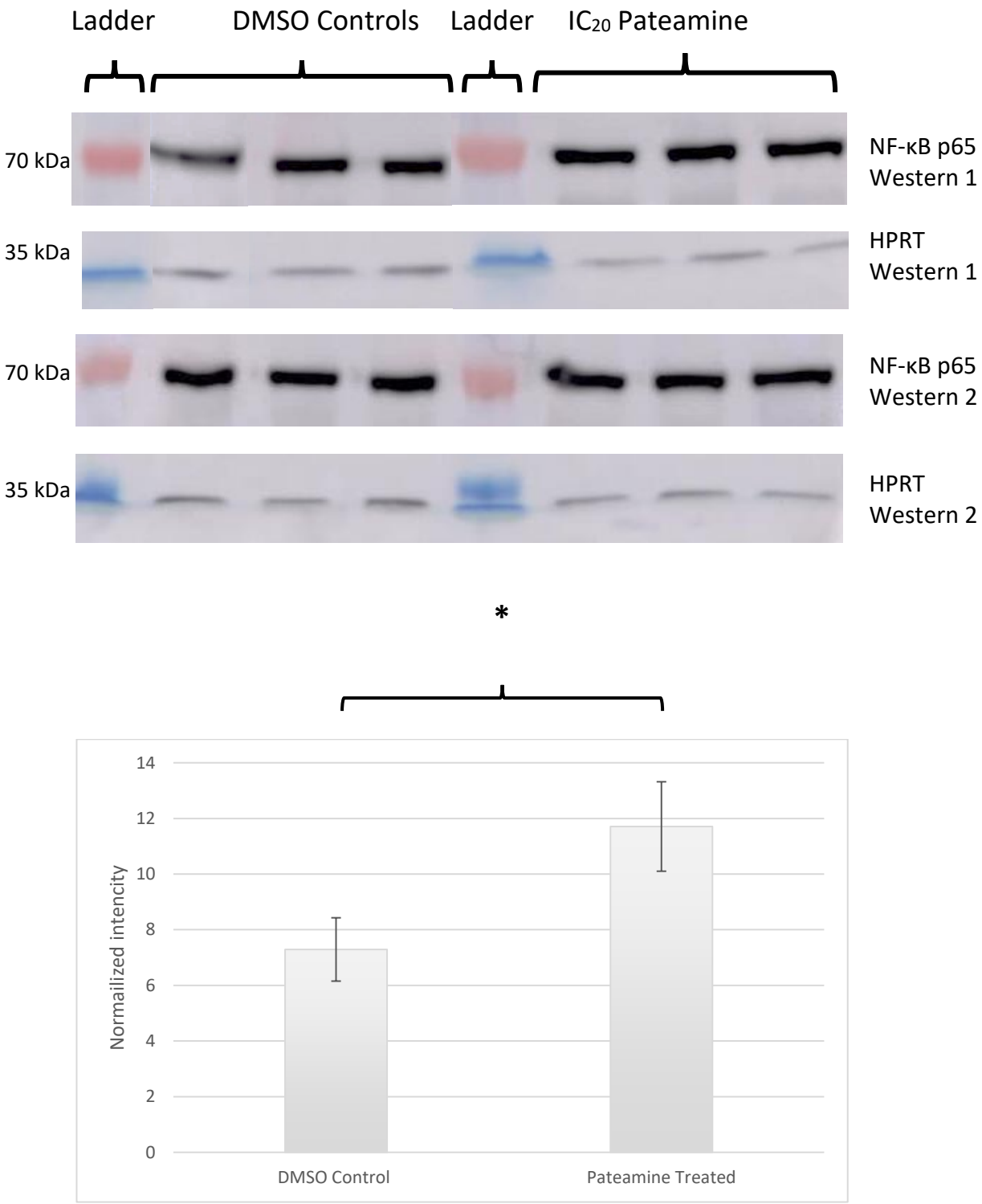

Figure 75. Expression of NF-κB p65 increases in response to treating with pateamine. Upper panels: DMSO control treated (left) and pateamine treated (right) cell protein extracts from LPS and PMA stimulated HL60 cells were separated with SDS-PAGE and immunoblotted against NF-κB p65 in two independent experiments (denoted western 1 and 2). Blot exposed for 1 min. Lower panel: when normalized to the HPRT loading control an increase in expression of NF-κB. The bar graph in the lower panel was compiled from the three biological replicates and two technical replicates and error bars denote standard deviation of the replicate experiments. $U_{statistic} < 0.01$ *determined by Mann-Whitney u test.*

3.4. Discussion

Pateamine has been identified as a potential treatment for certain forms of cancer, cachexia, viral infections, and Alzheimer's disease (Bottley et al., 2010; Di Marco et al., 2012; Parikh et al., 2012). However, translation initiation, the target of pateamine, is a fundamental pathway of all cells. Therefore, many cellular functions are likely to be affected as a result of pateamine treatment. The type and scale of the effect depends on the goal of the therapy. Therapies focused on inhibition of the expression of particular pateamine-sensitive proteins, such as for treating Alzheimer's disease, cachexia and viral infection, are likely to require reasonably low concentrations of pateamine. In contrast, the use of pateamine at sufficient concentrations to kill cells, as may be required for cancer therapies, may require much higher doses of pateamine. This higher treatment concentration will result in greater effects and is likely to cause reduced translation of additional transcripts with structure in their 5' UTRs. The aim of this study is to gain an understanding of the mechanisms underpinning the outcome of low concentration pateamine treatment.

To date, most studies have focused on treatment of eIF4A inhibitors at above IC_{50} concentrations and have identified direct effects on transcripts through, for example, ribosomal fingerprinting by Wolfe et al. which used 25 nM silvestrol compared to an IC_{50} of about 9 nM (Wolfe et al., 2014). In addition to evaluating effects at high concentrations, a number of these previous studies identified individual transcripts that were directly affected by an eIF4A inhibitor (Di Marco et al., 2012; Parikh et al., 2012) but are less informative for understanding the resultant cell-wide effects on expression. Yet studies with pateamine on cachexia have demonstrated that substantial biological responses can be observed when treating at concentrations that did not induce notable cell death (Di Marco et al., 2012). These changes may result from a profound effect on the proteome at much lower concentrations than would cause significant cell death. Treatments at these low concentrations could prove beneficial for conditions driven by aberrant expression or function of certain pateamine-sensitive proteins but less so for conditions requiring cell death such as cancer treatment.

From our proteomic expression analysis studies, we have identified a selection of cellular processes altered by pateamine treatment, even at very low levels of pateamine, and identified transcript-specific attributes which are differentially affected by pateamine under these conditions.

3.4.1. Selection of cell lines

Multiple factors were considered when selecting cell lines for this study. The HL60 cell line (a human myeloblastic leukaemia), the HT-29 (a colorectal adenocarcinoma cell line), the 1A9 (an ovarian endometrioid adenocarcinoma cell line) and three glioblastoma cell lines LN18, T98G, and the primary cell line NZG1003, were assessed. Preliminary growth curves and pateamine treatments were carried out on these cell lines to find the most appropriate line to use for the expression analysis. We found that 1A9 cell responses to pateamine were highly variable between experiments and a reliable IC_{20} and maximal sub-inhibitory concentration could not be obtained. We suspect that this was a result of the cells in the same culture having two different morphologies. We reasoned that these two morphologies likely also exhibited different protein expression profiles and as a result would not be suitable for producing meaningful outputs using mass spectrometry. The glioblastoma cell lines showed greater reproducibility in response to pateamine and were viable experimental candidates, however they exhibited slow growth rates, which was undesirable. Additionally, it is not known whether pateamine can cross the blood brain barrier, so glioblastoma may be a less relevant model should further anticancer focused experiments be planned.

Given their good growth characteristics and potential relevance as a model system, the HL60 and HT-29 cell lines were selected for carrying out follow-up proteomic analysis. Both cell lines have been used for label-free mass spectrometry expression analysis making them an appropriate cell line for this study (Nanni, 2009; Xiong, 2011). The HL60 cell line had the additional advantages as it has a history of use in pateamine studies (Bordeleau, 2005). Furthermore, being suspension cells allowed for simple and fast passaging and protein harvesting. Both cell lines also exhibited reliability and reproducibility when treated with pateamine, allowing us to establish a reliable maximum non-inhibitory and IC_{20} concentration. Additionally, the two cell lines being from different origins should result in the identification of a wider range of proteins in expression analysis. MTT analysis for the 1A9 and glioblastoma cell lines can be viewed in the supplementary data section (Supplementary data 25).

3.4.2. Selection of drug concentrations and treatment duration

As mentioned earlier (Section 1.4.5), previous studies have used high concentrations of eIF4A inhibitors to identify two motifs which lead to transcript sensitivity, Wolfe et al. (2014) for example used 25 nM silvestrol a concentration close to the IC_{100}. However, when distributed throughout the body the intercellular concentrations of drug are unlikely to be those reached in these *in vitro* experiments. Additionally, previous studies have treated for very short periods of time, 45 min for example by Wolfe et al., and as a result measure an acute response rather than identifying consequences of longer exposures to the drugs as would be seen in a clinical regimen. Our goal is to mimic the drug concentrations and treatment durations of pateamine if it was used as a clinical treatment for cachexia, viral infection, or Alzheimer's (Bottley et al., 2010; Di Marco et al., 2012; Slaine et al., 2017b). As such, we selected two low treatment concentrations of pateamine one at the maximum dose at which no growth inhibition is detectable and at 20% growth inhibition. Moreover, to mimic chronic dosing, a 72 hour exposure period was selected. Using this longer time period also gave time for the protein abundances to change as the cells would have undergone approximately two divisions. This means even proteins with long half-lives will greatly decrease in abundance if they are not being actively translated.

3.4.3. Cycloheximide control

The aim of our study was to identify specific proteins for which expression changes are disproportionately affected as a result of pateamine treatment. Treatment with pateamine is likely to affect the expression of many proteins to some extent but proteins which change relative to global protein levels will give greater insight into the effects of pateamine. It is therefore important to ensure the expression changes we are seeing are pateamine-specific and not simply a result of global translational suppression. To determine that our results were specific to pateamine, a cycloheximide treatment was also carried out to give a positive control for general protein synthesis inhibition that could be compared to our pateamine treatments. Cycloheximide is known to induce its anti-translational effects by inhibiting the translocation step of mRNA translation, a step required for the translation of all proteins equally. It therefore acts as an indiscriminate translation inhibitor (Schneider-Poetsch et al., 2010). However, biological systems are in constant flux with numerous feed-back mechanisms resulting in changes in gene expression. With this in mind, we still expected some

protein changes to occur as a result of cellular responses to the inhibition and cellular stress. Interestingly, we did not detect any significant protein expression changes on the cycloheximide controls when compared to the DMSO control when a 10 % FDR cut-off was applied. We suspect this may be a result of the low concentrations used in this study. The combination of low concentrations and the indiscriminate mode of action of cycloheximide may mean that all proteins were produced at slightly lower rates but consistently across the detected proteome. This effect would not have been seen directly as label-free mass spectrometry detects relative abundance and the amount of protein injected into the machine was normalized. Additionally, treatment at these low concentrations may be insufficient to induce a regulatory response, possibly in part due to the indiscriminate nature of cycloheximide, which keeps protein levels reduced but balanced relative to each other and not inducing direct transcript-specific effects. A substantial number of proteins are seen to change in our pateamine treatment expression experiments, this suggests that the responses observed are pateamine-specific and not simply the result of a global translational reduction.

Given that translation initiation is the most complex step of protein synthesis (Dever et al., 2016), it is also possible that perturbation of this function with pateamine affects more processes, triggering more expression changes than induced by cycloheximide.

3.4.4. Multiple test correction considerations

As mentioned above, quantitative analysis of the mass spectrometry data was carried out with the use of Scaffold analytical software. The output of this software produced a quantitative value for each sample and a t-test analysis of these values to identify a significant change. However, when a large number of proteins are identified in experiments of this sort, t-test analysis is not sufficiently statically robust to determine significant changes while limiting false positives (Noble, 2009). We initially attempted to address this issue by utilizing multiple test correction methods including Hochberg-Benjamini and Holm-Bonferroni corrections. However, these tests required levels of abundance change and low variability between replicates that were not realistic for our data set. This meant only 4 proteins in the IC_{20} pateamine HL60 experiments, none in the HL60 sub-inhibitory treatment, 2 in the HT-29 IC_{20} and 24 in the HT-29 sub-inhibitory treatment were considered to have significantly changed in abundance when using the Hochberg-Benjamini method and less using others methods. The nature of p-value calculation means it depends on the size effects, with larger

changes yielding lower p-values (Pascovici et al., 2016). In these experiments we are treating at very low inhibitory concentrations of pateamine, so effects are likely to be small for many proteins making it extremely difficult to achieve the required p-value. Pascovici et al. (2016) demonstrates this by comparing two slightly different populations with normal distributions, after multiple test correction no value was identified to be statistically different despite the two populations differing. This led to them to conclude that multiple testing corrections could be a useful tool but not an automatic requirement (Pascovici et al., 2016).

Although we decided to still carry out a multiple test correction, we selected a less stringent approach: FDR analysis using a q-value calculation (John D. Storey, 2002). This has been successfully applied to proteomic studies to avoid overly harsh multiple test corrections. This approach involves the analysis of the distribution of the t-test values of the whole dataset. From this distribution, it is possible to determine whether the p-value distribution is skewed, indicating a significant change. Using this information, a cut-off FDR can be chosen.

When analysing the protein abundance mass spectroscopy data, it was determined that an FDR of 10% would be used as few protein changes were large and consistent enough to fall below a 5% FDR cut off and this cut off has been used in previous expression studies when correcting for multiple testing (Ji et al., 2009). As a consequence of selecting this rather high FDR rate, it was important to keep in mind that a portion of these proteins may be false positives. For this reason, when carrying out analysis of these 10 % FDR protein lists, we limited the analysis to grouped analytical approaches such as gene ontology and motif enrichment analyses. These approaches were considered more robust, as false positives could be expected to be relatively randomly distributed across the proteome and so would generally only weaken any proposed statistical analysis.

3.4.5. Interpretation of ontological enrichments

When considering the up- and down-regulated proteins it was important to consider that there were likely to be various reasons why these proteins were changing in abundance. It is possible that in many cases the transcripts of these proteins were affected directly by pateamine, with pateamine treatment causing ribosomes to stall on particular regions of the 5’ UTR and sequestering the mRNAs into stress granules. However, another factor which could be contributing to expression changes is internal cellular mechanisms as a response to the translational stress induced by pateamine treatment.

Cells under stress can respond by changing the expression of a range of proteins, it would therefore be rational to expect that many of the proteins which are up- and down-regulated are the result of cellular responses to pateamine, instead of being directly affected by the drug. Given that pateamine targets eIF4AI, II & III proteins involved in translation initiation, mRNA splicing and nonsense mediated decay, we theorised that other proteins involved in these processes maybe be affected. As a response to mitigate the effects of pateamine on these processes, a cell could respond by up-regulating other proteins in these pathways in order to restore flux through the pathway. Conversely, other proteins could be down-regulated in these pathways through negative-feedback. Outside of proteins associated with translation and proteostasis, it is possible pateamine inhibition many result in some proteins in other pathways being down-regulated, resulting in a marked decrease in flux through those pathways. Linked positive or negative regulation impacting on the total proteome, for example through feedback responding to a reduction in a substrate or reduced demand for product processing.

The proteome could also be modified by secondary effects arising from the reduced expression of very select proteins which have a large effect on cellular protein level. Examples of this is transcription factors, where inhibited translation of one of these factors could have a large effect on many proteins under their control or proteolytic proteins that are more greatly required for homeostasis of proteins with a high turnover rate.

An additional effect which could be affecting the expression of some up-regulated proteins is the cellular availability of ribosomes. Inhibiting translation initiation of some transcripts will result in a drop in occupancy of ribosomes as they will no longer be occupied by these pateamine sensitive transcripts. As a result, translation of other transcripts can now progress at a higher rate. This effect, however, is not expected to have a major effect in our experiments as we only treated with very low doses so only a small proportion of cellular ribosomes will be freed up so demand will not greatly change.

These complex molecular pathways make prediction of overall responses difficult as proteomic expression is the result of the culmination of many of these pathways having both synergistic and interfering effects. Investigating these changing proteins with gene ontology enrichment analysis allows us to tease out trends in this data.

3.4.5.1. Proteasomal proteins

When carrying out string analysis on the combined up-regulated proteins list a cluster of 8 proteins were identified which were associated with proteasomal activity. Additionally, a statistical enrichment of proteasomal proteins was also observed in the combined up- and down-regulated protein GO enrichment analysis, with a p-value of 1.470×10^{-6} from 11 proteins. This demonstrates that pateamine treatment is perturbing normal protein degradation. To investigate this effect further our up-regulated proteins list was compared against studies investigating expression changes as a result of proteasomal inhibitor treatment. The proteome response from treatment with the proteasome inhibitor bortezomib was investigated by Uttenweiler-Joseph et al. in the NB4 cell line (Uttenweiler-Joseph et al., 2013). In that study, 130 proteins were seen to go up in abundance. When compared against our combined up-regulated proteins list only 5 proteins responded similarly to pateamine and bortezimib, being present in both data sets (ANXA2, EIF3C, PA2G4, SF3B2 and SRRT). When carrying out GO enrichment analysis of the bortezimib and pateamine up-regulated proteins alongside each other, both had a remarkable 76 GO biological process statistical enrichments in common. Some of the lowest p value matches between the two inhibitor treatments included mRNA metabolic process ($2.07x10^{-12}$, $1.11x10^{-19}$), translation ($1.37x10^{-08}$, $1.93x10^{-12}$), protein folding ($5.63457x10^{-06}$, $7.40x10^{-14}$), posttranscriptional regulation of gene expression ($1.19x10^{-13}$, $9.11x10^{-08}$), and viral process ($1.94205x10^{-07}$, $8.09x10^{-15}$) (bortezomib, pateamine respectively) (Supplementary data 27). Subtraction of the proteins linked to the GO terms identified in both pateamine and bortezomib led to the identification of a total of only 19 proteins not associated with any of these processes. This high degree of similarity between the two GO enrichments suggests, at these low concentrations, pateamine treatment has a major effect on the protein degradation pathway. It is possible pateamine may cause a loss of a key proteasomal protein, either directly or by inhibiting production of transcription factors, highlighting unexpected avenue for impact of pateamine treatment on the proteome. However, pateamine treatment does not appear to increase the abundance of proteins with shorter half-lives (Table 39), casting some doubt on this possible mechanism.

It is possible that the concentrations of pateamine used in this study only mildly inhibited the production of a proteasome-related proteins. This could have led to regulatory expression

changes, remedying the effects on the pathway resulting in no overall effect on protein degradation. Alternatively, as a result of pateamine induced changes in translation, some higher tier monitors of proteostasis may be activated which react similarly when either function being inhibited. This could explain why a proteasome inhibitor induces expression changes relating to mRNA metabolism, translation, and gene expression as much as a translation inhibitor links to proteasomal function. It is not clear if either of these effects is responsible for the actions of pateamine in low treatment conditions, as envisaged for cachexia and antiviral work. Future work will need to be undertaken to tease these details out.

This same effect was not observed when comparing our down-regulated list of proteins with bortezomib treated down-regulated proteins. Analysis yielded only 2 proteins common to both drug treatments and only 2 biological process ontologies in common when comparing GO enrichment analyses between the two inhibitors, both with much higher p-values.

3.4.5.2. Translation associated proteins

As might be expected many proteins involved in translation were observed to undergo a change in expression as a result of pateamine treatment. It is well established that pateamine inhibits the translation initiation factors eIF4AI & II which are involved in translation initiation. It is reasonable to expect that when translation initiation is inhibited certain feedback loops will be activated in the cell. This could result in an up-regulation and expression of proteins relating to translation attempting to ramp up translation and counteract the effect of the inhibitor. Conversely, by inhibiting translation initiation many downstream enzymes may no longer be active due to their target substrates not being present and upstream enzymes may no longer have the same demands for their products. This could result in down-regulation of these proteins as they are not required at the same levels of abundance. In our data we find enrichments relating to translation in both our up- and down-regulated proteins suggesting that both these feedback mechanisms are occurring.

3.4.5.3. mRNA metabolism proteins

In addition to inhibiting eIF4AI & II pateamine has been shown to inhibit eIF4AIII (Dang et al., 2009). As described in Section 1.4.2, the eIF4AIII protein acts as an anchoring protein that clamps onto pre-mRNAs holding the exon junction complex in place and is involved in non-sense mediated decay (Dang et al., 2009; Karousis et al., 2016). When analysing the proteins identified to have changed in expression mRNA splicing was statistically enriched in both the up- and down-regulated proteins (1.192×10^{-2} and 1.125×10^{-8} respectively). Showing that this pathway is being affected by pateamine treatment. Interestingly, proteins involved in nonsense mediated decay were also enriched but only in the up-regulated proteins (1.160×10^{-8}), with the down-regulated list failing to reach significance despite containing 11 proteins linked to this process. As described in Section 1.5.3, the eIF4A inhibitor hippuristanol has been shown to reduce the expression of the Alzheimer's disease associated proteins Tau and amyloid-β precursor protein (Bottley et al., 2010). Research on proteomic expression analysis with Alzheimer's disease model cell lines has also implicated dysregulation of spliceosome proteins (Nuzzo et al., 2017). When the Alzheimer's disease model was induced with the use of recombinant amyloid-β precursor protein, a marked decrease in expression of spliceosome proteins was observed (Nuzzo et al., 2017). The effects of pateamine on the spliceosome appear to be complex, with some components reducing in expression while others increase. As such, it is difficult to predict the outcomes of pateamine treatment on the spliceosome as a therapeutic strategy for Alzheimer's and further investigations would be needed.

Interestingly, ontologies relating to mRNA metabolism and splicing are also found to be enriched in the proteins found to change in abundance as a result of treatment with bortezimib (Uttenweiler-Joseph et al., 2013). The similarity of these datasets suggests this may be part of some sort of proteostatic control mechanism. An enrichment in nonsense-mediated decay however, it not seen in the bortezimib data set suggesting pateamine is inhibiting this pathway directly.

3.4.5.4. Nonsense mediated decay proteins

As mentioned above pateamine also inhibits eIF4AIII. In addition to being involved in mRNA splicing, eIF4AIII is also involved in nonsense mediated decay. This process serves to mitigate negative effects erroneous of mRNAs that contain a premature stop codon by inducing degradation of the transcript (Karousis et al., 2016). In our data we see an enrichment in ontologies relating to nonsense mediated decay in both our up and down-regulated protein lists. We were not surprised to see expression changes in this pathway as it is known to be directly affected by pateamine and the cell is likely to undergo regulatory changes to compensate.

3.4.5.5. Telomere-related proteins

An unexpected enrichment was also found relating to telomere maintenance. Although telomere associated proteins are regularly seen in our up-regulated proteins lists, the reasons for this enrichment are unclear. It is possible that pateamine directly inhibits the translation of a telomere maintenance protein or transcription factor leading to further expression changes in this pathway.

3.4.5.6. Summary of ontological enrichments

Taken together the ontological enrichment trends show that pateamine treatment is having a major effect on the protein synthesis pathway and supportive processes (Figure 76). Additionally, a number of processes which aren't directly involved in protein synthesis are also enriched. Many of the enrichments seen are not exclusive to the up- or down-regulated proteins lists, suggesting the responses are complex and highly dynamic (Figure 76).

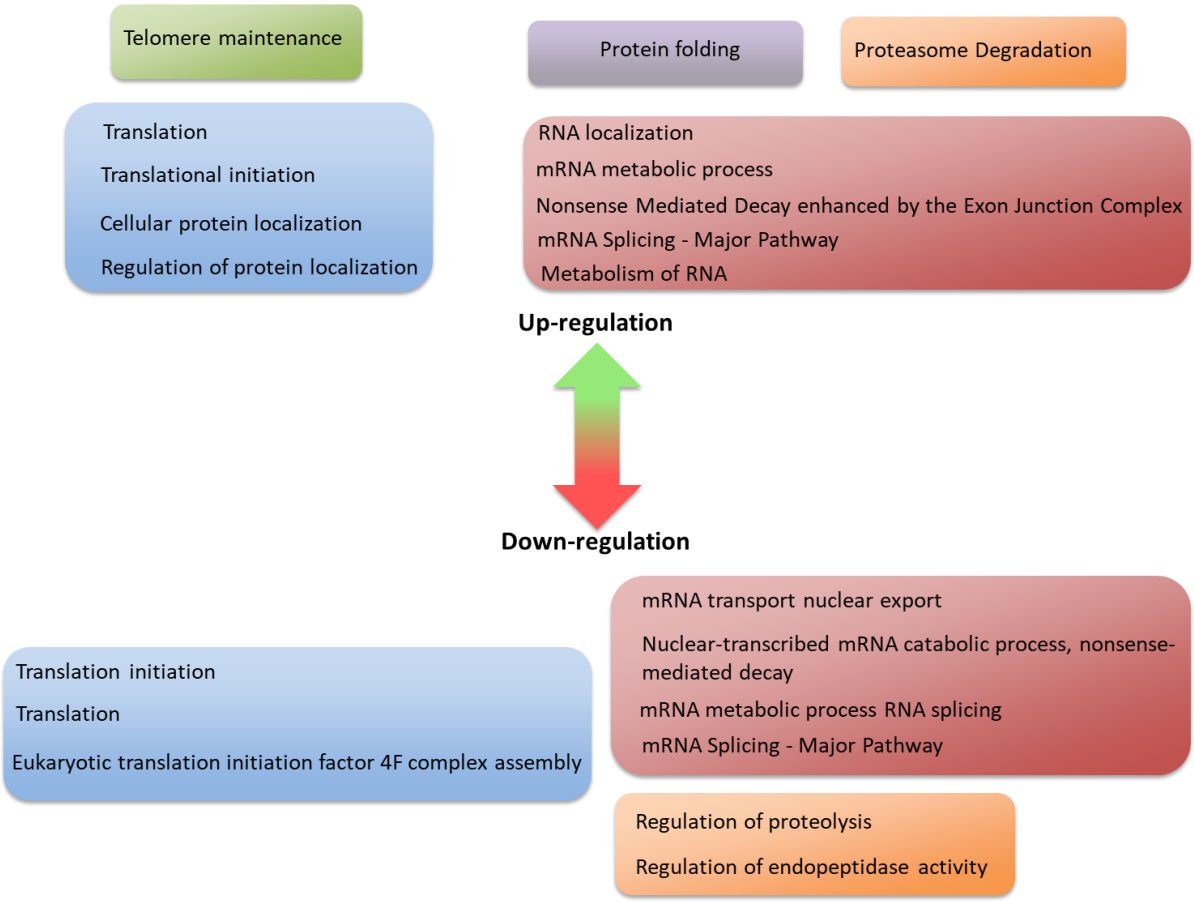

Figure 76. Human pateamine treatment protein abundance change enriched ontologies summary. Ontologies found in the up-regulated protein lists (top) and ontologies found in the down-regulated protein lists (bottom). Ontological enrichments are grouped in terms relating to: mRNA processing, protein degradation, translation and translation initiation, telomere maintenance and protein folding.

3.4.6. Hippuristanol versus pateamine A

Superoxide dismutase 1 (SOD1) and thioredoxin (TXN) are two proteins which have been identified to have to be unaffected by expression changes induced by the eIF4A inhibitor hippuristanol (Bottley et al., 2010). SOD1 is an enzyme involved in the detoxification of free superoxide radicals whereas TXN is known to be involved in a range of different redox reactions (Che et al., 2016; Matsuzawa, 2017). Both of these proteins have been identified to have potential neuroprotective properties (Iadecola et al., 1999; Masutani et al., 2004). When investigating the effects of hippuristanol on Alzheimer's disease model cells, Bottley et al. (2010) determined that hippuristanol treatment caused an increase in polysomes associating to the mRNAs of SOD1 and TXN. However, expression of TXN and SOD1 protein was unchanged as a result of hippuristanol treatment (Bottley et al., 2010). In contrast, from our proteomic expression data, both SOD1 and TXN proteins had significantly reduced expression

when HL60 cells were treated with IC_{20} concentrations of pateamine (0.27-fold change, p=0.00019; 0.18-fold change, p=0.0061 respectively (TIC)) (Supplementary data 11).

The mechanisms of pateamine and hippuristanol inhibition of eIF4A are known to differ (Dang et al., 2009; Lindqvist et al., 2008). Hippuristanol is known to prevent eIF4A from binding to transcripts (Lindqvist et al., 2008), whereas pateamine enhances the RNA binding and ATPase activity (Dang et al., 2009). The 5' UTR sequences of the SOD1 and TXN mRNA transcripts are relatively short (148 nucleotides and 63 nucleotides, respectively) and neither contain any long polypurine stretches in their 5' UTRs, making the reason for their down-regulation in our data unclear. Whilst these differences might be explained by differences in cell type, these expression changes in our data could suggest that inhibition of eIF4A with these two different inhibitors is not equivalent and these different modes of action may cause very different effects on global protein expression levels. Additionally, pateamine is known to inhibit eIF4AIII whereas hippuristanol is far less potent at inhibiting eIF4AIII when compared to eIF4AI & II (Lindqvist et al., 2008). This highlights another possible reason for differential effects between the two compounds. Although it is difficult to determine a direct link between exon junction complex function and SOD1 and TXN it is possible some follow-on responses or a link to the transcription factors responsible for their expression may be involved.

This difference in expression casts some doubt on whether pateamine could be a useful drug for the treatment of Alzheimer's disease. When analysing hippuristanol-induced expression changes, Bottley et al. (2010) determined that amyloid precursor protein and Tau both decreased in expression while SOD1, TXN and NDUFB2 expression was unaffected (Bottley et al., 2010). This meant that disease causing proteins were reduced while neuro-protective proteins were unchanged. Unfortunately, neither amyloid precursor protein nor Tau were identified in our proteomic data for comparison. However, the reduction in abundance of SOD1 and TXN suggests some neuroprotective effects will also be lost, possibly to the detriment of treatment outcomes.

3.4.7. Features of the 5’ UTR

The goal of our research is to investigate the effects of low concentrations of pateamine at levels that general protein translation is not inhibited. At these concentrations it was not clear whether we would see changes in expression of proteins with longer or structured 5’ UTRs, or 5’ UTRs with specific nucleotide sequences.

3.4.7.1. Interpretation of 5’ UTR length analysis

As previously reported, the length of the 5’ UTR on an mRNA transcript can influence its expression when eIF4A is being inhibited by small molecules (Iwasaki et al., 2016; Wolfe et al., 2014). For example, the translation of mRNA transcripts with longer 5’ UTRs is more greatly inhibited by high concentration treatments of rocaglamide A, with this effect not being the result of 5’ UTR structure stability (Iwasaki et al., 2016). It is possible that longer 5’ UTRs contain greater abundance of sequences susceptible to rocaglamide A, such as the reported polypurine motif (Iwasaki et al., 2016). When investigating the 5’ UTRs of the up- and down-regulated proteins in my study, this trend towards longer 5’ UTRs was not observed. It is likely this is result of the low concentrations of pateamine being used falling below a threshold as which these effects are seen. As described in Section 3.1.4, the intent of this study is to treat at low pateamine concentrations to identify low dose effects, meaning there is still abundant active eIF4A present to carry out normal transcript unwinding.

3.4.7.2. Interpretation of GC content analysis

As explained in Section 1.4.4 and illustrated in Figure 10, we suspected that inhibition by pateamine of expression of a protein possessing a highly structured 5’ UTR in its mRNA, relies on depletion of active cellular eIF4A. This would result from there no longer being sufficient functional eIF4A to unwind the 5’ UTR. No difference in GC content of the 5’ UTRs of up- or down-regulated proteins was identified with a mean content of 65.1% in the up-regulated and 65.7% in the down-regulated 5’ UTR list (See Section 3.3.6.3). Interestingly, these values are much higher than the mean human genome GC content of 41% (Lander et al., 2001) but is normal for human 5’ UTRs with the average 5’ UTR possessing a GC content greater than 60% (Zhang et al., 2004). The GC content being much higher in 5’ UTRs compared to the rest of the genome suggests a functional purpose. High GC content in 5’ UTRs has been corelated to reduced expression (Pelletier and Sonenberg, 1985) and it is believed this is the result of the 5’ UTRs being more stable, having a greater need for unwinding to be expressed. Not

seeing a difference in GC content of transcript 5' UTRs between our up- and down-regulated proteins suggests that at the concentrations of pateamine used in this study sufficient uninhibited eIF4A is still present to resolve secondary structure.

3.4.7.3. Interpretation of enriched motifs

As described in the results (Section 3.3.6.5.4), four major motifs were identified in our data. Three of these motifs, a TC and TA-rich motif and a GC-rich motif similar to the G-quadruplex motif identified by Wolfe et al. (2014), were observed to be statistically enriched in many of both our up- and down-regulated 5' UTR sequences. The fourth motif, a GA-rich polypurine motif was far more enriched in the down-regulated 5' UTR list and resembles the purine-rich stretch identified by Iwasaki et al. (2016) with the down-regulated 5' UTRs tending to have longer stretches of purines.

3.4.7.3.1. Technical aspects of the motif analysis

As with gene ontology analysis, motif enrichment analysis relies on a statistical background model. When carryout out motif enrichment searches with the MEME web tool, it is recommended that in addition to carrying out the standard searches some searches are carried out with shuffled sequences (Bailey et al., 2009). These shuffled sequences retain the nucleotide frequencies and size of the original data set but with the specific sequences randomized. This is done to gain a measure of the basal statistics of the dataset and allows us to confirm that the statistical E-values were the result of enriched motifs and not the composition and length of the dataset or search parameters. These were carried out and were a useful tool to check the standard significance cut-off value of 0.05. However, completely randomised sequence would not serve alone as an effective background. Although 5' UTRs are not actively translated they still contain a range of conserved features with functional significance (Araujo et al., 2012). These motifs can occur at a high frequency in 5' UTRs meaning that motif enrichment searches carried out without considering these will lead to identification of false positives. We addressed this, by also carrying out searches on a randomly selected 5' UTR list as described in Section 3.3.6.5.3.

Another influence on the motif analysis was that the search algorithm seemed to have some bias toward longer motifs, even if the longer motif had a higher E-values. For this reason, multiple searches were carried out with the maximum motif length constrained to various values. Additionally, during the course of this study Iwasaki et al. published a paper identifying

a polypurine motif which induced a tight binding of eIF4A to the transcript when inhibited by rocaglamide A (Iwasaki et al., 2016; Iwasaki et al., 2019). This binding effect may also occur when eIF4A is inhibited by pateamine, so a motif of a similar length could be involved. The number of motifs to find was also increased as the algorithm often did not find the lowest E-value motifs first. Additionally, when considering the settings to use for the motif enrichment searches, it was thought a transcript possessing more than one instance of a motif that causes a pateamine sensitivity should only serve to enhance its effect on expression. For this reason, the any number of repeats option was selected when carrying out the analysis.

3.4.7.3.2. Interpretation of the TC-rich motif

Motif enrichment analysis identified a TC-rich motif in both the up- and down-regulated protein 5' UTR sequence list (Figure 46 & 48 among others) Given that this motif was seen in the 5' UTRs in the mRNA of both up- and down-regulated proteins at very low E-values this sequence was not suspected to be sensitive to pateamine treatment. However, appearing in our analysis at such high significance suggested the motif was of functional significance. An example of a functional motif of this sort is the terminal oligopyrimidine tract. This is a regulatory element found in the 5' UTRs of some mRNAs. The element consists of a starting cytidine, which is then followed by a stretch of 5 to 15 pyrimidines (Caldarola et al., 2004). This element is commonly found in mRNAs coding for proteins involved in translation elongation and the ribosome (Caldarola et al., 2004). Finding a polypyrimidine tract as common throughout the 5' UTRs of pateamine-regulated proteins suggests a possible similar function, however it should be noted that the polypyrimidine tracts found in this study are not limited to the 5' UTR terminus. Part of this motif's functions may be to form interactions with proteins. One such protein known to interact with polypyrimidine stretches is polypyrimidine tract-binding protein (PTB) which functions as an mRNA splicing regulator (Clower et al., 2010). Binding of this or other proteins to the mRNA may also explain why this motif is seen as such high frequencies.

3.4.7.3.3. Interpretation of the TA-rich motif

In some of the motif searches a TA-rich motif is also identified. This is the least significant of the motifs and found in only a subset of searches. This motif is identified in both the up- and down-regulated protein 5' UTRs and it is currently unclear what functional role this sequence may have.

3.4.7.3.4. Interpretation of the GC-rich motif

Motif enrichment analysis of our pateamine-induced expression change 5' UTR sequences also yielded a repeating GC-rich motif consisting of one cytosine followed by two guanines. This motif has a strong resemblance to the motif identified by Wolfe et al proposed to form G-quadruplex structures. As described in Section 1.4.5, G-quadruplexes are highly stable RNA structures which form as a result of Hoogsteen base pairing between guanine nucleotides (Fay et al., 2017). G-quadruplex forming sequences have been found in the 5' UTR in more than 2900 genes and these genes are statistically enriched for a range of ontologies, including ontologies relating to translation and immune response (Huppert et al., 2008). Additionally, this G-quadruplex forming sequence has been found in the 5' UTRs of many proteins involved in the promotion of cancer phenotypes (Wolfe et al., 2014).

This motif identified from our proteomic expression data was found in 5' UTR from both our up and drown regulated proteins list at very low E-values and also enriched in the negative control list. This suggests that pateamine is not influencing the translation of G-quadruplex containing transcripts at the concentrations used in this study. Studies with the eIF4A inhibitor silvestrol have previously reported that silvestrol treatment caused the reduction of expression of transcripts with a G-quadruplex forming sequence within the 5' UTR (Wolfe et al., 2014). However, these silvestrol treatments were at concentrations which caused a growth inhibition greater than 20%. As discussed above, we suspect higher inhibitor concentrations will result in functional eIF4A depletion, causing these structured transcripts to have reduced expression.

Interestingly, a second similar motif was identified at a lower significance in some motif searches. This motif appears to have similar repetition pattern but with the nucleotides switched, with a guanine followed by two cytosines (Figure 57). It is unclear what functional role this motif may have.

3.4.7.3.5. Interpretation of the GA-rich motif

A purine-rich motif was identified which is substantially more enriched in the sequences of down-regulated 5' UTRs. This motif had a very low E-value, especially when searching for motifs with a maximum of 15 nucleotides in length ($E=3.20x10^{-36}$) (Figure 57) and is found in 27 unique 5' UTRs. At the time it was unclear why this motif would be differentially found in our down-regulated 5' UTR set. The model for suppression of translation in response to eIF4A inhibition that had just been proposed by Wolfe et al. (2014) was that down regulation could be explained by structural features in the transcript, such as G-quadruplexes. The purine-rich motif identified here was not suspected to increase 5' UTR structural stability. Soon after, Iwasaki et al. (2016) reported a similar stretch of purines in the 5' UTR of mRNA which reduced ribosomal occupancy on transcripts when treated with the eIF4A inhibitor rocaglamide A (Iwasaki et al., 2016). Further study of this interaction revealed that this purine stretch allows for the formation of a binding pocket allowing rocaglamide A to interact with both the mRNA and eIF4A stabilizing the interaction (Iwasaki et al., 2019). Although identified for rocaglamide A, this motif has not previously been described with pateamine treatment and strengthens the likelihood that rocaglamides and pateamine inhibit eIF4A by a similar mechanism.

We suspect that eIF4A is being induced to form a strong binding interaction with polypurine sequences when it is being inhibited by pateamine. This motif, which is in our down-regulated 5' UTR data, is similar to that previously observed in polysome profiling data with rocaglamide A (Iwasaki et al., 2016). Despite this suspicion, there is still some lack of clarity of the exact nature of the interaction. When investigating stretches of purines in our up- and down-regulated protein list, many up-regulated transcripts also contain polypurine stretches in their 5' UTR and when searching the combined up-regulated 5' UTRs motifs, some polypurine enrichment was detected. However, these motifs had much lower statistical significance, had far fewer contributing 5' UTR sequences and sites, and was less well defined with much higher pyridine base percentages through the motif (Figure 61). This may suggest that polypurine tracts are quite common in the 5' UTR of mRNAs but the interaction between pateamine, eIF4A and the mRNA transcript is more complex, with the interaction requiring adenine or guanine bases in precise sequences or that this inhibitory effect can often be overcome by other influencing factors. When the sequences are scanned by the MEME algorithm (Bailey et al., 2009) the motifs are identified in a different way than by eye, allowing pyrimidines in

certain positions at low frequencies within the motif and not seeing guanine and adenosines as equivalent. It might be that the interaction is similar to the Iwasaki – RocA interaction but it may be that some nucleotide positions matter more than others for a pateamine binding cleft to form.

It was thought that the inhibitory effects on expression associated with the polypurine motifs may depend on its position in the 5' UTR. To investigate this, the relative distances along the 5' UTR of all identified polypurine motifs graphed. The 7 nucleotide long polypurine motifs showed a reasonably random distribution along their respective 5' UTRs (Figure 64 & 67), suggesting the any inhibitory effect this motif may be having is independent of its position. Although the 15 nucleotide long motif was also found throughout the 5' UTR, there appeared to be some bias for it to be positioned in the first 20% of the 5' UTR and be closer to the guanine-cap in general (Figure 66 & 67). It is unclear why this trend was seen in our data. It is possible that polypurine stretches are more commonly found at this position, possibly serving a regulatory purpose and so they were more often found there. Alternatively, it may be that the expression inhibition caused by the polypurine motif is greater when it is at this location. Further investigations will help determine the reason this trend is seen in our data.

When only the transcripts containing the 15-nucleotide long purine-rich motif in their 5' UTR were analysed with g:Profiler, we do not see enrichment for translation initiation. This suggests the reduced abundance of these proteins is not linked to a response to translation initiation inhibition as would be expected if the reduction was a result of 5' UTR specific effects. This strengthens the likelihood that this motif is not enriched as a result correlated expression with a regulatory function. However, there is still a mild enrichment of the mRNA metabolic process and regulation of telomerase activity, with 9 of these 32 proteins relating to at least one of these two functions (Supplementary data 22).

3.4.8. Interpretation of western blot analysis

Although protein mass spectrometry is a powerful technique to identify abundance changes in a large amount of proteins, general identification and detection of quantitative changes, is heavily biased toward high abundance proteins. Low abundance proteins, such as transcription factors, can have large effects on the cell despite being expressed at very low abundances (Milo R, 2016). As a result, many protein changes which have significant biological influences have likely gone undetected in our proteomic analysis. For this reason, we also selected several other proteins for western blot analysis.

The proteins chosen for western blot analysis were selected for various reasons including their function, 5' UTR sequence and a previously reported sensitivity to pateamine. The iNOS protein has previously been identified by Di Marco et al. (2012) to be sensitive to pateamine. It was suspected to be the result of pateamine inducing eIF4A to bind and sequester the 5' UTR of iNOS mRNA (Di Marco et al., 2012). However, our treatments with pateamine were at concentrations low enough that we did not expect to see inhibition as a result of high 5' UTR secondary structure alone, as the majority of cellular eIF4A function remains unperturbed. We therefore wanted to investigate if iNOS expression still decreased at these low concentrations. As with iNOS, NF-κB p65 and p105 have implications in the muscle wasting disease cachexia. A number of transcription factors were chosen because they contained polypurine motifs in their 5' UTRs (NF-κB p105, GATA3, SOX6). In contrast, p65 shares a common biological function but lacks the polypurine motif. The iNOS protein was included as a control, given that it had been previously identified to be decreased in response to pateamine treatment. The functions of these proteins, and their responses to pateamine treatment are discussed below.

Three potential loading control proteins for the western blot were considered, HPRT, GAPDH and ACTB. When cross-checking these genes, it was found that the GAPDH was identified in the down-regulated proteins from our mass spectrometry screen and was excluded. Additionally, ACTB was found to have very high GC content in its 5' UTR and we were uncertain if this may affect expression when treating with pateamine. As a result, HPRT was chosen as the loading control from the western blot analysis.

3.4.8.1. Individual protein changes

3.4.8.1.1. Expression of iNOS

The protein iNOS produces nitric oxide, a reactive species implicated in the muscle wasting disease cachexia (Di Marco et al., 2012). Initially, iNOS was not detectable in the HL60 cell line sample. However, iNOS is induced by the NK-kB transcription factors, which are themselves constitutively expressed only at low levels. HL60 cells are a human leukocyte cell line which increase their expression of iNOS when activated in an immune response (Xue et al., 2018). Previous studies have been able to achieve this activation and the consequent increase in expression of enzymes associated with reactive nitrogen species, including iNOS, by stimulating HL60 with a combination of bacterial LPS and PMA (Rockett et al., 1998). To remedy the low iNOS expression in initial results, we attempted to induce the cell line to increase expression using this same method. In doing so, the HL60 cells acquired an adherent, macrophage-like morphology suggesting changes in expression were occurring. After LPS and PMA treatment, iNOS was expressed at detectable levels allowing for a quantitative analysis to be carried out.

As described in results Section 3.3.8.2, no detectable change in expression of iNOS was observed when pateamine treated and control samples were normalized to the HPRT loading control. This is likely a result of the drug concentrations used not being high enough to significantly reduce the amount of functional eIF4A. As described by Di Marco et al. (2012), it is suspected the reduction of iNOS was the result of its highly structured 5' UTR no longer being unwound for translation to occur (Di Marco et al., 2012). However, our pateamine treatments at IC_{20} should mean there is still ample eIF4A to unwind transcripts. In saying this, it is difficult to make some experimental comparisons between the two studies. Di Marco et al. (2012) carried out *in vivo* BALB/c mouse treatments at 20 μg kg^{-1} of pateamine making determination of an actual cellular pateamine concentration impossible. Additionally, muscle cells from *in vivo* mouse treatments were used for expression analysis meaning different regulation and expression mechanisms may be involved in iNOS expression. It is therefore possible that the reduction in iNOS expression seen by Di Marco et al. (2012) is a mouse-specific phenomenon. Although not a contiguous stretch, the mouse iNOS mRNA transcript has a region rich in purines close to the start codon with 13 purines with one C in the middle

(highlighted Table 40) which is more dense in purines than any region of the human iNOS 5' UTR.

Table 40. The 5' UTR sequences of human and mouse iNOS. Purines are in red and capitalized and a semi-contiguous polypurine stretch is highlighted.

Human: AtAActttGtAGcGAGtcGAAAActGAGGctccGGccGcAGAGAActcAGcctcAttcctG ctttAAAAtctctcGGccAcctttGAtGAGGGGActGGGcAGttctAGAcAGtcccGAAGt tctcAAGGcAcAGGtctcttcctGGtttGActGtccttAccccGGGGAGGcAGtGcAGccA GctGcAAGccccAcAGtGAAGAAcAtctGAGctcAAAtccAGAtAAGtGAcAtAAGtGAcc tGctttGtAAAGccAtAGAG
Mouse: GGccccAcGGGAcAcAGtGtcActGGtttGAAActtctcAGccAccttGGtGAAGGGActG AGctGttAGAGAcActtctGAGGctcctcAcGcttGGGtcttGttcActccAcGGAGtAGc ctAGtcAActGcAAGAGAAcGGAGAAcGttGGAtttGGAGcAGAAGtGcAAAGtctcAGAc

3.4.8.1.2. Expression of GATA3

GATA3 is a transcriptional activator involved in immune and inflammatory responses (Wan, 2014). As described in Section 3.3.8.2, the expression of GATA3 was not found to change as a result of an IC_{20} pateamine treatment. When selecting proteins for western blot analysis, GATA3 was specifically chosen because it possessed a long stretch of purine nucleotides in its mRNA 5' UTR (Supplementary data 26). We had hypothesized that this long polypurine tract would cause reduced expression as a result of pateamine treatment. It is not clear why this was not observed. In our mass spectrometry expression data, although there is a bias for the down-regulated proteins to possess a polypurine motif, long stretches of purines are still observed in the 5' UTRs of some proteins that were up-regulated. This suggests that although polypurine stretches may be important factors that influence expression other variables can have overriding effects.

3.4.8.1.3. Expression of NF-κB p65

The NF-κB p65 (RELA) transcription factor is involved in a wide range of cellular responses including inflammation, immunity, tumorigenesis, and apoptosis (Giridharan and Srinivasan, 2018). NF-κB p65 is known to reside in the cytoplasm until activated. This occurs when the bound inhibitor IκB is phosphorylated and degraded allowing migration into the nucleus where it activates gene transcription (Giridharan and Srinivasan, 2018). This protein was selected for the western blot analysis study due to its involvement in cachexia. Upon inspection of the mRNA transcript 5' UTR of NF-κB p65 is was hypothesized that expression would not be affected due to pateamine treatment as the 5' UTR did not possess any long polypurine tracts. Interestingly, when examined with western blot analysis pateamine treated samples consistently showed a moderate increase in expression. It is unclear why we are seeing this change in expression and we wondered if ribosome availability may have a part to play, even though we did not expect this to be a factor due to the relatively minor overall inhibition of translation intuition. It is also possible that the effects of pateamine on proteolysis is involved and the rate at which NF-κB p65 is degraded has been reduced. As described above, the action of NF-κB p65 is not intrinsically linked to its expression levels as it first needs to become activated to initiate transcription and functions in heterodimer complexes (Mulero et al., 2019). It is hence unclear if this expression change is having a direct effect on expression of other proteins or if NF-κB p65 is remaining in its inactive state despite being more abundant.

3.4.8.1.4. Expression of NF-κB p105

The NF-κB p105 transcription factor is involved in many cellular responses including inflammation, immunity and differentiation. Like NF-κB p65, NF-κBp105 is activated when IκB is phosphorylated and degraded allowing migration into the nucleus (Yu et al., 2016). Depending on which member of the NF-κB network it dimerizes with, NF-κB p105 can act as a transcriptional activator or repressor (Mulero et al., 2019). NF-κB p105 was selected for western blot analysis due it its role in cachexia. Analysis of the 5' UTR of the mRNA transcript of NF-κB p105 identified two long stretches of purines leading to us hypothesizing the expression of the protein will drop in response to pateamine treatment (Supplementary data 26). Upon western blot analysis it was observed that the expression of NF-κB p105 did not change as a result of pateamine treatment. It is unclear why this was the case and, along with the expression of GATA3 being unchanged, casts some doubt on the polypurine motif identified through our mass spectrometry experimentation as a major regulator of protein production under the conditions tested in this study. It is possible a more complex interaction is taking place requiring specific sequences for a stable interaction to occur between pateamine, the mRNA and eIF4A. It is also possible that the concentrations of pateamine used in this study were not enough to have a marked effect on translation of all mRNAs with polypurine motifs in the 5' UTR, meaning higher concentrations of pateamine may be needed.

3.4.9. Experimental limitations

3.4.9.1. Mass spectrometry protein detection limitations and biases

Mass spectrometry only detects a small part of the potential proteome of the cell and is biased toward higher abundance proteins (Fonslow et al., 2011), this engenders a degree of difficulty in gaining insight of the total proteome effects as we are only seeing snippets of the full picture. As described in Section 3.3.2, a range of modifications were made to the quantitative mass spectrometry pipeline to improve the number of proteins identified. These modifications included optimizations of the to the liquid chromatography gradient and analysis methods. After optimization we were capable of identifying up to 1439 proteins in a single experiment, of which less were consistently detected to allow for quantitative analysis. When considering the total proteins expressed in the cell, this is only a small snapshot of the proteins being expressed in human cells. This effect means that many protein abundance changes, especially relating to proteins expressed at low concentrations, have gone undetected. One factor that affected protein detection was the mass spectrometer used in this study. The LTQ Orbitrap XL mass spectrometer (Thermo Fisher), by mass spectrometer standards, is a reasonably old machine and does not have the sensitivity of newer models on the market. Additionally, experimentation using the mass spectrometer showed that polyethylene glycol (PEG) contamination was occurring with the method we used. Although multiple purification methods were carried out after the cell lysis step, including protein precipitation and C18 solid phase extraction, there was some PEG contamination from the Triton X-100 used for protein solubilization. When extraction methods not using PEG in the extraction process were used, the number of proteins identified in an experiment was improved. These two issues served to reduce the effectiveness of our analytical approach. Identification and quantification of a larger number of proteins would have proven beneficial to the subsequent analyses carried out including ontological enrichment and motif enrichment significance. Furthermore, detection of more proteins would have possibly allowed for the identification of additional, weaker biological trends and responses which were not apparent in our dataset.

3.4.9.2. Ontological analysis background limitations

Additional to the limitations of gathering data using mass spectrometry, the extraction method produced a bias for cytoplasmic proteins. Especially of note is that most translation-related proteins are expressed at high levels in dividing cells and are also found in the cytosol meaning that our identified protein pool was heavily biased toward translation-related proteins. Given that pateamine affects protein synthesis directly, it is reasonable to expect some proteins involved in translation to have altered expression profiles. However, this bias has the potential to cause an unrealistic balance to the proteins seen to be impacted in response to pateamine treatment.

To probe the changes in protein abundances and link them to cellular responses we unitized gene ontology enrichment analysis. GO analysis focuses on the molecular function, biological process and cellular localization of each protein in a list. The list of proteins that change in abundance is viewed as a whole and statistical analysis is used to determine whether any of these functions, processes or localizations are disproportionally represented in the dataset compared to a background list. When analysing ontological enrichment, a background gene list is often employed (Raudvere et al., 2019). Initially, a background set consisting of all proteins identified in any mass spectrometry experiment was considered. However, as noted above, the pool of identified proteins was relatively small and the extraction methodology biases detection towards translation-related proteins. This meant that the background set was closely matched to the list of all changing proteins, making this background inappropriate for these experiments. Instead, a default background of the entire proteome was used.

3.4.9.3. Cell treatment and analysis limitations

Although the cell lines' responses to pateamine were reasonably consistent, there was still some variation in the amount of cell death from passage to passage and this may have affected the proteomic responses measured especially in the maximum sub-inhibitory treatment samples. Given that we are giving such a low concentration of pateamine, giving an amount much lower could mean that there is no effect large enough to be detected. It is possible that this occurred in some of the sub-inhibitory HL60 pateamine quantitative protein samples, as after correcting for multiple testing very few proteins were identified to be changing in some mass spectrometry runs. This may be the result of pateamine inhibition not quite reaching a threshold required to elicit a biological response. Additionally, when samples were analysed with mass spectrometry some variation between proteins detected was also observed. For these reasons, at least 3 biological replicated and two technical replicates were carried out with each analysis to somewhat mitigate the variation of these two factors.

3.5. Conclusion

In this chapter we sought to test whether the effect of low concentrations of pateamine on human cell lines had a marked effect on the cellular protein landscape and determine which processes it was affecting. With the use of a proteomics-focused approach we identified a range of proteins which change in expression as a result of low concentration pateamine treatment. Ontological analysis of these proteins has highlighted a number of key cellular processes which are altered, including translation, translation initiation, protein degradation, mRNA splicing, nonsense-mediated decay, and telomere maintenance, providing insights into cellular regulatory responses to eIF4A inhibition. Regulatory effects appear to be the most major contributor to the changes in expression with 52% of the proteins identified being linked to the proteostasis pathway directly. These regulatory changes appear to be complex with some proteins being up-regulated and others down-regulated within the same process. Additionally, the ontological enrichments of the up-regulated proteins showed considerable similarity to proteins up-regulated when the proteasome is inhibited, suggesting pateamine treatment is affecting proteasome function or both conditions are inducing some sort of overarching regulatory mechanism. Analysis of the 5' UTRs of these proteins' mRNA transcripts has identified a motif likely to be pateamine-sensitive which causes reduced expression. This motif is similar to the motif observed by Iwasaki et al. (2016) when treating with rocaglamide A. We also investigated the expression of transcription factors linked to cachexia and some with polypurine motifs in their 5' UTRs, with the results suggesting the inhibitory effect of pateamine on polypurine tracts may be influenced by other factors which are yet to be determined. Taken together, these results identify some mRNA features that may influence a transcripts sensitivity and metabolic pathways which could be targeted when using pateamine as a therapeutic agent.

4. Chapter 4 – Global discussion

4.1. Introduction

Translation initiation factor eIF4A is essential for eukaryotic protein synthesis, and has been implicated in many human diseases including several cancers (Chan et al., 2019; Wolfe et al., 2014). Inhibition of eIF4A shows promise for the treatment of cachexia, viral infection, and Alzheimer's disease (Bottley et al., 2010; Cramer et al., 2018; Di Marco et al., 2012; Slaine et al., 2017b). The current model of eIF4A inhibition is that at higher concentrations of any eIF4A inhibitor the abundance of functional eIF4A is greatly reduced meaning 5' UTRs that have more stable secondary structure would not be unwound, resulting in reduced expression. Some eIF4A inhibitors such as silvestrol and potentially pateamine also have an additional effect at much lower concentrations as they are known to induce a strong binding of eIF4A to mRNA transcripts with particular 5' UTR sequences and reducing their translation (Iwasaki et al., 2019) (summarised in Figure 10). However, recent studies with hippuristanol have also demonstrated reduced expression of particular proteins at very low concentrations of inhibitor in spite of this inhibitor preventing eIF4A from binding mRNA (Cramer et al., 2018). This effect casts some doubt on the current model of low concentration inhibition. As some eIF4A inhibitors are poised to enter clinical trials (Cunningham et al., 2018), improved understanding and characterization of the cell-wide effects of eIF4A reduction and inhibition is of considerable value.

4.1.1. Research aims

In this body of research, we aimed to probe the effects of eIF4A reduction and inhibition on protein expression to gain a deeper understanding of the outcomes of eIF4A inhibition. This includes identifying the follow-on effects of inhibition and reduction of functional eIF4A on cellular pathways and identifying transcript-specific attributes that lead to disproportionate expression changes.

We proceeded to investigate this with the use of proteomic expression analysis methods to probe the effects of altered eIF4A function. This was carried out by establishing a gene deletion approach to reduce eIF4A expression in *Saccharomyces cerevisiae* that was then used for fluorescence microscopy and mass spectrometry to measure protein abundance change. Research was then transitioned to human cell lines and investigations carried out

with the eIF4A inhibitor pateamine and protein abundance changes identified using mass spectrometry and western blot approaches.

4.1.2. Hypothesis

We expected to see two separate effects when carrying this experimentation. The first is responses that are not unique to pateamine. These include proteomic expression changes in response to a drug treatment stress. Given that eIF4A is involved in translation initiation we expected expression changes in this pathway and pathways directly related in response to altered metabolite demand and feedback mechanisms. We did not expect this effect to be organism or condition specific and expected both yeast and human cell lines to show expression changes as a result of this response. Secondly, we expected expression changes of other proteins that weren't directly related to translation initiation but instead a result of specific attributes of the 5' UTR of the mRNA transcripts. These attributes include 5' UTR length, GC content and sequence motifs. Transcripts that have more highly structured 5' UTRs have a greater need for eIF4A helicase activity in order to be expressed. Previous work has highlighted G-quadruplex forming sequences in this regard (Wolfe et al., 2014). However, we were unsure to what extent this effect would be seen in this work, given such a mild inhibition of eIF4A function was used in these experiments. When this study began we were unaware of the potential for eIF4A inhibitors to induce clamping of eIF4A to specific 5' UTR sequences, reducing expression of these select transcripts (Iwasaki et al., 2019). Retrospectively, we may have expected this effect to be seen in the human cell line experiments when pateamine was used. This is because like rocaglamide A, pateamine is known to induce eIF4A to tightly bind RNA. With the new knowledge that this rocaglamide A induced binding occurs preferentially on some RNA sequences it would have been logical to suspect a similar effect may be seen with pateamine. We would not have expected to see this effect in yeast gene deletion experiments.

4.2. Pateamine vs eIF4A depletion

Pateamine A is a very scarce resource which is low in abundance and hard to obtain from its natural source as well as being difficult and costly to produce synthetically. This makes research in to pateamine difficult as the experimental approaches which could be utilized are severely limited. At the onset of this project, the total amount of pateamine we had at our disposal was less than 0.5 mg, making any large-scale yeast experimentation unfeasible and even limiting what could be done in human cells. Because of this issue the project was split into two parts: a yeast part focusing on reducing eIF4A protein function genetically and a human cell line part using the eIF4A inhibitor pateamine. Protein synthesis is a pathway that is a requirement for all eukaryotic life and the processes involved are relatively conserved (Petranovic et al., 2010). Therefore, despite these two models being considerably different in some ways, meaningful insights can still be gained from comparing the results of these two approaches and identifying common trends.

4.3. Comparison of experimental findings

When the enrichments of ontological processes are compared between the yeast and human cell line models, we see a significant degree of similarity in the processes affected by the perturbation of eIF4A function. Despite this similarity, there are some notable discrepancies that highlight both differences between pateamine treatment and eIF4A reduction and the organisms used.

4.3.1.1. Network effects on proteostasis

Altering the function of eIF4A, either through pateamine treatment or gene deletion, resulted in a general change in expression of proteins relating directly to translation and proteins involved in the protein production pipeline and ancillary processes downstream of translation. In both yeast and human cells translation initiation, translation, and protein folding processes are seen to have altered expression profiles when eIF4A function is perturbed. However, the effects appear to be farther reaching in the human cell model with protein localization and degradation processes also being affected. Reasons for this are unclear, although this might suggest that the human protein production pipeline is more dynamic allowing for a higher degree of regulation, or that *S. cerevisiae* is more robust to disruption of these processes. Alternately, these responses may not be a response to translation initiation inhibition, and it may be that pateamine is affecting the translation of key proteins involved in these pathways through transcript-specific effects, independent of pathway regulation. Although, it may be expected that a general downturn in protein synthesis may lead to a responsive down-regulation in protein degradation to maintain proteostasis. We were unsure to what extent this would be seen in our data given that the low concentrations of pateamine used should have a relatively small impact on overall protein production.

Unlike the yeast deletion model, ontologies relating to mRNA metabolic processes were seen in the human pateamine data. These enrichments may be the result of direct inhibition of this process by pateamine and may be eIF4AIII specific effects as described in Section 1.4.2. Previous studies suggest that pateamine inhibits translation initiation at lower concentrations than nonsense mediated decay but only slightly (Matthews et al., 2013), meaning that we could be inhibiting both processes. It is also possible that the inhibition of translation initiation is responsible for this enrichment as mRNA metabolism-related processes are immediately upstream of translation initiation in the proteostatic pathway. However, mRNA metabolism-related processes are not an enriched ontology in our yeast data possibly due to deletion of the *TIF1* or *TIF2* genes being more specific to translation initiation. This may suggest these enrichments are a direct effect of pateamine on eIF4AIII. Then again, as explained in Section 3.4.5.1, the similarity of our data to bortezimib suggests some overarching responses regulating proteostasis may be activated in both conditions driving this effect. Further

investigations will be required to identify which factor or factors are responsible for this enrichment.

Interestingly, although not seen in our data, *TIF1* function has previously been linked to mRNA metabolic processes. Prior to this study, investigations with the yeast gene deletion array identified 28 gene deletions that when paired with deletion of *TIF1* caused a significant reduction in growth (Venturi et al., 2018). These results painted a similar picture of the effects of eIF4A protein reduction on proteostasis-related processes with 17 of the gene deletion strains identified being involved in a proteostatic process (Venturi et al., 2018). These included proteins involved in mRNA metabolism, translation and protein trafficking. Although the latter two were also seen in our data, as mentioned above, mRNA metabolic processes were not. It may be that although correct mRNA preparation is beneficial for normal growth, when functional eIF4A is reduced, alterations to this pathway do no mitigate the negative effects of eIF4A reduction.

4.3.1.2. Effects on energy metabolism

The yeast deletion results have enrichments linked to energy regulation not seen in the human results. These enrichments are in processes relating to glycolysis, the citrate cycle and ATP generation. The nearest ontological enrichments seen in human cells following pateamine treatment are in broader ontological terms such as monosaccharide catabolic process and carbohydrate catabolic process, when multiple proteins lists are combined. This might suggest energy metabolism has a far greater part to play when translation initiation is inhibited in yeast compared to human cells, although the reasons for this are currently unclear and in need of further investigation.

4.3.1.3. Effects on amino acid metabolism

In addition to energy metabolism processes, amino acid metabolism-related processes are far more strongly enriched relative to other enrichments in the yeast experiments. In the yeast *tif1*Δ mass spectrometry experiment, amino acid biosynthesis was the most enriched ontology identified. In human cell lines, although still significant, amino acid metabolism appears to be proportionately less affected compared to translation and mRNA metabolism. It is unclear if this an actual differing biological response as amino acid metabolism is still enriched in human cells. This could be an effect from eIF4AIII inhibition or regulatory differences between species but further investigation will be needed to elucidate the cause of this trend.

4.3.1.4. Effects on telomere maintenance

One of the ontological enrichments we were most surprised to see related to telomere maintenance. This enrichment was seen in the human cell line experiments but was absent from the yeast results. This enrichment may be caused by an activity of pateamine that would not be seen in a gene deletion model. This result identifies a potential target of pateamine therapies for the treatment of cancers. Unlike normal somatic cells, most cancerous equivalents have activated expression of the telomerase gene (Shay and Wright, 2011). This allows them to divide indefinitely. If pateamine significantly affects proliferation through this mode of action cancerous cells will be more affected than many others in the body. However, of the 11 proteins linked to telomere maintenance 6 are also involved in protein folding, meaning some of the expression changes may be the result of other responses. Further investigation will be required to understand the reason and follow on consequences of expression changes in this pathway.

4.3.2. Motif enrichment trends

As described in Section 2.4.4.3, when searching the 5' UTRs of proteins identified to change as a result of *TIF1* or *TIF2* gene deletion, only a TC-rich motif sequence was consistently found to be enriched in all conditions.

This differs from the 5' UTRs of human proteins in which we identified a total of four different motifs enriched across all conditions. These motifs consisted of a GC-rich motif, a TC-rich motif, an AT-rich motif and a GA-rich polypurine motif. All but the GA-rich motif appeared to have similar enrichment in both the up- and down-regulated protein mRNA transcripts.

4.3.2.1. Polypurine motif

This polypurine motif was identified from the down-regulated proteins in human cell lines when using pateamine. In light of recent publications showing rocaglamide A induces a tight binding of eIF4A to mRNA (Iwasaki et al., 2019), we suspect this polypurine-related motif appears because pateamine induces tight binding of eIF4A to the mRNA transcript, preventing translation. As such, we would not expect to see this motif in our yeast data as no pateamine is present. Analysis of the yeast 5' UTRs did yield a motif somewhat rich in adenosines (Figure 34). This motif had segments of A-rich sequence and some other regions that were less consistent. It is unclear if this motif conveys a sensitivity of mRNA transcripts to reduced eIF4A function or appears only below the significance threshold by chance in this single combined list, having been observed above the significance threshold in other analysis both in up- and down-regulated 5' UTRs. This suggests that reduced eIF4A function and pateamine treatment are not equivalent, although further analysis with larger datasets will be required to determine if this motif has a genuine effect in yeast.

4.3.2.2. G-quadruplex forming motif

As described above, we suspected that we may identify the G-quadruplex forming motif described by Wolfe et al. (2014) in both our yeast and human down-regulated protein datasets. But we were unsure if eIF4A function would be reduced to levels low enough that stable 5' UTR secondary structures could not be resolved. In our human, pateamine treated, experiments the G-quadruplex motif was seen in both up- and down-regulated transcripts. This suggests repeated $(GGC)_n$ the motifs are common in human 5' UTRs. However, being identified at high rates in the up-regulated proteins shows that these structures were easily unwound during translation initiation. Indeed, growing evidence suggests that potential G-quadruplex forming sequences in 5' UTRs do not form stable folded structures (Jodoin and Perreault, 2018). We suspect that the low concentrations of pateamine used in this study was the reason we did not see reduced expression from G-quadruplex containing 5' UTRs, with eIF4A function not being reduced enough for structure-dependent effects to be seen. The yeast studies do not clarify the interaction between eIF4A and G-quadruplexes. Consistent with this ambiguous situation for G-quadruplex motifs, it is notable that the G-quadruplex reporter system did not show reduced GFP expression upon eIF4A disruption. Additionally, no G-quadruplex-related sequence was enriched in any of the 5' UTRs analysed.

This motif being absent in our yeast data could be explained in two ways. Firstly, it is possible this sequence is not commonly seen in yeast 5' UTRs, meaning it would not be found in our enrichment analysis. Secondly, it is possible that deletion of one of the two TIF genes does not result in a sufficient reduction of eIF4A to impact on mRNA secondary structure resolution.

More motifs were identified to be enriched in our experimentation with human cells compared to yeast suggesting there are additional mechanisms for control of translation or other upstream processes in human 5' UTRs.

4.3.3. Limitations of comparing models

Clearly, there are two major limitations with comparing these two models. Firstly, yeast and human cell lines have significantly different genetic backgrounds and regulatory mechanisms. Despite this, yeast and human cells possess a great degree of similarity in protein synthesis machinery (Taylor and Triggle, 2007) and both need an effective response mechanism to react to stresses. Due to conservation, these responses are likely quite similar. Secondly, although pateamine and gene deletion both serve to disrupt the function of eIF4A these conditions cannot be considered completely equivalent. Pateamine inhibits translation initiation by inducing a tight binding of eIF4A to the mRNA (Low et al., 2007), which could induce different transcript-specific and general regulatory effects (Iwasaki et al., 2016; Wolfe et al., 2014). Pateamine treatment is also multi-faceted by directly inhibiting both eIF4AI & II, and eIF4A III meaning two processes, translation initiation and mRNA metabolism, are being affected simultaneously. This will likely lead to more complex and varied responses and expression changes. When considering the effects of pateamine on eIF4A an additional potentially confounding issue arises. Although not established, due to the similarity of eIF4AIII to eIF4AI and II pateamine likely inhibits eIF4AIII by a similar mechanism. This means that pateamine may also induce tight binding of eIF4AIII to mRNA, anchoring the spliceosome complex and possibly inducing degradation of the transcript through nonsense mediated decay and providing an additional mechanism for altered protein expression which would only be seen in the human cell line pateamine experiments. Notably, eIF4AIII binds within the ORF, rather than the 5' UTR of the transcript, and so influences of its interaction with mRNA will not have been evident in the 5' UTR features investigated in this work.

4.4. Future directions

Although our research has provided an improved understanding of the consequences of eIF4A inhibition, further characterization is required to refine the current model. Future experiments in both yeast and human cell lines could build on and strengthen the findings outlined in this study.

4.4.1. Pateamine treatments of yeast

Due to yeast cells requiring much higher concentrations of pateamine to retard growth compared to mammalian cells most of our research so far has been focused on the reducing eIF4A function by reducing abundance or out competing WT eIF4A with a less efficient mutant. Although this has the potential to provide valuable insights into eIF4A function and pateamine inhibition, recent research suggests that inhibition of eIF4A with some inhibitors is more complex than just reducing the catalytic turnover of eIF4A. Thus, it would be of value to investigate the differential effects that pateamine treatment has compared to decreased function. The Victoria University of Wellington chemistry department has recently produced additional pateamine to be used for experimentation. This opens the possibility to carry out experiments which were not previously possible. Carrying out pateamine-treated yeast expression screens has the potential to give improved insights into how pateamine treatment differs from general eIF4A reduction allowing for direct comparison between the two conditions. This investigation could be approached with both mass spectrometry and GFP library-based analysis with mutants more sensitive to pateamine such as a Δ*PDR1/3* or Δ*ERG6* strain, as the genetic background reducing the amount of pateamine required (Emter et al., 2002; Fardeau et al., 2007).

4.4.2. Additional yeast reporters of translation initiation inhibition

As described in Section 2.3.1.2, we were able to produce a GFP reporter yeast strain with the GFP gene immediately downstream from a G-quadruplex motif as a method to visualise eIF4A function. This was at a time before Iwasaki et al. (2016) reported a polypurine motif found in the 5′ UTRs of genes disproportionately affected by the inhibition of eIF4A with rocaglamide A. A reporter strain with a 5′ UTR containing a stretch of purines could be made to investigate other approaches to mimic the effects of pateamine inhibition. This reporter system could even be combined with the G-quadruplex reporter construct with the two 5′ UTRs linked to different colour fluorescent proteins that could be used to compare gain of function eIF4A inhibition against drugs such as pateamine and loss of function eIF4A inhibition by drugs like hippuristanol. This reporter would also be useful for probing concentration-related effects investigating if low pateamine concentrations reduce expression of the polypurine motif and higher concentrations reduce expression of the structured G-quadruplex motif. A thirdly this reporter could be used for discovery of other drugs that inhibit eIF4A and could be screened against drug libraries. Production of this reporter is likely to be relatively simple as the difficult to produce, high GC content G-quadruplex 5′ UTR reporter strain has already been made and transformation of this strain with a polypurine containing 5′ UTR should be relatively easy.

4.4.3. Acute yeast deletion models

As described in Sections 2.2.12 & 2.2.15, the *TIF1* and *TIF2* deletion mutants used in this study were obtained from yeast gene deletion libraries. These libraries have gone through many generations since their production, allowing for long-term adaptation and selection in response to the gene deletion. The expression changes seen in our experiments are likely a combination of both long-term adaptation and shorter-term regulatory effects but it is unclear which expression changes are caused by each effect. Follow-up experiments could be carried out which involve producing new deletion strains and carrying out the same expression profile experiments. These new deletion strains will have far fewer replications preventing the development of long-term adaptations, meaning the changes observed would be the result of acute cellular responses, more closely mimicking a drug treatment. Alternatively, strains with the *TIF1* and/or *TIF2* loci under controllable promoters could be produced allowing induction of acute reductions in functional eIF4A.

4.4.4. Human cell hippuristanol, RNAi or CRISPR

As described in Section 4.3.3, when investigating the differences between reduced functional eIF4A and inhibition of eIF4A with pateamine, a major limitation is the comparison between yeast and human models. As an alternative, or in addition to carrying out pateamine treatments in yeast, the abundance of functional eIF4A could be reduced in human cells with the use of RNAi or CRISPR based approaches or by treating cells with hippuristanol. The results could then be compared against existing data from this study to identify responses specific to each condition. A CRISPR-based approach could also be used to introduce the P147L pateamine-resistance mutation into eIF4AI and II or eIF4AIII. This would allow us to isolate pateamine-induced inhibition to only one of these proteins and their associated pathways at a time.

4.4.5. mRNA expression analysis

When using protein expression data obtained from quantitative mass spectrometry, it became clear that we were measuring the culmination of numerous effects of pateamine treatment. Most notable of these is that not only were we detecting changes directly caused by pateamine inhibiting translation initiation in a transcript-dependent manor but also cell-controlled expression changes in response to the inhibition stress and resource requirements. It would be expected that the abundance of the mRNA transcripts affected by pateamine would remain largely unchanged, whereas transcripts of proteins with changed expression due to cellular regulation will be up or down-regulated. It may therefore prove beneficial in future to carryout quantitative reverse transcription PCR or RNAseq experiments. This will allow for the separation of these two effects influencing protein abundance allowing for more in-depth analysis and identification of pateamine-sensitive transcript attributes and the regulatory feedback mechanisms of human cells undergoing pateamine inhibition.

4.4.6. In-depth analysis of NF-κB p65 and p105 and iNOS

As described in Section 3.3.8, when treating human cells with pateamine we did not detect a decrease in expression of the NF-κB p105 or iNOS proteins. This was not as we had expected as there is a polypurine stretch in the 5' UTR of the NF-κB p105 mRNA that we expected would lead to inhibited translation during pateamine treatment. Additionally, iNOS expression has previously been shown to decrease upon pateamine treatment in mouse models. It is unclear if this is due to the concentrations of pateamine being insufficient to induce this effect, whether polypurine based effects on NF-κB p105 are more complex, or if the differences in iNOS expression is a result of the models used given the difference in the 5' UTRs between mouse and human iNOS. To investigate this further, by titrating pateamine concentrations and analysing the western blot we could determine if higher pateamine concentrations are required to see changes in expression of these proteins. In addition to NF-κB p105 and iNOS, unexpected results were seen when measuring the expression of NF-κB p65 with an increase in expression being observed. Additionally, the influence of pateamine at these low concentrations in a mouse cell line could be investigated. This deserves further investigation to understand the origin of this effect.

4.4.7. Production of larger proteomic datasets

As described in Section 3.4.9.1, the presence of PEG in protein extracts and the limitations of the mass spectrometer used for this study significantly reduced that number of proteins identified in this experimental approach. There are likely to be far more proteins changing in abundance than we successfully identified in each experiment which could drastically improve the ontological and motif enrichment analyses if they were detected. Since these experiments were carried out, a protein extraction method that does not use PEG has been optimized in our lab and a new mass spectrometer has been bought. Preliminary experiments with this altered preparation method on the new spectrometer identified approximately 5 times the total number of proteins identified in our runs. These experimental runs also took significantly less time to complete. Repeating the analysis with newer equipment and methodology has the potential to drastically improve the statistical power of our study, giving potential to find more subtle ontological enrichments, rarer motifs and strengthening enrichments of dubious motifs such as the yeast A-rich motif.

4.5. Final conclusion

This body of research focused on the translation initiation factor eIF4A and inhibition of its normal cellular function. Our aim was to gain a deeper understanding of the outcomes of eIF4A inhibition, finding key processes that were affected and identify mRNA attributes that led to reduced expression of specific proteins. We approached this examination in two distinct ways, carrying out protein expression analysis using both yeast eIF4A gene deletion mutants and with the eIF4A inhibitor pateamine in human cells. Important differences to previous studies on eIF4A inhibition were the use of the highly potent inhibitor, pateamine; evaluation of effects of inhibition under conditions with little effect on cell proliferation, as would be required for treatment of cachexia or viral infections; and the application of systems biology tools evaluating a whole cell response, rather than focusing on select proteins or transcripts. Although we do see expression changes in translation, translation initiation, and protein folding in both models, our data suggest that treatment with pateamine and reduction in the amount of functional eIF4A are not equivalent. Pateamine has further reaching effects on the proteostatic pathway stretching from mRNA processing to proteolysis; has eIF4AIII inhibition-related effects with significant expression changes in spliceosome-related proteins; and appears to induce 5' UTR sequence-specific effects reducing the expression of polypurine tracts containing 5' UTRs. These additional targets and effects of pateamine induce a more varied change to the proteome than reduction in functional eIF4A alone. From these findings we have gained an improved understanding of the effects of low concentration eIF4A inhibition and identified areas of interest for future research.

5. References

Abdelkrim, Y.Z., Harigua-Souiai, E., Barhoumi, M., Banroques, J., Blondel, A., Guizani, I., and Tanner, N.K. (2018). The steroid derivative 6-aminocholestanol inhibits the DEAD-box helicase eIF4A (LieIF4A) from the Trypanosomatid parasite Leishmania by perturbing the RNA and ATP binding sites. Mol Biochem Parasitol *226*, 9-19.

Amberg, D.C. (2005). Methods in Yeast Genetics: A Cold Spring Harbor Laboratory Course Manual, 2005 Edition (Cold Spring Harbor Laboratory Press).

Andreou, A.Z., and Klostermeier, D. (2013). The DEAD-box helicase eIF4A: Paradigm or the odd one out? RNA Biol *10*, 19-32.

Andreou, A.Z., and Klostermeier, D. (2014). eIF4B and eIF4G jointly stimulate eIF4A ATPase and unwinding activities by modulation of the eIF4A conformational cycle. J Mol Biol *426*, 51-61.

Ankney, J.A., Muneer, A., and Chen, X. (2018). Relative and Absolute Quantitation in Mass Spectrometry-Based Proteomics. Annu Rev Anal Chem (Palo Alto Calif) *11*, 49-77.

Aoyagi, T., Terracina, K.P., Raza, A., Matsubara, H., and Takabe, K. (2015). Cancer cachexia, mechanism and treatment. World J Gastrointest Oncol *7*, 17-29.

Araujo, P.R., Yoon, K., Ko, D., Smith, A.D., Qiao, M., Suresh, U., Burns, S.C., and Penalva, L.O. (2012). Before It Gets Started: Regulating Translation at the 5' UTR. Comp Funct Genomics *2012*, 475731.

Asara, J.M., Christofk, H.R., Freimark, L.M., and Cantley, L.C. (2008). A label-free quantification method by MS/MS TIC compared to SILAC and spectral counting in a proteomics screen. Proteomics *8*, 994-999.

Babendure, J.R., Babendure, J.L., Ding, J.H., and Tsien, R.Y. (2006). Control of mammalian translation by mRNA structure near caps. RNA *12*, 851-861.

Bailey, T.L., Boden, M., Buske, F.A., Frith, M., Grant, C.E., Clementi, L., Ren, J., Li, W.W., and Noble, W.S. (2009). MEME SUITE: tools for motif discovery and searching. Nucleic Acids Res *37*, W202-208.

Bailey. T, and Elkan. C (1994). Fitting a mixture model by expectation maximization to discover motifs in biopolymers. Proceedings of the Second International Conference on Intelligent Systems for Molecular Biology, 28-36.

Banez-Coronel, M., Ayhan, F., Tarabochia, A.D., Zu, T., Perez, B.A., Tusi, S.K., Pletnikova, O., Borchelt, D.R., Ross, C.A., Margolis, R.L.*, et al.* (2015). RAN Translation in Huntington Disease. Neuron *88*, 667-677.

Beaudoin, M.E., Poirel, V.J., and Krushel, L.A. (2008). Regulating amyloid precursor protein synthesis through an internal ribosomal entry site. In Nucleic Acids Res, pp. 6835-6847.

Beuchet, P., el Kihel, L., Dherbomez, M., Charles, G., and Letourneux, Y. (1998). Synthesis of 6(alpha, beta)-aminocholestanols as ergosterol biosynthesis inhibitors. Bioorg Med Chem Lett *8*, 3627-3630.

Bhat, M., Robichaud, N., Hulea, L., Sonenberg, N., Pelletier, J., and Topisirovic, I. (2015). Targeting the translation machinery in cancer. Nat Rev Drug Discov *14*, 261-278.

Bhatia-Kissova, I., and Camougrand, N. (2010). Mitophagy in yeast: actors and physiological roles. FEMS Yeast Res *10*, 1023-1034.

Biedenkopf, N., Lange-Grunweller, K., Schulte, F.W., Weisser, A., Muller, C., Becker, D., Becker, S., Hartmann, R.K., and Grunweller, A. (2017). The natural compound silvestrol is a potent inhibitor of Ebola virus replication. Antiviral Res *137*, 76-81.

Bircham, P.W. (2014). The use of high-throughput microscopy in the characterisation of phenotypes associated with the Unfolded Protein Response in Saccharomyces cerevisiae. In Cell and Molecular Bioscience (Victoria University of Wellington: Victoria University of Wellington).

Bircham, P.W., Maass, D.R., Roberts, C.A., Kiew, P.Y., Low, Y.S., Yegambaram, M., Matthews, J., Jack, C.A., and Atkinson, P.H. (2011). Secretory pathway genes assessed by high-throughput microscopy and synthetic genetic array analysis. Mol Biosyst *7*, 2589-2598.

Boone, C., Bussey, H., and Andrews, B.J. (2007). Exploring genetic interactions and networks with yeast. Nat Rev Genet *8*, 437-449.

Bordeleau, M., Robert, F., Gerard, B., Lindqvist, Chen, S., Wendel, H., Brem, B., Greger, H., Lowe, S., Porco, J.J*., et al.* (2008). Therapeutic suppression of translation initiation modulates chemosensitivity in a mouse lymphoma model (J Clin Invest).
Bordeleau, M.E., Matthews, J., Wojnar, J.M., Lindqvist, L., Novac, O., Jankowsky, E., Sonenberg, N., Northcote, P., Teesdale-Spittle, P., and Pelletier, J. (2005). Stimulation of mammalian translation initiation factor eIF4A activity by a small molecule inhibitor of eukaryotic translation. Proc Natl Acad Sci U S A *102*, 10460-10465.
Bordeleau, M.E., Mori, A., Oberer, M., Lindqvist, L., Chard, L.S., Higa, T., Belsham, G.J., Wagner, G., Tanaka, J., and Pelletier, J. (2006). Functional characterization of IRESes by an inhibitor of the RNA helicase eIF4A. Nat Chem Biol *2*, 213-220.
Bosch, P.J., Peng, L., and Kivell, B.M. (2015). Proteomics Analysis of Dorsal Striatum Reveals Changes in Synaptosomal Proteins following Methamphetamine Self-Administration in Rats. PLoS One *10*.
Bottley, A., Phillips, N.M., Webb, T.E., Willis, A.E., and Spriggs, K.A. (2010). eIF4A inhibition allows translational regulation of mRNAs encoding proteins involved in Alzheimer's disease. PLoS One *5*.
Boussemart, L., Malka-Mahieu, H., Girault, I., Allard, D., Hemmingsson, O., Tomasic, G., Thomas, M., Basmadjian, C., Ribeiro, N., Thuaud, F*., et al.* (2014). eIF4F is a nexus of resistance to anti-BRAF and anti-MEK cancer therapies. Nature *513*, 105-109.
Bradshaw, R., and Dennis, E. (2009). Handbook of Cell Signaling, 2 edn (Academic Press).
Breker, M., Gymrek, M., and Schuldiner, M. (2013). A novel single-cell screening platform reveals proteome plasticity during yeast stress responses. Journal of Cell Biology *200*, 839-850.
Buchan, J.R., Muhlrad, D., and Parker, R. (2008). P bodies promote stress granule assembly in Saccharomyces cerevisiae. In J Cell Biol, pp. 441-455.
Buchan, J.R., Yoon, J.H., and Parker, R. (2011). Stress-specific composition, assembly and kinetics of stress granules in Saccharomyces cerevisiae. J Cell Sci *124*, 228-239.
Caldarola, S., Amaldi, F., Proud, C.G., and Loreni, F. (2004). Translational regulation of terminal oligopyrimidine mRNAs induced by serum and amino acids involves distinct signaling events. J Biol Chem *279*, 13522-13531.
CDC, U.S.D.O.H.A.H.S. (2017). Seasonal flu death estimate increases worldwide.
Cencic, R., and Pelletier, J. (2016). Hippuristanol - A potent steroid inhibitor of eukaryotic initiation factor 4A. Translation (Austin) *4*.
Chan, K., Robert, F., Oertlin, C., Kapeller-Libermann, D., Avizonis, D., Gutierrez, J., Handly-Santana, A., Doubrovin, M., Park, J., Schoepfer, C*., et al.* (2019). eIF4A supports an oncogenic translation program in pancreatic ductal adenocarcinoma. Nat Commun *10*, 5151.
Che, M., Wang, R., Wang, H.Y., and Zheng, X.S. (2016). Expanding roles of superoxide dismutases in cell regulation and cancer. Drug Discov Today *21*, 143-149.
Chen, Y., Knosel, T., Kristiansen, G., Pietas, A., Garber, M.E., Matsuhashi, S., Ozaki, I., and Petersen, I. (2003). Loss of PDCD4 expression in human lung cancer correlates with tumour progression and prognosis. J Pathol *200*, 640-646.
Chen, Z.H., Qi, J.J., Wu, Q.N., Lu, J.H., Liu, Z.X., Wang, Y., Hu, P.S., Li, T., Lin, J.F., Wu, X.Y*., et al.* (2019). Eukaryotic initiation factor 4A2 promotes experimental metastasis and oxaliplatin resistance in colorectal cancer. J Exp Clin Cancer Res *38*, 196.
Cheng, J., Gao, F., Chen, X., Wu, J., Xing, C., Lv, Z., Xu, W., Xie, Q., Wu, L., Ye, S*., et al.* (2014). Prohibitin-2 promotes hepatocellular carcinoma malignancy progression in hypoxia based on a label-free quantitative proteomics strategy. Mol Carcinog *53*, 820-832.
Chong, Y.T., Cox, M.J., and Andrews, B. (2012). Proteome-wide screens in Saccharomyces cerevisiae using the yeast GFP collection. Adv Exp Med Biol *736*, 169-178.
Clower, C.V., Chatterjee, D., Wang, Z., Cantley, L.C., Vander Heiden, M.G., and Krainer, A.R. (2010). The alternative splicing repressors hnRNP A1/A2 and PTB influence pyruvate kinase isoform expression and cell metabolism. Proc Natl Acad Sci U S A *107*, 1894-1899.

Cramer, Z., Sadek, J., Vazquez, G.G., Di Marco, S., Pause, A., Pelletier, J., and Gallouzi, I.E. (2018). eIF4A inhibition prevents the onset of cytokine-induced muscle wasting by blocking the STAT3 and iNOS pathways. Sci Rep *8*.
Cunningham, T.A., Chapman, E., and Schatz, J.H. (2018). eIF4A inhibition: ready for primetime? In Oncotarget, pp. 35515-35516.
Dang, Y., Kedersha, N., Low, W.K., Romo, D., Gorospe, M., Kaufman, R., Anderson, P., and Liu, J.O. (2006). Eukaryotic initiation factor 2alpha-independent pathway of stress granule induction by the natural product pateamine A. J Biol Chem *281*, 32870-32878.
Dang, Y., Low, W.K., Xu, J., Gehring, N.H., Dietz, H.C., Romo, D., and Liu, J.O. (2009). Inhibition of nonsense-mediated mRNA decay by the natural product pateamine A through eukaryotic initiation factor 4AIII. J Biol Chem *284*, 23613-23621.
Decker, C.J., and Parker, R. (2012). P-Bodies and Stress Granules: Possible Roles in the Control of Translation and mRNA Degradation. Cold Spring Harb Perspect Biol *4*.
DeLuna, A., Springer, M., Kirschner, M.W., and Kishony, R. (2010). Need-based up-regulation of protein levels in response to deletion of their duplicate genes. PLoS Biol *8*, e1000347.
Dever, T.E., Kinzy, T.G., and Pavitt, G.D. (2016). Mechanism and Regulation of Protein Synthesis in Saccharomyces cerevisiae. In Genetics, pp. 65-107.
Di Marco, S., Cammas, A., Lian, X.J., Kovacs, E.N., Ma, J.F., Hall, D.T., Mazroui, R., Richardson, J., Pelletier, J., and Gallouzi, I.E. (2012). The translation inhibitor pateamine A prevents cachexia-induced muscle wasting in mice. In Nat Commun, pp. 896-.
Duina, A.A., Miller, M.E., and Keeney, J.B. (2014). Budding Yeast for Budding Geneticists: A Primer on the Saccharomyces cerevisiae Model System. Genetics *197*, 33-48.
Duncan, R., and Hershey, J.W. (1983). Identification and quantitation of levels of protein synthesis initiation factors in crude HeLa cell lysates by two-dimensional polyacrylamide gel electrophoresis. J Biol Chem *258*, 7228-7235.
Eberle, J., Krasagakis, K., and Orfanos, C.E. (1997). Translation initiation factor eIF-4A1 mRNA is consistently overexpressed in human melanoma cells in vitro. Int J Cancer *71*, 396-401.
Effector_Therapeutics (2019). Study of eFT226 in Subjects With Selected Advanced Solid Tumor Malignancies (U.S. National Library of Medicine).
Emter, R., Heese-Peck, A., and Kralli, A. (2002). ERG6 and PDR5 regulate small lipophilic drug accumulation in yeast cells via distinct mechanisms. FEBS Lett *521*, 57-61.
Fardeau, V., Lelandais, G., Oldfield, A., Salin, H., Lemoine, S., Garcia, M., Tanty, V., Le Crom, S., Jacq, C., and Devaux, F. (2007). The central role of PDR1 in the foundation of yeast drug resistance. J Biol Chem *282*, 5063-5074.
Fay, M.M., and Anderson, P.J. (2018). The Role of RNA in Biological Phase Separations. J Mol Biol *430*, 4685-4701.
Fay, M.M., Lyons, S.M., and Ivanov, P. (2017). RNA G-quadruplexes in biology: principles and molecular mechanisms. J Mol Biol *429*, 2127-2147.
Fonslow, B.R., Carvalho, P.C., Academia, K., Freeby, S., Xu, T., Nakorchevsky, A., Paulus, A., and Yates, J.R. (2011). Improvements in proteomic metrics of low abundance proteins through proteome equalization using ProteoMiner prior to MudPIT. J Proteome Res *10*, 3690-3700.
Gelperin, D.M., White, M.A., Wilkinson, M.L., Kon, Y., Kung, L.A., Wise, K.J., Lopez-Hoyo, N., Jiang, L., Piccirillo, S., Yu, H.*, et al.* (2005). Biochemical and genetic analysis of the yeast proteome with a movable ORF collection. Genes Dev *19*, 2816-2826.
Giaever, G., Chu, A.M., Ni, L., Connelly, C., Riles, L., Veronneau, S., Dow, S., Lucau-Danila, A., Anderson, K., Andre, B.*, et al.* (2002). Functional profiling of the Saccharomyces cerevisiae genome. Nature *418*, 387-391.
Giridharan, S., and Srinivasan, M. (2018). Mechanisms of NF-κB p65 and strategies for therapeutic manipulation. J Inflamm Res *11*, 407-419.
Goryanin, I., and Goryachev, A. (2012). Advances in Systems Biology, 1 edn (Springer-Verlag New York).

Grant, C.E., Bailey, T.L., and Noble, W.S. (2011). FIMO: scanning for occurrences of a given motif. Bioinformatics *27*, 1017-1018.
Green, K.M., Linsalata, A.E., and Todd, P.K. (2016). RAN translation—what makes it run? Brain Res *1647*, 30-42.
Grillo, G., Turi, A., Licciulli, F., Mignone, F., Liuni, S., Banfi, S., Gennarino, V.A., Horner, D.S., Pavesi, G., Picardi, E.*, et al.* (2010). UTRdb and UTRsite (RELEASE 2010): a collection of sequences and regulatory motifs of the untranslated regions of eukaryotic mRNAs. In Nucleic Acids Res, pp. D75-80.
He, F., and Jacobson, A. (2015). Nonsense-Mediated mRNA Decay: Degradation of Defective Transcripts Is Only Part of the Story. Annu Rev Genet *49*, 339-366.
Heim, R., Cubitt, A.B., and Tsien, R.Y. (1995). Improved green fluorescence. Nature *373*, 663-664.
Hilbert, M., Kebbel, F., Gubaev, A., and Klostermeier, D. (2011). eIF4G stimulates the activity of the DEAD box protein eIF4A by a conformational guidance mechanism. Nucleic Acids Res *39*, 2260-2270.
Ho, B., Baryshnikova, A., and Brown, G.W. (2018). Unification of Protein Abundance Datasets Yields a Quantitative Saccharomyces cerevisiae Proteome. Cell Syst *6*, 192-205.e193.
Hofer, S., Kainz, K., Zimmermann, A., Bauer, M.A., Pendl, T., Poglitsch, M., Madeo, F., and Carmona-Gutierrez, D. (2018). Studying Huntington's Disease in Yeast: From Mechanisms to Pharmacological Approaches. Front Mol Neurosci *11*.
Huh, W.K., Falvo, J.V., Gerke, L.C., Carroll, A.S., Howson, R.W., Weissman, J.S., and O'Shea, E.K. (2003). Global analysis of protein localization in budding yeast. Nature *425*, 686-691.
Huppert, J.L., Bugaut, A., Kumari, S., and Balasubramanian, S. (2008). G-quadruplexes: the beginning and end of UTRs. In Nucleic Acids Res, pp. 6260-6268.
Iadecola, C., Zhang, F., Niwa, K., Eckman, C., Turner, S.K., Fischer, E., Younkin, S., Borchelt, D.R., Hsiao, K.K., and Carlson, G.A. (1999). SOD1 rescues cerebral endothelial dysfunction in mice overexpressing amyloid precursor protein. Nat Neurosci *2*, 157-161.
Iwasaki, S., Floor, S.N., and Ingolia, N.T. (2016). Rocaglates convert DEAD-box protein eIF4A into a sequence-selective translational repressor. Nature *534*, 558-561.
Iwasaki, S., Iwasaki, W., Takahashi, M., Sakamoto, A., Watanabe, C., Shichino, Y., Floor, S.N., Fujiwara, K., Mito, M., Dodo, K.*, et al.* (2019). The Translation Inhibitor Rocaglamide Targets a Bimolecular Cavity between eIF4A and Polypurine RNA. Mol Cell *73*, 738-748 e739.
Janke, C., Magiera, M.M., Rathfelder, N., Taxis, C., Reber, S., Maekawa, H., Moreno-Borchart, A., Doenges, G., Schwob, E., Schiebel, E.*, et al.* (2004). A versatile toolbox for PCR-based tagging of yeast genes: new fluorescent proteins, more markers and promoter substitution cassettes. Yeast *21*, 947-962.
Ji, R.R., de Silva, H., Jin, Y., Bruccoleri, R.E., Cao, J., He, A., Huang, W., Kayne, P.S., Neuhaus, I.M., Ott, K.H.*, et al.* (2009). Transcriptional profiling of the dose response: a more powerful approach for characterizing drug activities. PLoS Comput Biol *5*, e1000512.
Jin, C., Rajabi, H., Rodrigo, C.M., Porco, J.A., Jr., and Kufe, D. (2013). Targeting the eIF4A RNA helicase blocks translation of the MUC1-C oncoprotein. Oncogene *32*, 2179-2188.
Jodoin, R., and Perreault, J.P. (2018). G-quadruplexes formation in the 5'UTRs of mRNAs associated with colorectal cancer pathways. PLoS One *13*.
Jonikas, M.C., Collins, S.R., Denic, V., Oh, E., Quan, E.M., Schmid, V., Weibezahn, J., Schwappach, B., Walter, P., Weissman, J.S.*, et al.* (2009). Comprehensive characterization of genes required for protein folding in the endoplasmic reticulum. Science *323*, 1693-1697.
Kachroo, A.H., Laurent, J.M., Yellman, C.M., Meyer, A.G., Wilke, C.O., and Marcotte, E.M. (2015). Evolution. Systematic humanization of yeast genes reveals conserved functions and genetic modularity. Science *348*, 921-925.
Karousis, E.D., Nasif, S., and Muhlemann, O. (2016). Nonsense-mediated mRNA decay: novel mechanistic insights and biological impact. Wiley Interdiscip Rev RNA *7*, 661-682.
Kearse, M.G., Green, K.M., Krans, A., Rodriguez, C.M., Linsalata, A.E., Goldstrohm, A.C., and Todd, P.K. (2016). CGG Repeat associated non-AUG translation utilizes a cap-dependent, scanning mechanism of initiation to produce toxic proteins. Mol Cell *62*, 314-322.

Kim, S., Hwang, B.Y., Su, B.N., Chai, H., Mi, Q., Kinghorn, A.D., Wild, R., and Swanson, S.M. (2007). Silvestrol, a potential anticancer rocaglate derivative from Aglaia foveolata, induces apoptosis in LNCaP cells through the mitochondrial/apoptosome pathway without activation of executioner caspase-3 or -7. Anticancer Res *27*, 2175-2183.
Kimball, S.R. (2017). Leucine-Induced Upregulation of Terminal Oligopyrimidine mRNA Translation in Skeletal Muscle: Just the Tip of the Iceberg? J Nutr *147*, 1603-1604.
Kitahata, S., Yakushiji, F., and Ichikawa, S. (2017). Impact of the structures of macrocyclic Michael acceptors on covalent proteasome inhibition. Chem Sci *8*, 6959-6963.
Korneeva, N.L., First, E.A., Benoit, C.A., and Rhoads, R.E. (2005). Interaction between the NH2-terminal domain of eIF4A and the central domain of eIF4G modulates RNA-stimulated ATPase activity. J Biol Chem *280*, 1872-1881.
Kressler, D., de la Cruz, J., Rojo, M., and Linder, P. (1997). Fal1p is an essential DEAD-box protein involved in 40S-ribosomal-subunit biogenesis in Saccharomyces cerevisiae. Mol Cell Biol *17*, 7283-7294.
Krey, J.F., Wilmarth, P.A., Shin, J.B., Klimek, J., Sherman, N.E., Jeffery, E.D., Choi, D., David, L.L., and Barr-Gillespie, P.G. (2014). Accurate Label-Free Protein Quantitation with High- and Low-Resolution Mass Spectrometers. J Proteome Res *13*, 1034-1044.
Kuznetsov, G., Xu, Q., Rudolph-Owen, L., Tendyke, K., Liu, J., Towle, M., Zhao, N., Marsh, J., Agoulnik, S., Twine, N*., et al.* (2009). Potent in vitro and in vivo anticancer activities of des-methyl, des-amino pateamine A, a synthetic analogue of marine natural product pateamine A. Mol Cancer Ther *8*, 1250-1260.
Lander, E.S., Linton, L.M., Birren, B., Nusbaum, C., Zody, M.C., Baldwin, J., Devon, K., Dewar, K., Doyle, M., FitzHugh, W*., et al.* (2001). Initial sequencing and analysis of the human genome. Nature *409*, 860-921.
Laurent, J.M., Young, J.H., Kachroo, A.H., and Marcotte, E.M. (2016). Efforts to make and apply humanized yeast. In Brief Funct Genomics, pp. 155-163.
Le Hir, H., Gatfield, D., Izaurralde, E., and Moore, M.J. (2001). The exon-exon junction complex provides a binding platform for factors involved in mRNA export and nonsense-mediated mRNA decay. Embo j *20*, 4987-4997.
Lee, P.Y., Costumbrado, J., Hsu, C.Y., and Kim, Y.H. (2012a). Agarose Gel Electrophoresis for the Separation of DNA Fragments. J Vis Exp.
Lee, S., Liu, B., Huang, S.X., Shen, B., and Qian, S.B. (2012b). Global mapping of translation initiation sites in mammalian cells at single-nucleotide resolution. In Proc Natl Acad Sci U S A, pp. E2424-2432.
Leppek, K., Das, R., and Barna, M. (2018). Functional 5' UTR mRNA structures in eukaryotic translation regulation and how to find them. Nat Rev Mol Cell Biol *19*, 158-174.
Liang, S., Zhou, Y., Chen, Y., Ke, G., Wen, H., and Wu, X. (2014). Decreased expression of EIF4A1 after preoperative brachytherapy predicts better tumor-specific survival in cervical cancer. Int J Gynecol Cancer *24*, 908-915.
Lin, Z., and Li, W.H. (2012). Evolution of 5' untranslated region length and gene expression reprogramming in yeasts. Mol Biol Evol *29*, 81-89.
Lindqvist, L., Oberer, M., Reibarkh, M., Cencic, R., Bordeleau, M.E., Vogt, E., Marintchev, A., Tanaka, J., Fagotto, F., Altmann, M*., et al.* (2008). Selective Pharmacological Targeting of a DEAD Box RNA Helicase. In PLoS One.
Liu, T., Nair, S.J., Lescarbeau, A., Belani, J., Peluso, S., Conley, J., Tillotson, B., O'Hearn, P., Smith, S., Slocum, K*., et al.* (2012). Synthetic silvestrol analogues as potent and selective protein synthesis inhibitors. J Med Chem *55*, 8859-8878.
Low, W.K., Dang, Y., Bhat, S., Romo, D., and Liu, J.O. (2007). Substrate-dependent targeting of eukaryotic translation initiation factor 4A by pateamine A: negation of domain-linker regulation of activity. Chem Biol *14*, 715-727.

Low, W.K., Dang, Y., Schneider-Poetsch, T., Shi, Z., Choi, N.S., Merrick, W.C., Romo, D., and Liu, J.O. (2005). Inhibition of eukaryotic translation initiation by the marine natural product pateamine A. Mol Cell *20*, 709-722.
Ly, T., Endo, A., Brenes, A., Gierlinski, M., Afzal, V., Pawellek, A., and Lamond, A.I. (2018). Proteome-wide analysis of protein abundance and turnover remodelling during oncogenic transformation of human breast epithelial cells. Wellcome Open Res *3*.
Masutani, H., Bai, J., Kim, Y.C., and Yodoi, J. (2004). Thioredoxin as a neurotrophic cofactor and an important regulator of neuroprotection. Mol Neurobiol *29*, 229-242.
Matsuzawa, A. (2017). Thioredoxin and redox signaling: Roles of the thioredoxin system in control of cell fate. Arch Biochem Biophys *617*, 101-105.
Matthews, J.H. (2010). The Molecular Pharmacology Of Pateamine A. In Biomedical Science (Victoria University of Wellington: Victoria University of Wellington).
Matthews, J.H., Maass, D.R., Northcote, P.T., Atkinson, P.H., and Teesdale-Spittle, P.H. (2013). The cellular target specificity of pateamine A. Z Naturforsch C J Biosci *68*, 406-415.
Mazumder, A., Pesudo, L.Q., McRee, S., Bathe, M., and Samson, L.D. (2013). Genome-wide single-cell-level screen for protein abundance and localization changes in response to DNA damage in S. cerevisiae. Nucleic Acids Res *41*, 9310-9324.
Michalkova-Papajova, D., Obernauerova, M., and Subik, J. (2000). Role of the PDR gene network in yeast susceptibility to the antifungal antibiotic mucidin. Antimicrob Agents Chemother *44*, 418-420.
Milo R, P.R., Orme N (2016). Cell Biology by the Numbers. In Yale J Biol Med, pp. 425-426.
Mokrejs, M., Masek, T., Vopalensky, V., Hlubucek, P., Delbos, P., and Pospisek, M. (2010). IRESite--a tool for the examination of viral and cellular internal ribosome entry sites. Nucleic Acids Res *38*, D131-136.
Mosmann, T. (1983). Rapid colorimetric assay for cellular growth and survival: application to proliferation and cytotoxicity assays. J Immunol Methods *65*, 55-63.
Mulero, M.C., Wang, V.Y.F., Huxford, T., and Ghosh, G. (2019). Genome reading by the NF-κB transcription factors. In Nucleic Acids Res, pp. 9967-9989.
Nagarajan, N., Ng, P., and Keich, U. (2006). Refining motif finders with E-value calculations. RECOMB on Regulatory Genomics.
Newman, J.R., Ghaemmaghami, S., Ihmels, J., Breslow, D.K., Noble, M., DeRisi, J.L., and Weissman, J.S. (2006). Single-cell proteomic analysis of S. cerevisiae reveals the architecture of biological noise. Nature *441*, 840-846.
Nitiss, J., and Heitman, J. (2007). Yeast as a Tool in Cancer Research (Springer).
Noble, W.S. (2009). How does multiple testing correction work? Nat Biotechnol *27*, 1135-1137.
Northcote, P.T., Blunt, J.W., and Munro, M.H.G. (1991). Pateamine: a potent cytotoxin from the New Zealand Marine sponge, mycale sp. Tetrahedron Letters *32*, 6411-6414.
Nuzzo, D., Inguglia, L., Walters, J., Picone, P., and Di Carlo, M. (2017). A Shotgun Proteomics Approach Reveals a New Toxic Role for Alzheimer's Disease Abeta Peptide: Spliceosome Impairment. J Proteome Res *16*, 1526-1541.
Parikh, D., Dougan, J., Li, J., Romo, D., Moorman, N.J., Graves, L.M., and Graves, P.R. (2012). Des-methyl, Des-amino pateamine A, a Synthetic Analogue of Marine Natural Product Pateamine A, Sensitizes Non-small Cell Lung Cancer Cells to Radiation and Enhances BAX Expression. International Journal of Radiation Oncology • Biology • Physics *84*, S701-S702.
Pascovici, D., Handler, D.C., Wu, J.X., and Haynes, P.A. (2016). Multiple testing corrections in quantitative proteomics: A useful but blunt tool. Proteomics *16*, 2448-2453.
Paulo, J.A. (2013). Practical and Efficient Searching in Proteomics: A Cross Engine Comparison. Webmedcentral *4*.
Pelletier, J., and Sonenberg, N. (1985). Insertion mutagenesis to increase secondary structure within the 5' noncoding region of a eukaryotic mRNA reduces translational efficiency. Cell *40*, 515-526.
Peters, T.L., Tillotson, J., Yeomans, A.M., Wilmore, S., Lemm, E., Jimenez-Romero, C., Amador, L.A., Li, L., Amin, A.D., Pongtornpipat, P.*, et al.* (2018). Target-Based Screening against eIF4A1 Reveals the

Marine Natural Product Elatol as a Novel Inhibitor of Translation Initiation with In Vivo Antitumor Activity. Clin Cancer Res *24*, 4256-4270.
Petranovic, D., Tyo, K., Vemuri, G.N., and Nielsen, J. (2010). Prospects of yeast systems biology for human health: integrating lipid, protein and energy metabolism. FEMS Yeast Res *10*, 1046-1059.
Raudvere, U., Kolberg, L., Kuzmin, I., Arak, T., Adler, P., Peterson, H., and Vilo, J. (2019). g:Profiler: a web server for functional enrichment analysis and conversions of gene lists (2019 update). Nucleic Acids Res *47*, W191-w198.
Rockett, K.A., Brookes, R., Udalova, I., Vidal, V., Hill, A.V., and Kwiatkowski, D. (1998). 1,25-Dihydroxyvitamin D3 induces nitric oxide synthase and suppresses growth of Mycobacterium tuberculosis in a human macrophage-like cell line. Infect Immun *66*, 5314-5321.
Romo, D., Choi, N.S., Li, S., Buchler, I., Shi, Z., and Liu, J.O. (2004). Evidence for separate binding and scaffolding domains in the immunosuppressive and antitumor marine natural product, pateamine a: design, synthesis, and activity studies leading to a potent simplified derivative. J Am Chem Soc *126*, 10582-10588.
Romo, D., Rzasa, R.M., Shea, H.A., Park, K., Langenhan, J.M., Sun, L., Akhiezer, A., and Liu, J.O. (1998). Total Synthesis and Immunosuppressive Activity of (−)-Pateamine A and Related Compounds: Implementation of a β-Lactam-Based Macrocyclization. Journal of the American Chemical Society *120*, 12237-12254.
Saiki, R.K., Gelfand, D. H., Stoffel, S., Scharf, S. J., Higuchi, R., Horn, G. T., Mullis, K. B., & Erlich, H. A. (1988). Primer-directed enzymatic amplification of DNA with a thermostable DNA polymerase. Science.
Schirmer, E.C., Yates, J.R., 3rd, and Gerace, L. (2003). MudPIT: A powerful proteomics tool for discovery. Discov Med *3*, 38-39.
Schneider-Poetsch, T., Ju, J., Eyler, D.E., Dang, Y., Bhat, S., Merrick, W.C., Green, R., Shen, B., and Liu, J.O. (2010). Inhibition of Eukaryotic Translation Elongation by Cycloheximide and Lactimidomycin. Nat Chem Biol *6*, 209-217.
Shaner, N.C., Campbell, R.E., Steinbach, P.A., Giepmans, B.N., Palmer, A.E., and Tsien, R.Y. (2004). Improved monomeric red, orange and yellow fluorescent proteins derived from Discosoma sp. red fluorescent protein. In Nat Biotechnol (United States), pp. 1567-1572.
Shay, J.W., and Wright, W.E. (2011). Role of telomeres and telomerase in cancer. Semin Cancer Biol *21*, 349-353.
Singh, J., Petter, R.C., Baillie, T.A., and Whitty, A. (2011). The resurgence of covalent drugs. Nat Rev Drug Discov *10*, 307-317.
Singh, K.K., Wachsmuth, L., Kulozik, A.E., and Gehring, N.H. (2013). Two mammalian MAGOH genes contribute to exon junction complex composition and nonsense-mediated decay. In RNA Biol, pp. 1291-1298.
Slaine, P.D., Kleer, M., Smith, N.K., Khaperskyy, D.A., and McCormick, C. (2017a). Stress Granule-Inducing Eukaryotic Translation Initiation Factor 4A Inhibitors Block Influenza A Virus Replication. Viruses *9*.
Slaine, P.D., Kleer, M., Smith, N.K., Khaperskyy, D.A., and McCormick, C. (2017b). Stress Granule-Inducing Eukaryotic Translation Initiation Factor 4A Inhibitors Block Influenza A Virus Replication. In Viruses.
Smith, B.J. (1984). SDS Polyacrylamide Gel Electrophoresis of Proteins. In Proteins Methods in Molecular Biology (Humana Press).
Storey, J. (2002). A direct approach to false discovery rates. Journal of the Royal Statistical Society.
Storey, J.D., and Tibshirani, R. (2003). Statistical significance for genomewide studies. Proc Natl Acad Sci U S A *100*, 9440-9445.
Suizu, T., Iimura, Y., Gomi, K., Takahashi, K., Hara, S., and Yoshizawa, K. (1989). l-Canavanine Resistance as a Positive Selectable Marker in Diploid Yeast Transformation through Integral Disruption of the CAN 1 Gene. Agricultural and Biological Chemistry *53*, 431-436.

Sun, Y., Atas, E., Lindqvist, L.M., Sonenberg, N., Pelletier, J., and Meller, A. (2014). Single-molecule kinetics of the eukaryotic initiation factor 4AI upon RNA unwinding. Structure *22*, 941-948.
Svitkin, Y.V., Pause, A., Haghighat, A., Pyronnet, S., Witherell, G., Belsham, G.J., and Sonenberg, N. (2001). The requirement for eukaryotic initiation factor 4A (eIF4A) in translation is in direct proportion to the degree of mRNA 5' secondary structure. Rna *7*, 382-394.
Swisher, K.D., and Parker, R. (2010). Localization to, and effects of Pbp1, Pbp4, Lsm12, Dhh1, and Pab1 on stress granules in Saccharomyces cerevisiae. PLoS One *5*, e10006.
Szklarczyk, D., Gable, A.L., Lyon, D., Junge, A., Wyder, S., Huerta-Cepas, J., Simonovic, M., Doncheva, N.T., Morris, J.H., Bork, P*., et al.* (2019a). STRING v11: protein–protein association networks with increased coverage, supporting functional discovery in genome-wide experimental datasets. In Nucleic Acids Res, pp. D607-613.
Szklarczyk, D., Gable, A.L., Lyon, D., Junge, A., Wyder, S., Huerta-Cepas, J., Simonovic, M., Doncheva, N.T., Morris, J.H., Bork, P*., et al.* (2019b). STRING v11: protein-protein association networks with increased coverage, supporting functional discovery in genome-wide experimental datasets. Nucleic Acids Res *47*, D607-d613.
Taylor, J.B., and Triggle, D.J. (2007). Comprehensive Medicinal Chemistry II, 2 edn (Elsevier Science).
Therapeutics, E. (2019). Study of eFT226 in Subjects With Selected Advanced Solid Tumor Malignancies (U.S. National Library of Medicine).
Tisdale, M.J. (2009). Mechanisms of cancer cachexia. Physiol Rev *89*, 381-410.
Towbin, H., Staehelin, T., and Gordon, J. (1979). Electrophoretic transfer of proteins from polyacrylamide gels to nitrocellulose sheets: procedure and some applications. Proc Natl Acad Sci U S A *76*, 4350-4354.
Treusch, S., Hamamichi, S., Goodman, J.L., Matlack, K.E., Chung, C.Y., Baru, V., Shulman, J.M., Parrado, A., Bevis, B.J., Valastyan, J.S*., et al.* (2011). Functional links between Abeta toxicity, endocytic trafficking, and Alzheimer's disease risk factors in yeast. Science *334*, 1241-1245.
Trudgian, D.C., Fischer, R., Guo, X., Kessler, B.M., and Mirzaei, H. (2014). GOAT--a simple LC-MS/MS gradient optimization tool. Proteomics *14*, 1467-1471.
Tsumuraya, T., Ishikawa, C., Machijima, Y., Nakachi, S., Senba, M., Tanaka, J., and Mori, N. (2011). Effects of hippuristanol, an inhibitor of eIF4A, on adult T-cell leukemia. Biochem Pharmacol *81*, 713-722.
Tu, C., Sheng, Q., Li, J., Ma, D., Shen, X., Wang, X., Shyr, Y., Yi, Z., and Qu, J. (2015). Optimization of Search Engines and Postprocessing Approaches to Maximize Peptide and Protein Identification for High-Resolution Mass Data. J Proteome Res *14*, 4662-4673.
Uttenweiler-Joseph, S., Bouyssie, D., Calligaris, D., Lutz, P.G., Monsarrat, B., and Burlet-Schiltz, O. (2013). Quantitative proteomic analysis to decipher the differential apoptotic response of bortezomib-treated APL cells before and after retinoic acid differentiation reveals involvement of protein toxicity mechanisms. Proteomics *13*, 37-47.
Venturi, V. (2012). The Genetic Profiles Of Tif1 And Tif2 Duplicate Genes. In Biology (Victoria University of Wellington).
Venturi, V., Little, R., Bircham, P.W., Rodigheri Brito, J., Atkinson, P.H., Maass, D.R., and Teesdale-Spittle, P.H. (2018). Characterisation of the biological response of Saccharomyces cerevisiae to the loss of an allele of the eukaryotic initiation factor 4A. Biochem Biophys Res Commun *496*, 1082-1087.
Veo, B.L., and Krushel, L.A. (2009). Translation initiation of the human tau mRNA through an internal ribosomal entry site. J Alzheimers Dis *16*, 271-275.
von der Haar, T. (2007). Optimized Protein Extraction for Quantitative Proteomics of Yeasts. PLoS One *2*.
Waldron, J.A., Tack, D.C., Ritchey, L.E., Gillen, S.L., Wilczynska, A., Turro, E., Bevilacqua, P.C., Assmann, S.M., Bushell, M., and Le Quesne, J. (2019). mRNA structural elements immediately upstream of the start codon dictate dependence upon eIF4A helicase activity. Genome Biol *20*, 300.
Wan, Y.Y. (2014). GATA3: a master of many trades in immune regulation. Trends Immunol *35*, 233-242.

Wang, Q., and Yang, H.S. (2019). The role of Pdcd4 in tumor suppression and protein translation. Biol Cell.
Wang, W.B., Boing, S., Zhou, X.Q., Ji, P., Dong, Y., Yao, Q., and Muller-Tidow, C. (2002). Identification of metastasis-associated genes in early stage non-small cell lung cancer by subtractive hybridization. Sheng Wu Hua Xue Yu Sheng Wu Wu Li Xue Bao (Shanghai) *34*, 273-278.
Weissman, J., Guthrie, C., and Fink, G.R. (2010). Guide to Yeast Genetics: Functional Genomics, Proteomics, and Other Systems Analysis, Vol 470 (Elsevier).
Winzeler, E.A., Shoemaker, D.D., Astromoff, A., Liang, H., Anderson, K., Andre, B., Bangham, R., Benito, R., Boeke, J.D., Bussey, H.*, et al.* (1999). Functional characterization of the S. cerevisiae genome by gene deletion and parallel analysis. Science *285*, 901-906.
Wolfe, A.L., Singh, K., Zhong, Y., Drewe, P., Rajasekhar, V.K., Sanghvi, V.R., Mavrakis, K.J., Jiang, M., Roderick, J.E., Van der Meulen, J.*, et al.* (2014). RNA G-quadruplexes cause eIF4A-dependent oncogene translation in cancer. Nature *513*, 65-70.
Wood, V., Gwilliam, R., Rajandream, M.A., Lyne, M., Lyne, R., Stewart, A., Sgouros, J., Peat, N., Hayles, J., Baker, S.*, et al.* (2002). The genome sequence of Schizosaccharomyces pombe. Nature *415*, 871-880.
Xue, Q., Yan, Y., Zhang, R., and Xiong, H. (2018). Regulation of iNOS on Immune Cells and Its Role in Diseases. Int J Mol Sci *19*.
Yang, X., Shen, Y., Garre, E., Hao, X., Krumlinde, D., Cvijović, M., Arens, C., Nyström, T., Liu, B., and Sunnerhagen, P. (2014). Stress Granule-Defective Mutants Deregulate Stress Responsive Transcripts. In PLoS Genet.
Yanguez, E., Castello, A., Welnowska, E., Carrasco, L., Goodfellow, I., and Nieto, A. (2011). Functional impairment of eIF4A and eIF4G factors correlates with inhibition of influenza virus mRNA translation. Virology *413*, 93-102.
Yeastgenome.org. SGD all ORFs 5prime UTRs.
Yu, F.S., Lin, M.L., Hsu, S.C., Yu, C.C., Huang, Y.P., Kuo, Y.H., and Chung, J.G. (2016). 4-Hydroxybutenolide impairs cell migration, and invasion of human oral cancer SCC-4 cells via the inhibition of NF-kappaB and MAPK signaling pathways. Int J Oncol *49*, 579-588.
Zhang, L., Kasif, S., Cantor, C.R., and Broude, N.E. (2004). GC/AT-content spikes as genomic punctuation marks. In Proc Natl Acad Sci U S A, pp. 16855-16860.
Zhu, W., Smith, J.W., and Huang, C.M. (2010). Mass Spectrometry-Based Label-Free Quantitative Proteomics. J Biomed Biotechnol *2010*.
Zhuo, C.X., and Furstner, A. (2018). Catalysis-Based Total Syntheses of Pateamine A and DMDA-Pat A. J Am Chem Soc *140*, 10514-10523.
Ziehr, B., Lenarcic, E., Cecil, C., and Moorman, N.J. (2016). The eIF4AIII RNA helicase is a critical determinant of human cytomegalovirus replication. Virology *489*, 194-201.

Supplementary data

1. Yeast tif1Δ *GFP screen ontological enrichments*

source	Term name	Term id	Adjusted p value
GO:BP	cytoplasmic translation	GO:0002181	5.50E-23
GO:BP	organonitrogen compound biosynthetic process	GO:1901566	5.93E-15
GO:BP	amide biosynthetic process	GO:0043604	1.14E-13
GO:BP	translation	GO:0006412	1.11E-12
GO:BP	peptide biosynthetic process	GO:0043043	1.66E-12
GO:BP	cellular amide metabolic process	GO:0043603	4.73E-12
GO:BP	peptide metabolic process	GO:0006518	2.62E-11
GO:BP	ribonucleoprotein complex biogenesis	GO:0022613	4.65E-11
GO:BP	ribosome biogenesis	GO:0042254	6.79E-10
GO:BP	cytoplasmic translational initiation	GO:0002183	1.00E-04
GO:BP	formation of cytoplasmic translation initiation complex	GO:0001732	2.90E-04
GO:BP	ribonucleoprotein complex subunit organization	GO:0071826	3.25E-04
GO:BP	ribonucleoprotein complex assembly	GO:0022618	6.09E-04
GO:BP	ribosome assembly	GO:0042255	2.18E-03
GO:BP	cellular amino acid biosynthetic process	GO:0008652	3.03E-03
GO:BP	rRNA processing	GO:0006364	4.04E-03
GO:BP	glutamine family amino acid biosynthetic process	GO:0009084	5.00E-03
GO:BP	ribosomal small subunit biogenesis	GO:0042274	7.19E-03
GO:BP	arginine biosynthetic process	GO:0006526	7.65E-03
GO:BP	rRNA metabolic process	GO:0016072	1.01E-02
GO:BP	GDP-mannose biosynthetic process	GO:0009298	1.19E-02
GO:BP	GDP-mannose metabolic process	GO:0019673	1.19E-02
GO:BP	alpha-amino acid biosynthetic process	GO:1901607	3.93E-02
GO:BP	rRNA export from nucleus	GO:0006407	4.61E-02
GO:BP	arginine metabolic process	GO:0006525	4.61E-02
GO:BP	rRNA transport	GO:0051029	4.61E-02
GO:CC	ribonucleoprotein complex	GO:1990904	1.80E-20
GO:CC	cytosolic ribosome	GO:0022626	3.31E-20
GO:CC	cytosolic part	GO:0044445	2.77E-19
GO:CC	ribosome	GO:0005840	1.77E-17
GO:CC	ribosomal subunit	GO:0044391	2.46E-15
GO:CC	cytosolic small ribosomal subunit	GO:0022627	3.52E-13
GO:CC	cytosol	GO:0005829	1.13E-12
GO:CC	small ribosomal subunit	GO:0015935	5.79E-10
GO:CC	cytosolic large ribosomal subunit	GO:0022625	5.62E-07
GO:CC	cytoplasmic stress granule	GO:0010494	2.25E-06
GO:CC	cytoplasmic ribonucleoprotein granule	GO:0036464	1.71E-04
GO:CC	ribonucleoprotein granule	GO:0035770	1.71E-04

GO:CC	large ribosomal subunit	GO:0015934	2.07E-04
GO:CC	eukaryotic 48S preinitiation complex	GO:0033290	6.26E-04
GO:CC	translation preinitiation complex	GO:0070993	2.82E-03
GO:CC	nucleolar part	GO:0044452	3.42E-02
GO:CC	RNA polymerase I complex	GO:0005736	3.63E-02
KEGG	Ribosome	KEGG:03010	7.69E-11
WP	Cytoplasmic Ribosomal Proteins	WP:WP210	3.34E-04
WP	Colanic Acid Building Blocks Biosynthesis	WP:WP121	1.97E-02
WP	Translation Factors	WP:WP32	2.52E-02

2. Yeast mass spectrometry ontological enrichments tif1Δ down-regulated proteins

source	Term name	Term id	Adjusted p-value
GO:BP	cellular amino acid biosynthetic process	GO:0008652	8.31E-06
GO:BP	alpha-amino acid biosynthetic process	GO:1901607	7.48E-05
GO:BP	carboxylic acid biosynthetic process	GO:0046394	3.29E-04
GO:BP	organic acid biosynthetic process	GO:0016053	3.29E-04
GO:BP	cellular amino acid metabolic process	GO:0006520	4.11E-04
GO:BP	aspartate family amino acid biosynthetic process	GO:0009067	8.64E-04
GO:BP	small molecule metabolic process	GO:0044281	2.09E-03
GO:BP	small molecule biosynthetic process	GO:0044283	2.10E-03
GO:BP	alpha-amino acid metabolic process	GO:1901605	2.37E-03
GO:BP	aspartate family amino acid metabolic process	GO:0009066	6.01E-03
GO:BP	carboxylic acid metabolic process	GO:0019752	8.98E-03
GO:BP	oxoacid metabolic process	GO:0043436	1.39E-02
GO:BP	organonitrogen compound biosynthetic process	GO:1901566	1.45E-02
GO:BP	organic acid metabolic process	GO:0006082	1.45E-02
GO:BP	translational initiation	GO:0006413	4.05E-02
GO:CC	cytoplasmic stress granule	GO:0010494	1.40E-03
GO:CC	cytoplasmic ribonucleoprotein granule	GO:0036464	9.71E-03
GO:CC	ribonucleoprotein granule	GO:0035770	9.71E-03
KEGG	Biosynthesis of amino acids	KEGG:01230	9.18E-05
KEGG	Lysine biosynthesis	KEGG:00300	5.95E-03
KEGG	Metabolic pathways	KEGG:01100	1.27E-02
KEGG	Biosynthesis of secondary metabolites	KEGG:01110	2.27E-02
WP	Asparagine Biosynthesis	WP:WP67	4.99E-02

3. Yeast mass spectrometry ontological enrichments tif1Δ up-regulated proteins

source	Term name	Term id	Adjusted p-value
GO:BP	cytoplasmic translation	GO:0002181	2.17E-03
GO:BP	proton transmembrane transport	GO:1902600	2.52E-03
GO:BP	ATP synthesis coupled proton transport	GO:0015986	9.83E-03
GO:BP	energy coupled proton transport, down electrochemical gradient	GO:0015985	9.83E-03
GO:BP	ATP biosynthetic process	GO:0006754	9.83E-03
GO:BP	cellular amide metabolic process	GO:0043603	1.20E-02
GO:BP	monovalent inorganic cation transport	GO:0015672	2.03E-02
GO:BP	purine ribonucleoside triphosphate biosynthetic process	GO:0009206	2.30E-02
GO:BP	purine nucleoside triphosphate biosynthetic process	GO:0009145	2.30E-02
GO:BP	purine ribonucleoside triphosphate metabolic process	GO:0009205	2.30E-02
GO:BP	purine nucleoside triphosphate metabolic process	GO:0009144	3.08E-02
GO:BP	ribonucleoside triphosphate metabolic process	GO:0009199	4.05E-02
GO:BP	ribonucleoside triphosphate biosynthetic process	GO:0009201	4.05E-02
GO:BP	purine ribonucleotide biosynthetic process	GO:0009152	4.74E-02
GO:CC	proton-transporting two-sector ATPase complex	GO:0016469	9.98E-06
GO:CC	cytosol	GO:0005829	2.11E-05
GO:CC	cytosolic ribosome	GO:0022626	1.15E-04
GO:CC	proton-transporting two-sector ATPase complex, catalytic domain	GO:0033178	2.14E-04
GO:CC	cytosolic part	GO:0044445	2.54E-04
GO:CC	ribosome	GO:0005840	7.52E-04
GO:CC	proton-transporting ATP synthase complex	GO:0045259	8.93E-04
GO:CC	mitochondrial proton-transporting ATP synthase complex	GO:0005753	8.93E-04
GO:CC	ribosomal subunit	GO:0044391	2.20E-03
GO:CC	mitochondrial nucleoid	GO:0042645	3.02E-03
GO:CC	nucleoid	GO:0009295	3.02E-03
GO:CC	mitochondrial intermembrane space	GO:0005758	3.09E-03
GO:CC	organelle envelope lumen	GO:0031970	4.29E-03
GO:CC	proton-transporting ATP synthase, stator stalk	GO:0045265	2.51E-02
GO:CC	mitochondrial proton-transporting ATP synthase, stator stalk	GO:0000274	2.51E-02
GO:CC	cytosolic large ribosomal subunit	GO:0022625	3.65E-02
GO:CC	mitochondrion	GO:0005739	4.04E-02
GO:CC	inner mitochondrial membrane protein complex	GO:0098800	4.80E-02
KEGG	Oxidative phosphorylation	KEGG:00190	2.89E-04
KEGG	Ribosome	KEGG:03010	3.17E-03
WP	Principle Pathways of Carbon Metabolism	WP:WP112	1.02E-02
WP	Cytoplasmic Ribosomal Proteins	WP:WP210	2.17E-02

4. Yeast mass spectrometry ontological enrichments tif2Δ down-regulated proteins

source	Term name	Term id	Adjusted p-value
GO:BP	carbohydrate metabolic process	GO:0005975	1.88E-08
GO:BP	trehalose metabolic process	GO:0005991	2.99E-05
GO:BP	nucleobase-containing small molecule metabolic process	GO:0055086	7.92E-05
GO:BP	small molecule metabolic process	GO:0044281	8.54E-05
GO:BP	generation of precursor metabolites and energy	GO:0006091	9.25E-05
GO:BP	trehalose biosynthetic process	GO:0005992	0.00015
GO:BP	oxidation-reduction process	GO:0055114	0.00026
GO:BP	disaccharide biosynthetic process	GO:0046351	0.000297
GO:BP	oligosaccharide biosynthetic process	GO:0009312	0.000531
GO:BP	purine ribonucleotide metabolic process	GO:0009150	0.000558
GO:BP	purine nucleotide metabolic process	GO:0006163	0.000751
GO:BP	ribonucleotide metabolic process	GO:0009259	0.001409
GO:BP	carbohydrate derivative metabolic process	GO:1901135	0.001583
GO:BP	response to oxidative stress	GO:0006979	0.001834
GO:BP	ribose phosphate metabolic process	GO:0019693	0.00222
GO:BP	purine-containing compound metabolic process	GO:0072521	0.002516
GO:BP	monocarboxylic acid metabolic process	GO:0032787	0.003511
GO:BP	pyruvate metabolic process	GO:0006090	0.00358
GO:BP	trehalose metabolism in response to stress	GO:0070413	0.004646
GO:BP	nucleotide metabolic process	GO:0009117	0.004953
GO:BP	hexose metabolic process	GO:0019318	0.005651
GO:BP	nucleoside phosphate metabolic process	GO:0006753	0.005988
GO:BP	response to heat	GO:0009408	0.006139
GO:BP	disaccharide metabolic process	GO:0005984	0.006545
GO:BP	cellular response to oxidative stress	GO:0034599	0.007423
GO:BP	response to temperature stimulus	GO:0009266	0.010635
GO:BP	oligosaccharide metabolic process	GO:0009311	0.011895
GO:BP	monosaccharide metabolic process	GO:0005996	0.01233
GO:BP	nucleoside diphosphate phosphorylation	GO:0006165	0.013652
GO:BP	nucleotide phosphorylation	GO:0046939	0.015604
GO:BP	glucose metabolic process	GO:0006006	0.015664
GO:BP	nucleoside diphosphate metabolic process	GO:0009132	0.020154
GO:BP	carbohydrate catabolic process	GO:0016052	0.026139
GO:BP	carbohydrate biosynthetic process	GO:0016051	0.027855
GO:BP	organophosphate metabolic process	GO:0019637	0.030029
GO:BP	ATP metabolic process	GO:0046034	0.035674
GO:CC	mitochondrion	GO:0005739	0.010123
GO:CC	nucleoid	GO:0009295	0.012053
GO:CC	mitochondrial nucleoid	GO:0042645	0.012053
GO:CC	mitochondrial intermembrane space	GO:0005758	0.023337

GO:CC	organelle envelope lumen	GO:0031970	0.032073
KEGG	Starch and sucrose metabolism	KEGG:00500	5.26E-05
KEGG	Biosynthesis of antibiotics	KEGG:01130	8.76E-05
KEGG	Metabolic pathways	KEGG:01100	0.000103
KEGG	Carbon metabolism	KEGG:01200	0.001184
KEGG	Biosynthesis of secondary metabolites	KEGG:01110	0.002126
KEGG	Amino sugar and nucleotide sugar metabolism	KEGG:00520	0.003291
KEGG	Glycolysis / Gluconeogenesis	KEGG:00010	0.004782
KEGG	Galactose metabolism	KEGG:00052	0.011467
KEGG	Citrate cycle (TCA cycle)	KEGG:00020	0.035444
WP	Principle Pathways of Carbon Metabolism	WP:WP112	6.46E-06
WP	Trehalose Anabolism	WP:WP398	0.000808
WP	Glycolysis and Gluconeogenesis	WP:WP515	0.036168
WP	Glycerol Teichoic Acid Biosynthesis	WP:WP563	0.049969

5. Yeast mass spectrometry ontological enrichments tif2Δ up-regulated proteins

source	Term name	Term id	Adjusted p-value
GO:BP	translation	GO:0006412	6.00E-11
GO:BP	peptide biosynthetic process	GO:0043043	7.54E-11
GO:BP	organonitrogen compound biosynthetic process	GO:1901566	9.75E-11
GO:BP	peptide metabolic process	GO:0006518	3.62E-10
GO:BP	amide biosynthetic process	GO:0043604	7.57E-10
GO:BP	cellular amide metabolic process	GO:0043603	1.19E-08
GO:BP	tRNA aminoacylation for protein translation	GO:0006418	2.05E-07
GO:BP	tRNA aminoacylation	GO:0043039	3.95E-07
GO:BP	amino acid activation	GO:0043038	3.95E-07
GO:BP	ncRNA metabolic process	GO:0034660	9E-05
GO:BP	cellular amino acid metabolic process	GO:0006520	0.000179
GO:BP	cytoplasmic translation	GO:0002181	0.006426
GO:BP	regulation of translational fidelity	GO:0006450	0.009219
GO:BP	translational elongation	GO:0006414	0.012349
GO:BP	'de novo' cotranslational protein folding	GO:0051083	0.012456
GO:BP	translational frameshifting	GO:0006452	0.019824
GO:BP	translational termination	GO:0006415	0.0206
GO:BP	carboxylic acid metabolic process	GO:0019752	0.034793
GO:CC	polysome	GO:0005844	1.05E-05
GO:CC	ribonucleoprotein complex	GO:1990904	1.14E-05
GO:CC	cytoplasmic stress granule	GO:0010494	0.000563
GO:CC	cytoplasmic ribonucleoprotein granule	GO:0036464	0.005281
GO:CC	ribonucleoprotein granule	GO:0035770	0.005281
GO:CC	cytosolic ribosome	GO:0022626	0.020888
KEGG	Aminoacyl-tRNA biosynthesis	KEGG:00970	9.83E-07
WP	Cytoplasmic tRNA Synthetases	WP:WP219	1.62E-05

6. Yeast mass spectrometry ontological enrichments tif2Δ down-regulated proteins not corrected for multiple testing

source	Term name	Term id	Adjusted p-value
GO:BP	carbohydrate metabolic process	GO:0005975	9.51E-10
GO:BP	generation of precursor metabolites and energy	GO:0006091	1.08E-06
GO:BP	oxidation-reduction process	GO:0055114	1.29E-06
GO:BP	small molecule metabolic process	GO:0044281	7.46E-06
GO:BP	response to oxidative stress	GO:0006979	1.48E-05
GO:BP	nucleobase-containing small molecule metabolic process	GO:0055086	4.52E-05
GO:BP	carbohydrate derivative metabolic process	GO:1901135	0.000111
GO:BP	trehalose metabolic process	GO:0005991	0.000241
GO:BP	cellular response to oxidative stress	GO:0034599	0.000369
GO:BP	ribonucleotide metabolic process	GO:0009259	0.000786
GO:BP	trehalose biosynthetic process	GO:0005992	0.000819
GO:BP	hexose metabolic process	GO:0019318	0.001009
GO:BP	ribose phosphate metabolic process	GO:0019693	0.001354
GO:BP	disaccharide biosynthetic process	GO:0046351	0.001621
GO:BP	purine ribonucleotide metabolic process	GO:0009150	0.002192
GO:BP	monosaccharide metabolic process	GO:0005996	0.002739
GO:BP	oligosaccharide biosynthetic process	GO:0009312	0.002886
GO:BP	purine nucleotide metabolic process	GO:0006163	0.003017
GO:BP	pyruvate metabolic process	GO:0006090	0.00311
GO:BP	monocarboxylic acid metabolic process	GO:0032787	0.004205
GO:BP	nucleotide metabolic process	GO:0009117	0.006259
GO:BP	carbohydrate catabolic process	GO:0016052	0.007135
GO:BP	nucleoside diphosphate phosphorylation	GO:0006165	0.007231
GO:BP	carbohydrate biosynthetic process	GO:0016051	0.007736
GO:BP	nucleoside phosphate metabolic process	GO:0006753	0.00779
GO:BP	nucleotide phosphorylation	GO:0046939	0.00849
GO:BP	purine-containing compound metabolic process	GO:0072521	0.010968
GO:BP	nucleoside diphosphate metabolic process	GO:0009132	0.011538
GO:BP	nucleotide-sugar metabolic process	GO:0009225	0.015674
GO:BP	glucose metabolic process	GO:0006006	0.017063
GO:BP	mannose metabolic process	GO:0006013	0.017141
GO:BP	trehalose metabolism in response to stress	GO:0070413	0.017141
GO:BP	response to abiotic stimulus	GO:0009628	0.018583
GO:BP	response to stress	GO:0006950	0.032866
GO:BP	carboxylic acid metabolic process	GO:0019752	0.036628
GO:BP	organophosphate metabolic process	GO:0019637	0.048621
GO:BP	disaccharide metabolic process	GO:0005984	0.049023
GO:CC	mitochondrial intermembrane space	GO:0005758	0.003292
GO:CC	mitochondrion	GO:0005739	0.003871

GO:CC	organelle envelope lumen	GO:0031970	0.005016
GO:CC	cytoplasmic stress granule	GO:0010494	0.005892
GO:CC	proton-transporting ATP synthase, catalytic core	GO:0045267	0.033168
GO:CC	mitochondrial proton-transporting ATP synthase, catalytic core	GO:0005754	0.033168
GO:CC	cytosol	GO:0005829	0.036814
KEGG	Carbon metabolism	KEGG:01200	4.14E-05
KEGG	Biosynthesis of antibiotics	KEGG:01130	6.24E-05
KEGG	Metabolic pathways	KEGG:01100	0.000117
KEGG	Biosynthesis of secondary metabolites	KEGG:01110	0.000191
KEGG	Fructose and mannose metabolism	KEGG:00051	0.000286
KEGG	Starch and sucrose metabolism	KEGG:00500	0.000997
KEGG	Amino sugar and nucleotide sugar metabolism	KEGG:00520	0.00261
KEGG	Glycolysis / Gluconeogenesis	KEGG:00010	0.007782
WP	Principle Pathways of Carbon Metabolism	WP:WP112	2.1E-05
WP	Trehalose Anabolism	WP:WP398	0.006127
WP	Colanic Acid Building Blocks Biosynthesis	WP:WP121	0.04999

7. Yeast mass spectrometry ontological enrichments tif2Δ up-regulated proteins not corrected for multiple testing

source	Term name	Term id	Adjusted p-value
GO:BP	amide biosynthetic process	GO:0043604	8.36E-20
GO:BP	translation	GO:0006412	9.78E-20
GO:BP	organonitrogen compound biosynthetic process	GO:1901566	1.16E-19
GO:BP	peptide biosynthetic process	GO:0043043	1.49E-19
GO:BP	peptide metabolic process	GO:0006518	2.60E-18
GO:BP	cellular amide metabolic process	GO:0043603	1.69E-17
GO:BP	cytoplasmic translation	GO:0002181	5.45E-13
GO:BP	tRNA aminoacylation for protein translation	GO:0006418	1.94E-06
GO:BP	cellular amino acid metabolic process	GO:0006520	2.11E-06
GO:BP	amino acid activation	GO:0043038	4.02E-06
GO:BP	tRNA aminoacylation	GO:0043039	4.02E-06
GO:BP	carboxylic acid metabolic process	GO:0019752	6.97E-05
GO:BP	oxoacid metabolic process	GO:0043436	0.000148
GO:BP	organic acid metabolic process	GO:0006082	0.000161
GO:BP	'de novo' cotranslational protein folding	GO:0051083	0.001055
GO:BP	translational elongation	GO:0006414	0.001583
GO:BP	small molecule metabolic process	GO:0044281	0.001776
GO:BP	ncRNA metabolic process	GO:0034660	0.0021
GO:BP	ribosome biogenesis	GO:0042254	0.004177
GO:BP	regulation of translational fidelity	GO:0006450	0.004431
GO:BP	ribonucleoprotein complex biogenesis	GO:0022613	0.007287
GO:BP	'de novo' protein folding	GO:0006458	0.01885
GO:BP	rRNA-containing ribonucleoprotein complex export from nucleus	GO:0071428	0.025141
GO:BP	nuclear transport	GO:0051169	0.035416
GO:BP	nucleocytoplasmic transport	GO:0006913	0.035416
GO:BP	ribosomal small subunit assembly	GO:0000028	0.040179
GO:BP	GMP metabolic process	GO:0046037	0.041342
GO:BP	GMP biosynthetic process	GO:0006177	0.041342
GO:CC	ribonucleoprotein complex	GO:1990904	1.46E-13
GO:CC	cytosolic ribosome	GO:0022626	2.28E-11
GO:CC	cytosolic part	GO:0044445	1.63E-09
GO:CC	cytosol	GO:0005829	4.75E-09
GO:CC	polysome	GO:0005844	2.65E-08
GO:CC	ribosomal subunit	GO:0044391	1.17E-07
GO:CC	ribosome	GO:0005840	1.17E-07
GO:CC	cytoplasmic stress granule	GO:0010494	5.22E-06
GO:CC	cytosolic small ribosomal subunit	GO:0022627	3.34E-05
GO:CC	ribonucleoprotein granule	GO:0035770	0.000174
GO:CC	cytoplasmic ribonucleoprotein granule	GO:0036464	0.000174

GO:CC	cytosolic large ribosomal subunit	GO:0022625	0.000247
GO:CC	small ribosomal subunit	GO:0015935	0.001007
GO:CC	large ribosomal subunit	GO:0015934	0.010611
GO:CC	multi-eIF complex	GO:0043614	0.049826
KEGG	Aminoacyl-tRNA biosynthesis	KEGG:00970	2.12E-05
KEGG	Ribosome	KEGG:03010	2.17E-05
KEGG	Biosynthesis of secondary metabolites	KEGG:01110	0.007957
KEGG	Biosynthesis of amino acids	KEGG:01230	0.046514
WP	Cytoplasmic tRNA Synthetases	WP:WP219	0.002243
HP	Macrocytic anemia	HP:0001972	0.015113

8. Supplementary table tif1Δ mass spectrometry quantitative data

Gene name	Accession Number	T-Test (P-Value) TIC	Fold Change TIC	q-value TIC	T-Test (P-Value) iBAQ	Fold Change iBAQ	q-value iBAQ
TY1B-JR1	YJ11B_YEAST	0.00026	0.2907	0.1221	0.023	0.2427	0.4644
LSP1	LSP1_YEAST	0.00095	1.9939	0.2192	0.016	1.6280	0.3965
ABP1	ABP1_YEAST	0.0014	0.4274	0.2192	0.0091	0.4006	0.3101
RPS20	RS20_YEAST	0.0022	1.7620	0.2583	0.3	1.3214	0.6613
ADH6	ADH6_YEAST	0.0035	0.2164	0.2877	0.057	0.3654	0.5452
LEU1	LEUC_YEAST	0.0053	13.0388	0.2877	0.00023	18.6903	0.0418
RPL10	RL10_YEAST	0.0058	1.5324	0.2877	0.019	1.7435	0.4361
GPP1	GPP1_YEAST	0.0068	0.5428	0.2877	0.062	0.4332	0.5452
FAA4	LCF4_YEAST	0.0068	0.1024	0.2877	0.21	0.0813	0.6432
LYS21	HOSM_YEAST	0.0069	0.2263	0.2877	0.063	0.3605	0.5452
RPL4A	RL4A_YEAST	0.0082	1.2493	0.2877	0.23	1.2755	0.6613
HSP12	HSP12_YEAST	0.0083	4.0949	0.2877	0.034	4.6867	0.5452
CCS1	CCS1_YEAST	0.0086	0.0305	0.2877	0.00042	0.0087	0.0572
CCP1	CCPR_YEAST	0.0087	9.2383	0.2877	0.0081	29.3721	0.3053
THO1	THO1_YEAST	0.0093	0.2674	0.2877	0.065	0.3883	0.5452
TY1B-DR3	YD12B_YEAST	0.0098	0.2040	0.2877	0.00014	0.1832	0.0382
LSC1	SUCA_YEAST	0.013	3.2686	0.3355	0.26	2.5811	0.6613
VMA4	VATE_YEAST	0.014	1.4232	0.3355	0.95	0.9764	0.8899
RIB3	RIB3_YEAST	0.014	0.3001	0.3355	0.35	0.5787	0.6613
POR1	VDAC1_YEAST	0.015	1.4485	0.3355	0.19	1.5299	0.6432
PAB1	PABP_YEAST	0.015	0.7780	0.3355	0.12	0.7605	0.5670
ATP2	ATPB_YEAST	0.018	1.9539	0.3843	0.026	2.0847	0.4888
PGM2	PGM2_YEAST	0.019	4.4765	0.3880	0.007	8.7861	0.3053
TIF1	IF4A_YEAST	0.02	0.5696	0.3914	0.069	0.3377	0.5452
RPL11A	RL11A_YEAST	0.021	1.3734	0.3945	0.74	1.0890	0.8318
PRX1	PRX1_YEAST	0.022	11.6108	0.3974	0.0016	4.2986	0.1745
PRE1	PSB4_YEAST	0.023	0.3063	0.4001	0.52	0.7876	0.7500
QCR2	QCR2_YEAST	0.025	2.8257	0.4049	0.0084	4.3760	0.3053
ECM33	ECM33_YEAST	0.025	0.4536	0.4049	0.25	0.4875	0.6613
ARC1	ARC1_YEAST	0.026	0.6599	0.4071	0.8	0.9377	0.8403
GPD1	GPD1_YEAST	0.027	2.3759	0.4091	0.026	3.3128	0.4888
TIF5	IF5_YEAST	0.033	0.4993	0.4462	0.095	0.4136	0.5670
PRO2	PROA_YEAST	0.033	0.3657	0.4462	0.046	0.4123	0.5452
TUB1	TBA1_YEAST	0.034	0.6516	0.4462	0.064	0.4582	0.5452
ATP4	ATPF_YEAST	0.035	16.8065	0.4462	0.055	35.8659	0.5452
ASN1	ASNS1_YEAST	0.035	0.3251	0.4462	0.037	0.2670	0.5452
HIS1	HIS1_YEAST	0.036	0.2741	0.4462	0.04	0.2599	0.5452
LYS12	LYS12_YEAST	0.037	0.3625	0.4462	0.16	0.0776	0.6230
RPS0B	RSSA2_YEAST	0.038	1.4887	0.4462	0.61	1.1933	0.7806

THR1	KHSE_YEAST	0.038	0.1811	0.4462	0.039	0.1982	0.5452
ASN2	ASNS2_YEAST	0.039	0.4010	0.4468	0.049	0.3103	0.5452
ALD4	ALDH4_YEAST	0.04	4.1536	0.4473	0.035	6.8190	0.5452
HIR2	HIR2_YEAST	0.041	0.0164	0.4478	0.32	0.0067	0.6613
RRB1	RRB1_YEAST	0.043	0.1058	0.4523	0.19	0.0663	0.6432
PMA1	PMA1_YEAST	0.044	0.9149	0.4523	0.11	0.7848	0.5670
CRP1	CRP1_YEAST	0.046	0.4464	0.4523	0.26	0.3419	0.6613
URA2	PYR1_YEAST	0.048	0.3296	0.4523	0.04	0.2645	0.5452
ACS2	ACS2_YEAST	0.049	2.4556	0.4523	0.056	2.6353	0.5452
NIP1	EIF3C_YEAST	0.049	0.4575	0.4523	0.18	0.5527	0.6432
FCY1	FCY1_YEAST	0.055	0.1868	0.4613	0.008	0.2116	0.3053
HOM2	DHAS_YEAST	0.059	0.5215	0.4621	0.04	0.3488	0.5452
SSC1	HSP77_YEAST	0.06	0.7034	0.4621	0.028	0.6863	0.5088
ATP1	ATPA_YEAST	0.064	1.7333	0.4697	0.014	2.5492	0.3816
ARO4	AROG_YEAST	0.065	0.4859	0.4697	0.034	0.4474	0.5452
MDH1	MDHM_YEAST	0.074	3.7953	0.4697	0.049	6.9808	0.5452
RPS27B	RS27B_YEAST	0.076	1.9416	0.4697	0.0001	2.1284	0.0382
ATP5	ATPO_YEAST	0.077	9.4914	0.4697	0.02	6.3197	0.4361
SBP1	SSBP1_YEAST	0.083	1.5598	0.4935	0.0061	1.8471	0.3053
GRX2	GLRX2_YEAST	0.11	2.2802	0.5016	0.02	2.6014	0.4361
RPS5	RS5_YEAST	0.12	1.5576	0.5078	0.022	1.8905	0.4613
CPR1	CYPH_YEAST	0.14	1.2076	0.5097	0.0058	1.4120	0.3053
PUB1	PUB1_YEAST	0.16	3.0008	0.5385	0.0069	0.2030	0.3053
YLR257W	YL257_YEAST	0.18	0.3910	0.5385	0.003	0.1358	0.2726
PST2	PST2_YEAST	0.23	1.5512	0.5484	0.042	1.6879	0.5452
RPL8B	RL8B_YEAST	0.25	1.2016	0.5728	0.033	1.2821	0.5452
SIS1	SIS1_YEAST	0.27	0.5699	0.5794	0.0054	0.5775	0.3053
HSP150	HS150_YEAST	0.33	1.9887	0.5797	0.011	5.8849	0.3528
TEF4	EF1G2_YEAST	0.33	1.2830	0.5797	0.047	3.5505	0.5452
PDI1	PDI_YEAST	0.46	0.8967	0.6052	0.012	0.7060	0.3634
ADH4	ADH4_YEAST	0.48	1.2711	0.6194	0.043	1.8346	0.5452
VMA1	VATA_YEAST	0.52	1.0921	0.6350	0.0049	1.2828	0.3053
YRB1	YRB1_YEAST	0.53	0.6319	0.6350	0.013	0.4942	0.3730
NHP6A	NHP6A_YEAST	0.54	0.8274	0.6373	0.015	0.3686	0.3894
HXK2	HXKB_YEAST	0.77	0.9521	0.7105	0.041	0.6365	0.5452

9. Supplementary table tif2Δ mass spectrometry quantitative data

Gene name	Accession Number	T-Test (P-Value) TIC	Fold Change TIC	q-value TIC	T-Test (P-Value) iBAQ	Fold Change iBAQ	q-value iBAQ
PGM2	PGM2_YEAST	0.0001	0.1167	0.0079	0.00029	0.0696	0.0092
ARP2	ARP2_YEAST	0.0001	0.1258	0.0079	0.011	0.3065	0.0688
HSP12	HSP12_YEAST	0.0001	0.1452	0.0079	0.0001	0.1239	0.0064
HSP26	HSP26_YEAST	0.0001	0.4521	0.0079	0.0001	0.3548	0.0064
ILV3	ILV3_YEAST	0.0001	7.4572	0.0079	0.00017	7.2876	0.0090
NOP56	NOP56_YEAST	0.0003	3.1389	0.0198	0.032	6.9511	0.1121
HXK1	HXKA_YEAST	0.00038	0.3961	0.0215	0.0001	0.3887	0.0064
SSE1	HSP7F_YEAST	0.00047	1.4203	0.0233	0.00074	1.5776	0.0197
GLK1	HXKG_YEAST	0.0007	0.2601	0.0305	0.0001	0.1973	0.0064
YDR341C	SYRC_YEAST	0.00077	2.0099	0.0305	0.041	2.5502	0.1210
ILS1	SYIC_YEAST	0.00093	3.2123	0.0335	0.0021	3.0572	0.0319
YGP1	YGP1_YEAST	0.0012	0.0267	0.0368	0.0077	0.0001	0.0584
PST2	PST2_YEAST	0.0013	0.5227	0.0368	0.065	0.3470	0.1606
POR1	VDAC1_YEAST	0.0013	0.7083	0.0368	0.0057	0.6073	0.0554
RPL35A	RL35A_YEAST	0.0017	1.3089	0.0450	0.97	1.0034	0.6075
LSP1	LSP1_YEAST	0.0023	0.6799	0.0570	0.0017	0.7479	0.0319
APE1	AMPL_YEAST	0.0028	0.3514	0.0617	0.041	0.3435	0.1210
GRE3	GRE3_YEAST	0.0028	0.6042	0.0617	0.11	0.4126	0.1981
TIF1	IF4A_YEAST	0.0032	0.6360	0.0668	0.00028	0.6320	0.0092
YDL124W	KAR_YEAST	0.0034	0.4145	0.0674	0.00025	0.3678	0.0092
HSP31	HSP31_YEAST	0.0039	0.1383	0.0737	0.19	0.1673	0.2622
GLY1	GLY1_YEAST	0.0042	2.1592	0.0757	0.092	1.3460	0.1850
EXG1	EXG1_YEAST	0.0045	0.1952	0.0760	0.066	0.2158	0.1618
PEP4	CARP_YEAST	0.0046	0.4959	0.0760	0.002	0.4804	0.0319
THS1	SYTC_YEAST	0.0053	2.1458	0.0841	0.085	2.2300	0.1806
CCP1	CCPR_YEAST	0.0061	0.1790	0.0893	0.068	0.3333	0.1629
KAP123	IMB4_YEAST	0.0062	1.6368	0.0893	0.041	1.6613	0.1210
GPD1	GPD1_YEAST	0.0063	0.6106	0.0893	0.00023	0.7099	0.0092
CDC60	SYLC_YEAST	0.0069	2.7954	0.0917	0.03	2.3149	0.1087
ALA1	SYA_YEAST	0.0072	3.7390	0.0917	0.0001	2.8737	0.0064
CPR3	CYPC_YEAST	0.0074	0.5582	0.0917	0.005	0.5753	0.0542
PAA1	PAA1_YEAST	0.0074	2.4943	0.0917	0.0071	1.9255	0.0566
TRP5	TRP_YEAST	0.008	1.8371	0.0962	0.016	1.8204	0.0810
NOP58	NOP58_YEAST	0.0085	1.9783	0.0992	0.13	1.8413	0.2170
YMR315W	YM94_YEAST	0.0092	0.3592	0.1014	0.00097	0.3380	0.0238
TIF35	EIF3G_YEAST	0.0097	2.8479	0.1040	0.013	2.8442	0.0754
TUF1	EFTU_YEAST	0.013	0.3849	0.1228	0.002	0.4936	0.0319
NIP1	EIF3C_YEAST	0.013	6.8473	0.1228	0.0085	3.8825	0.0630
CAR2	OAT_YEAST	0.015	0.5564	0.1322	0.0046	0.3992	0.0542

ATP2	ATPB_YEAST	0.018	0.7515	0.1428	0.013	0.6731	0.0754
YNL134C	YNN4_YEAST	0.019	0.5672	0.1478	0.021	0.5021	0.0905
EFT1	EF2_YEAST	0.022	1.2428	0.1587	0.011	1.3761	0.0688
MDH1	MDHM_YEAST	0.022	0.5901	0.1587	0.021	0.5266	0.0905
UGP1	UGPA1_YEAST	0.024	0.6500	0.1610	0.0029	0.4968	0.0402
RPS23B	RS23B_YEAST	0.027	1.5443	0.1610	0.025	1.3333	0.0996
ALD4	ALDH4_YEAST	0.028	0.3568	0.1610	0.007	0.3770	0.0566
RTC3	SDO1L_YEAST	0.029	0.0230	0.1620	0.019	ND	0.0891
PYC1	PYC1_YEAST	0.032	0.1569	0.1678	0.0088	0.0010	0.0631
PNC1	PNC1_YEAST	0.033	0.2536	0.1678	0.0016	0.1911	0.0319
TSL1	TSL1_YEAST	0.033	0.0402	0.1678	0.0041	0.0005	0.0523
VMA6	VA0D_YEAST	0.033	1.4478	0.1678	0.0054	1.4096	0.0554
TDH1	G3P1_YEAST	0.035	0.8268	0.1721	0.0013	0.7685	0.0276
MRP8	MRP8_YEAST	0.035	0.2890	0.1721	0.0018	0.3900	0.0319
RPL42B	RL44B_YEAST	0.036	2.1874	0.1721	0.018	4.2327	0.0856
ILV2	ILVB_YEAST	0.042	2.0089	0.1874	0.011	2.1685	0.0688
GRS1	SYG_YEAST	0.044	1.6096	0.1897	0.0051	1.8910	0.0542
TPS1	TPS1_YEAST	0.045	0.1183	0.1899	0.015	0.0166	0.0771
TAL1	TAL1_YEAST	0.047	0.8002	0.1922	0.0058	0.7573	0.0554
IDP1	IDHP_YEAST	0.048	0.4866	0.1943	0.015	0.2165	0.0771
IMD4	IMDH4_YEAST	0.05	1.5645	0.1983	0.014	1.7218	0.0769
TKL1	TKT1_YEAST	0.052	1.2934	0.2021	0.018	1.4421	0.0856
HRI1	HRI1_YEAST	0.054	1.4317	0.2021	0.021	1.5720	0.0905
LSC2	SUCB_YEAST	0.055	0.1022	0.2039	0.0028	0.0745	0.0402
GUS1	SYEC_YEAST	0.069	1.7506	0.2300	0.025	1.8305	0.0996
TDH3	G3P3_YEAST	0.08	0.9288	0.2623	0.015	0.8858	0.0771
RDL1	RDL1_YEAST	0.082	0.4034	0.2645	0.0033	0.4616	0.0438
RPL26B	RL26B_YEAST	0.087	1.1987	0.2696	0.0045	1.1729	0.0542
PRB1	PRTB_YEAST	0.09	0.5523	0.2713	0.024	0.6168	0.0981
HCH1	HCH1_YEAST	0.093	2.1958	0.2713	0.014	5.4153	0.0769
HSP104	HS104_YEAST	0.096	0.6867	0.2740	0.0074	0.5216	0.0575
ZPS1	ZPS1_YEAST	0.11	1.1069	0.2929	0.0066	1.1323	0.0554
GRX2	GLRX2_YEAST	0.12	0.4442	0.3132	0.018	0.5941	0.0856
ERP1	ERP1_YEAST	0.13	0.7220	0.3264	0.021	0.3493	0.0905
ATP1	ATPA_YEAST	0.15	0.8817	0.3420	0.013	0.7296	0.0754
GLC7	PP12_YEAST	0.16	0.6478	0.3487	0.0011	0.2440	0.0250
IMD3	IMDH3_YEAST	0.2	1.2363	0.3987	0.0051	1.6868	0.0542
YNK1	NDK_YEAST	0.21	0.6504	0.4005	0.0063	0.4890	0.0554
YEF3	EF3A_YEAST	0.21	1.2770	0.4005	0.013	1.5187	0.0754
FRS1	SYFB_YEAST	0.26	1.3352	0.4280	0.0091	2.2121	0.0631
SSB1	SSB1_YEAST	0.28	1.1075	0.4408	0.015	1.2123	0.0771
DBP5	DBP5_YEAST	0.28	1.4122	0.4408	0.02	5.2599	0.0905
FAS2	FAS2_YEAST	0.31	0.8280	0.4572	0.022	0.7357	0.0923
SSZ1	SSZ1_YEAST	0.32	1.1390	0.4633	0.017	1.4480	0.0847
SSB2	SSB2_YEAST	0.32	1.0962	0.4633	0.024	1.1998	0.0981

ADE5,7	PUR2_YEAST	0.35	1.4750	0.4821	0.0096	3.0813	0.0651
RPL26A	RL26A_YEAST	0.37	1.1005	0.4892	0.0091	1.1639	0.0631
GPP1	GPP1_YEAST	0.38	1.0617	0.4926	0.00057	1.5432	0.0165
PMI40	MPI_YEAST	0.39	0.7955	0.5023	0.0066	0.6409	0.0554
CPR1	CYPH_YEAST	0.42	0.9133	0.5207	0.0066	0.7309	0.0554
PBI2	IPB2_YEAST	0.43	0.8346	0.5216	0.022	0.3737	0.0923
ABF2	ABF2_YEAST	0.71	0.9038	0.6674	0.0061	0.3757	0.0554
OLA1	OLA1_YEAST	0.85	0.9601	0.7220	0.021	1.2839	0.0905
ATP7	ATP7_YEAST	0.87	0.9352	0.7318	0.014	0.2636	0.0769
RPS8A	RS8A_YEAST	0.9	0.9835	0.7403	0.01	1.1400	0.0664

10. Yeast randomly selected 5′ UTR list, length and sequence obtained from Lin et al.

Random ORF	5′ UTR length	GC content (%)
YKL071W	883	32.28
YNR051C	743	33.11
YFL050C	741	37.11
YDL134C	530	32.26
YDR389W	524	36.64
YDL137W	520	39.62
YMR075W	508	37.99
YOR011W-A	496	29.84
YDR125C	475	32.21
YNR004W	461	33.84
YBR212W	433	30.25
YPL058C	425	34.59
YPL216W	411	32.85
YPL018W	398	43.72
YLR431C	392	33.67
YBL055C	387	38.76
YKL101W	386	34.97
YHR071W	381	28.87
YOL055C	380	33.95
YOL123W	378	25.13
YPL151C	375	34.67
YDR420W	374	34.22
YNL268W	372	39.25
YHL033C	353	27.20
YMR100W	346	29.48
YNR044W	345	32.75
YJL213W	338	44.97
YKL151C	337	39.76
YLR224W	329	39.51
YFL055W	323	36.84
YOL158C	319	31.03
YJR090C	300	34.33
YER164W	298	32.55
YMR102C	294	31.63
YJL160C	289	30.45
YKL103C	288	35.07
YDL089W	283	37.46
YOL105C	278	33.81
YJL129C	277	32.49
YPL154C	275	28.00
YIL033C	273	41.03

Random ORF	5′ UTR length	GC content (%)
YOL002C	265	33.21
YIL007C	264	43.94
YNL078W	262	38.55
YDR001C	253	32.81
YDR251W	252	34.13
YAL005C	250	35.20
YGL194C-A	248	31.45
YGL114W	244	33.61
YPL042C	239	30.54
YNL068C	237	34.18
YFL036W	236	38.14
YGR144W	233	25.32
YGR161W-C	229	44.98
YIL016W	227	38.77
YKL046C	227	38.33
YKR017C	225	38.67
YBR239C	218	30.28
YDR515W	216	29.17
YNL183C	216	34.72
YER033C	215	40.47
YER033C	215	40.47
YOR212W	213	35.21
YIL146C	211	40.76
YLR220W	210	25.24
YLR312C	210	34.76
YMR070W	208	28.85
YBR183W	206	25.73
YJL184W	205	35.61
YGR233C	202	30.20
YLR328W	202	28.71
YLR087C	201	41.29
YML126C	200	41.00
YIL107C	199	30.65
YKL184W	198	31.31
YJL116C	196	37.24
YPR109W	196	34.18
YKL105C	195	34.36
YKL105C	195	34.36
YBR283C	193	43.52
YNL275W	193	38.34
YJR056C	189	31.75

YER159C	188	27.66
YKL112W	188	39.89
YLR116W	188	31.91
YDR054C	186	35.48
YOR114W	185	36.22
YPL262W	183	36.61
YDR009W	182	38.46
YGL140C	182	35.71
YEL037C	178	30.34
YNL007C	177	37.29
YBR078W	175	29.14
YLR083C	174	25.29
YLR299W	174	38.51
YNL331C	173	31.79
YOL113W	172	40.12
YPR127W	172	26.16
YPL028W	171	39.77
YOR070C	168	34.52
YPR141C	168	28.57
YBR020W	165	24.24
YJR109C	165	34.55
YGR017W	164	36.59
YML043C	158	34.81
YBR145W	156	30.77
YDL066W	154	45.45
YDR292C	154	37.01
YKR069W	154	27.27
YKL006W	153	34.64
YCR011C	151	25.17
YJL177W	151	28.48
YMR081C	151	41.06
YPR065W	151	32.45
YDR297W	150	36.67
YDR297W	150	36.67
YLR422W	150	32.00
YOR061W	150	31.33
YDR026C	149	26.17
YOR304W	149	31.54
YJL101C	148	38.51
YDR045C	147	31.97
YPL092W	147	35.37
YBR081C	142	29.58
YJR102C	142	27.46
YDR387C	140	39.29

YKR067W	140	40.71
YOR110W	140	32.14
YOR110W	140	32.14
YIR011C	138	42.75
YPL133C	138	37.68
YPL133C	138	37.68
YPL023C	137	43.07
YOR361C	136	33.09
YJL093C	136	37.50
YKR097W	136	23.53
YML081W	136	43.38
YJL084C	135	40.74
YIL074C	134	38.81
YNL087W	130	30.77
YBR218C	128	35.16
YKL016C	128	35.94
YBL101C	127	40.16
YNL207W	127	29.92
YDR224C	125	27.20
YNL063W	123	40.65
YPR041W	122	35.25
YBR194W	121	28.93
YPL247C	121	27.27
YLR265C	120	34.17
YNR032W	120	38.33
YDR507C	119	31.09
YOL116W	119	33.61
YBR029C	118	31.36
YHL009C	118	23.73
YLR454W	116	36.21
YMR217W	116	35.34
YPR081C	113	34.51
YLR237W	112	34.82
YLR225C	109	27.52
YBL029C-A	108	26.85
YFR030W	107	40.19
YFR005C	105	43.81
YFR005C	105	43.81
YGR225W	105	25.71
YAL007C	104	36.54
YDL193W	104	25.96
YGR125W	103	30.10
YJL161W	103	26.21
YLR114C	102	32.35

YKL087C	100	26.00	YML027W	77	42.86
YKL087C	100	26.00	YBL042C	76	34.21
YDL130W	97	31.96	YFR017C	76	52.63
YLR427W	97	36.08	YDR421W	75	34.67
YML064C	97	36.08	YGL082W	75	36.00
YOR283W	97	37.11	YPL046C	75	37.33
YOR352W	95	32.63	YJR076C	74	36.49
YOR352W	95	32.63	YKR089C	74	32.43
YFR016C	94	29.79	YBL050W	73	32.88
YGR183C	94	25.53	YPL206C	73	42.47
YFL022C	93	44.09	YDL106C	72	33.33
YJL163C	93	33.33	YFR050C	72	20.83
YGL039W	92	31.52	YGL086W	72	30.56
YGR231C	92	38.04	YPL053C	72	29.17
YGL207W	90	36.67	YBL038W	71	42.25
YOR191W	90	40.00	YBR231C	71	36.62
YMR307W	89	24.72	YDL136W	71	38.03
YBR199W	88	39.77	YDR411C	71	39.44
YJR041C	88	36.36	YGR123C	71	30.99
YLR424W	88	35.23	YGR123C	71	30.99
YNL165W	87	39.08	YHR092C	71	29.58
YPL234C	85	36.47	YIR025W	71	45.07
YLR167W	84	30.95	YKL216W	71	30.99
YMR132C	84	25.00	YBR052C	70	37.14
YOL032W	84	26.19	YDR070C	70	17.14
YPL246C	84	40.48	YFL046W	70	31.43
YDR145W	83	40.96	YGR030C	70	42.86
YLL041C	83	38.55	YGR100W	70	35.71
YBR114W	82	37.80	YHR121W	70	38.57
YGR020C	82	32.93	YKL045W	70	45.71
YGR031W	82	39.02	YMR086W	70	41.43
YAL027W	81	37.04	YMR299C	70	31.43
YGL186C	81	34.57	YPL119C	70	28.57
YGL186C	81	34.57	YER019W	68	36.76
YML046W	81	43.21	YER149C	68	25.00
YMR281W	81	33.33	YGL146C	68	26.47
YOR133W	81	38.27	YJR144W	68	36.76
YHR021C	80	27.50	YDL183C	67	29.85
YIL120W	80	28.75	YGR004W	67	38.81
YMR002W	80	26.25	YOR087W	67	29.85
YMR205C	80	33.75	YPL067C	67	35.82
YPR181C	80	50.00	YPR182W	67	50.75
YLR173W	78	37.18	YBR041W	66	33.33
YLR173W	78	37.18	YJL078C	65	33.85

YKR004C	65	33.85	YKL159C	56	28.57
YLR292C	65	35.38	YKL159C	56	28.57
YLR292C	65	35.38	YOR006C	56	30.36
YML029W	65	36.92	YOR154W	56	26.79
YBR058C-A	64	29.69	YBR094W	55	27.27
YLL006W	64	31.25	YER095W	55	36.36
YLR439W	64	31.25	YGR112W	55	34.55
YNL115C	64	29.69	YLR166C	55	32.73
YDR353W	63	33.33	YML100W	55	32.73
YHR019C	63	26.98	YNL023C	55	23.64
YDR330W	62	37.10	YNL234W	55	50.91
YHR064C	62	29.03	YHR013C	54	33.33
YIL026C	62	38.71	YNL001W	54	33.33
YNL191W	62	35.48	YOR293W	54	38.89
YBL025W	61	32.79	YDR305C	53	26.42
YDR104C	61	27.87	YGL105W	53	32.08
YGR060W	61	32.79	YJL044C	53	33.96
YKR039W	61	26.23	YCL002C	52	38.46
YMR302C	61	29.51	YJR069C	52	25.00
YOL019W-A	61	39.34	YJR069C	52	25.00
YEL060C	60	25.00	YML095C	52	23.08
YGL087C	60	28.33	YOL025W	52	40.38
YMR006C	60	31.67	YPL178W	52	25.00
YOL107W	60	28.33	YBR200W	51	35.29
YDR152W	59	40.68	YER087C-B	51	17.65
YGL107C	59	47.46	YER087C-B	51	17.65
YML069W	59	32.20	YKR077W	51	31.37
YML069W	59	32.20	YKR077W	51	31.37
YDR400W	58	48.28	YLR086W	51	41.18
YER021W	58	29.31	YLR086W	51	41.18
YJR122W	58	48.28	YLR193C	51	27.45
YKL057C	58	31.03	YLR278C	51	37.25
YLR057W	58	44.83	YML032C	51	50.98
YBR265W	57	31.58	YMR259C	51	37.25
YCL036W	57	52.63	YOL022C	51	35.29
YGL244W	57	31.58	YPL217C	51	37.25
YHR191C	57	22.81	YAL041W	50	50.00
YHR191C	57	22.81	YCL059C	50	22.00
YMR077C	57	38.60	YGR261C	50	36.00
YMR208W	57	35.09	YHR074W	50	42.00
YOL041C	57	33.33	YLR241W	50	34.00
YOL041C	57	33.33	YOL061W	50	52.00
YOR272W	57	33.33	YPR190C	50	32.00
YJL058C	56	23.21	YBL080C	49	40.82

YER009W	49	32.65	YNL225C	41	29.27
YLR129W	49	40.82	YGL179C	40	25.00
YLR419W	49	24.49	YGL179C	40	25.00
YML073C	49	32.65	YGL233W	40	37.50
YNL118C	49	22.45	YJL074C	40	40.00
YOL010W	49	38.78	YPR164W	40	37.50
YBR070C	48	31.25	YHR154W	39	38.46
YDL208W	48	41.67	YLR027C	39	23.08
YBR159W	47	40.43	YJL096W	38	39.47
YDR481C	47	46.81	YMR128W	38	26.32
YFR051C	47	38.30	YNL130C	38	28.95
YOR254C	47	27.66	YOR063W	38	34.21
YDL064W	46	39.13	YPL111W	38	26.32
YHR017W	46	23.91	YPL144W	38	44.74
YLL007C	45	33.33	YPR067W	38	42.11
YDL100C	45	33.33	YKL155C	37	40.54
YEL006W	45	31.11	YKL155C	37	40.54
YNL069C	45	33.33	YNL039W	37	45.95
YBR034C	44	31.82	YPL074W	37	40.54
YBR204C	44	47.73	YDR034W-B	36	27.78
YDL230W	44	38.64	YGR117C	36	27.78
YDL230W	44	38.64	YJR073C	36	47.22
YDR379C-A	44	29.55	YOL057W	36	38.89
YJL212C	44	50.00	YPL220W	36	33.33
YKL060C	44	34.09	YPR188C	36	38.89
YKR095W-A	44	38.64	YCL026C-B	35	28.57
YLR003C	44	13.64	YDL007W	35	22.86
YLL038C	43	46.51	YHR127W	35	40.00
YAL056W	43	41.86	YNL141W	35	17.14
YGL153W	43	32.56	YNL141W	35	17.14
YGL209W	43	25.58	YOR077W	35	40.00
YOR304C-A	43	30.23	YOR350C	35	42.86
YPL263C	43	27.91	YPL176C	35	25.71
YPR118W	43	37.21	YDR035W	34	35.29
YBR097W	42	33.33	YIL062C	34	26.47
YBR222C	42	47.62	YJL034W	34	41.18
YJL201W	42	47.62	YJL151C	34	32.35
YMR157C	42	38.10	YMR033W	34	29.41
YPR022C	42	28.57	YDR236C	33	45.45
YDR204W	41	34.15	YGR275W	33	39.39
YGR246C	41	34.15	YIL127C	33	51.52
YGR262C	41	24.39	YLR104W	33	39.39
YMR174C	41	24.39	YLR165C	33	36.36
YNL006W	41	39.02	YOR201C	33	39.39

YPL193W	33	36.36
YDR030C	32	37.50
YGR274C	32	40.63
YDR179C	31	35.48
YDR179C	31	35.48
YDR332W	31	32.26
YDR506C	31	22.58
YIL112W	31	35.48
YCR016W	30	30.00
YMR251W-A	30	13.33
YOR040W	30	43.33
YOR271C	30	40.00
YPL226W	30	43.33
YDR041W	29	41.38
YMR011W	29	20.69
YBR229C	28	21.43
YKL014C	28	32.14
YDR518W	27	48.15
YGR080W	27	40.74
YNL135C	27	22.22
YGR129W	26	34.62
YIR014W	26	57.69
YLR362W	26	38.46
YMR209C	26	46.15
YPL210C	26	26.92
YPL229W	26	19.23
YAR018C	25	36.00
YCL008C	25	24.00
YCL008C	25	24.00
YDR409W	25	32.00
YEL031W	25	40.00
YDR435C	24	41.67
YOR080W	24	41.67
YBL031W	23	30.43
YBR061C	23	8.70
YGR015C	23	21.74
YML049C	23	47.83
YDR484W	22	31.82
YCR083W	21	38.10
YKR088C	21	42.86
YOL102C	21	47.62
YJL207C	20	45.00
YKL088W	20	40.00
YPL055C	20	20.00
YPR025C	20	30.00
YPR025C	20	30.00
YPR134W	20	35.00
YDR183W	19	10.53
YOR158W	19	26.32
YHR111W	18	22.22
YJR002W	18	44.44
YNL262W	18	50.00
YKR007W	17	23.53
YCL054W	16	43.75
YLR022C	16	43.75
YGR016W	14	21.43
YJR135W-A	13	30.77
YAL033W	12	33.33
YAL033W	12	33.33
YLR010C	12	8.33
YDR107C	9	11.11
YNR038W	9	44.44
YLR007W	6	66.67
YBR062C	5	0.00
YBL046W	4	50.00
YIL009W	4	25.00
mean	**109.93**	**34.19**
stdev	**111.26**	**7.56**
median	**68.00**	**34.18**

11. HL60 IC_{20} pateamine treatment mass spectrometry data

Gene name	Accession Number	T-Test (P-Value) TIC	Fold Change TIC	q-value TIC	T-Test (P-Value) iBAQ	Fold Change iBAQ	q-value iBAQ
SZRD1_HUMAN	SZRD1	0.014	0.0544	0.0738	0.043	0.0039	0.1237
NECP2_HUMAN	NECAP2	0.028	0.0911	0.0976	0.14	0.0074	0.1999
GELS_HUMAN	GSN	0.0017	0.1113	0.0487	0.1	0.2665	0.1648
GTSF1_HUMAN	GTSF1	0.00029	0.1387	0.0269	0.0061	0.1136	0.0763
BT3L4_HUMAN	BTF3L4	0.0082	0.1838	0.0667	0.51	0.6756	0.4066
THIO_HUMAN	TXN	0.0061	0.1847	0.0609	0.22	0.6042	0.2550
COX5A_HUMAN	COX5A	0.028	0.1907	0.0976	0.018	0.1609	0.0936
RLA2_HUMAN	RPLP2	0.002	0.2115	0.0487	0.044	0.4982	0.1247
CASP1_HUMAN	CASP1	0.019	0.2133	0.0872	0.19	0.3525	0.2362
ITPA_HUMAN	ITPA	0.0086	0.2191	0.0672	0.03	0.0904	0.1090
PRDX5_HUMAN	PRDX5	0.017	0.2222	0.0813	0.0011	0.1818	0.0612
TCTP_HUMAN	TPT1	0.014	0.2259	0.0738	0.02	0.1933	0.0937
PFD6_HUMAN	PFDN6	0.025	0.2323	0.0974	0.022	0.4665	0.0973
LSM1_HUMAN	LSM1	0.01	0.2538	0.0672	0.17	0.2429	0.2210
FABP5_HUMAN	FABP5	0.0076	0.2656	0.0638	0.049	0.3929	0.1286
SODC_HUMAN	SOD1	0.00019	0.2707	0.0220	0.0022	0.2763	0.0612
EF1B_HUMAN	EEF1B2	0.0094	0.2737	0.0672	0.035	0.3278	0.1167
MTPN_HUMAN	MTPN	0.0065	0.2885	0.0609	0.0087	0.1920	0.0831
CHSP1_HUMAN	CARHSP1	0.028	0.3224	0.0976	0.041	0.3796	0.1217
LSP1_HUMAN	LSP1	0.029	0.3271	0.0989	0.038	0.2312	0.1183
TRA2B_HUMAN	TRA2B	0.025	0.3333	0.0974	0.38	1.1806	0.3392
HINT1_HUMAN	HINT1	0.025	0.3720	0.0974	0.092	0.4424	0.1648
RS12_HUMAN	RPS12	0.003	0.3929	0.0497	0.0058	0.3683	0.0747
RPE_HUMAN	RPE	0.013	0.3956	0.0726	0.02	0.5149	0.0937
RFA3_HUMAN	RPA3	0.012	0.4155	0.0713	0.18	0.7452	0.2288
FPPS_HUMAN	FDPS	0.023	0.4325	0.0970	0.16	0.5905	0.2154
OSTF1_HUMAN	OSTF1	0.013	0.4370	0.0726	0.19	0.2905	0.2362
PROF1_HUMAN	PFN1	0.0007	0.4513	0.0316	0.0001	0.5273	0.0283
RINI_HUMAN	RNH1	0.0066	0.4627	0.0609	0.089	0.4698	0.1648
LGUL_HUMAN	GLO1	0.022	0.4645	0.0945	0.029	0.6636	0.1067
MIF_HUMAN	MIF	0.027	0.4757	0.0976	0.0064	0.4844	0.0763
COMT_HUMAN	COMT	0.0067	0.4782	0.0609	0.072	0.4705	0.1488
IF5A1_HUMAN	EIF5A	0.01	0.4816	0.0672	0.00085	0.3007	0.0612
CYBP_HUMAN	CACYBP	0.001	0.4821	0.0357	0.0045	0.5820	0.0654
HNRPD_HUMAN	HNRNPD	0.00075	0.4946	0.0316	0.00035	0.5267	0.0496
TPIS_HUMAN	TPI1	0.0077	0.5046	0.0638	0.014	0.7592	0.0872
LYSC_HUMAN	LYZ	0.024	0.5110	0.0974	0.015	0.1860	0.0895
PEBP1_HUMAN	PEBP1	0.019	0.5125	0.0872	0.0018	0.6750	0.0612
VPS4B_HUMAN	VPS4B	0.028	0.5484	0.0976	0.0001	0.2461	0.0283

RBBP7_HUMAN	RBBP7	0.0042	0.5530	0.0567	0.4	0.8351	0.3472
PQBP1_HUMAN	PQBP1	0.0097	0.5571	0.0672	0.36	0.7713	0.3296
RS21_HUMAN	RPS21	0.0054	0.5592	0.0596	0.13	0.7163	0.1919
PTBP1_HUMAN	PTBP1	0.0001	0.5596	0.0155	0.01	0.7282	0.0831
CALR_HUMAN	CALR	0.013	0.5634	0.0726	0.08	0.7784	0.1564
ARPC5_HUMAN	ARPC5	0.011	0.5677	0.0680	0.014	0.7490	0.0872
HNRPQ_HUMAN	SYNCRIP	0.00043	0.5819	0.0285	0.071	0.9232	0.1485
PIMT_HUMAN	PCMT1	0.0042	0.5831	0.0567	0.016	0.4167	0.0907
LASP1_HUMAN	LASP1	0.0056	0.5852	0.0604	0.048	0.5179	0.1271
RS29_HUMAN	RPS29	0.011	0.5879	0.0680	0.45	0.9686	0.3801
SRSF1_HUMAN	SRSF1	0.0092	0.6002	0.0672	0.046	0.7683	0.1254
HCLS1_HUMAN	HCLS1	0.0085	0.6038	0.0672	0.028	0.6829	0.1044
UB2L3_HUMAN	UBE2L3	0.026	0.6200	0.0976	0.023	0.6120	0.0973
RL32_HUMAN	RPL32	0.022	0.6230	0.0945	0.017	0.5006	0.0927
HMGB1_HUMAN	HMGB1	0.028	0.6410	0.0976	0.01	0.4137	0.0831
DPYL2_HUMAN	DPYSL2	0.011	0.6422	0.0680	0.057	0.5720	0.1387
CBX3_HUMAN	CBX3	0.014	0.6480	0.0738	0.12	0.7786	0.1833
HMGB2_HUMAN	HMGB2	0.011	0.6505	0.0680	0.0021	0.4975	0.0612
GPX1_HUMAN	GPX1	0.0027	0.6590	0.0497	0.77	1.1240	0.5208
SRS11_HUMAN	SRSF11	0.023	0.6694	0.0970	0.24	0.9812	0.2715
GDIR2_HUMAN	ARHGDIB	0.011	0.6976	0.0680	0.0029	0.6181	0.0625
ALDOC_HUMAN	ALDOC	0.0036	0.7042	0.0567	0.66	1.0444	0.4759
ROA1_HUMAN	HNRNPA1	0.012	0.7201	0.0713	0.16	0.8999	0.2154
PCBP1_HUMAN	PCBP1	0.0038	0.7275	0.0567	0.66	1.0107	0.4759
PGK1_HUMAN	PGK1	0.0099	0.7324	0.0672	0.0066	0.9020	0.0763
PSME1_HUMAN	PSME1	0.013	0.7902	0.0726	0.19	0.7911	0.2362
TCPQ_HUMAN	CCT8	0.0093	1.1171	0.0672	0.083	1.2165	0.1595
EZRI_HUMAN	EZR	0.018	1.1451	0.0843	0.34	1.1057	0.3294
PCNA_HUMAN	PCNA	0.003	1.1774	0.0497	0.21	0.8526	0.2480
MOES_HUMAN	MSN	0.0046	1.2387	0.0577	0.14	1.1695	0.1999
FKBP4_HUMAN	FKBP4	0.016	1.2755	0.0781	0.25	1.3582	0.2746
CAPZB_HUMAN	CAPZB	0.0043	1.3146	0.0567	0.012	0.6840	0.0840
RU2A_HUMAN	SNRPA1	0.015	1.3315	0.0773	0.39	1.3985	0.3427
RACK1_HUMAN	RACK1	0.0044	1.3464	0.0567	0.012	1.4616	0.0840
DDX5_HUMAN	DDX5	0.015	1.3474	0.0773	0.016	1.4775	0.0907
HS90B_HUMAN	HSP90AB1	0.0027	1.4403	0.0497	0.02	1.4152	0.0937
UBP14_HUMAN	USP14	0.024	1.4965	0.0974	0.15	1.4453	0.2089
GNAI2_HUMAN	GNAI2	0.0053	1.5389	0.0596	0.072	2.3968	0.1488
FLNA_HUMAN	FLNA	0.025	1.5441	0.0974	0.011	1.9551	0.0831
SAHH_HUMAN	AHCY	0.018	1.5583	0.0843	0.026	1.5720	0.1016
HS90A_HUMAN	HSP90AA1	0.012	1.5845	0.0713	0.017	1.3996	0.0927
RS10_HUMAN	RPS10	0.014	1.6395	0.0738	0.33	1.1897	0.3253
GRP75_HUMAN	HSPA9	0.0029	1.6681	0.0497	0.0019	1.5752	0.0612
SND1_HUMAN	SND1	0.016	1.7397	0.0781	0.02	2.2165	0.0937
GBB2_HUMAN	GNB2	0.02	1.8181	0.0900	0.3	1.5168	0.3053

H4_HUMAN	HIST1H4A	0.014	1.8388	0.0738	0.18	2.1916	0.2288
PSME3_HUMAN	PSME3	0.026	1.8390	0.0976	0.084	2.9342	0.1598
IMB1_HUMAN	KPNB1	0.016	1.8682	0.0781	0.039	1.9014	0.1195
PSA4_HUMAN	PSMA4	0.027	1.8947	0.0976	0.06	2.0695	0.1394
H32_HUMAN	HIST2H3A	0.026	1.9530	0.0976	0.038	3.6531	0.1183
HS71B_HUMAN	HSPA1B	0.029	1.9975	0.0989	0.0018	1.9374	0.0612
TRAP1_HUMAN	TRAP1	0.013	2.0568	0.0726	0.025	1.5724	0.0998
ATPO_HUMAN	ATP5PO	0.01	2.1041	0.0672	0.01	2.9002	0.0831
ATPG_HUMAN	ATP5F1C	0.0067	2.1636	0.0609	0.008	2.0789	0.0831
ACON_HUMAN	ACO2	0.0063	2.1824	0.0609	0.061	3.1055	0.1400
AIFM1_HUMAN	AIFM1	0.027	2.2338	0.0976	0.061	2.2147	0.1400
SERC_HUMAN	PSAT1	0.0058	2.2436	0.0609	0.023	1.9355	0.0973
C1TC_HUMAN	MTHFD1	0.016	2.2502	0.0781	0.037	2.2889	0.1183
RS18_HUMAN	RPS18	0.0018	2.2890	0.0487	0.023	1.8275	0.0973
UBP5_HUMAN	USP5	0.0077	2.3178	0.0638	0.02	2.2482	0.0937
DNJB1_HUMAN	DNAJB1	0.0094	2.3193	0.0672	0.0023	4.4792	0.0612
SYHC_HUMAN	HARS	0.016	2.3560	0.0781	0.011	5.1184	0.0831
SYEP_HUMAN	EPRS	0.0074	2.4684	0.0638	0.064	2.0937	0.1423
CPIN1_HUMAN	CIAPIN1	0.0017	2.4694	0.0487	0.013	3.2750	0.0872
SYFB_HUMAN	FARSB	0.022	2.4887	0.0945	0.0018	3.1969	0.0612
ECHA_HUMAN	HADHA	0.0021	2.4953	0.0487	0.037	2.4144	0.1183
PSB4_HUMAN	PSMB4	0.00057	2.5607	0.0294	0.12	1.6559	0.1833
SF3B3_HUMAN	SF3B3	0.022	2.5847	0.0945	0.035	2.1375	0.1167
IF4G1_HUMAN	EIF4G1	0.002	2.8485	0.0487	0.0026	2.3698	0.0612
RCC1_HUMAN	RCC1	0.002	2.8549	0.0487	0.011	4.3329	0.0831
QCR2_HUMAN	UQCRC2	0.0054	3.3508	0.0596	0.0027	3.6518	0.0612
DFFA_HUMAN	DFFA	0.0076	3.3776	0.0638	0.0003	4.3195	0.0496
IMDH1_HUMAN	IMPDH1	0.003	3.8961	0.0497	0.07	3.6916	0.1480
TOIP1_HUMAN	TOR1AIP1	0.003	4.0512	0.0497	0.0031	4.6962	0.0625
PDC6I_HUMAN	PDCD6IP	0.0052	4.0528	0.0596	0.0044	2.9118	0.0654
ACPH_HUMAN	APEH	0.0001	4.1653	0.0155	0.0042	3.8166	0.0654
ASNA_HUMAN	ASNA1	0.0044	4.1869	0.0567	0.0083	3.2328	0.0831
CHIP_HUMAN	STUB1	0.024	4.1940	0.0974	0.04	3.4061	0.1206
NDUS3_HUMAN	NDUFS3	0.0065	4.5896	0.0609	0.039	5.0043	0.1195
RL13A_HUMAN	RPL13A	0.004	4.7754	0.0567	0.0068	3.3600	0.0771
RM01_HUMAN	MRPL1	0.025	4.7882	0.0974	0.09	183.0860	0.1648
DPP3_HUMAN	DPP3	0.0053	4.7940	0.0596	0.043	6.0950	0.1237
IF2A_HUMAN	EIF2S1	0.027	5.0304	0.0976	0.021	5.4743	0.0968
NSUN2_HUMAN	NSUN2	0.001	5.5168	0.0357	0.037	4.7518	0.1183
ODO2_HUMAN	DLST	0.00054	5.5348	0.0294	0.00096	117.7035	0.0612
ANM1_HUMAN	PRMT1	0.027	5.6661	0.0976	0.079	3.5095	0.1564
DPOD2_HUMAN	POLD2	0.022	6.2302	0.0945	0.0054	3.5969	0.0742
PRC2A_HUMAN	PRRC2A	0.017	6.6688	0.0813	0.018	8.1594	0.0936
FBRL_HUMAN	FBL	0.0097	6.7028	0.0672	0.0031	6.6964	0.0625
EIF3H_HUMAN	EIF3H	0.011	7.1754	0.0680	0.15	138.45	0.2089

SYSC_HUMAN	SARS	0.0001	9.1313	0.0155	0.16	259824	0.2154
EIF3E_HUMAN	EIF3E	0.0024	12.0464	0.0497	0.0027	1109733	0.0612
RM15_HUMAN	MRPL15	0.029	13.9634	0.0989	0.0026	269.2801	0.0612
EIF3C_HUMAN	EIF3C	0.028	21.6708	0.0976	0.23	1749524	0.2655
EFTS_HUMAN	TSFM	0.024	34.2440	0.0974	0.11	266.252	0.1746
SRPRB_HUMAN	SRPRB	0.00037	46.6003	0.0285	0.002	575.563	0.0612
RU1C_HUMAN	SNRPC	0.061	0.0354	0.1257	0.0093	0.0008	0.0831
SAE1_HUMAN	SAE1	0.11	0.1713	0.1570	0.015	0.0431	0.0895
NUP62_HUMAN	NUP62	0.12	0.5025	0.1632	0.025	0.1078	0.0998
TEBP_HUMAN	PTGES3	0.046	0.4841	0.1105	0.023	0.1314	0.0973
WDR61_HUMAN	WDR61	0.13	0.2502	0.1670	0.02	0.1423	0.0937
AN32A_HUMAN	ANP32A	0.085	0.3841	0.1444	0.011	0.1627	0.0831
RAVR1_HUMAN	RAVER1	0.11	0.2673	0.1570	0.011	0.2205	0.0831
AN32B_HUMAN	ANP32B	0.21	0.3664	0.2126	0.015	0.3295	0.0895
ECHM_HUMAN	ECHS1	0.074	0.3692	0.1351	0.025	0.3917	0.0998
SET_HUMAN	SET	0.056	0.4592	0.1208	0.0018	0.4000	0.0612
LEG1_HUMAN	LGALS1	0.045	0.4710	0.1098	0.0038	0.4145	0.0654
RD23A_HUMAN	RAD23A	0.099	0.4559	0.1511	0.018	0.4228	0.0936
RL35_HUMAN	RPL35	0.7	0.6934	0.4078	0.012	0.4237	0.0840
HDGF_HUMAN	HDGF	0.031	0.5768	0.1020	0.011	0.4368	0.0831
PRS6B_HUMAN	PSMC4	0.054	0.4174	0.1181	0.02	0.4554	0.0937
THIC_HUMAN	ACAT2	0.072	0.8306	0.1341	0.0058	0.4926	0.0747
NUCB2_HUMAN	NUCB2	0.17	0.4683	0.1886	0.012	0.4962	0.0840
NLTP_HUMAN	SCP2	0.14	0.5330	0.1713	0.0042	0.5208	0.0654
NTF2_HUMAN	NUTF2	0.15	0.3013	0.1748	0.01	0.5231	0.0831
PARK7_HUMAN	PARK7	0.036	0.5135	0.1046	0.0044	0.5233	0.0654
CH10_HUMAN	HSPE1	0.097	0.5522	0.1511	0.002	0.5791	0.0612
COX5B_HUMAN	COX5B	0.57	0.8141	0.3587	0.0079	0.6513	0.0831
PAK2_HUMAN	PAK2	0.063	0.6734	0.1259	0.022	0.6910	0.0973
DUT_HUMAN	DUT	0.14	0.9212	0.1713	0.023	0.7737	0.0973
ROA2_HUMAN	HNRNPA2B1	0.2	0.9240	0.2089	0.014	0.8526	0.0872
IMDH2_HUMAN	IMPDH2	0.96	0.9656	0.4782	0.014	1.2185	0.0872
PUR9_HUMAN	ATIC	1	0.9262	0.4887	0.025	1.2188	0.0998
TCPG_HUMAN	CCT3	0.092	1.2028	0.1492	0.0038	1.2323	0.0654
TCPB_HUMAN	CCT2	0.89	0.9172	0.4586	0.025	1.2605	0.0998
PDIA1_HUMAN	P4HB	0.51	0.9902	0.3408	0.0094	1.2730	0.0831
PA2G4_HUMAN	PA2G4	0.97	0.9958	0.4811	0.0043	1.3069	0.0654
GRP78_HUMAN	HSPA5	0.072	1.0845	0.1341	0.024	1.3168	0.0998
ARPC3_HUMAN	ARPC3	0.21	0.8214	0.2126	0.012	1.3442	0.0840
PHB_HUMAN	PHB	0.13	1.1941	0.1670	0.018	1.3877	0.0936
ACTS_HUMAN	ACTA1	0.058	1.4421	0.1227	0.013	1.4418	0.0872
RAN_HUMAN	RAN	0.77	0.9446	0.4266	0.019	1.4432	0.0937
IF4A3_HUMAN	EIF4A3	0.2	1.5848	0.2089	0.014	1.4672	0.0872
TCPZ_HUMAN	CCT6A	0.43	1.1405	0.3077	0.015	1.4719	0.0895
IF4A1_HUMAN	EIF4A1	0.062	1.0711	0.1259	0.0092	1.5018	0.0831

RL38_HUMAN	RPL38	0.035	2.1308	0.1046	0.012	1.5111	0.0840
HSP7C_HUMAN	HSPA8	0.087	1.1600	0.1446	0.0011	1.5152	0.0612
ATPA_HUMAN	ATP5F1A	0.31	1.1474	0.2586	0.0018	1.5255	0.0612
PSA6_HUMAN	PSMA6	0.1	1.2569	0.1511	0.019	1.5274	0.0937
GANAB_HUMAN	GANAB	0.5	0.9531	0.3375	0.02	1.5285	0.0937
H2AV_HUMAN	H2AFV	0.74	1.0240	0.4200	0.011	1.5811	0.0831
IF5_HUMAN	EIF5	0.097	1.3960	0.1511	0.0062	1.6902	0.0763
PPIB_HUMAN	PPIB	0.24	1.2083	0.2262	0.011	1.6910	0.0831
RL13_HUMAN	RPL13	0.11	1.1975	0.1570	0.0065	1.7557	0.0763
RSSA_HUMAN	RPSA	0.12	1.9813	0.1632	0.0055	1.7748	0.0742
PSD11_HUMAN	PSMD11	0.084	1.3965	0.1437	0.014	1.8137	0.0872
PPAC_HUMAN	ACP1	0.14	1.3404	0.1713	0.0051	1.8219	0.0723
PDIA4_HUMAN	PDIA4	0.032	1.7102	0.1038	0.017	1.9234	0.0927
RSMB_HUMAN	SNRPB	0.99	0.9565	0.4858	0.00062	1.9247	0.0612
RL24_HUMAN	RPL24	0.42	1.5868	0.3062	0.0097	1.9619	0.0831
NUP50_HUMAN	NUP50	0.71	1.1348	0.4095	0.025	1.9629	0.0998
PURA2_HUMAN	ADSS	0.11	1.4015	0.1570	0.016	1.9718	0.0907
RS3_HUMAN	RPS3	0.097	1.7144	0.1511	0.02	1.9794	0.0937
CISY_HUMAN	CS	0.89	0.8252	0.4586	0.016	2.1221	0.0907
SF3B2_HUMAN	SF3B2	0.04	1.8094	0.1060	0.0077	2.1498	0.0831
METK2_HUMAN	MAT2A	0.037	2.4547	0.1046	0.018	2.2366	0.0936
ERF3A_HUMAN	GSPT1	0.75	1.2646	0.4226	0.014	2.2639	0.0872
PSB6_HUMAN	PSMB6	0.088	2.9350	0.1457	0.0032	2.3578	0.0625
MTDC_HUMAN	MTHFD2	0.059	0.7026	0.1227	0.0097	2.4608	0.0831
SRRT_HUMAN	SRRT	0.35	1.3008	0.2741	0.011	2.4686	0.0831
CPSF7_HUMAN	CPSF7	0.29	1.7466	0.2486	0.025	2.4823	0.0998
ACADM_HUMAN	ACADM	0.16	2.3111	0.1823	0.013	2.6996	0.0872
NONO_HUMAN	NONO	0.44	1.4516	0.3120	0.0077	2.7877	0.0831
LMNB2_HUMAN	LMNB2	0.03	1.8911	0.1015	0.02	2.7969	0.0937
CSDE1_HUMAN	CSDE1	0.097	3.1874	0.1511	0.0039	2.8039	0.0654
LYPA1_HUMAN	LYPLA1	0.12	2.7551	0.1632	0.023	3.0093	0.0973
PTN6_HUMAN	PTPN6	0.047	2.8897	0.1123	0.021	3.2521	0.0968
ABCE1_HUMAN	ABCE1	0.11	2.6193	0.1570	0.022	3.5791	0.0973
4F2_HUMAN	SLC3A2	0.059	4.5638	0.1227	0.017	3.6540	0.0927
TFR1_HUMAN	TFRC	0.037	2.0045	0.1046	0.016	3.9496	0.0907
SNX1_HUMAN	SNX1	0.04	3.1814	0.1060	0.0018	6.5040	0.0612
ERF1_HUMAN	ETF1	0.043	6.1854	0.1072	0.0041	9.2214	0.0654
ATD3A_HUMAN	ATAD3A	0.072	6.1726	0.1341	0.023	9.7929	0.0973
BCLF1_HUMAN	BCLAF1	0.04	13.2800	0.1060	0.01	25.2933	0.0831
RPR1B_HUMAN	RPRD1B	0.046	10.7177	0.1105	0.023	357.105	0.0973

12. HT-29 IC_{20} pateamine treatment mass spectrometry data

Accession Number	Gene name	T-Test (P-Value) TIC	Fold Change TIC	q-value TIC	T-Test (P-Value) iBAQ	Fold Change iBAQ	q-value iBAQ
CTF8A_HUMAN	CHTF8	0.0034	0.1216	0.0937	0.028	0.0175	0.2102
CATA_HUMAN	CAT	0.0001	0.6685	0.0141	0.9	1.1580	0.6582
K2C8_HUMAN	KRT8	0.001	1.6453	0.0551	0.00046	2.7314	0.0414
SRSF6_HUMAN	SRSF6	0.0034	2.4768	0.0937	0.0021	1.7570	0.0570
SAFB1_HUMAN	SAFB	0.00077	3.5771	0.0551	0.00057	6.7566	0.0414
LIMA1_HUMAN	LIMA1	0.0033	3.6281	0.0937	0.00085	8.2501	0.0414
SAFB2_HUMAN	SAFB2	0.00085	4.0496	0.0551	0.0015	6.6254	0.0507
SF3A2_HUMAN	SF3A2	0.0016	12.4250	0.0772	0.00074	5.5418	0.0414
ES8L1_HUMAN	EPS8L1	0.0019	24.1710	0.0814	0.0069	85.0693	0.1191
ZN185_HUMAN	ZNF185	0.00011	26.6189	0.0141	0.0001	51.6306	0.0285
TRXR1_HUMAN	TXNRD1	0.00093	27.8827	0.0551	0.014	6.5749	0.1630
AK1BA_HUMAN	AKR1B10	0.0032	38.8551	0.0937	0.0077	1047.7089	0.1218
LA_HUMAN	SSB	0.0001	150.9017	0.0141	0.0001	461.0307	0.0285
K1C20_HUMAN	KRT20	0.0028	170.2230	0.0937	0.0045	264.0866	0.1070
ROA1_HUMAN	HNRNPA1	0.23	1.0824	0.2360	0.0018	1.5627	0.0513
RL7_HUMAN	RPL7	0.45	1.0960	0.2993	0.0016	1.6631	0.0507
STIP1_HUMAN	STIP1	0.063	1.2855	0.1785	0.00049	1.8712	0.0414
ROA3_HUMAN	HNRNPA3	0.25	1.1083	0.2417	0.0011	1.8859	0.0448
CAPG_HUMAN	CAPG	0.52	1.0155	0.3210	0.0017	2.6841	0.0510
RL10A_HUMAN	RPL10A	0.28	1.7536	0.2542	0.003	2.9627	0.0769
LRC59_HUMAN	LRRC59	0.14	1.6219	0.2054	0.00078	3.0617	0.0414
TB182_HUMAN	TNKS1BP1	0.013	1.7086	0.1320	0.0011	3.4700	0.0448
SF3B2_HUMAN	SF3B2	0.026	2.5776	0.1653	0.0016	3.8091	0.0507
MISP_HUMAN	MISP	0.0039	3.7455	0.1003	0.0005	5.4455	0.0414
HS90B_HUMAN	HSP90AB1	0.0078	2.9903	0.1248	0.00044	6.2291	0.0414
DNJA2_HUMAN	DNAJA2	0.01	5.2620	0.1248	0.00087	6.9413	0.0414
HS90A_HUMAN	HSP90AA1	0.031	5.3839	0.1653	0.0013	8.5881	0.0494
RPN1_HUMAN	RPN1	0.0062	6.7608	0.1157	0.0006	15.0853	0.0414
FIP1_HUMAN	FIP1L1	0.053	3.1202	0.1785	0.0031	384.1343	0.0769

13. HT-29 sun-inhibitory pateamine treatment mass spectrometry data

Gene name	Accession Number	T-Test (P-Value) TIC	Fold Change TIC	q-value TIC	T-Test (P-Value) iBAQ	Fold Change iBAQ	q-value iBAQ
FUBP3_HUMAN	FUBP3	0.00023	0.0020	0.0227	0.00012	0.0020	0.0125
THIM_HUMAN	ACAA2	0.00081	0.0034	0.0440	0.039	0.0000	0.3012
MISP_HUMAN	MISP	0.003	0.0052	0.0721	0.0096	0.0018	0.1604
P66B_HUMAN	GATAD2B	0.0001	0.0127	0.0227	0.042	0.0107	0.3039
TIAR_HUMAN	TIAL1	0.0044	0.0144	0.0786	0.0083	0.0000	0.1573
DBNL_HUMAN	DBNL	0.00026	0.0160	0.0227	0.00039	0.0005	0.0250
NSF1C_HUMAN	NSFL1C	0.0033	0.0163	0.0721	0.021	0.0026	0.2467
PRPF3_HUMAN	PRPF3	0.0031	0.0193	0.0721	0.36	0.0000	0.5581
FBRL_HUMAN	FBL	0.004	0.0202	0.0749	0.00067	0.0182	0.0329
ESTD_HUMAN	ESD	0.0018	0.0368	0.0544	0.0096	0.0329	0.1604
CAPG_HUMAN	CAPG	0.0023	0.0418	0.0624	0.01	0.0901	0.1604
BUB3_HUMAN	BUB3	0.00084	0.0453	0.0440	0.0001	0.0080	0.0119
P53_HUMAN	TP53	0.00064	0.0755	0.0387	0.0001	0.0024	0.0119
CATA_HUMAN	CAT	0.0001	0.0789	0.0227	0.0003	0.0074	0.0209
ROA3_HUMAN	HNRNPA3	0.00021	0.1123	0.0227	0.0001	0.0137	0.0119
DHSO_HUMAN	SORD	0.0036	0.1134	0.0726	0.094	0.0551	0.4810
RL3_HUMAN	RPL3	0.0033	0.1567	0.0721	0.0099	0.1408	0.1604
HNRPL_HUMAN	HNRNPL	0.0013	0.1721	0.0465	0.026	0.1140	0.2750
CAPR1_HUMAN	CAPRIN1	0.0029	0.2028	0.0721	0.26	0.2244	0.5581
UB2D2_HUMAN	UBE2D2	0.00097	0.2031	0.0449	0.11	0.2858	0.5183
PSPC1_HUMAN	PSPC1	0.00096	0.2234	0.0449	0.00022	0.1143	0.0200
PABP1_HUMAN	PABPC1	0.0018	0.2485	0.0544	0.03	0.1741	0.2750
UBQL1_HUMAN	UBQLN1	0.005	0.2821	0.0874	0.0001	0.0648	0.0119
TB182_HUMAN	TNKS1BP1	0.0058	0.2974	0.0928	0.028	0.2134	0.2750
RS4X_HUMAN	RPS4X	0.0012	0.3000	0.0465	0.0077	0.2039	0.1529
RL18A_HUMAN	RPL18A	0.0041	0.3190	0.0750	0.013	0.3315	0.1838
FUBP1_HUMAN	FUBP1	0.0026	0.3382	0.0681	0.0001	0.2340	0.0119
RBM14_HUMAN	RBM14	0.0004	0.3506	0.0314	0.023	0.3594	0.2628
IF4H_HUMAN	EIF4H	0.0017	0.3693	0.0544	0.0011	0.1223	0.0399
KHDR1_HUMAN	KHDRBS1	0.0005	0.3705	0.0357	0.059	0.3696	0.3672
IF4B_HUMAN	EIF4B	0.0056	0.4126	0.0928	0.00097	0.4549	0.0397
G3P_HUMAN	GAPDH	0.0017	0.4403	0.0544	0.001	0.3246	0.0397
ROA1_HUMAN	HNRNPA1	0.00015	0.4647	0.0227	0.00027	0.3265	0.0205
HNRH1_HUMAN	HNRNPH1	0.0059	0.5336	0.0928	0.00063	0.2530	0.0328
PDIA3_HUMAN	PDIA3	0.0011	0.6077	0.0455	0.031	0.3316	0.2750
RL4_HUMAN	RPL4	0.0013	0.6667	0.0465	0.001	0.4846	0.0397
K2C8_HUMAN	KRT8	0.0058	1.7420	0.0928	0.047	1.6360	0.3187
TCPB_HUMAN	CCT2	0.00022	2.0010	0.0227	0.027	1.8735	0.2750
CISY_HUMAN	CS	0.0036	2.0173	0.0726	0.39	1.4558	0.5737

TCPE_HUMAN	CCT5	0.0006	2.1506	0.0387	0.05	1.8126	0.3336
GSTP1_HUMAN	GSTP1	0.00026	2.7518	0.0227	0.0067	2.6997	0.1397
SEPT2_HUMAN	SEPT2	0.004	3.0259	0.0749	0.055	2.4429	0.3502
AN32A_HUMAN	ANP32A	0.0054	3.0701	0.0923	0.03	6.5054	0.2750
PDIA1_HUMAN	P4HB	0.0011	3.4840	0.0455	0.011	4.7107	0.1668
RS5_HUMAN	RPS5	0.0037	3.5712	0.0727	0.0025	4.4597	0.0695
HS90B_HUMAN	HSP90AB1	0.0035	4.6177	0.0726	0.008	7.4843	0.1552
EF1D_HUMAN	EEF1D	0.0021	7.9951	0.0590	0.03	4.1483	0.2750
AN32B_HUMAN	ANP32B	0.0032	9.8036	0.0721	0.21	6.5437	0.5581
RB11B_HUMAN	RAB11B	0.002	28.1119	0.0582	0.0001	48.9652	0.0119
RTN4_HUMAN	RTN4	0.0001	79.4428	0.0227	0.21	244412	0.5581
ROA0_HUMAN	HNRNPA0	0.048	0.2052	0.2755	0.0011	0.0004	0.0399
PA1B3_HUMAN	PAFAH1B3	0.037	0.2438	0.2465	0.002	0.0756	0.0618
HNRPF_HUMAN	HNRNPF	0.016	0.1879	0.1677	0.0022	0.0928	0.0655
PA1B2_HUMAN	PAFAH1B2	0.31	0.5710	0.5090	0.0039	0.1339	0.0957
RCC1_HUMAN	RCC1	0.042	0.3931	0.2581	0.0001	0.1487	0.0119
GSTK1_HUMAN	GSTK1	0.082	1.8592	0.3422	0.00063	0.1935	0.0328
ALDOA_HUMAN	ALDOA	0.0075	0.3684	0.1113	0.001	0.1989	0.0397
TXND5_HUMAN	TXNDC5	0.037	0.6433	0.2465	0.0019	0.2944	0.0609
FUBP2_HUMAN	KHSRP	0.023	0.5562	0.2127	0.00024	0.3523	0.0200
HP1B3_HUMAN	HP1BP3	0.035	0.3928	0.2372	0.0033	0.3959	0.0834
ROA2_HUMAN	HNRNPA2B1	0.039	0.6639	0.2534	0.0033	0.4253	0.0834
ADT2_HUMAN	SLC25A5	0.011	2.2179	0.1466	0.0013	2.1521	0.0452
SETLP_HUMAN	SETSIP	0.01	2.2061	0.1379	0.0025	2.1887	0.0695
HMGB1_HUMAN	HMGB1	0.13	2.0132	0.4276	0.0031	3.1388	0.0834
TALDO_HUMAN	TALDO1	0.028	2.5769	0.2268	0.0017	5.1063	0.0567
ANXA2_HUMAN	ANXA2	0.0096	2.3195	0.1348	0.00057	6.2931	0.0328

14. Ontological enrichments HL60 down-regulated proteins

source	Term name	Term id	Adjusted p-value
GO:BP	aromatic compound catabolic process	GO:0019439	1.95E-11
GO:BP	nucleobase-containing compound catabolic process	GO:0034655	2.19E-11
GO:BP	organic cyclic compound catabolic process	GO:1901361	5.61E-11
GO:BP	heterocycle catabolic process	GO:0046700	1.19E-10
GO:BP	cellular nitrogen compound catabolic process	GO:0044270	1.23E-10
GO:BP	mRNA metabolic process	GO:0016071	4.38E-10
GO:BP	mRNA catabolic process	GO:0006402	5.69E-08
GO:BP	RNA catabolic process	GO:0006401	2.33E-07
GO:BP	nuclear export	GO:0051168	6.29E-06
GO:BP	nucleocytoplasmic transport	GO:0006913	2.83E-05
GO:BP	nuclear transport	GO:0051169	3.14E-05
GO:BP	interspecies interaction between organisms	GO:0044419	3.53E-05
GO:BP	protein export from nucleus	GO:0006611	3.61E-05
GO:BP	symbiotic process	GO:0044403	8.15E-05
GO:BP	regulation of mRNA metabolic process	GO:1903311	1.49E-04
GO:BP	viral process	GO:0016032	1.73E-04
GO:BP	RNA splicing, via transesterification reactions	GO:0000375	2.73E-04
GO:BP	mRNA splicing, via spliceosome	GO:0000398	2.06E-03
GO:BP	RNA splicing, via transesterification reactions with bulged adenosine as nucleophile	GO:0000377	2.06E-03
GO:BP	regulation of cysteine-type endopeptidase activity involved in apoptotic process	GO:0043281	2.50E-03
GO:BP	RNA splicing	GO:0008380	2.94E-03
GO:BP	small molecule biosynthetic process	GO:0044283	3.94E-03
GO:BP	regulation of cysteine-type endopeptidase activity	GO:2000116	5.69E-03
GO:BP	methylglyoxal metabolic process	GO:0009438	8.04E-03
GO:BP	viral gene expression	GO:0019080	1.02E-02
GO:BP	peptide metabolic process	GO:0006518	1.21E-02
GO:BP	SRP-dependent cotranslational protein targeting to membrane	GO:0006614	1.53E-02
GO:BP	regulation of endopeptidase activity	GO:0052548	1.54E-02
GO:BP	mRNA processing	GO:0006397	1.58E-02
GO:BP	mRNA transport	GO:0051028	1.79E-02
GO:BP	nuclear-transcribed mRNA catabolic process	GO:0000956	1.83E-02
GO:BP	cotranslational protein targeting to membrane	GO:0006613	2.05E-02
GO:BP	positive regulation of organelle organization	GO:0010638	2.07E-02
GO:BP	regulation of peptidase activity	GO:0052547	2.73E-02
GO:BP	protein targeting to ER	GO:0045047	3.18E-02
GO:BP	regulation of nucleocytoplasmic transport	GO:0046822	3.18E-02
GO:BP	monocarboxylic acid metabolic process	GO:0032787	3.52E-02
GO:BP	regulation of intracellular protein transport	GO:0033157	3.53E-02

GO:BP	establishment of protein localization to organelle	GO:0072594	3.83E-02
GO:BP	establishment of protein localization to endoplasmic reticulum	GO:0072599	3.91E-02
GO:CC	ribonucleoprotein complex	GO:1990904	9.23E-07
GO:CC	cytosolic ribosome	GO:0022626	3.49E-03
GO:CC	cytosolic part	GO:0044445	6.54E-03
GO:CC	ficolin-1-rich granule lumen	GO:1904813	8.09E-03
GO:CC	ficolin-1-rich granule	GO:0101002	8.09E-03
GO:CC	secretory granule lumen	GO:0034774	3.96E-02
GO:CC	cytoplasmic vesicle lumen	GO:0060205	4.31E-02
GO:CC	vesicle lumen	GO:0031983	4.50E-02
KEGG	Carbon metabolism	KEGG:01200	1.46E-02
KEGG	Ribosome	KEGG:03010	3.05E-02
KEGG	Spliceosome	KEGG:03040	3.05E-02
REAC	Metabolism of RNA	REAC:R-HSA-8953854	6.37E-09
REAC	mRNA Splicing – Major Pathway	REAC:R-HSA-72163	9.60E-05
REAC	mRNA Splicing	REAC:R-HSA-72172	1.44E-04
REAC	Processing of Capped Intron-Containing Pre-mRNA	REAC:R-HSA-72203	1.55E-04
REAC	Signaling by ROBO receptors	REAC:R-HSA-376176	5.65E-04
REAC	Eukaryotic Translation Elongation	REAC:R-HSA-156842	1.03E-03
REAC	Influenza Life Cycle	REAC:R-HSA-168255	1.57E-03
REAC	Infectious disease	REAC:R-HSA-5663205	1.86E-03
REAC	Influenza Infection	REAC:R-HSA-168254	2.61E-03
REAC	Regulation of expression of SLITs and ROBOs	REAC:R-HSA-9010553	6.18E-03
REAC	Influenza Viral RNA Transcription and Replication	REAC:R-HSA-168273	1.02E-02
REAC	Peptide chain elongation	REAC:R-HSA-156902	1.05E-02
REAC	Viral mRNA Translation	REAC:R-HSA-192823	1.05E-02
REAC	Eukaryotic Translation Termination	REAC:R-HSA-72764	1.35E-02
REAC	Selenocysteine synthesis	REAC:R-HSA-2408557	1.35E-02
REAC	Nonsense Mediated Decay (NMD) independent of the Exon Junction Complex (EJC)	REAC:R-HSA-975956	1.52E-02

REAC	Formation of a pool of free 40S subunits	REAC:R-HSA-72689	2.14E-02
REAC	L13a-mediated translational silencing of Ceruloplasmin expression	REAC:R-HSA-156827	3.60E-02
REAC	GTP hydrolysis and joining of the 60S ribosomal subunit	REAC:R-HSA-72706	3.79E-02
REAC	SRP-dependent cotranslational protein targeting to membrane	REAC:R-HSA-1799339	3.79E-02
REAC	Gene and protein expression by JAK-STAT after Interleukin-12 stimulation	REAC:R-HSA-8950505	4.23E-02
REAC	Nonsense Mediated Decay (NMD) enhanced by the Exon Junction Complex (EJC)	REAC:R-HSA-975957	4.38E-02
REAC	Nonsense-Mediated Decay (NMD)	REAC:R-HSA-927802	4.38E-02
REAC	Selenoamino acid metabolism	REAC:R-HSA-2408522	4.59E-02
WP	Cytoplasmic Ribosomal Proteins	WP:WP477	1.16E-02

15. Ontological enrichments HL60 up-regulated proteins

source	Term name	Term id	Adjusted p-value
GO:BP	protein folding	GO:0006457	4.44E-14
GO:BP	nucleobase-containing compound catabolic process	GO:0034655	8.67E-14
GO:BP	heterocycle catabolic process	GO:0046700	7.28E-13
GO:BP	cellular nitrogen compound catabolic process	GO:0044270	7.61E-13
GO:BP	RNA catabolic process	GO:0006401	1.04E-12
GO:BP	aromatic compound catabolic process	GO:0019439	1.44E-12
GO:BP	mRNA catabolic process	GO:0006402	1.45E-12
GO:BP	translation	GO:0006412	2.51E-12
GO:BP	mRNA metabolic process	GO:0016071	3.89E-12
GO:BP	organic cyclic compound catabolic process	GO:1901361	5.08E-12
GO:BP	peptide biosynthetic process	GO:0043043	6.17E-12
GO:BP	viral process	GO:0016032	1.13E-11
GO:BP	amide biosynthetic process	GO:0043604	1.27E-11
GO:BP	symbiotic process	GO:0044403	6.20E-11
GO:BP	posttranscriptional regulation of gene expression	GO:0010608	9.37E-11
GO:BP	interspecies interaction between organisms	GO:0044419	2.69E-10
GO:BP	chaperone-mediated protein folding	GO:0061077	3.39E-10
GO:BP	peptide metabolic process	GO:0006518	5.33E-10
GO:BP	translational initiation	GO:0006413	7.58E-10
GO:BP	nuclear-transcribed mRNA catabolic process, nonsense-mediated decay	GO:0000184	4.48E-09
GO:BP	cytoplasmic translation	GO:0002181	8.75E-09
GO:BP	nuclear-transcribed mRNA catabolic process	GO:0000956	3.16E-08
GO:BP	ribonucleoprotein complex biogenesis	GO:0022613	8.97E-08
GO:BP	establishment of protein localization to organelle	GO:0072594	5.06E-07
GO:BP	ribonucleoprotein complex assembly	GO:0022618	1.79E-06
GO:BP	cytoplasmic translational initiation	GO:0002183	2.64E-06
GO:BP	ribonucleoprotein complex subunit organization	GO:0071826	3.77E-06
GO:BP	cellular response to heat	GO:0034605	4.27E-06
GO:BP	response to unfolded protein	GO:0006986	6.38E-06
GO:BP	cellular amino acid metabolic process	GO:0006520	6.41E-06
GO:BP	protein targeting to ER	GO:0045047	7.42E-06
GO:BP	establishment of protein localization to endoplasmic reticulum	GO:0072599	1.06E-05
GO:BP	regulation of translation	GO:0006417	1.25E-05
GO:BP	response to topologically incorrect protein	GO:0035966	2.53E-05
GO:BP	protein localization to organelle	GO:0033365	4.93E-05
GO:BP	response to heat	GO:0009408	6.12E-05
GO:BP	protein localization to endoplasmic reticulum	GO:0070972	6.79E-05
GO:BP	regulation of cellular amide metabolic process	GO:0034248	7.07E-05
GO:BP	regulation of catabolic process	GO:0009894	1.27E-04

GO:BP	response to temperature stimulus	GO:0009266	1.81E-04
GO:BP	'de novo' posttranslational protein folding	GO:0051084	2.42E-04
GO:BP	protein catabolic process	GO:0030163	2.48E-04
GO:BP	regulation of cellular response to stress	GO:0080135	3.70E-04
GO:BP	regulation of DNA-templated transcription in response to stress	GO:0043620	4.05E-04
GO:BP	'de novo' protein folding	GO:0006458	4.75E-04
GO:BP	protein refolding	GO:0042026	4.75E-04
GO:BP	regulation of mRNA binding	GO:1902415	4.88E-04
GO:BP	positive regulation of protein localization to Cajal body	GO:1904871	4.88E-04
GO:BP	regulation of protein localization to Cajal body	GO:1904869	4.88E-04
GO:BP	SRP-dependent cotranslational protein targeting to membrane	GO:0006614	5.99E-04
GO:BP	positive regulation of establishment of protein localization to telomere	GO:1904851	8.09E-04
GO:BP	protein localization to nuclear body	GO:1903405	8.09E-04
GO:BP	protein localization to Cajal body	GO:1904867	8.09E-04
GO:BP	protein stabilization	GO:0050821	8.37E-04
GO:BP	establishment of protein localization to membrane	GO:0090150	8.55E-04
GO:BP	cotranslational protein targeting to membrane	GO:0006613	8.87E-04
GO:BP	regulation of protein catabolic process	GO:0042176	9.84E-04
GO:BP	cellular response to unfolded protein	GO:0034620	1.05E-03
GO:BP	regulation of protein stability	GO:0031647	1.07E-03
GO:BP	regulation of RNA binding	GO:1905214	1.26E-03
GO:BP	regulation of establishment of protein localization to telomere	GO:0070203	1.26E-03
GO:BP	regulation of hematopoietic stem cell differentiation	GO:1902036	1.29E-03
GO:BP	protein targeting to membrane	GO:0006612	1.83E-03
GO:BP	protein localization to nucleoplasm	GO:1990173	1.89E-03
GO:BP	regulation of establishment of protein localization to chromosome	GO:0070202	1.89E-03
GO:BP	positive regulation of protein localization to chromosome, telomeric region	GO:1904816	1.89E-03
GO:BP	regulation of cellular response to heat	GO:1900034	2.21E-03
GO:BP	chaperone cofactor-dependent protein refolding	GO:0051085	2.76E-03
GO:BP	cellular response to topologically incorrect protein	GO:0035967	3.20E-03
GO:BP	regulation of transcription from RNA polymerase II promoter in response to stress	GO:0043618	3.31E-03
GO:BP	hematopoietic stem cell differentiation	GO:0060218	3.36E-03
GO:BP	telomere maintenance	GO:0000723	3.55E-03
GO:BP	regulation of protein localization to chromosome, telomeric region	GO:1904814	3.78E-03
GO:BP	regulation of hematopoietic progenitor cell differentiation	GO:1901532	3.94E-03

GO:BP	positive regulation of telomerase RNA localization to Cajal body	GO:1904874	5.12E-03
GO:BP	telomere organization	GO:0032200	6.68E-03
GO:BP	formation of cytoplasmic translation initiation complex	GO:0001732	6.79E-03
GO:BP	viral transcription	GO:0019083	7.33E-03
GO:BP	regulation of cellular catabolic process	GO:0031329	8.39E-03
GO:BP	regulation of cellular amino acid metabolic process	GO:0006521	9.49E-03
GO:BP	regulation of telomerase RNA localization to Cajal body	GO:1904872	1.13E-02
GO:BP	chaperone-mediated protein complex assembly	GO:0051131	1.13E-02
GO:BP	establishment of protein localization to telomere	GO:0070200	1.13E-02
GO:BP	positive regulation of DNA biosynthetic process	GO:2000573	1.24E-02
GO:BP	positive regulation of DNA metabolic process	GO:0051054	1.30E-02
GO:BP	proteasome-mediated ubiquitin-dependent protein catabolic process	GO:0043161	1.40E-02
GO:BP	DNA biosynthetic process	GO:0071897	1.42E-02
GO:BP	telomerase RNA localization to Cajal body	GO:0090671	1.42E-02
GO:BP	purine ribonucleoside monophosphate biosynthetic process	GO:0009168	1.42E-02
GO:BP	purine nucleoside monophosphate biosynthetic process	GO:0009127	1.42E-02
GO:BP	RNA localization to Cajal body	GO:0090670	1.42E-02
GO:BP	telomerase RNA localization	GO:0090672	1.42E-02
GO:BP	RNA localization to nucleus	GO:0090685	1.42E-02
GO:BP	telomere maintenance via telomerase	GO:0007004	1.48E-02
GO:BP	protein targeting	GO:0006605	1.51E-02
GO:BP	viral gene expression	GO:0019080	1.54E-02
GO:BP	cytokine-mediated pathway	GO:0019221	1.62E-02
GO:BP	T cell receptor pathway	GO:0050852	1.74E-02
GO:BP	RNA-dependent DNA biosynthetic process	GO:0006278	1.74E-02
GO:BP	regulation of cellular protein catabolic process	GO:1903362	1.81E-02
GO:BP	mitotic cell cycle process	GO:1903047	1.83E-02
GO:BP	positive regulation of mRNA binding	GO:1902416	2.03E-02
GO:BP	antigen processing and presentation of exogenous peptide antigen via MHC class I, TAP-dependent	GO:0002479	2.40E-02
GO:BP	positive regulation of protein localization to nucleus	GO:1900182	2.59E-02
GO:BP	purine ribonucleoside triphosphate metabolic process	GO:0009205	2.59E-02
GO:BP	regulation of nuclease activity	GO:0032069	2.64E-02
GO:BP	regulation of transcription from RNA polymerase II promoter in response to hypoxia	GO:0061418	3.01E-02
GO:BP	regulation of stem cell differentiation	GO:2000736	3.23E-02
GO:BP	positive regulation of RNA binding	GO:1905216	3.23E-02
GO:BP	regulation of translational initiation	GO:0006446	3.24E-02

GO:BP	antigen processing and presentation of exogenous peptide antigen via MHC class I	GO:0042590	3.24E-02
GO:BP	viral life cycle	GO:0019058	3.31E-02
GO:BP	telomere maintenance via telomere lengthening	GO:0010833	3.74E-02
GO:BP	proteasomal ubiquitin-independent protein catabolic process	GO:0010499	3.80E-02
GO:BP	ribonucleoside triphosphate metabolic process	GO:0009199	4.01E-02
GO:BP	tumor necrosis factor-mediated pathway	GO:0033209	4.15E-02
GO:BP	cellular response to decreased oxygen levels	GO:0036294	4.18E-02
GO:BP	anaphase-promoting complex-dependent catabolic process	GO:0031145	4.30E-02
GO:BP	regulation of cellular amine metabolic process	GO:0033238	4.60E-02
GO:BP	purine nucleoside triphosphate metabolic process	GO:0009144	4.60E-02
GO:CC	pigment granule	GO:0048770	2.75E-12
GO:CC	melanosome	GO:0042470	2.75E-12
GO:CC	ribonucleoprotein complex	GO:1990904	2.89E-12
GO:CC	chaperone complex	GO:0101031	1.78E-08
GO:CC	cytosolic part	GO:0044445	3.12E-08
GO:CC	focal adhesion	GO:0005925	4.60E-07
GO:CC	cell-substrate adherens junction	GO:0005924	5.15E-07
GO:CC	cell-substrate junction	GO:0030055	6.20E-07
GO:CC	ficolin-1-rich granule lumen	GO:1904813	3.37E-06
GO:CC	ficolin-1-rich granule	GO:0101002	3.37E-06
GO:CC	mitochondrial matrix	GO:0005759	5.36E-06
GO:CC	cytosolic ribosome	GO:0022626	1.32E-05
GO:CC	ribosomal subunit	GO:0044391	1.89E-05
GO:CC	ribosome	GO:0005840	2.52E-05
GO:CC	adherens junction	GO:0005912	4.03E-05
GO:CC	anchoring junction	GO:0070161	5.93E-05
GO:CC	proteasome complex	GO:0000502	1.04E-04
GO:CC	endopeptidase complex	GO:1905369	1.15E-04
GO:CC	chaperonin-containing T-complex	GO:0005832	1.34E-04
GO:CC	polysome	GO:0005844	1.88E-04
GO:CC	peptidase complex	GO:1905368	7.88E-04
GO:CC	eukaryotic 48S preinitiation complex	GO:0033290	8.48E-04
GO:CC	organelle inner membrane	GO:0019866	9.43E-04
GO:CC	nucleolus	GO:0005730	1.17E-03
GO:CC	translation preinitiation complex	GO:0070993	1.87E-03
GO:CC	secretory granule lumen	GO:0034774	3.13E-03
GO:CC	cytoplasmic vesicle lumen	GO:0060205	3.52E-03
GO:CC	vesicle lumen	GO:0031983	3.73E-03
GO:CC	cytosolic small ribosomal subunit	GO:0022627	4.14E-03
GO:CC	proteasome core complex	GO:0005839	5.28E-03
GO:CC	zona pellucida receptor complex	GO:0002199	5.59E-03
GO:CC	mitochondrial inner membrane	GO:0005743	5.84E-03

GO:CC	catalytic step 2 spliceosome	GO:0071013	7.07E-03
GO:CC	cell body	GO:0044297	9.69E-03
GO:CC	endoplasmic reticulum chaperone complex	GO:0034663	1.19E-02
GO:CC	COP9 signalosome	GO:0008180	2.94E-02
GO:CC	small ribosomal subunit	GO:0015935	4.69E-02
GO:CC	mitochondrial envelope	GO:0005740	4.72E-02
KEGG	RNA transport	KEGG:03013	3.23E-04
KEGG	Ribosome	KEGG:03010	4.64E-04
KEGG	Protein processing in endoplasmic reticulum	KEGG:04141	4.91E-04
KEGG	Proteasome	KEGG:03050	1.42E-03
KEGG	Antigen processing and presentation	KEGG:04612	1.64E-02
KEGG	Spliceosome	KEGG:03040	2.01E-02
REAC	Translation	REAC:R-HSA-72766	9.35E-15
REAC	Metabolism of RNA	REAC:R-HSA-8953854	5.56E-11
REAC	Regulation of expression of SLITs and ROBOs	REAC:R-HSA-9010553	7.02E-11
REAC	GTP hydrolysis and joining of the 60S ribosomal subunit	REAC:R-HSA-72706	2.75E-10
REAC	Eukaryotic Translation Initiation	REAC:R-HSA-72613	6.75E-10
REAC	Cap-dependent Translation Initiation	REAC:R-HSA-72737	6.75E-10
REAC	L13a-mediated translational silencing of Ceruloplasmin expression	REAC:R-HSA-156827	3.91E-09
REAC	Signaling by ROBO receptors	REAC:R-HSA-376176	4.22E-09
REAC	Ribosomal scanning and start codon recognition	REAC:R-HSA-72702	8.24E-09
REAC	Infectious disease	REAC:R-HSA-5663205	9.26E-08
REAC	Translation initiation complex formation	REAC:R-HSA-72649	1.90E-07
REAC	Activation of the mRNA upon binding of the cap-binding complex and eIFs, and subsequent binding to 43S	REAC:R-HSA-72662	2.25E-07
REAC	Metabolism of amino acids and derivatives	REAC:R-HSA-71291	5.61E-07
REAC	Axon guidance	REAC:R-HSA-422475	8.63E-07
REAC	Nonsense-Mediated Decay (NMD)	REAC:R-HSA-927802	1.18E-06
REAC	Nonsense Mediated Decay (NMD) enhanced by the Exon Junction Complex (EJC)	REAC:R-HSA-975957	1.18E-06

REAC	Attenuation phase	REAC:R-HSA-3371568	1.36E-06
REAC	Eukaryotic Translation Termination	REAC:R-HSA-72764	1.49E-06
REAC	Nonsense Mediated Decay (NMD) independent of the Exon Junction Complex (EJC)	REAC:R-HSA-975956	1.87E-06
REAC	Formation of a pool of free 40S subunits	REAC:R-HSA-72689	3.59E-06
REAC	Cellular responses to stress	REAC:R-HSA-2262752	6.59E-06
REAC	Influenza Life Cycle	REAC:R-HSA-168255	1.19E-05
REAC	Selenoamino acid metabolism	REAC:R-HSA-2408522	1.53E-05
REAC	Formation of the ternary complex, and subsequently, the 43S complex	REAC:R-HSA-72695	2.47E-05
REAC	Influenza Infection	REAC:R-HSA-168254	2.55E-05
REAC	AUF1 (hnRNP D0) binds and destabilizes mRNA	REAC:R-HSA-450408	3.36E-05
REAC	HSF1-dependent transactivation	REAC:R-HSA-3371571	5.58E-05
REAC	Cellular response to heat stress	REAC:R-HSA-3371556	1.23E-04
REAC	Cellular responses to external stimuli	REAC:R-HSA-8953897	1.68E-04
REAC	Selenocysteine synthesis	REAC:R-HSA-2408557	2.40E-04
REAC	Host Interactions of HIV factors	REAC:R-HSA-162909	2.99E-04
REAC	Influenza Viral RNA Transcription and Replication	REAC:R-HSA-168273	5.30E-04
REAC	The role of GTSE1 in G2/M progression after G2 checkpoint	REAC:R-HSA-8852276	6.76E-04
REAC	HSP90 chaperone cycle for steroid hormone receptors (SHR)	REAC:R-HSA-3371497	8.31E-04
REAC	Folding of actin by CCT/TriC	REAC:R-HSA-390450	9.35E-04
REAC	SRP-dependent cotranslational protein targeting to membrane	REAC:R-HSA-1799339	1.14E-03
REAC	Regulation of mRNA stability by proteins that bind AU-rich elements	REAC:R-HSA-450531	1.29E-03
REAC	Peptide chain elongation	REAC:R-HSA-156902	1.82E-03
REAC	Viral mRNA Translation	REAC:R-HSA-192823	1.82E-03

REAC	Cooperation of PDCL (PhLP1) and TriC/CCT in G-protein beta folding	REAC:R-HSA-6814122	1.86E-03
REAC	Hedgehog ligand biogenesis	REAC:R-HSA-5358346	2.04E-03
REAC	Purine ribonucleoside monophosphate biosynthesis	REAC:R-HSA-73817	2.17E-03
REAC	Eukaryotic Translation Elongation	REAC:R-HSA-156842	2.53E-03
REAC	Regulation of PTEN stability and activity	REAC:R-HSA-8948751	3.06E-03
REAC	RUNX1 regulates transcription of genes involved in differentiation of HSCs	REAC:R-HSA-8939236	3.61E-03
REAC	Regulation of RUNX2 expression and activity	REAC:R-HSA-8939902	3.70E-03
REAC	Cross-presentation of soluble exogenous antigens (endosomes)	REAC:R-HSA-1236978	5.27E-03
REAC	Regulation of activated PAK-2p34 by proteasome mediated degradation	REAC:R-HSA-211733	5.27E-03
REAC	Nucleobase biosynthesis	REAC:R-HSA-8956320	5.83E-03
REAC	Regulation of ornithine decarboxylase (ODC)	REAC:R-HSA-350562	5.92E-03
REAC	Vpu mediated degradation of CD4	REAC:R-HSA-180534	6.63E-03
REAC	p53-Independent DNA Damage Response	REAC:R-HSA-69610	6.63E-03
REAC	p53-Independent G1/S DNA damage checkpoint	REAC:R-HSA-69613	6.63E-03
REAC	Ubiquitin-dependent degradation of Cyclin D	REAC:R-HSA-75815	6.63E-03
REAC	Autodegradation of the E3 ubiquitin ligase COP1	REAC:R-HSA-349425	6.63E-03
REAC	Ubiquitin Mediated Degradation of Phosphorylated Cdc25A	REAC:R-HSA-69601	6.63E-03
REAC	Negative regulation of NOTCH4 signaling	REAC:R-HSA-9604323	7.42E-03
REAC	Vif-mediated degradation of APOBEC3G	REAC:R-HSA-180585	7.42E-03
REAC	Regulation of Apoptosis	REAC:R-HSA-169911	7.42E-03
REAC	Antiviral mechanism by IFN-stimulated genes	REAC:R-HSA-1169410	7.53E-03
REAC	Regulation of RUNX3 expression and activity	REAC:R-HSA-8941858	8.27E-03
REAC	FBXL7 down-regulates AURKA during mitotic entry and in early mitosis	REAC:R-HSA-8854050	9.21E-03

REAC	Degradation of AXIN	REAC:R-HSA-4641257	9.21E-03
REAC	SCF-beta-TrCP mediated degradation of Emi1	REAC:R-HSA-174113	9.21E-03
REAC	Hh mutants that don't undergo autocatalytic processing are degraded by ERAD	REAC:R-HSA-5362768	1.02E-02
REAC	HIV Infection	REAC:R-HSA-162906	1.12E-02
REAC	Stabilization of p53	REAC:R-HSA-69541	1.13E-02
REAC	Degradation of DVL	REAC:R-HSA-4641258	1.13E-02
REAC	Metabolism of polyamines	REAC:R-HSA-351202	1.25E-02
REAC	Hh mutants abrogate ligand secretion	REAC:R-HSA-5387390	1.38E-02
REAC	NIK→noncanonical NF-kB signaling	REAC:R-HSA-5676590	1.38E-02
REAC	CDT1 association with the CDC6:ORC:origin complex	REAC:R-HSA-68827	1.38E-02
REAC	Synthesis of DNA	REAC:R-HSA-69239	1.43E-02
REAC	Degradation of GLI2 by the proteasome	REAC:R-HSA-5610783	1.52E-02
REAC	Degradation of GLI1 by the proteasome	REAC:R-HSA-5610780	1.52E-02
REAC	GLI3 is processed to GLI3R by the proteasome	REAC:R-HSA-5610785	1.52E-02
REAC	SCF(Skp2)-mediated degradation of p27/p21	REAC:R-HSA-187577	1.52E-02
REAC	Dectin-1 mediated noncanonical NF-kB signaling	REAC:R-HSA-5607761	1.52E-02
REAC	MAPK6/MAPK4 signaling	REAC:R-HSA-5687128	1.64E-02
REAC	Defective CFTR causes cystic fibrosis	REAC:R-HSA-5678895	1.67E-02
REAC	Cytokine Signaling in Immune system	REAC:R-HSA-1280215	1.99E-02
REAC	Autodegradation of Cdh1 by Cdh1:APC/C	REAC:R-HSA-174084	2.01E-02
REAC	Asymmetric localization of PCP proteins	REAC:R-HSA-4608870	2.20E-02
REAC	DNA Replication	REAC:R-HSA-69306	2.28E-02
REAC	Oxygen-dependent proline hydroxylation of Hypoxia-inducible Factor Alpha	REAC:R-HSA-1234176	2.63E-02

REAC	p53-Dependent G1 DNA Damage Response	REAC:R-HSA-69563	2.63E-02
REAC	p53-Dependent G1/S DNA damage checkpoint	REAC:R-HSA-69580	2.63E-02
REAC	Activation of NF-kappaB in B cells	REAC:R-HSA-1169091	2.86E-02
REAC	APC/C:Cdc20 mediated degradation of Securin	REAC:R-HSA-174154	2.86E-02
REAC	Regulation of HSF1-mediated heat shock response	REAC:R-HSA-3371453	2.86E-02
REAC	Assembly of the pre-replicative complex	REAC:R-HSA-68867	3.11E-02
REAC	G1/S DNA Damage Checkpoints	REAC:R-HSA-69615	3.11E-02
REAC	Regulation of RAS by GAPs	REAC:R-HSA-5658442	3.11E-02
REAC	The citric acid (TCA) cycle and respiratory electron transport	REAC:R-HSA-1428517	3.48E-02
REAC	Orc1 removal from chromatin	REAC:R-HSA-68949	3.96E-02
REAC	ESR-mediated signaling	REAC:R-HSA-8939211	4.17E-02
REAC	ABC-family proteins mediated transport	REAC:R-HSA-382556	4.18E-02
REAC	Cytosolic tRNA aminoacylation	REAC:R-HSA-379716	4.22E-02
REAC	APC/C:Cdh1 mediated degradation of Cdc20 and other APC/C:Cdh1 targeted proteins in late mitosis/early G1	REAC:R-HSA-174178	4.29E-02
REAC	CDK-mediated phosphorylation and removal of Cdc6	REAC:R-HSA-69017	4.29E-02
REAC	Cdc20:Phospho-APC/C mediated degradation of Cyclin A	REAC:R-HSA-174184	4.29E-02
REAC	mRNA Splicing – Major Pathway	REAC:R-HSA-72163	4.52E-02
REAC	APC:Cdc20 mediated degradation of cell cycle proteins prior to satisfaction of the cell cycle checkpoint	REAC:R-HSA-179419	4.63E-02
WP	Translation Factors	WP:WP107	3.52E-05
WP	Cytoplasmic Ribosomal Proteins	WP:WP477	2.36E-03
WP	Trans-sulfuration and one carbon metabolism	WP:WP2525	5.69E-03
WP	Proteasome Degradation	WP:WP183	2.06E-02
WP	Purine metabolism	WP:WP4224	2.08E-02
WP	Parkin-Ubiquitin Proteasomal System pathway	WP:WP2359	3.41E-02

16. Ontological enrichments HT-29 IC_{20} up-regulated proteins

source	Term name	Term id	Adjusted p-value
GO:BP	mRNA metabolic process	GO:0016071	7.29E-07
GO:BP	RNA processing	GO:0006396	2.81E-05
GO:BP	mRNA processing	GO:0006397	5.67E-04
GO:BP	telomere maintenance via telomerase	GO:0007004	4.20E-03
GO:BP	RNA-dependent DNA biosynthetic process	GO:0006278	4.71E-03
GO:BP	telomere maintenance via telomere lengthening	GO:0010833	7.99E-03
GO:BP	nucleic acid transport	GO:0050657	1.13E-02
GO:BP	RNA transport	GO:0050658	1.13E-02
GO:BP	mRNA splicing, via spliceosome	GO:0000398	1.18E-02
GO:BP	RNA splicing, via transesterification reactions with bulged adenosine as nucleophile	GO:0000377	1.18E-02
GO:BP	establishment of RNA localization	GO:0051236	1.22E-02
GO:BP	RNA splicing, via transesterification reactions	GO:0000375	1.23E-02
GO:BP	RNA localization	GO:0006403	2.69E-02
GO:BP	nucleobase-containing compound transport	GO:0015931	3.36E-02
GO:BP	RNA splicing	GO:0008380	4.39E-02
GO:BP	telomerase holoenzyme complex assembly	GO:1905323	4.86E-02
GO:CC	catalytic step 2 spliceosome	GO:0071013	1.27E-03
GO:CC	melanosome	GO:0042470	3.08E-03
GO:CC	pigment granule	GO:0048770	3.08E-03
GO:CC	dendritic growth cone	GO:0044294	1.51E-02
GO:CC	adherens junction	GO:0005912	2.16E-02
GO:CC	anchoring junction	GO:0070161	2.51E-02
GO:CC	spliceosomal complex	GO:0005681	2.87E-02
GO:CC	dendrite terminus	GO:0044292	3.79E-02
GO:CC	ribonucleoprotein complex	GO:1990904	3.88E-02
KEGG	Spliceosome	KEGG:03040	4.35E-04
KEGG	Protein processing in endoplasmic reticulum	KEGG:04141	2.26E-02
REAC	Uptake and function of diphtheria toxin	REAC:R-HSA-5336415	3.11E-05
REAC	mRNA Splicing – Major Pathway	REAC:R-HSA-72163	1.86E-04
REAC	mRNA Splicing	REAC:R-HSA-72172	2.41E-04
REAC	Metabolism of RNA	REAC:R-HSA-8953854	3.45E-04
REAC	HSP90 chaperone cycle for steroid hormone receptors (SHR)	REAC:R-HSA-3371497	9.30E-04
REAC	Processing of Capped Intron-Containing Pre-mRNA	REAC:R-HSA-72203	9.81E-04
REAC	Uptake and actions of bacterial toxins	REAC:R-HSA-5339562	3.49E-03
WP	mRNA Processing	WP:WP411	1.85E-02

17. Ontological enrichments HT-29 sub-inhibitory up-regulated proteins

source	Term name	Term id	Adjusted p value
GO:BP	regulation of cellular protein localization	GO:1903827	2.39E-02
GO:BP	interleukin-12-mediated pathway	GO:0035722	2.68E-02
GO:BP	cellular response to interleukin-12	GO:0071349	3.05E-02
GO:BP	positive regulation of cellular protein localization	GO:1903829	3.10E-02
GO:BP	response to interleukin-12	GO:0070671	3.24E-02
GO:BP	regulation of cellular localization	GO:0060341	4.53E-02
GO:CC	chaperone complex	GO:0101031	2.08E-04
GO:CC	secretory granule lumen	GO:0034774	2.35E-03
GO:CC	cytoplasmic vesicle lumen	GO:0060205	2.49E-03
GO:CC	vesicle lumen	GO:0031983	2.57E-03
GO:CC	chaperonin-containing T-complex	GO:0005832	7.84E-03
GO:CC	melanosome	GO:0042470	2.78E-02
GO:CC	pigment granule	GO:0048770	2.78E-02
GO:CC	ficolin-1-rich granule lumen	GO:1904813	4.54E-02
GO:CC	ficolin-1-rich granule	GO:0101002	4.54E-02
REAC	Interleukin-12 signaling	REAC:R-HSA-9020591	1.45E-02
REAC	Interleukin-12 family signaling	REAC:R-HSA-447115	2.59E-02
REAC	Folding of actin by CCT/TriC	REAC:R-HSA-390450	2.94E-02

18. Ontological enrichments HT-29 sub-inhibitory down-regulated proteins

source	Term name	Term id	Adjusted p-value
GO:BP	mRNA metabolic process	GO:0016071	5.31E-08
GO:BP	RNA splicing, via transesterification reactions	GO:0000375	2.93E-06
GO:BP	RNA splicing	GO:0008380	3.00E-05
GO:BP	mRNA splicing, via spliceosome	GO:0000398	4.14E-05
GO:BP	RNA splicing, via transesterification reactions with bulged adenosine as nucleophile	GO:0000377	4.14E-05
GO:BP	translational initiation	GO:0006413	8.69E-05
GO:BP	mRNA processing	GO:0006397	1.60E-04
GO:BP	RNA processing	GO:0006396	1.11E-03
GO:BP	regulation of RNA splicing	GO:0043484	4.07E-03
GO:BP	translation	GO:0006412	4.90E-03
GO:BP	peptide metabolic process	GO:0006518	5.25E-03
GO:BP	peptide biosynthetic process	GO:0043043	6.78E-03
GO:BP	mRNA catabolic process	GO:0006402	1.09E-02
GO:BP	posttranscriptional regulation of gene expression	GO:0010608	1.81E-02
GO:BP	RNA catabolic process	GO:0006401	2.18E-02
GO:BP	regulation of translation	GO:0006417	3.24E-02
GO:BP	amide biosynthetic process	GO:0043604	3.48E-02
GO:BP	nuclear-transcribed mRNA catabolic process, nonsense-mediated decay	GO:0000184	3.64E-02
GO:BP	nuclear-transcribed mRNA catabolic process	GO:0000956	3.96E-02
GO:CC	ribonucleoprotein complex	GO:1990904	9.03E-14
GO:CC	catalytic step 2 spliceosome	GO:0071013	1.61E-05
GO:CC	spliceosomal complex	GO:0005681	9.72E-05
GO:CC	ribonucleoprotein granule	GO:0035770	3.39E-04
GO:CC	cytoplasmic stress granule	GO:0010494	4.81E-03
GO:CC	polysome	GO:0005844	8.62E-03
GO:CC	adherens junction	GO:0005912	1.45E-02
GO:CC	focal adhesion	GO:0005925	1.55E-02
GO:CC	cell-substrate adherens junction	GO:0005924	1.62E-02
GO:CC	cell-substrate junction	GO:0030055	1.75E-02
GO:CC	anchoring junction	GO:0070161	1.76E-02
GO:CC	cytosolic ribosome	GO:0022626	3.84E-02
GO:CC	cytoplasmic ribonucleoprotein granule	GO:0036464	4.86E-02
KEGG	Protein processing in endoplasmic reticulum	KEGG:04141	1.15E-02
KEGG	Carbon metabolism	KEGG:01200	3.40E-02
REAC	Metabolism of RNA	REAC:R-HSA-8953854	1.35E-08
REAC	L13a-mediated translational silencing of Ceruloplasmin expression	REAC:R-HSA-156827	4.73E-05

REAC	mRNA Splicing – Major Pathway	REAC:R-HSA-72163	7.46E-05
REAC	Cap-dependent Translation Initiation	REAC:R-HSA-72737	7.61E-05
REAC	Eukaryotic Translation Initiation	REAC:R-HSA-72613	7.61E-05
REAC	mRNA Splicing	REAC:R-HSA-72172	1.04E-04
REAC	Processing of Capped Intron-Containing Pre-mRNA	REAC:R-HSA-72203	6.48E-04
REAC	FGFR2 alternative splicing	REAC:R-HSA-6803529	7.31E-04
REAC	GTP hydrolysis and joining of the 60S ribosomal subunit	REAC:R-HSA-72706	1.05E-03
REAC	Nonsense Mediated Decay (NMD) independent of the Exon Junction Complex (EJC)	REAC:R-HSA-975956	8.22E-03
REAC	Translation initiation complex formation	REAC:R-HSA-72649	2.04E-02
REAC	Nonsense Mediated Decay (NMD) enhanced by the Exon Junction Complex (EJC)	REAC:R-HSA-975957	2.04E-02
REAC	Nonsense-Mediated Decay (NMD)	REAC:R-HSA-927802	2.04E-02
REAC	Activation of the mRNA upon binding of the cap-binding complex and eIFs, and subsequent binding to 43S	REAC:R-HSA-72662	2.18E-02
REAC	Translation	REAC:R-HSA-72766	2.70E-02
REAC	Signaling by FGFR2	REAC:R-HSA-5654738	3.17E-02
REAC	Deadenylation of mRNA	REAC:R-HSA-429947	3.30E-02
WP	mRNA Processing	WP:WP411	2.65E-02

19. Ontological enrichments of all down-regulated proteins combined

source	Term name	Term id	Adjusted p-value
GO:BP	mRNA metabolic process	GO:0016071	3.62E-18
GO:BP	nucleobase-containing compound catabolic process	GO:0034655	8.85E-15
GO:BP	aromatic compound catabolic process	GO:0019439	2.00E-14
GO:BP	organic cyclic compound catabolic process	GO:1901361	8.14E-14
GO:BP	heterocycle catabolic process	GO:0046700	8.66E-14
GO:BP	cellular nitrogen compound catabolic process	GO:0044270	9.07E-14
GO:BP	mRNA catabolic process	GO:0006402	8.20E-13
GO:BP	RNA catabolic process	GO:0006401	6.91E-12
GO:BP	RNA splicing, via transesterification reactions	GO:0000375	3.11E-10
GO:BP	RNA splicing	GO:0008380	2.26E-08
GO:BP	RNA splicing, via transesterification reactions with bulged adenosine as nucleophile	GO:0000377	2.44E-08
GO:BP	mRNA splicing, via spliceosome	GO:0000398	2.44E-08
GO:BP	interspecies interaction between organisms	GO:0044419	8.14E-08
GO:BP	symbiotic process	GO:0044403	1.19E-07
GO:BP	peptide metabolic process	GO:0006518	1.50E-07
GO:BP	translational initiation	GO:0006413	4.37E-07
GO:BP	mRNA processing	GO:0006397	4.68E-07
GO:BP	viral process	GO:0016032	8.20E-07
GO:BP	regulation of mRNA metabolic process	GO:1903311	8.56E-07
GO:BP	nuclear-transcribed mRNA catabolic process	GO:0000956	1.16E-06
GO:BP	nuclear-transcribed mRNA catabolic process, nonsense-mediated decay	GO:0000184	3.47E-06
GO:BP	SRP-dependent cotranslational protein targeting to membrane	GO:0006614	4.73E-06
GO:BP	nuclear export	GO:0051168	5.24E-06
GO:BP	cotranslational protein targeting to membrane	GO:0006613	7.81E-06
GO:BP	translation	GO:0006412	8.29E-06
GO:BP	establishment of protein localization to organelle	GO:0072594	1.38E-05
GO:BP	peptide biosynthetic process	GO:0043043	1.56E-05
GO:BP	protein targeting to ER	GO:0045047	1.65E-05
GO:BP	establishment of protein localization to endoplasmic reticulum	GO:0072599	2.34E-05
GO:BP	RNA processing	GO:0006396	3.80E-05
GO:BP	viral gene expression	GO:0019080	4.80E-05
GO:BP	protein localization to organelle	GO:0033365	5.77E-05
GO:BP	monosaccharide catabolic process	GO:0046365	7.51E-05
GO:BP	nucleocytoplasmic transport	GO:0006913	1.00E-04
GO:BP	nuclear transport	GO:0051169	1.12E-04
GO:BP	protein localization to endoplasmic reticulum	GO:0070972	1.49E-04
GO:BP	viral transcription	GO:0019083	1.80E-04

GO:BP	protein export from nucleus	GO:0006611	2.02E-04
GO:BP	regulation of RNA splicing	GO:0043484	2.09E-04
GO:BP	protein targeting	GO:0006605	2.40E-04
GO:BP	amide biosynthetic process	GO:0043604	3.63E-04
GO:BP	posttranscriptional regulation of gene expression	GO:0010608	4.57E-04
GO:BP	glucose catabolic process	GO:0006007	4.77E-04
GO:BP	NADH metabolic process	GO:0006734	1.65E-03
GO:BP	regulation of mRNA stability	GO:0043488	1.79E-03
GO:BP	regulation of RNA stability	GO:0043487	2.31E-03
GO:BP	RNA localization	GO:0006403	2.66E-03
GO:BP	canonical glycolysis	GO:0061621	2.90E-03
GO:BP	glucose catabolic process to pyruvate	GO:0061718	2.90E-03
GO:BP	NADH regeneration	GO:0006735	2.90E-03
GO:BP	regulation of nucleocytoplasmic transport	GO:0046822	2.99E-03
GO:BP	small molecule biosynthetic process	GO:0044283	3.21E-03
GO:BP	cellular detoxification	GO:1990748	3.43E-03
GO:BP	glycolytic process through glucose-6-phosphate	GO:0061620	3.51E-03
GO:BP	glycolytic process through fructose-6-phosphate	GO:0061615	3.51E-03
GO:BP	mRNA transport	GO:0051028	3.55E-03
GO:BP	NAD metabolic process	GO:0019674	3.57E-03
GO:BP	monocarboxylic acid metabolic process	GO:0032787	3.58E-03
GO:BP	nucleic acid transport	GO:0050657	3.90E-03
GO:BP	protein targeting to membrane	GO:0006612	3.90E-03
GO:BP	RNA transport	GO:0050658	3.90E-03
GO:BP	establishment of RNA localization	GO:0051236	4.47E-03
GO:BP	alternative mRNA splicing, via spliceosome	GO:0000380	4.60E-03
GO:BP	positive regulation of multi-organism process	GO:0043902	4.61E-03
GO:BP	regulation of mRNA catabolic process	GO:0061013	5.12E-03
GO:BP	hexose catabolic process	GO:0019320	8.66E-03
GO:BP	regulation of multi-organism process	GO:0043900	8.84E-03
GO:BP	detoxification	GO:0098754	1.48E-02
GO:BP	cellular oxidant detoxification	GO:0098869	2.01E-02
GO:BP	regulation of alternative mRNA splicing, via spliceosome	GO:0000381	2.61E-02
GO:BP	methylglyoxal metabolic process	GO:0009438	2.66E-02
GO:BP	regulation of mRNA splicing, via spliceosome	GO:0048024	2.77E-02
GO:BP	nucleobase-containing compound transport	GO:0015931	2.83E-02
GO:BP	pyruvate metabolic process	GO:0006090	3.88E-02
GO:BP	regulation of translation	GO:0006417	3.94E-02
GO:BP	carbohydrate catabolic process	GO:0016052	3.98E-02
GO:BP	interleukin-12-mediated pathway	GO:0035722	4.89E-02
GO:CC	ribonucleoprotein complex	GO:1990904	2.36E-18
GO:CC	cytosolic ribosome	GO:0022626	1.54E-06
GO:CC	ficolin-1-rich granule lumen	GO:1904813	6.45E-06
GO:CC	ficolin-1-rich granule	GO:0101002	6.45E-06
GO:CC	polysome	GO:0005844	1.61E-05

GO:CC	spliceosomal complex	GO:0005681	3.08E-05
GO:CC	catalytic step 2 spliceosome	GO:0071013	4.89E-05
GO:CC	cytosolic part	GO:0044445	6.74E-05
GO:CC	secretory granule lumen	GO:0034774	1.55E-04
GO:CC	cytoplasmic vesicle lumen	GO:0060205	1.78E-04
GO:CC	vesicle lumen	GO:0031983	1.91E-04
GO:CC	ribonucleoprotein granule	GO:0035770	2.00E-04
GO:CC	ribosomal subunit	GO:0044391	3.53E-04
GO:CC	focal adhesion	GO:0005925	3.72E-04
GO:CC	cell-substrate adherens junction	GO:0005924	4.06E-04
GO:CC	cell-substrate junction	GO:0030055	4.68E-04
GO:CC	adherens junction	GO:0005912	5.74E-04
GO:CC	anchoring junction	GO:0070161	8.14E-04
GO:CC	cytosolic large ribosomal subunit	GO:0022625	1.27E-03
GO:CC	ribosome	GO:0005840	3.06E-03
GO:CC	cytoplasmic ribonucleoprotein granule	GO:0036464	7.31E-03
GO:CC	polysomal ribosome	GO:0042788	2.51E-02
GO:CC	cytoplasmic stress granule	GO:0010494	2.84E-02
KEGG	Carbon metabolism	KEGG:01200	2.81E-05
KEGG	Ribosome	KEGG:03010	9.95E-05
KEGG	Spliceosome	KEGG:03040	6.22E-03
KEGG	Biosynthesis of amino acids	KEGG:01230	1.04E-02
KEGG	Amyotrophic lateral sclerosis (ALS)	KEGG:05014	1.49E-02
KEGG	Fructose and mannose metabolism	KEGG:00051	3.00E-02
REAC	Metabolism of RNA	REAC:R-HSA-8953854	6.77E-17
REAC	mRNA Splicing – Major Pathway	REAC:R-HSA-72163	1.09E-08
REAC	mRNA Splicing	REAC:R-HSA-72172	2.12E-08
REAC	L13a-mediated translational silencing of Ceruloplasmin expression	REAC:R-HSA-156827	3.40E-08
REAC	Eukaryotic Translation Initiation	REAC:R-HSA-72613	8.19E-08
REAC	Cap-dependent Translation Initiation	REAC:R-HSA-72737	8.19E-08
REAC	Processing of Capped Intron-Containing Pre-mRNA	REAC:R-HSA-72203	8.79E-08
REAC	GTP hydrolysis and joining of the 60S ribosomal subunit	REAC:R-HSA-72706	5.38E-07
REAC	Eukaryotic Translation Elongation	REAC:R-HSA-156842	9.58E-07
REAC	Nonsense Mediated Decay (NMD) independent of the Exon Junction Complex (EJC)	REAC:R-HSA-975956	1.20E-06

REAC	Signaling by ROBO receptors	REAC:R-HSA-376176	1.75E-06
REAC	Regulation of expression of SLITs and ROBOs	REAC:R-HSA-9010553	6.57E-06
REAC	Influenza Life Cycle	REAC:R-HSA-168255	7.43E-06
REAC	Viral mRNA Translation	REAC:R-HSA-192823	8.85E-06
REAC	Peptide chain elongation	REAC:R-HSA-156902	8.85E-06
REAC	Nonsense-Mediated Decay (NMD)	REAC:R-HSA-927802	9.07E-06
REAC	Nonsense Mediated Decay (NMD) enhanced by the Exon Junction Complex (EJC)	REAC:R-HSA-975957	9.07E-06
REAC	Selenocysteine synthesis	REAC:R-HSA-2408557	1.35E-05
REAC	Eukaryotic Translation Termination	REAC:R-HSA-72764	1.35E-05
REAC	Influenza Infection	REAC:R-HSA-168254	1.60E-05
REAC	Formation of a pool of free 40S subunits	REAC:R-HSA-72689	2.98E-05
REAC	Influenza Viral RNA Transcription and Replication	REAC:R-HSA-168273	3.78E-05
REAC	Infectious disease	REAC:R-HSA-5663205	6.63E-05
REAC	SRP-dependent cotranslational protein targeting to membrane	REAC:R-HSA-1799339	7.92E-05
REAC	Selenoamino acid metabolism	REAC:R-HSA-2408522	1.10E-04
REAC	Translation	REAC:R-HSA-72766	5.51E-04
REAC	Translation initiation complex formation	REAC:R-HSA-72649	8.13E-04
REAC	Activation of the mRNA upon binding of the cap-binding complex and eIFs, and subsequent binding to 43S	REAC:R-HSA-72662	9.13E-04
REAC	Major pathway of rRNA processing in the nucleolus and cytosol	REAC:R-HSA-6791226	9.35E-04
REAC	rRNA processing in the nucleus and cytosol	REAC:R-HSA-8868773	1.57E-03
REAC	FGFR2 alternative splicing	REAC:R-HSA-6803529	2.21E-03
REAC	rRNA processing	REAC:R-HSA-72312	2.55E-03
REAC	Gluconeogenesis	REAC:R-HSA-70263	6.44E-03

REAC	Ribosomal scanning and start codon recognition	REAC:R-HSA-72702	1.12E-02
REAC	Axon guidance	REAC:R-HSA-422475	1.42E-02
REAC	Gene and protein expression by JAK-STAT after Interleukin-12 stimulation	REAC:R-HSA-8950505	1.53E-02
REAC	Glycolysis	REAC:R-HSA-70171	2.32E-02
REAC	Interleukin-12 signaling	REAC:R-HSA-9020591	4.35E-02
WP	Cytoplasmic Ribosomal Proteins	WP:WP477	1.99E-05
WP	mRNA Processing	WP:WP411	4.56E-03
WP	Amyotrophic lateral sclerosis (ALS)	WP:WP2447	1.37E-02
WP	Glycolysis and Gluconeogenesis	WP:WP534	3.10E-02

20. Ontological enrichments of all up-regulated proteins combined

source	Term name	Term id	Adjusted p-value
GO:BP	mRNA metabolic process	GO:0016071	1.90E-19
GO:BP	nucleobase-containing compound catabolic process	GO:0034655	3.52E-17
GO:BP	heterocycle catabolic process	GO:0046700	5.04E-16
GO:BP	mRNA catabolic process	GO:0006402	5.12E-16
GO:BP	cellular nitrogen compound catabolic process	GO:0044270	5.32E-16
GO:BP	RNA catabolic process	GO:0006401	6.49E-16
GO:BP	aromatic compound catabolic process	GO:0019439	1.18E-15
GO:BP	organic cyclic compound catabolic process	GO:1901361	5.71E-15
GO:BP	protein folding	GO:0006457	4.27E-14
GO:BP	viral process	GO:0016032	7.48E-14
GO:BP	symbiotic process	GO:0044403	9.20E-14
GO:BP	interspecies interaction between organisms	GO:0044419	5.80E-13
GO:BP	translation	GO:0006412	2.60E-12
GO:BP	peptide biosynthetic process	GO:0043043	7.02E-12
GO:BP	nuclear-transcribed mRNA catabolic process	GO:0000956	7.14E-12
GO:BP	translational initiation	GO:0006413	2.41E-11
GO:BP	nuclear-transcribed mRNA catabolic process, nonsense-mediated decay	GO:0000184	2.79E-11
GO:BP	amide biosynthetic process	GO:0043604	3.22E-11
GO:BP	peptide metabolic process	GO:0006518	1.72E-10
GO:BP	ribonucleoprotein complex biogenesis	GO:0022613	8.19E-10
GO:BP	chaperone-mediated protein folding	GO:0061077	6.55E-09
GO:BP	cytoplasmic translation	GO:0002181	1.17E-08
GO:BP	posttranscriptional regulation of gene expression	GO:0010608	2.33E-08
GO:BP	protein targeting to ER	GO:0045047	3.16E-08
GO:BP	protein localization to endoplasmic reticulum	GO:0070972	4.27E-08
GO:BP	establishment of protein localization to endoplasmic reticulum	GO:0072599	5.04E-08
GO:BP	establishment of protein localization to organelle	GO:0072594	7.28E-08
GO:BP	ribonucleoprotein complex assembly	GO:0022618	8.41E-08
GO:BP	ribonucleoprotein complex subunit organization	GO:0071826	2.08E-07
GO:BP	SRP-dependent cotranslational protein targeting to membrane	GO:0006614	1.90E-06
GO:BP	protein localization to organelle	GO:0033365	2.41E-06
GO:BP	cotranslational protein targeting to membrane	GO:0006613	3.29E-06
GO:BP	RNA localization	GO:0006403	5.57E-06
GO:BP	positive regulation of protein localization to Cajal body	GO:1904871	1.34E-05
GO:BP	regulation of protein localization to Cajal body	GO:1904869	1.34E-05
GO:BP	establishment of protein localization to membrane	GO:0090150	1.36E-05

GO:BP	cytoplasmic translational initiation	GO:0002183	1.79E-05
GO:BP	telomere maintenance via telomerase	GO:0007004	2.11E-05
GO:BP	positive regulation of establishment of protein localization to telomere	GO:1904851	2.67E-05
GO:BP	protein localization to nuclear body	GO:1903405	2.67E-05
GO:BP	protein localization to Cajal body	GO:1904867	2.67E-05
GO:BP	RNA-dependent DNA biosynthetic process	GO:0006278	2.73E-05
GO:BP	protein targeting to membrane	GO:0006612	4.41E-05
GO:BP	viral gene expression	GO:0019080	4.41E-05
GO:BP	regulation of establishment of protein localization to telomere	GO:0070203	4.86E-05
GO:BP	telomere maintenance	GO:0000723	5.23E-05
GO:BP	cellular response to heat	GO:0034605	7.15E-05
GO:BP	positive regulation of protein localization to chromosome, telomeric region	GO:1904816	8.27E-05
GO:BP	protein localization to nucleoplasm	GO:1990173	8.27E-05
GO:BP	regulation of establishment of protein localization to chromosome	GO:0070202	8.27E-05
GO:BP	telomere maintenance via telomere lengthening	GO:0010833	8.85E-05
GO:BP	protein refolding	GO:0042026	9.84E-05
GO:BP	response to heat	GO:0009408	1.08E-04
GO:BP	telomere organization	GO:0032200	1.23E-04
GO:BP	response to unfolded protein	GO:0006986	1.31E-04
GO:BP	viral transcription	GO:0019083	1.39E-04
GO:BP	protein stabilization	GO:0050821	1.48E-04
GO:BP	regulation of protein localization to chromosome, telomeric region	GO:1904814	2.06E-04
GO:BP	cellular amino acid metabolic process	GO:0006520	2.89E-04
GO:BP	positive regulation of DNA biosynthetic process	GO:2000573	2.89E-04
GO:BP	positive regulation of DNA metabolic process	GO:0051054	3.01E-04
GO:BP	positive regulation of telomerase RNA localization to Cajal body	GO:1904874	3.07E-04
GO:BP	DNA biosynthetic process	GO:0071897	3.37E-04
GO:BP	RNA processing	GO:0006396	4.06E-04
GO:BP	regulation of catabolic process	GO:0009894	4.50E-04
GO:BP	response to temperature stimulus	GO:0009266	4.79E-04
GO:BP	regulation of protein stability	GO:0031647	4.95E-04
GO:BP	response to topologically incorrect protein	GO:0035966	4.96E-04
GO:BP	regulation of mRNA metabolic process	GO:1903311	6.09E-04
GO:BP	regulation of translation	GO:0006417	6.54E-04
GO:BP	establishment of protein localization to telomere	GO:0070200	8.57E-04
GO:BP	regulation of telomerase RNA localization to Cajal body	GO:1904872	8.57E-04
GO:BP	positive regulation of telomere maintenance via telomerase	GO:0032212	1.04E-03

GO:BP	RNA localization to Cajal body	GO:0090670	1.15E-03
GO:BP	telomerase RNA localization to Cajal body	GO:0090671	1.15E-03
GO:BP	telomerase RNA localization	GO:0090672	1.15E-03
GO:BP	RNA localization to nucleus	GO:0090685	1.15E-03
GO:BP	'de novo' posttranslational protein folding	GO:0051084	1.24E-03
GO:BP	regulation of mRNA binding	GO:1902415	1.54E-03
GO:BP	positive regulation of telomere maintenance via telomere lengthening	GO:1904358	1.75E-03
GO:BP	mRNA processing	GO:0006397	1.78E-03
GO:BP	regulation of cellular response to stress	GO:0080135	1.86E-03
GO:BP	protein localization to membrane	GO:0072657	2.07E-03
GO:BP	'de novo' protein folding	GO:0006458	2.42E-03
GO:BP	regulation of deoxyribonuclease activity	GO:0032070	2.55E-03
GO:BP	regulation of nuclease activity	GO:0032069	2.56E-03
GO:BP	protein targeting	GO:0006605	3.00E-03
GO:BP	regulation of cellular amide metabolic process	GO:0034248	3.34E-03
GO:BP	regulation of RNA binding	GO:1905214	3.97E-03
GO:BP	regulation of DNA-templated transcription in response to stress	GO:0043620	3.97E-03
GO:BP	regulation of protein catabolic process	GO:0042176	4.89E-03
GO:BP	cytokine-mediated pathway	GO:0019221	4.94E-03
GO:BP	ribosome biogenesis	GO:0042254	4.95E-03
GO:BP	tumor necrosis factor-mediated pathway	GO:0033209	5.87E-03
GO:BP	mRNA splicing, via spliceosome	GO:0000398	6.05E-03
GO:BP	RNA splicing, via transesterification reactions with bulged adenosine as nucleophile	GO:0000377	6.05E-03
GO:BP	nucleocytoplasmic transport	GO:0006913	6.25E-03
GO:BP	regulation of DNA metabolic process	GO:0051052	6.68E-03
GO:BP	RNA splicing, via transesterification reactions	GO:0000375	6.68E-03
GO:BP	nuclear transport	GO:0051169	6.91E-03
GO:BP	interleukin-12-mediated pathway	GO:0035722	7.52E-03
GO:BP	establishment of protein localization to chromosome	GO:0070199	7.56E-03
GO:BP	regulation of hematopoietic stem cell differentiation	GO:1902036	8.09E-03
GO:BP	protein catabolic process	GO:0030163	8.51E-03
GO:BP	cellular response to interleukin-12	GO:0071349	9.66E-03
GO:BP	cellular response to unfolded protein	GO:0034620	1.01E-02
GO:BP	positive regulation of protein localization to nucleus	GO:1900182	1.06E-02
GO:BP	response to interleukin-12	GO:0070671	1.09E-02
GO:BP	protein localization to chromosome, telomeric region	GO:0070198	1.10E-02
GO:BP	chaperone cofactor-dependent protein refolding	GO:0051085	1.10E-02
GO:BP	regulation of cellular catabolic process	GO:0031329	1.11E-02

GO:BP	positive regulation of telomere maintenance	GO:0032206	1.23E-02
GO:BP	regulation of DNA biosynthetic process	GO:2000278	1.23E-02
GO:BP	regulation of cellular protein localization	GO:1903827	1.37E-02
GO:BP	regulation of cellular response to heat	GO:1900034	1.38E-02
GO:BP	neutrophil degranulation	GO:0043312	1.45E-02
GO:BP	positive regulation of cellular protein localization	GO:1903829	1.52E-02
GO:BP	neutrophil activation involved in immune response	GO:0002283	1.56E-02
GO:BP	regulation of telomere maintenance via telomerase	GO:0032210	1.72E-02
GO:BP	RNA splicing	GO:0008380	1.92E-02
GO:BP	neutrophil activation	GO:0042119	2.06E-02
GO:BP	neutrophil mediated immunity	GO:0002446	2.06E-02
GO:BP	hematopoietic stem cell differentiation	GO:0060218	2.07E-02
GO:BP	formation of cytoplasmic translation initiation complex	GO:0001732	2.12E-02
GO:BP	nuclear export	GO:0051168	2.28E-02
GO:BP	granulocyte activation	GO:0036230	2.40E-02
GO:BP	regulation of hematopoietic progenitor cell differentiation	GO:1901532	2.42E-02
GO:BP	regulation of transcription from RNA polymerase II promoter in response to stress	GO:0043618	2.50E-02
GO:BP	cellular response to topologically incorrect protein	GO:0035967	2.95E-02
GO:BP	regulation of cellular protein catabolic process	GO:1903362	3.42E-02
GO:BP	chaperone-mediated protein complex assembly	GO:0051131	3.51E-02
GO:BP	ribosomal small subunit assembly	GO:0000028	3.51E-02
GO:BP	regulation of telomere maintenance via telomere lengthening	GO:1904356	3.86E-02
GO:BP	ncRNA metabolic process	GO:0034660	4.39E-02
GO:BP	purine ribonucleoside monophosphate biosynthetic process	GO:0009168	4.41E-02
GO:BP	purine nucleoside monophosphate biosynthetic process	GO:0009127	4.41E-02
GO:BP	leukocyte degranulation	GO:0043299	4.55E-02
GO:BP	regulation of cellular amino acid metabolic process	GO:0006521	4.64E-02
GO:BP	positive regulation of mRNA binding	GO:1902416	4.93E-02
GO:CC	melanosome	GO:0042470	8.82E-15
GO:CC	pigment granule	GO:0048770	8.82E-15
GO:CC	ribonucleoprotein complex	GO:1990904	2.27E-14
GO:CC	chaperone complex	GO:0101031	1.75E-11
GO:CC	cytosolic part	GO:0044445	1.34E-10
GO:CC	focal adhesion	GO:0005925	2.17E-10
GO:CC	cell-substrate adherens junction	GO:0005924	2.53E-10

GO:CC	cell-substrate junction	GO:0030055	3.26E-10
GO:CC	adherens junction	GO:0005912	2.57E-09
GO:CC	anchoring junction	GO:0070161	4.61E-09
GO:CC	cytosolic ribosome	GO:0022626	4.20E-08
GO:CC	ficolin-1-rich granule	GO:0101002	2.38E-07
GO:CC	ficolin-1-rich granule lumen	GO:1904813	2.38E-07
GO:CC	ribosomal subunit	GO:0044391	3.30E-07
GO:CC	ribosome	GO:0005840	8.93E-07
GO:CC	chaperonin-containing T-complex	GO:0005832	3.40E-06
GO:CC	mitochondrial matrix	GO:0005759	8.91E-06
GO:CC	catalytic step 2 spliceosome	GO:0071013	1.38E-05
GO:CC	nucleolus	GO:0005730	3.91E-05
GO:CC	polysome	GO:0005844	6.65E-05
GO:CC	secretory granule lumen	GO:0034774	2.20E-04
GO:CC	cytoplasmic vesicle lumen	GO:0060205	2.55E-04
GO:CC	vesicle lumen	GO:0031983	2.75E-04
GO:CC	proteasome complex	GO:0000502	5.44E-04
GO:CC	endopeptidase complex	GO:1905369	6.02E-04
GO:CC	cytosolic small ribosomal subunit	GO:0022627	7.19E-04
GO:CC	spliceosomal complex	GO:0005681	1.54E-03
GO:CC	eukaryotic 48S preinitiation complex	GO:0033290	2.11E-03
GO:CC	large ribosomal subunit	GO:0015934	2.78E-03
GO:CC	cytosolic large ribosomal subunit	GO:0022625	3.60E-03
GO:CC	peptidase complex	GO:1905368	3.96E-03
GO:CC	translation preinitiation complex	GO:0070993	4.64E-03
GO:CC	organelle inner membrane	GO:0019866	5.31E-03
GO:CC	U2 snRNP	GO:0005686	7.25E-03
GO:CC	zona pellucida receptor complex	GO:0002199	1.07E-02
GO:CC	mitochondrial nucleoid	GO:0042645	1.16E-02
GO:CC	nucleoid	GO:0009295	1.16E-02
GO:CC	cell body	GO:0044297	1.21E-02
GO:CC	proteasome core complex	GO:0005839	1.30E-02
GO:CC	small ribosomal subunit	GO:0015935	1.33E-02
GO:CC	mitochondrial inner membrane	GO:0005743	2.11E-02
GO:CC	U2-type precatalytic spliceosome	GO:0071005	2.17E-02
GO:CC	endoplasmic reticulum chaperone complex	GO:0034663	2.27E-02
GO:CC	precatalytic spliceosome	GO:0071011	2.39E-02
GO:CC	midbody	GO:0030496	4.21E-02
GO:CC	U2-type spliceosomal complex	GO:0005684	4.79E-02
GO:CC	polysomal ribosome	GO:0042788	4.97E-02
KEGG	Ribosome	KEGG:03010	9.42E-06
KEGG	Spliceosome	KEGG:03040	7.16E-05
KEGG	Protein processing in endoplasmic reticulum	KEGG:04141	1.14E-04
KEGG	RNA transport	KEGG:03013	2.52E-03
KEGG	Proteasome	KEGG:03050	4.90E-03

REAC	Translation	REAC:R-HSA-72766	3.88E-17
REAC	Metabolism of RNA	REAC:R-HSA-8953854	1.46E-15
REAC	GTP hydrolysis and joining of the 60S ribosomal subunit	REAC:R-HSA-72706	2.76E-12
REAC	Regulation of expression of SLITs and ROBOs	REAC:R-HSA-9010553	2.99E-12
REAC	Cap-dependent Translation Initiation	REAC:R-HSA-72737	8.22E-12
REAC	Eukaryotic Translation Initiation	REAC:R-HSA-72613	8.22E-12
REAC	L13a-mediated translational silencing of Ceruloplasmin expression	REAC:R-HSA-156827	3.72E-11
REAC	Signaling by ROBO receptors	REAC:R-HSA-376176	3.55E-10
REAC	Infectious disease	REAC:R-HSA-5663205	9.66E-10
REAC	Ribosomal scanning and start codon recognition	REAC:R-HSA-72702	5.21E-09
REAC	Eukaryotic Translation Termination	REAC:R-HSA-72764	8.30E-09
REAC	Nonsense Mediated Decay (NMD) independent of the Exon Junction Complex (EJC)	REAC:R-HSA-975956	1.11E-08
REAC	Nonsense Mediated Decay (NMD) enhanced by the Exon Junction Complex (EJC)	REAC:R-HSA-975957	1.25E-08
REAC	Nonsense-Mediated Decay (NMD)	REAC:R-HSA-927802	1.25E-08
REAC	Selenoamino acid metabolism	REAC:R-HSA-2408522	1.42E-08
REAC	Formation of a pool of free 40S subunits	REAC:R-HSA-72689	2.59E-08
REAC	Metabolism of amino acids and derivatives	REAC:R-HSA-71291	3.58E-08
REAC	Translation initiation complex formation	REAC:R-HSA-72649	1.05E-07
REAC	Activation of the mRNA upon binding of the cap-binding complex and eIFs, and subsequent binding to 43S	REAC:R-HSA-72662	1.27E-07
REAC	Influenza Life Cycle	REAC:R-HSA-168255	2.31E-07
REAC	Influenza Infection	REAC:R-HSA-168254	6.04E-07
REAC	Cellular responses to stress	REAC:R-HSA-2262752	6.74E-07
REAC	SRP-dependent cotranslational protein targeting to membrane	REAC:R-HSA-1799339	1.20E-06
REAC	Axon guidance	REAC:R-HSA-422475	1.22E-06
REAC	Eukaryotic Translation Elongation	REAC:R-HSA-156842	1.49E-06
REAC	Selenocysteine synthesis	REAC:R-HSA-2408557	1.49E-06
REAC	Attenuation phase	REAC:R-HSA-3371568	5.59E-06
REAC	Influenza Viral RNA Transcription and Replication	REAC:R-HSA-168273	8.88E-06
REAC	Formation of the ternary complex, and subsequently, the 43S complex	REAC:R-HSA-72695	9.40E-06
REAC	Peptide chain elongation	REAC:R-HSA-156902	1.09E-05
REAC	Viral mRNA Translation	REAC:R-HSA-192823	1.09E-05

REAC	HSP90 chaperone cycle for steroid hormone receptors (SHR)	REAC:R-HSA-3371497	2.17E-05
REAC	Cellular responses to external stimuli	REAC:R-HSA-8953897	3.14E-05
REAC	Folding of actin by CCT/TriC	REAC:R-HSA-390450	3.77E-05
REAC	mRNA Splicing – Major Pathway	REAC:R-HSA-72163	4.29E-05
REAC	mRNA Splicing	REAC:R-HSA-72172	7.39E-05
REAC	AUF1 (hnRNP D0) binds and destabilizes mRNA	REAC:R-HSA-450408	2.05E-04
REAC	HSF1-dependent transactivation	REAC:R-HSA-3371571	2.24E-04
REAC	Processing of Capped Intron-Containing Pre-mRNA	REAC:R-HSA-72203	2.47E-04
REAC	Host Interactions of HIV factors	REAC:R-HSA-162909	3.28E-04
REAC	Cooperation of PDCL (PhLP1) and TriC/CCT in G-protein beta folding	REAC:R-HSA-6814122	4.74E-04
REAC	Regulation of mRNA stability by proteins that bind AU-rich elements	REAC:R-HSA-450531	8.00E-04
REAC	Cellular response to heat stress	REAC:R-HSA-3371556	8.82E-04
REAC	Major pathway of rRNA processing in the nucleolus and cytosol	REAC:R-HSA-6791226	2.32E-03
REAC	The role of GTSE1 in G2/M progression after G2 checkpoint	REAC:R-HSA-8852276	3.87E-03
REAC	rRNA processing in the nucleus and cytosol	REAC:R-HSA-8868773	4.00E-03
REAC	Purine ribonucleoside monophosphate biosynthesis	REAC:R-HSA-73817	5.54E-03
REAC	rRNA processing	REAC:R-HSA-72312	6.66E-03
REAC	Formation of tubulin folding intermediates by CCT/TriC	REAC:R-HSA-389960	8.28E-03
REAC	Hedgehog ligand biogenesis	REAC:R-HSA-5358346	9.48E-03
REAC	Prefoldin mediated transfer of substrate to CCT/TriC	REAC:R-HSA-389957	1.21E-02
REAC	Interleukin-12 signaling	REAC:R-HSA-9020591	1.39E-02
REAC	Regulation of PTEN stability and activity	REAC:R-HSA-8948751	1.41E-02
REAC	Nucleobase biosynthesis	REAC:R-HSA-8956320	1.48E-02
REAC	Regulation of RUNX2 expression and activity	REAC:R-HSA-8939902	1.69E-02
REAC	Uptake and function of diphtheria toxin	REAC:R-HSA-5336415	1.81E-02
REAC	Cross-presentation of soluble exogenous antigens (endosomes)	REAC:R-HSA-1236978	1.99E-02

REAC	Regulation of activated PAK-2p34 by proteasome mediated degradation	REAC:R-HSA-211733	1.99E-02
REAC	HIV Infection	REAC:R-HSA-162906	2.09E-02
REAC	Regulation of ornithine decarboxylase (ODC)	REAC:R-HSA-350562	2.23E-02
REAC	RUNX1 regulates transcription of genes involved in differentiation of HSCs	REAC:R-HSA-8939236	2.33E-02
REAC	Ubiquitin Mediated Degradation of Phosphorylated Cdc25A	REAC:R-HSA-69601	2.50E-02
REAC	p53-Independent DNA Damage Response	REAC:R-HSA-69610	2.50E-02
REAC	Ubiquitin-dependent degradation of Cyclin D	REAC:R-HSA-75815	2.50E-02
REAC	Vpu mediated degradation of CD4	REAC:R-HSA-180534	2.50E-02
REAC	Autodegradation of the E3 ubiquitin ligase COP1	REAC:R-HSA-349425	2.50E-02
REAC	p53-Independent G1/S DNA damage checkpoint	REAC:R-HSA-69613	2.50E-02
REAC	Cooperation of Prefoldin and TriC/CCT in actin and tubulin folding	REAC:R-HSA-389958	2.77E-02
REAC	Negative regulation of NOTCH4 signaling	REAC:R-HSA-9604323	2.78E-02
REAC	Vif-mediated degradation of APOBEC3G	REAC:R-HSA-180585	2.78E-02
REAC	Regulation of Apoptosis	REAC:R-HSA-169911	2.78E-02
REAC	Regulation of RUNX3 expression and activity	REAC:R-HSA-8941858	3.10E-02
REAC	Antiviral mechanism by IFN-stimulated genes	REAC:R-HSA-1169410	3.38E-02
REAC	FBXL7 down-regulates AURKA during mitotic entry and in early mitosis	REAC:R-HSA-8854050	3.44E-02
REAC	SCF-beta-TrCP mediated degradation of Emi1	REAC:R-HSA-174113	3.44E-02
REAC	Degradation of AXIN	REAC:R-HSA-4641257	3.44E-02
REAC	Cytokine Signaling in Immune system	REAC:R-HSA-1280215	3.81E-02
REAC	Hh mutants that don’t undergo autocatalytic processing are degraded by ERAD	REAC:R-HSA-5362768	3.81E-02
REAC	Stabilization of p53	REAC:R-HSA-69541	4.21E-02
REAC	Degradation of DVL	REAC:R-HSA-4641258	4.21E-02
REAC	Interleukin-12 family signaling	REAC:R-HSA-447115	4.21E-02
REAC	Metabolism of polyamines	REAC:R-HSA-351202	4.65E-02
WP	Translation Factors	WP:WP107	1.68E-05
WP	Cytoplasmic Ribosomal Proteins	WP:WP477	2.58E-05
WP	Proteasome Degradation	WP:WP183	1.02E-02
WP	Trans-sulfuration and one carbon metabolism	WP:WP2525	1.86E-02
WP	mRNA Processing	WP:WP411	3.56E-02

21. Ontological enrichments of all up- and down-regulated proteins combined in HL60 and HT-29 cell lines

source	Term name	Term id	Adjusted p-value
GO:BP	mRNA metabolic process	GO:0016071	2.29E-37
GO:BP	nucleobase-containing compound catabolic process	GO:0034655	3.41E-32
GO:BP	aromatic compound catabolic process	GO:0019439	2.27E-30
GO:BP	heterocycle catabolic process	GO:0046700	4.34E-30
GO:BP	cellular nitrogen compound catabolic process	GO:0044270	4.78E-30
GO:BP	mRNA catabolic process	GO:0006402	8.61E-30
GO:BP	organic cyclic compound catabolic process	GO:1901361	4.19E-29
GO:BP	RNA catabolic process	GO:0006401	8.77E-29
GO:BP	symbiotic process	GO:0044403	1.19E-22
GO:BP	interspecies interaction between organisms	GO:0044419	4.38E-22
GO:BP	viral process	GO:0016032	8.87E-22
GO:BP	translational initiation	GO:0006413	3.93E-21
GO:BP	peptide metabolic process	GO:0006518	7.50E-21
GO:BP	translation	GO:0006412	1.01E-20
GO:BP	nuclear-transcribed mRNA catabolic process, nonsense-mediated decay	GO:0000184	3.64E-20
GO:BP	nuclear-transcribed mRNA catabolic process	GO:0000956	4.52E-20
GO:BP	peptide biosynthetic process	GO:0043043	5.40E-20
GO:BP	amide biosynthetic process	GO:0043604	8.18E-18
GO:BP	protein targeting to ER	GO:0045047	2.46E-16
GO:BP	establishment of protein localization to organelle	GO:0072594	5.18E-16
GO:BP	establishment of protein localization to endoplasmic reticulum	GO:0072599	5.85E-16
GO:BP	protein localization to endoplasmic reticulum	GO:0070972	3.85E-15
GO:BP	SRP-dependent cotranslational protein targeting to membrane	GO:0006614	4.54E-15
GO:BP	cotranslational protein targeting to membrane	GO:0006613	1.39E-14
GO:BP	posttranscriptional regulation of gene expression	GO:0010608	3.13E-14
GO:BP	protein localization to organelle	GO:0033365	6.81E-14
GO:BP	protein folding	GO:0006457	1.40E-13
GO:BP	RNA splicing, via transesterification reactions	GO:0000375	3.83E-13
GO:BP	viral gene expression	GO:0019080	1.60E-12
GO:BP	RNA splicing, via transesterification reactions with bulged adenosine as nucleophile	GO:0000377	1.50E-11
GO:BP	mRNA splicing, via spliceosome	GO:0000398	1.50E-11
GO:BP	viral transcription	GO:0019083	2.03E-11
GO:BP	regulation of mRNA metabolic process	GO:1903311	2.88E-11
GO:BP	mRNA processing	GO:0006397	3.29E-11
GO:BP	RNA splicing	GO:0008380	4.30E-11

GO:BP	protein targeting to membrane	GO:0006612	1.49E-10
GO:BP	protein targeting	GO:0006605	7.04E-10
GO:BP	RNA processing	GO:0006396	7.29E-10
GO:BP	cytoplasmic translation	GO:0002181	8.53E-10
GO:BP	establishment of protein localization to membrane	GO:0090150	1.10E-09
GO:BP	ribonucleoprotein complex biogenesis	GO:0022613	4.93E-09
GO:BP	RNA localization	GO:0006403	6.59E-09
GO:BP	chaperone-mediated protein folding	GO:0061077	1.16E-08
GO:BP	nuclear export	GO:0051168	1.38E-08
GO:BP	regulation of translation	GO:0006417	2.49E-08
GO:BP	ribonucleoprotein complex assembly	GO:0022618	6.76E-08
GO:BP	nucleocytoplasmic transport	GO:0006913	1.46E-07
GO:BP	protein export from nucleus	GO:0006611	1.72E-07
GO:BP	nuclear transport	GO:0051169	1.76E-07
GO:BP	ribonucleoprotein complex subunit organization	GO:0071826	2.08E-07
GO:BP	interleukin-12-mediated pathway	GO:0035722	3.16E-07
GO:BP	regulation of cellular amide metabolic process	GO:0034248	4.54E-07
GO:BP	cellular response to interleukin-12	GO:0071349	5.14E-07
GO:BP	response to interleukin-12	GO:0070671	6.50E-07
GO:BP	protein stabilization	GO:0050821	1.23E-06
GO:BP	regulation of mRNA stability	GO:0043488	1.23E-06
GO:BP	positive regulation of DNA biosynthetic process	GO:2000573	1.26E-06
GO:BP	regulation of catabolic process	GO:0009894	1.4E-06
GO:BP	regulation of RNA stability	GO:0043487	1.92E-06
GO:BP	regulation of protein stability	GO:0031647	1.93E-06
GO:BP	DNA biosynthetic process	GO:0071897	4.17E-06
GO:BP	response to heat	GO:0009408	5.85E-06
GO:BP	regulation of mRNA catabolic process	GO:0061013	8E-06
GO:BP	neutrophil degranulation	GO:0043312	8.44E-06
GO:BP	cellular response to heat	GO:0034605	8.84E-06
GO:BP	neutrophil activation involved in immune response	GO:0002283	9.67E-06
GO:BP	regulation of cellular catabolic process	GO:0031329	1.13E-05
GO:BP	neutrophil activation	GO:0042119	1.58E-05
GO:BP	neutrophil mediated immunity	GO:0002446	1.58E-05
GO:BP	telomere maintenance	GO:0000723	1.63E-05
GO:BP	protein localization to membrane	GO:0072657	1.83E-05
GO:BP	granulocyte activation	GO:0036230	2.04E-05
GO:BP	RNA transport	GO:0050658	3.3E-05
GO:BP	nucleic acid transport	GO:0050657	3.3E-05
GO:BP	establishment of RNA localization	GO:0051236	4.15E-05
GO:BP	regulation of DNA biosynthetic process	GO:2000278	4.18E-05
GO:BP	telomere organization	GO:0032200	4.9E-05
GO:BP	regulation of multi-organism process	GO:0043900	5.05E-05

GO:BP	leukocyte degranulation	GO:0043299	6.27E-05
GO:BP	regulation of cellular response to stress	GO:0080135	8.21E-05
GO:BP	myeloid cell activation involved in immune response	GO:0002275	9.3E-05
GO:BP	regulation of apoptotic pathway	GO:2001233	0.000103
GO:BP	RNA export from nucleus	GO:0006405	0.000105
GO:BP	response to temperature stimulus	GO:0009266	0.00012
GO:BP	myeloid leukocyte mediated immunity	GO:0002444	0.000122
GO:BP	'de novo' posttranslational protein folding	GO:0051084	0.000136
GO:BP	telomere maintenance via telomere lengthening	GO:0010833	0.000137
GO:BP	regulation of cellular amino acid metabolic process	GO:0006521	0.000141
GO:BP	positive regulation of DNA metabolic process	GO:0051054	0.000155
GO:BP	nucleobase-containing compound transport	GO:0015931	0.000164
GO:BP	cellular response to oxidative stress	GO:0034599	0.000182
GO:BP	regulation of protein localization to Cajal body	GO:1904869	0.000271
GO:BP	positive regulation of protein localization to Cajal body	GO:1904871	0.000271
GO:BP	positive regulation of multi-organism process	GO:0043902	0.000275
GO:BP	telomere maintenance via telomerase	GO:0007004	0.000295
GO:BP	apoptotic pathway	GO:0097190	0.000314
GO:BP	regulation of cellular protein localization	GO:1903827	0.000319
GO:BP	'de novo' protein folding	GO:0006458	0.000337
GO:BP	response to unfolded protein	GO:0006986	0.000346
GO:BP	regulation of oxidative stress-induced intrinsic apoptotic pathway	GO:1902175	0.000368
GO:BP	generation of precursor metabolites and energy	GO:0006091	0.00037
GO:BP	RNA-dependent DNA biosynthetic process	GO:0006278	0.000389
GO:BP	regulation of protein complex assembly	GO:0043254	0.000508
GO:BP	protein localization to nuclear body	GO:1903405	0.000535
GO:BP	positive regulation of establishment of protein localization to telomere	GO:1904851	0.000535
GO:BP	protein localization to Cajal body	GO:1904867	0.000535
GO:BP	chaperone-mediated protein complex assembly	GO:0051131	0.000556
GO:BP	leukocyte activation involved in immune response	GO:0002366	0.000599
GO:BP	positive regulation of cellular protein localization	GO:1903829	0.000627
GO:BP	chaperone cofactor-dependent protein refolding	GO:0051085	0.00063
GO:BP	antigen processing and presentation of exogenous peptide antigen via MHC class I, TAP-dependent	GO:0002479	0.000661
GO:BP	cell activation involved in immune response	GO:0002263	0.000678
GO:BP	positive regulation of protein localization to nucleus	GO:1900182	0.00075

GO:BP	regulation of establishment of protein localization to telomere	GO:0070203	0.000968
GO:BP	cellular response to toxic substance	GO:0097237	0.00097
GO:BP	cytoplasmic translational initiation	GO:0002183	0.001033
GO:BP	regulation of cellular response to heat	GO:1900034	0.001086
GO:BP	antigen processing and presentation of exogenous peptide antigen via MHC class I	GO:0042590	0.001086
GO:BP	regulation of intrinsic apoptotic pathway	GO:2001242	0.001114
GO:BP	cellular response to decreased oxygen levels	GO:0036294	0.001148
GO:BP	regulation of cellular protein catabolic process	GO:1903362	0.001361
GO:BP	protein localization to nucleoplasm	GO:1990173	0.001637
GO:BP	regulation of establishment of protein localization to chromosome	GO:0070202	0.001637
GO:BP	positive regulation of protein localization to chromosome, telomeric region	GO:1904816	0.001637
GO:BP	response to topologically incorrect protein	GO:0035966	0.00168
GO:BP	regulation of DNA-templated transcription in response to stress	GO:0043620	0.001793
GO:BP	mRNA transport	GO:0051028	0.001838
GO:BP	regulation of cellular amine metabolic process	GO:0033238	0.001942
GO:BP	hematopoietic stem cell differentiation	GO:0060218	0.001942
GO:BP	regulation of nuclease activity	GO:0032069	0.002119
GO:BP	ribonucleoprotein complex export from nucleus	GO:0071426	0.00231
GO:BP	ribonucleoprotein complex localization	GO:0071166	0.00251
GO:BP	regulated exocytosis	GO:0045055	0.002672
GO:BP	cellular amino acid metabolic process	GO:0006520	0.00286
GO:BP	regulation of protein catabolic process	GO:0042176	0.002889
GO:BP	positive regulation of telomere maintenance	GO:0032206	0.00296
GO:BP	cellular response to oxygen levels	GO:0071453	0.003252
GO:BP	cellular response to hypoxia	GO:0071456	0.003306
GO:BP	cellular detoxification	GO:1990748	0.003511
GO:BP	protein localization to nucleus	GO:0034504	0.00354
GO:BP	positive regulation of telomere maintenance via telomere lengthening	GO:1904358	0.003729
GO:BP	purine-containing compound metabolic process	GO:0072521	0.003908
GO:BP	regulation of protein localization to chromosome, telomeric region	GO:1904814	0.004032
GO:BP	purine nucleotide metabolic process	GO:0006163	0.004153
GO:BP	myeloid leukocyte activation	GO:0002274	0.004208
GO:BP	ATP metabolic process	GO:0046034	0.004597
GO:BP	regulation of hematopoietic stem cell differentiation	GO:1902036	0.005159
GO:BP	protein refolding	GO:0042026	0.005423
GO:BP	positive regulation of organelle organization	GO:0010638	0.005656
GO:BP	positive regulation of telomerase RNA localization to Cajal body	GO:1904874	0.005971
GO:BP	exocytosis	GO:0006887	0.006262

GO:BP	regulation of RNA splicing	GO:0043484	0.006407
GO:BP	regulation of innate immune response	GO:0045088	0.006956
GO:BP	tumor necrosis factor-mediated pathway	GO:0033209	0.007059
GO:BP	purine ribonucleoside triphosphate metabolic process	GO:0009205	0.007265
GO:BP	drug metabolic process	GO:0017144	0.007581
GO:BP	regulation of transcription from RNA polymerase II promoter in response to stress	GO:0043618	0.007596
GO:BP	protein catabolic process	GO:0030163	0.007653
GO:BP	regulation of mRNA processing	GO:0050684	0.007976
GO:BP	regulation of DNA metabolic process	GO:0051052	0.008093
GO:BP	regulation of oxidative stress-induced cell death	GO:1903201	0.008114
GO:BP	regulation of protein localization to nucleus	GO:1900180	0.00824
GO:BP	cytokine-mediated pathway	GO:0019221	0.008709
GO:BP	regulation of transcription from RNA polymerase II promoter in response to hypoxia	GO:0061418	0.009047
GO:BP	activation of innate immune response	GO:0002218	0.009416
GO:BP	antigen processing and presentation of peptide antigen via MHC class I	GO:0002474	0.009751
GO:BP	regulation of translational initiation	GO:0006446	0.01007
GO:BP	negative regulation of cell cycle process	GO:0010948	0.010773
GO:BP	intrinsic apoptotic pathway	GO:0097193	0.011196
GO:BP	alternative mRNA splicing, via spliceosome	GO:0000380	0.012418
GO:BP	intrinsic apoptotic pathway in response to oxidative stress	GO:0008631	0.012629
GO:BP	positive regulation of response to biotic stimulus	GO:0002833	0.01268
GO:BP	viral life cycle	GO:0019058	0.013236
GO:BP	ribonucleoside triphosphate metabolic process	GO:0009199	0.013758
GO:BP	purine ribonucleotide metabolic process	GO:0009150	0.014723
GO:BP	anaphase-promoting complex-dependent catabolic process	GO:0031145	0.015221
GO:BP	negative regulation of translation	GO:0017148	0.015713
GO:BP	nucleotide metabolic process	GO:0009117	0.015762
GO:BP	establishment of protein localization to telomere	GO:0070200	0.016385
GO:BP	regulation of telomerase RNA localization to Cajal body	GO:1904872	0.016385
GO:BP	purine nucleoside triphosphate metabolic process	GO:0009144	0.016814
GO:BP	regulation of mRNA binding	GO:1902415	0.017199
GO:BP	response to antibiotic	GO:0046677	0.017668
GO:BP	nucleoside triphosphate metabolic process	GO:0009141	0.017964
GO:BP	regulation of proteasomal protein catabolic process	GO:0061136	0.019062
GO:BP	nucleoside phosphate metabolic process	GO:0006753	0.020105

GO:BP	regulation of hematopoietic progenitor cell differentiation	GO:1901532	0.020433
GO:BP	regulation of cell cycle process	GO:0010564	0.020679
GO:BP	regulation of nucleocytoplasmic transport	GO:0046822	0.021201
GO:BP	RNA localization to Cajal body	GO:0090670	0.02195
GO:BP	RNA localization to nucleus	GO:0090685	0.02195
GO:BP	telomerase RNA localization	GO:0090672	0.02195
GO:BP	telomerase RNA localization to Cajal body	GO:0090671	0.02195
GO:BP	regulation of response to biotic stimulus	GO:0002831	0.022326
GO:BP	positive regulation of innate immune response	GO:0045089	0.022549
GO:BP	nucleobase-containing small molecule metabolic process	GO:0055086	0.02278
GO:BP	detoxification	GO:0098754	0.023765
GO:BP	negative regulation of apoptotic process	GO:0043066	0.023947
GO:BP	cellular protein complex disassembly	GO:0043624	0.024096
GO:BP	regulation of cellular response to oxidative stress	GO:1900407	0.024698
GO:BP	ribonucleotide metabolic process	GO:0009259	0.025308
GO:BP	regulation of telomerase activity	GO:0051972	0.026464
GO:BP	monosaccharide catabolic process	GO:0046365	0.027248
GO:BP	small molecule biosynthetic process	GO:0044283	0.027261
GO:BP	regulation of deoxyribonuclease activity	GO:0032070	0.028309
GO:BP	cellular response to aldehyde	GO:0110096	0.028309
GO:BP	response to endoplasmic reticulum stress	GO:0034976	0.030911
GO:BP	positive regulation of telomere maintenance via telomerase	GO:0032212	0.032573
GO:BP	regulation of alternative mRNA splicing, via spliceosome	GO:0000381	0.033863
GO:BP	proteasome-mediated ubiquitin-dependent protein catabolic process	GO:0043161	0.035763
GO:BP	ribose phosphate metabolic process	GO:0019693	0.035763
GO:BP	cellular response to unfolded protein	GO:0034620	0.035922
GO:BP	negative regulation of programmed cell death	GO:0043069	0.037931
GO:BP	negative regulation of cellular amide metabolic process	GO:0034249	0.038061
GO:BP	regulation of RNA binding	GO:1905214	0.043933
GO:BP	ribosome biogenesis	GO:0042254	0.045378
GO:BP	glucose catabolic process	GO:0006007	0.045941
GO:BP	positive regulation of telomerase activity	GO:0051973	0.045941
GO:BP	cellular component disassembly	GO:0022411	0.048597
GO:CC	ribonucleoprotein complex	GO:1990904	2.35E-32
GO:CC	cytosolic part	GO:0044445	3.39E-17
GO:CC	cytosolic ribosome	GO:0022626	1.57E-16
GO:CC	focal adhesion	GO:0005925	2.78E-15
GO:CC	cell-substrate adherens junction	GO:0005924	3.53E-15
GO:CC	cell-substrate junction	GO:0030055	5.24E-15

GO:CC	ficolin-1-rich granule	GO:0101002	6.69E-14
GO:CC	ficolin-1-rich granule lumen	GO:1904813	6.69E-14
GO:CC	adherens junction	GO:0005912	2.22E-13
GO:CC	ribosomal subunit	GO:0044391	4.62E-13
GO:CC	anchoring junction	GO:0070161	5.46E-13
GO:CC	polysome	GO:0005844	3.77E-12
GO:CC	pigment granule	GO:0048770	7.81E-12
GO:CC	melanosome	GO:0042470	7.81E-12
GO:CC	ribosome	GO:0005840	1.32E-11
GO:CC	chaperone complex	GO:0101031	5.03E-11
GO:CC	catalytic step 2 spliceosome	GO:0071013	6.25E-10
GO:CC	secretory granule lumen	GO:0034774	1.02E-09
GO:CC	cytoplasmic vesicle lumen	GO:0060205	1.36E-09
GO:CC	vesicle lumen	GO:0031983	1.56E-09
GO:CC	spliceosomal complex	GO:0005681	1.96E-08
GO:CC	cytosolic large ribosomal subunit	GO:0022625	2.10E-08
GO:CC	mitochondrial matrix	GO:0005759	2.94E-07
GO:CC	cytosolic small ribosomal subunit	GO:0022627	3.30E-07
GO:CC	large ribosomal subunit	GO:0015934	1.06E-06
GO:CC	proteasome complex	GO:0000502	1.46E-06
GO:CC	endopeptidase complex	GO:1905369	1.72E-06
GO:CC	polysomal ribosome	GO:0042788	5.83E-06
GO:CC	GAIT complex	GO:0097452	1.55E-05
GO:CC	peptidase complex	GO:1905368	3.48E-05
GO:CC	small ribosomal subunit	GO:0015935	5.04E-05
GO:CC	chaperonin-containing T-complex	GO:0005832	5.48E-05
GO:CC	nucleolus	GO:0005730	9.24E-05
GO:CC	ribonucleoprotein granule	GO:0035770	0.000102
GO:CC	cytoplasmic ribonucleoprotein granule	GO:0036464	0.001476
GO:CC	secretory granule	GO:0030141	0.00344
GO:CC	nuclear speck	GO:0016607	0.004004
GO:CC	nuclear body	GO:0016604	0.005257
GO:CC	cell body	GO:0044297	0.007584
GO:CC	eukaryotic translation initiation factor 4F complex	GO:0016281	0.009929
GO:CC	perinuclear region of cytoplasm	GO:0048471	0.010334
GO:CC	cytoplasmic stress granule	GO:0010494	0.013735
GO:CC	eukaryotic 48S preinitiation complex	GO:0033290	0.018506
GO:CC	azurophil granule lumen	GO:0035578	0.021734
GO:CC	organelle inner membrane	GO:0019866	0.023663
GO:CC	U2-type spliceosomal complex	GO:0005684	0.025373
GO:CC	U2-type precatalytic spliceosome	GO:0071005	0.031322
GO:CC	precatalytic spliceosome	GO:0071011	0.035051
GO:CC	translation preinitiation complex	GO:0070993	0.040022
KEGG	Ribosome	KEGG:03010	1.98E-11

KEGG	Protein processing in endoplasmic reticulum	KEGG:04141	5.48E-07
KEGG	Spliceosome	KEGG:03040	5.78E-07
KEGG	Carbon metabolism	KEGG:01200	3.25E-06
KEGG	Biosynthesis of amino acids	KEGG:01230	0.000241
KEGG	Proteasome	KEGG:03050	0.001378
KEGG	RNA transport	KEGG:03013	0.004583
KEGG	Antigen processing and presentation	KEGG:04612	0.005293
REAC	Metabolism of RNA	REAC:R-HSA-8953854	1.59E-30
REAC	Translation	REAC:R-HSA-72766	1.63E-22
REAC	Cap-dependent Translation Initiation	REAC:R-HSA-72737	6.68E-22
REAC	Eukaryotic Translation Initiation	REAC:R-HSA-72613	6.68E-22
REAC	L13a-mediated translational silencing of Ceruloplasmin expression	REAC:R-HSA-156827	1.21E-21
REAC	GTP hydrolysis and joining of the 60S ribosomal subunit	REAC:R-HSA-72706	1.61E-21
REAC	Regulation of expression of SLITs and ROBOs	REAC:R-HSA-9010553	3.56E-20
REAC	Signaling by ROBO receptors	REAC:R-HSA-376176	1.14E-18
REAC	Nonsense Mediated Decay (NMD) independent of the Exon Junction Complex (EJC)	REAC:R-HSA-975956	2.04E-17
REAC	Eukaryotic Translation Termination	REAC:R-HSA-72764	1.96E-16
REAC	Nonsense-Mediated Decay (NMD)	REAC:R-HSA-927802	2.16E-16
REAC	Nonsense Mediated Decay (NMD) enhanced by the Exon Junction Complex (EJC)	REAC:R-HSA-975957	2.16E-16
REAC	Infectious disease	REAC:R-HSA-5663205	1.11E-15
REAC	Formation of a pool of free 40S subunits	REAC:R-HSA-72689	1.56E-15
REAC	Eukaryotic Translation Elongation	REAC:R-HSA-156842	3.13E-15
REAC	Selenoamino acid metabolism	REAC:R-HSA-2408522	3.67E-15
REAC	Influenza Life Cycle	REAC:R-HSA-168255	4.03E-15
REAC	Influenza Infection	REAC:R-HSA-168254	2.50E-14
REAC	Selenocysteine synthesis	REAC:R-HSA-2408557	4.69E-14
REAC	Ribosomal scanning and start codon recognition	REAC:R-HSA-72702	1.83E-13
REAC	Translation initiation complex formation	REAC:R-HSA-72649	1.83E-13
REAC	mRNA Splicing – Major Pathway	REAC:R-HSA-72163	2.02E-13
REAC	SRP-dependent cotranslational protein targeting to membrane	REAC:R-HSA-1799339	2.51E-13
REAC	Viral mRNA Translation	REAC:R-HSA-192823	2.56E-13
REAC	Peptide chain elongation	REAC:R-HSA-156902	2.56E-13
REAC	Activation of the mRNA upon binding of the cap-binding complex and eIFs, and subsequent binding to 43S	REAC:R-HSA-72662	2.57E-13
REAC	mRNA Splicing	REAC:R-HSA-72172	6.48E-13
REAC	Influenza Viral RNA Transcription and Replication	REAC:R-HSA-168273	1.02E-12
REAC	Processing of Capped Intron-Containing Pre-mRNA	REAC:R-HSA-72203	7.08E-12
REAC	Metabolism of amino acids and derivatives	REAC:R-HSA-71291	4.02E-11
REAC	Axon guidance	REAC:R-HSA-422475	7.21E-11

REAC	Cellular responses to stress	REAC:R-HSA-2262752	2.98E-09
REAC	Formation of the ternary complex, and subsequently, the 43S complex	REAC:R-HSA-72695	4.15E-08
REAC	Major pathway of rRNA processing in the nucleolus and cytosol	REAC:R-HSA-6791226	7.00E-08
REAC	rRNA processing in the nucleus and cytosol	REAC:R-HSA-8868773	1.98E-07
REAC	rRNA processing	REAC:R-HSA-72312	5.23E-07
REAC	Cellular responses to external stimuli	REAC:R-HSA-8953897	7.80E-07
REAC	Interleukin-12 signaling	REAC:R-HSA-9020591	2.57E-06
REAC	Regulation of mRNA stability by proteins that bind AU-rich elements	REAC:R-HSA-450531	3.28E-06
REAC	Gene and protein expression by JAK-STAT after Interleukin-12 stimulation	REAC:R-HSA-8950505	3.75E-06
REAC	Attenuation phase	REAC:R-HSA-3371568	3.87E-06
REAC	AUF1 (hnRNP D0) binds and destabilizes mRNA	REAC:R-HSA-450408	1.22E-05
REAC	Interleukin-12 family signaling	REAC:R-HSA-447115	2.22E-05
REAC	Host Interactions of HIV factors	REAC:R-HSA-162909	6.51E-05
REAC	HSP90 chaperone cycle for steroid hormone receptors (SHR)	REAC:R-HSA-3371497	0.000234
REAC	Cellular response to heat stress	REAC:R-HSA-3371556	0.000259
REAC	HSF1-dependent transactivation	REAC:R-HSA-3371571	0.000321
REAC	Folding of actin by CCT/TriC	REAC:R-HSA-390450	0.000597
REAC	The role of GTSE1 in G2/M progression after G2 checkpoint	REAC:R-HSA-8852276	0.000699
REAC	Regulation of activated PAK-2p34 by proteasome mediated degradation	REAC:R-HSA-211733	0.0007
REAC	Apoptosis	REAC:R-HSA-109581	0.000892
REAC	Autodegradation of the E3 ubiquitin ligase COP1	REAC:R-HSA-349425	0.000988
REAC	Programmed Cell Death	REAC:R-HSA-5357801	0.001119
REAC	Regulation of Apoptosis	REAC:R-HSA-169911	0.001167
REAC	Neutrophil degranulation	REAC:R-HSA-6798695	0.00168
REAC	Stabilization of p53	REAC:R-HSA-69541	0.002188
REAC	Detoxification of Reactive Oxygen Species	REAC:R-HSA-3299685	0.005036
REAC	Hedgehog ligand biogenesis	REAC:R-HSA-5358346	0.006634
REAC	Cross-presentation of soluble exogenous antigens (endosomes)	REAC:R-HSA-1236978	0.006718
REAC	Deadenylation of mRNA	REAC:R-HSA-429947	0.007147
REAC	Oxygen-dependent proline hydroxylation of Hypoxia-inducible Factor Alpha	REAC:R-HSA-1234176	0.007531
REAC	p53-Dependent G1/S DNA damage checkpoint	REAC:R-HSA-69580	0.007531
REAC	p53-Dependent G1 DNA Damage Response	REAC:R-HSA-69563	0.007531
REAC	Regulation of ornithine decarboxylase (ODC)	REAC:R-HSA-350562	0.007812
REAC	HIV Infection	REAC:R-HSA-162906	0.007836
REAC	ER-Phagosome pathway	REAC:R-HSA-1236974	0.00784
REAC	Ubiquitin-dependent degradation of Cyclin D	REAC:R-HSA-75815	0.009053
REAC	Ubiquitin Mediated Degradation of Phosphorylated Cdc25A	REAC:R-HSA-69601	0.009053

REAC	Vpu mediated degradation of CD4	REAC:R-HSA-180534	0.009053
REAC	p53-Independent DNA Damage Response	REAC:R-HSA-69610	0.009053
REAC	p53-Independent G1/S DNA damage checkpoint	REAC:R-HSA-69613	0.009053
REAC	G1/S DNA Damage Checkpoints	REAC:R-HSA-69615	0.009637
REAC	Vif-mediated degradation of APOBEC3G	REAC:R-HSA-180585	0.010455
REAC	Negative regulation of NOTCH4 signaling	REAC:R-HSA-9604323	0.010455
REAC	Regulation of PTEN stability and activity	REAC:R-HSA-8948751	0.010865
REAC	Regulation of RUNX3 expression and activity	REAC:R-HSA-8941858	0.012034
REAC	Regulation of RUNX2 expression and activity	REAC:R-HSA-8939902	0.013724
REAC	Degradation of AXIN	REAC:R-HSA-4641257	0.013809
REAC	SCF-beta-TrCP mediated degradation of Emi1	REAC:R-HSA-174113	0.013809
REAC	FBXL7 down-regulates AURKA during mitotic entry and in early mitosis	REAC:R-HSA-8854050	0.013809
REAC	Prefoldin mediated transfer of substrate to CCT/TriC	REAC:R-HSA-389957	0.014355
REAC	MAPK6/MAPK4 signaling	REAC:R-HSA-5687128	0.014543
REAC	Cdc20:Phospho-APC/C mediated degradation of Cyclin A	REAC:R-HSA-174184	0.015377
REAC	Hh mutants that don't undergo autocatalytic processing are degraded by ERAD	REAC:R-HSA-5362768	0.015797
REAC	Deadenylation-dependent mRNA decay	REAC:R-HSA-429914	0.015797
REAC	APC:Cdc20 mediated degradation of cell cycle proteins prior to satisfaction of the cell cycle checkpoint	REAC:R-HSA-179419	0.017195
REAC	Cooperation of PDCL (PhLP1) and TriC/CCT in G-protein beta folding	REAC:R-HSA-6814122	0.017634
REAC	Degradation of DVL	REAC:R-HSA-4641258	0.018019
REAC	Metabolism of polyamines	REAC:R-HSA-351202	0.020496
REAC	Cellular response to hypoxia	REAC:R-HSA-1234174	0.021382
REAC	APC/C:Cdc20 mediated degradation of mitotic proteins	REAC:R-HSA-176409	0.021382
REAC	NIK→noncanonical NF-kB signaling	REAC:R-HSA-5676590	0.02325
REAC	CDT1 association with the CDC6:ORC:origin complex	REAC:R-HSA-68827	0.02325
REAC	Hh mutants abrogate ligand secretion	REAC:R-HSA-5387390	0.02325
REAC	Activation of APC/C and APC/C:Cdc20 mediated degradation of mitotic proteins	REAC:R-HSA-176814	0.023779
REAC	SCF(Skp2)-mediated degradation of p27/p21	REAC:R-HSA-187577	0.026305
REAC	Dectin-1 mediated noncanonical NF-kB signaling	REAC:R-HSA-5607761	0.026305
REAC	Degradation of GLI1 by the proteasome	REAC:R-HSA-5610780	0.026305
REAC	Degradation of GLI2 by the proteasome	REAC:R-HSA-5610783	0.026305
REAC	GLI3 is processed to GLI3R by the proteasome	REAC:R-HSA-5610785	0.026305
REAC	PTEN Regulation	REAC:R-HSA-6807070	0.029623
REAC	Defective CFTR causes cystic fibrosis	REAC:R-HSA-5678895	0.029688
REAC	Regulation of APC/C activators between G1/S and early anaphase	REAC:R-HSA-176408	0.035762
REAC	Antigen processing-Cross presentation	REAC:R-HSA-1236975	0.036511

REAC	Synthesis of DNA	REAC:R-HSA-69239	0.036605
REAC	Autodegradation of Cdh1 by Cdh1:APC/C	REAC:R-HSA-174084	0.037543
REAC	Cooperation of Prefoldin and TriC/CCT in actin and tubulin folding	REAC:R-HSA-389958	0.038357
REAC	Asymmetric localization of PCP proteins	REAC:R-HSA-4608870	0.042073
REAC	Purine ribonucleoside monophosphate biosynthesis	REAC:R-HSA-73817	0.049643
REAC	HSF1 activation	REAC:R-HSA-3371511	0.049643
REAC	Beta oxidation of octanoyl-CoA to hexanoyl-CoA	REAC:R-HSA-77348	0.049706
WP	Cytoplasmic Ribosomal Proteins	WP:WP477	5.75E-12
WP	Translation Factors	WP:WP107	1.53E-08
WP	mRNA Processing	WP:WP411	2.18E-05
WP	Proteasome Degradation	WP:WP183	0.001693
WP	Parkin-Ubiquitin Proteasomal System pathway	WP:WP2359	0.022498
WP	Purine metabolism	WP:WP4224	0.048474

22. Ontological enrichment analysis of genes found to have at least one instance of the 15 nt polypurine motif in their 5′ UTR from all down-regulated proteins found in the human cell line experiments. Terms size was limited to less than 1000 genes and the biological processes database was used.

source	Term name	Term id	Adjusted p-value
GO:BP	regulation of mRNA metabolic process	GO:1903311	0.002916
GO:BP	regulation of telomerase activity	GO:0051972	0.003043
GO:BP	positive regulation of telomerase RNA reverse transcriptase activity	GO:1905663	0.005562
GO:BP	protein-DNA complex assembly	GO:0065004	0.010165
GO:BP	regulation of telomerase RNA reverse transcriptase activity	GO:1905661	0.016667
GO:BP	posttranscriptional regulation of gene expression	GO:0010608	0.019862
GO:BP	protein-DNA complex subunit organization	GO:0071824	0.024031
GO:BP	negative regulation of mRNA metabolic process	GO:1903312	0.024098
GO:BP	mRNA metabolic process	GO:0016071	0.024689
GO:BP	regulation of mRNA stability	GO:0043488	0.027707
GO:BP	regulation of RNA stability	GO:0043487	0.031647
GO:BP	DNA conformation change	GO:0071103	0.034625
GO:BP	DNA biosynthetic process	GO:0071897	0.03983
GO:BP	regulation of mRNA catabolic process	GO:0061013	0.048408

23. 5' UTRs randomly chosen as a control list (UTRdb accession format)

5HSAA086530BA086532,	5HSAA004104BA004104,	5HSAA066146BA066324,
5HSAA058130BA058133,	5HSAA029152BA029163,	5HSAA019083BA019083,
5HSAA032178BA032179,	5HSAA047802BA047803,	5HSAA081916BA081916,
5HSAA017228BA017804,	5HSAA102315BA102315,	5HSAA044953BA044953,
5HSAA065319BA065319,	5HSAA030450BA030450,	5HSAA066031BA066031,
5HSAA106508BA106509,	5HSAA116023BA116023,	5HSAA066653BA066653,
5HSAA060716BA060719,	5HSAA042799BA042799,	5HSAA010920BA010920,
5HSAA001825BA001825,	5HSAA044094BA044095,	5HSAA121866BA121866,
5HSAA037091BA037091,	5HSAA103639BA103642,	5HSAA014072BA014199,
5HSAA098339BA098339,	5HSAA065697BA065697,	5HSAA000848BA000863,
5HSAA038558BA038559,	5HSAA009755BA009755,	5HSAA029046BA029046,
5HSAA095366BA095373,	5HSAA093410BA093410,	5HSAA049159BA049159,
5HSAA030157BA030157,	5HSAA063274BA063274,	5HSAA008350BA008364,
5HSAA120815BA120815,	5HSAA058312BA058312,	5HSAA048328BA048329,
5HSAA012641BA012641,	5HSAA091337BA091340,	5HSAA014437BA014437,
5HSAA076177BA076177,	5HSAA059672BA059687,	5HSAA031687BA031691,
5HSAA073156BA073156,	5HSAA090918BA090924,	5HSAA017925BA017925,
5HSAA021287BA021288,	5HSAA011639BA011639,	5HSAA101510BA101512,
5HSAA031773BA031773,	5HSAA026465BA026466,	5HSAA097462BA097462,
5HSAA053172BA053182,	5HSAA110636BA110636,	5HSAA071863BA071864,
5HSAA047879BA047879,	5HSAA047685BA047685,	5HSAA075423BA075428,
5HSAA093392BA093392,	5HSAA107486BA107490,	5HSAA092639BA092639,
5HSAA110636BA110639,	5HSAA072527BA072538,	5HSAA114717BA114717,
5HSAA083169BA083219,	5HSAA054872BA054872,	5HSAA067404BA067404,
5HSAA102663BA102663,	5HSAA026070BA026070,	5HSAA024095BA024164,
5HSAA050463BA050463,	5HSAA060012BA060020,	5HSAA000930BA000931,
5HSAA081555BA081557,	5HSAA026364BA026365,	5HSAA006721BA006722,
5HSAA044304BA044304,	5HSAA011131BA011139,	5HSAA069777BA069777,
5HSAA055088BA055088,	5HSAA024655BA024655,	5HSAA085125BA085125,
5HSAA072046BA072046,	5HSAA027654BA027654,	5HSAA114368BA114368,

5HSAA045069BA045069,	5HSAA095907BA095907,	5HSAA076423BA076425,
5HSAA114818BA114818,	5HSAA012842BA012854,	5HSAA022547BA022547,
5HSAA121409BA121418,	5HSAA099824BA099826,	5HSAA033737BA033737,
5HSAA103862BA103862,	5HSAA047455BA047459,	5HSAA097233BA097251,
5HSAA008884BA008884,	5HSAA015124BA015124,	5HSAA037294BA037294,
5HSAA075547BA075561,	5HSAA072819BA072819,	5HSAA082289BA082306,
5HSAA106624BA106624,	5HSAA085863BA085868,	5HSAA067058BA067059,
5HSAA102706BA102706,	5HSAA071805BA071805,	5HSAA018297BA018301,
5HSAA066877BA066879,	5HSAA120863BA120863,	5HSAA114666BA114666,
5HSAA014602BA014602,	5HSAA093737BA093737,	5HSAA080070BA080070,
5HSAA121700BA121702,	5HSAA107988BA108030,	5HSAA029036BA029036,
5HSAA102316BA102317,	5HSAA052800BA052866,	5HSAA035328BA035331,
5HSAA081291BA081293,	5HSAA118888BA118889,	5HSAA031740BA031740,
5HSAA087115BA087115,	5HSAA096811BA096811,	5HSAA071788BA071788,
5HSAA030949BA030951,	5HSAA000598BA000598,	5HSAA000669BA000670,
5HSAA081622BA081622		

24. Enriched 5′ UTR motifs found in control 5′ UTR list consisting of 136 genes

Length range	E-value	Number of motif instances	Length of motif	Motif
5-20	$2.5x10^{-32}$	108	20	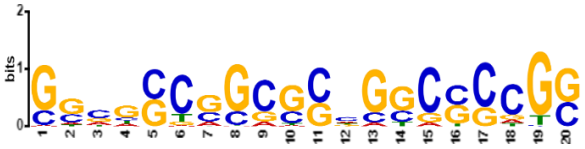
	$4.2x10^{-32}$	51	20	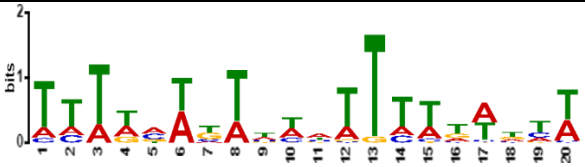
	$2.5x10^{-12}$	46	15	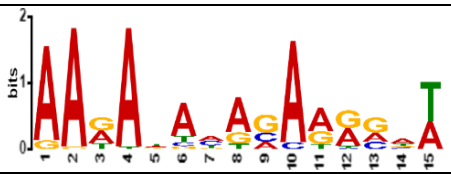
	$1.3x10^{-6}$	14	15	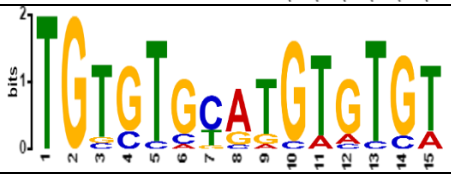
	$8.5x10^{-5}$	21	15	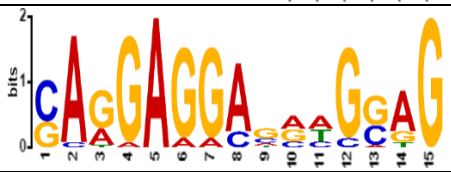
5-15	$4.1x10^{-26}$	42	15	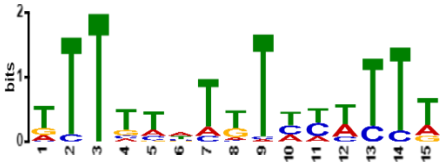
	$2.0x10^{-15}$	62	15	
	$3.7x10^{-14}$	54	15	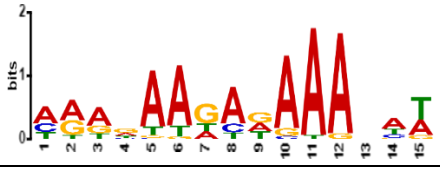
	$1.3x10^{-6}$	14	15	
	$1.6x10^{-2}$	26	15	

5-10	1.2x10-012	35	10	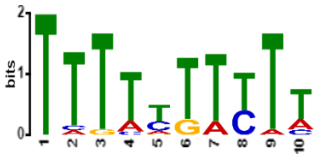
	1.3x10-009	39	8	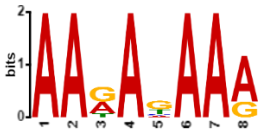
	2.0x10-009	55	10	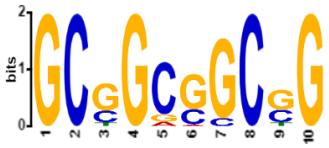
	4.6x10-002	15	10	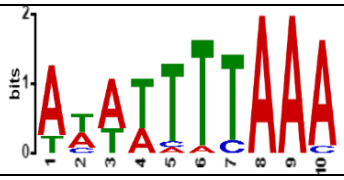

25. Glioblastoma multiforme and 1A9 cell lines pateamine treatment MTTs

Glioblastoma cell lines were cultured in RPMI 1640 with 10% FCS and 1% penstrep. MTT pateamine treatments were prepared using the same method used for HT-29 cells (Section 3.2.2)

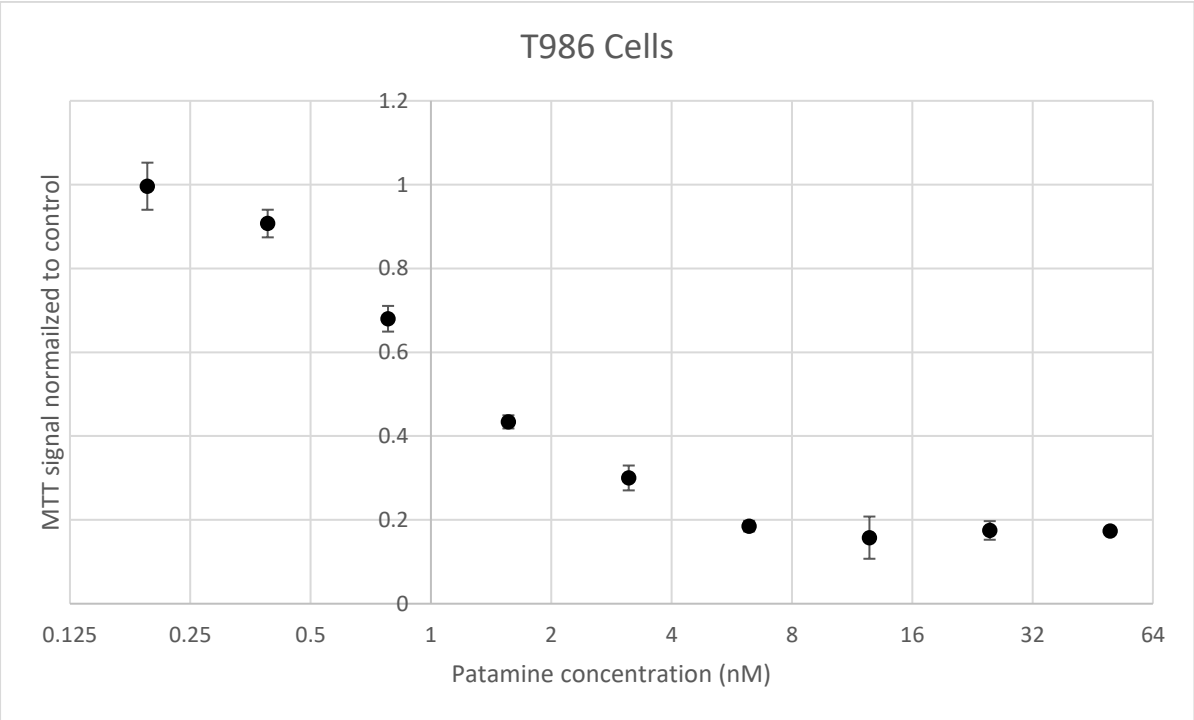

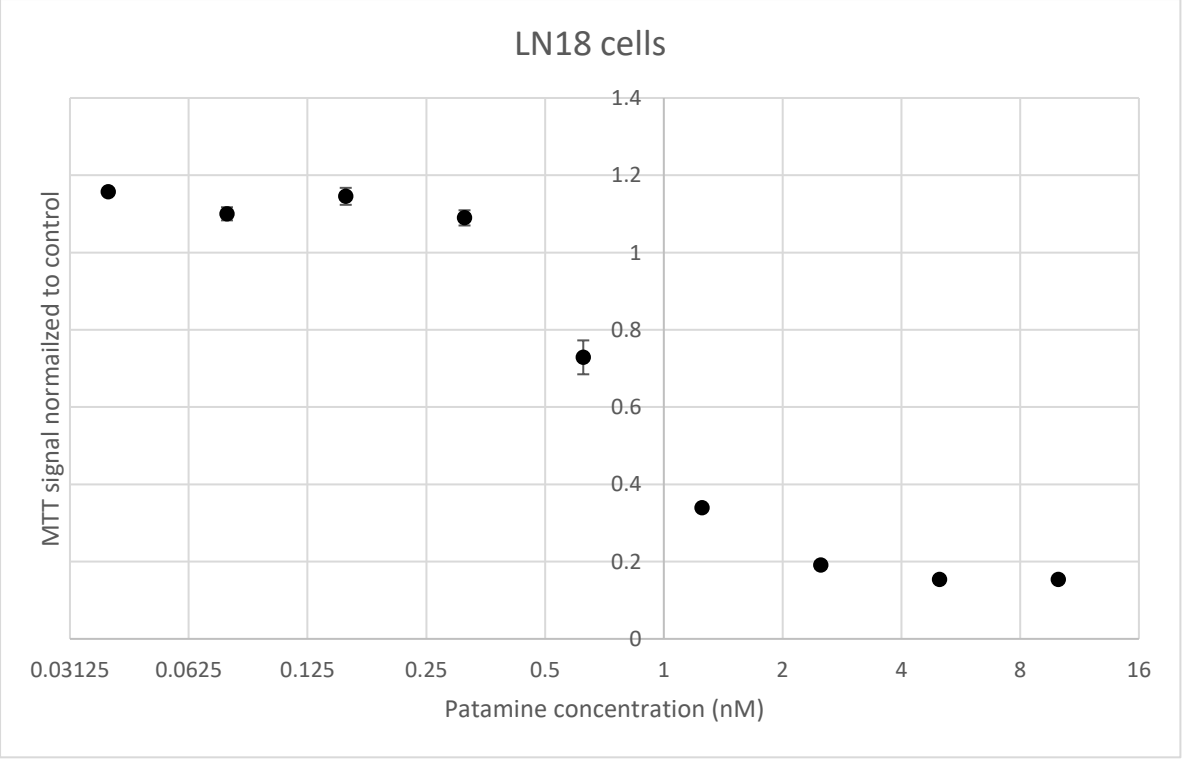

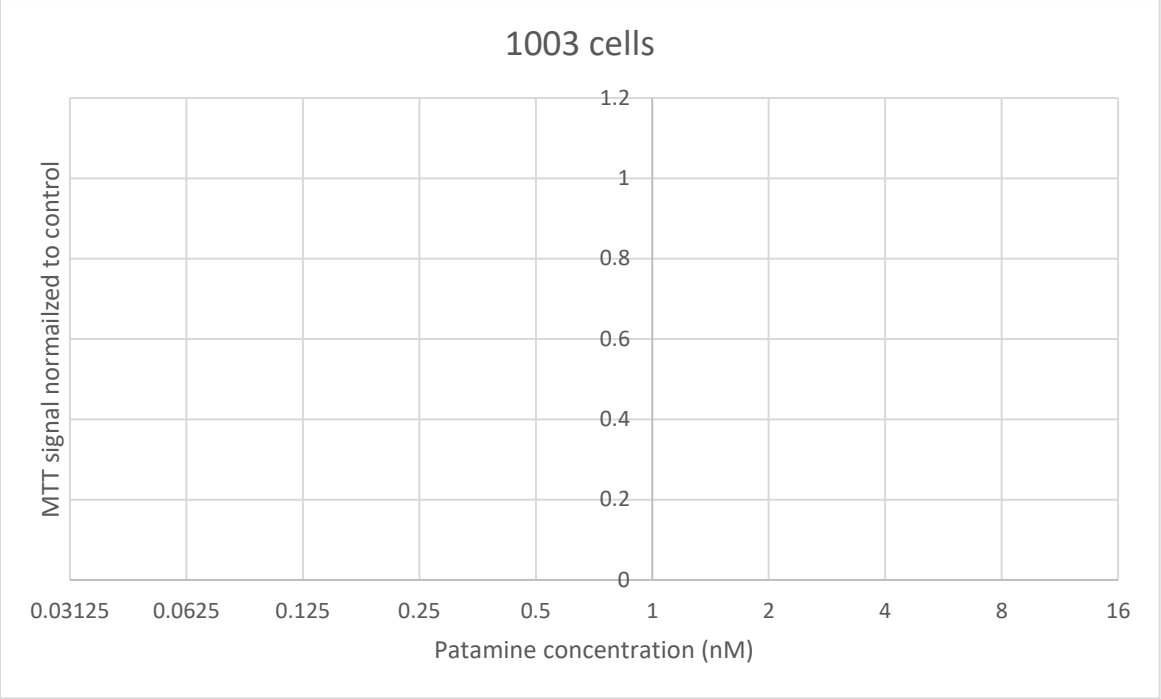

The 1A9 cell line was cultured in DMEM media with 10% FCS and 1% penstrep. MTT pateamine treatments were prepared using the same method used for HT-29 cells (Section 3.2.2)

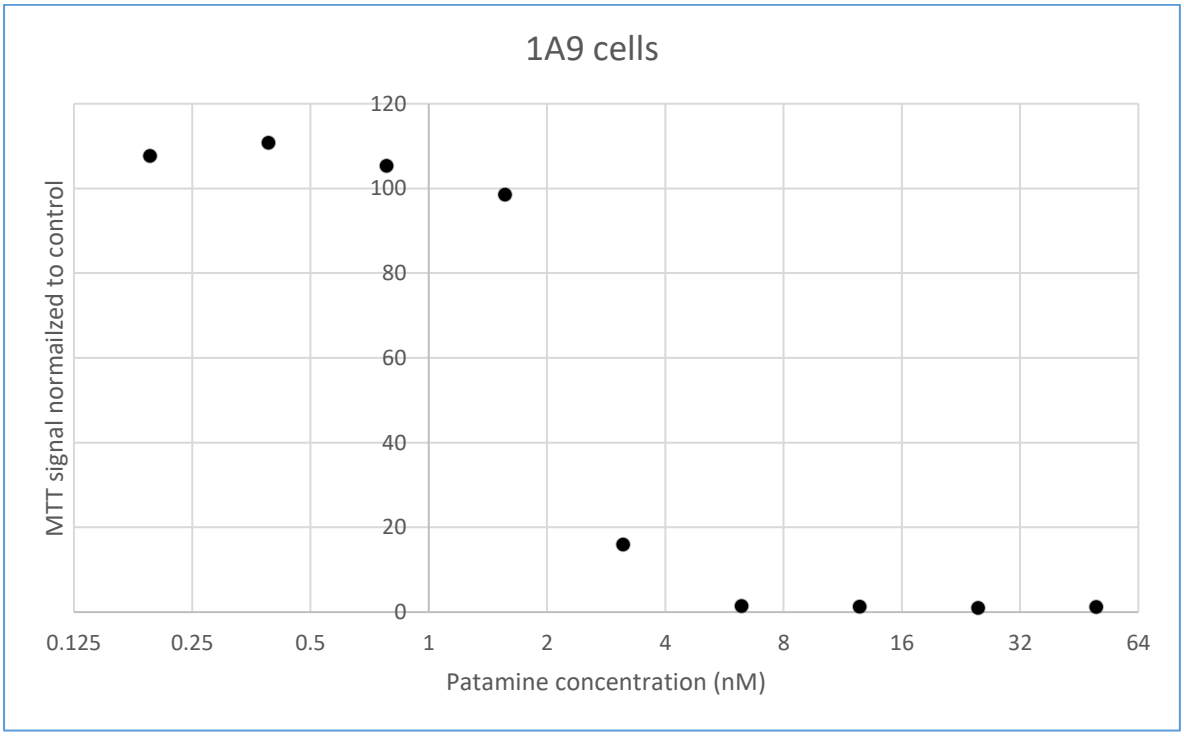

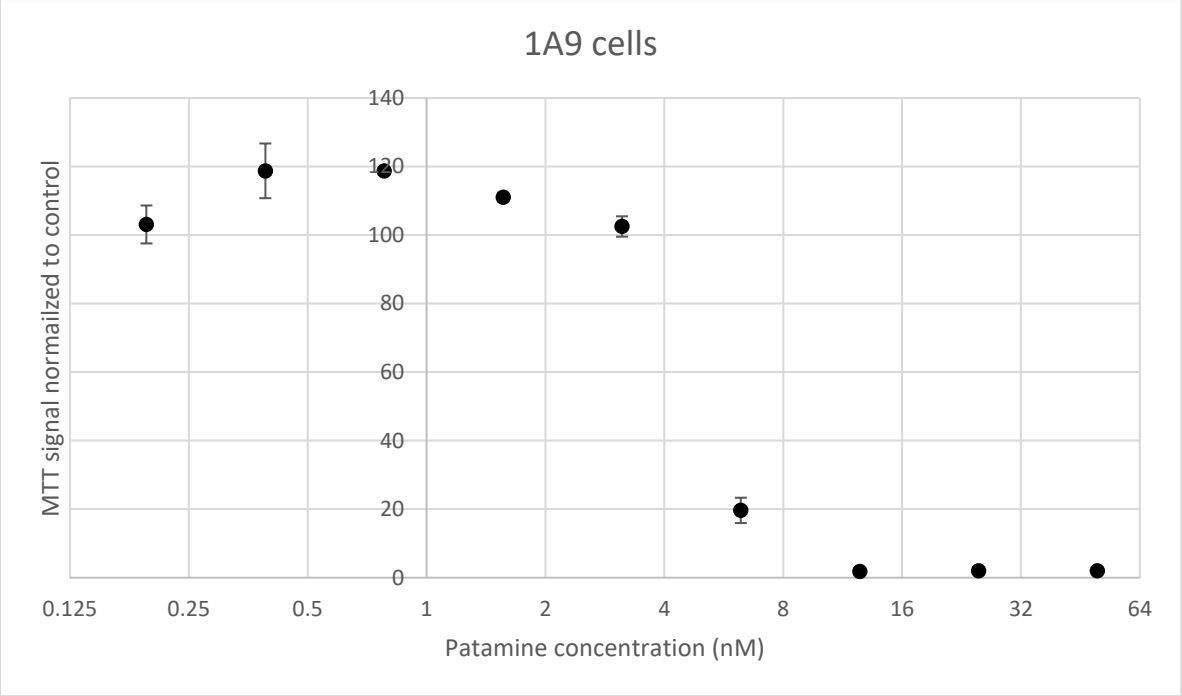
1A9 cells
MTT signal normalized to control
140
120
100
80
60
40
20
0
0.125
0.25
0.5
1
2
4
8
16
32
64
Patamine concentration (nM)

26. 5' UTR sequences proteins selected for western blot analysis

RELA/NFKB p65

AGCGCGCAGGCGCGGCCGGATTCCGGGCAGTGACGCGACGGCGGGCCGCGCGGCGCATTTCCGCCTCT
GGCGAATGGCTCGTCTGTAGTGCACGCCGCGGGCCCAGCTGCGACCCCGGCCCCGCCCCCGGGACCCC
GGCC

PPCPCPCPPPCPCPPCCPPPTTCCPPPCPPTPPCPCPPCPPCPPPCCPCPCPPCPCPTTTCCPCCTCT
PPCPPPTPPCTCPTCTPTPPTPCPCPCCPCPPPCCCPPCTPCPPCCCCPPCCCCPCCCCCPPPPCCCC
PPCC

NFKB1 NFkB p105

GTGAGAGAGTGAGCGAGACAGAAAGAGAGAGAAGTGCACCAGCGAGCCGGGGCAGGAAGAGGAGGTTT
CGCCACCGGAGCGGCCCGGCGACGCGCTGACAGCTTCCCCTGCCCTTCCCGTCGGTCGGGCCGCCAGC
CGCCGC

AGCCCTCGGCCTGCACGCAGCCACCGGCCCCGCTCCCGGAGCCCAGCGCCGCCGAGGCCGCAGCCGCC
CGGCCAGTAAGGCGGCGCCGCCGCCCGGCCACCGCGCGCCCTGCGCTTCCCTCCGCCCGCGCTGCGGC
CATGGC

GCGGCGCTGACTGGCCTGGCCCGGCCCCGCCGCGCTCCCGCTCGCCCCGACCCGCACTCGGGCCCGCC
CGGGCTCCGGCCTGCCGCCGCCTCTTCCTTCTCCAGCCGGCAGGCCCGCGCCGCTTAGGAGGGAGAGC
CCACCC

GCGCCAGGAGGCCGAACGCGGACTCGCCACCCGGCTTCAGA

PTPPPPPPPTPPPCPPPPCPPPPPPPPPPPPPPPTPCPCCPPCPPPCCPPPPCPPPPPPPPPPPTTT
CPCCPCCPPPPCPPCCCPPCPPCPCPCTPPCPPCTTCCCCTPCCCTTCCCPTCPPTCPPPCCPCCPPC
CPCCPC

PPCCCTCPPCCTPCPCPCPPCCPCCPPCCCCPCTCCCPPPPCCCPPCPCCPCCPPPPCCPCPPCCPCC
CPPCCPPTPPPPCPPCPCCPCCPCCCPPCCPCCPCPCPCCCTPCPCTTCCCTCCPCCCPCPCTPCPPC
CPTPPC

PCPPCPCTPPCTPPCCTPPCCCPPCCCCPCCPCPCTCCCPCTCPCCCCPPCCCPCPCTCPPPCCCPCC
CPPPCTCCPPCCTPCCPCCPCCTCTTCCTTCTCCPPCCPPCPPPCCCPCPCCPCTT**PPPPPPPPPPP**C
CCPCCC

PCPCCPPPPPPCCPPPCPCPPPCTCPCCPCCCPPCTTCPPP

iNOS

ATAACTTTGTAGCGAGTCGAAAACTGAGGCTCCGGCCGCAGAGAACTCAGCCTCATTCCTGCTTTAAA
ATCTCTCGGCCACCTTTGATGAGGGGACTGGGCAGTTCTAGACAGTCCCGAAGTTCTCAAGGCACAGG
TCTCTTCCTGGTTTGACTGTCCTTACCCCGGGGAGGCAGTGCAGCCAGCTGCAAGCCCCACAGTGAAG
AACATCTGAGCTCAAATCCAGATAAGTGACATAAGTGACCTGCTTTGTAAAGCCATAGAG

PT**PP**CTTT**P**T**PP**C**PPP**TC**PPPPP**CT**PPPP**CTCC**PP**CC**P**C**PPPPPP**CTC**PP**CCTC**P**TTCCT**P**CTTT**PPP**
PTCTCTC**PP**CC**P**CCTTT**PP**T**PPPPPPP**CT**PPP**C**PP**TTCT**PPP**C**PP**TCCC**PPPP**TTCTC**PPPP**C**P**C**PPP**
TCTCTTCCT**PP**TTT**PP**CT**P**TCCTT**P**CCCC**PPPPPPP**C**PP**T**P**C**PP**CC**PP**CT**P**C**PPP**CCCC**P**C**PP**T**PPPP**
PPC**P**TCT**PPP**CTC**PPP**TCC**PPP**T**PPP**T**PP**C**P**T**PPP**T**PP**CCT**P**CTTT**P**T**PPPP**CC**P**T**PPPP**

Known to respond to pateamine. Some relatively polypurine rich regions.

GATA3

UTR not validated in UTRdb

GGCGCCGTCTTGATACTTTCAGAAAGAATGCATTCCCTGTAAAAAAAAAAAAAAAAATACTGAGAGAGG
GAGAGAGAGAGAGAAGAAGAGAGAGAGACGGAGGGAGAGCGAGACAGAGCGAGCAACGCAATCTGACC
GAGCAGGTCGTACGCCGCCGCCTCCTCCTCCTCTCTGCTCTTCGCTACCCAGGTGACCCGAGGAGGGA
CTCCGCCTCCGAGCGGCTGAGGACCCCGGTGCAGAGGAGCCTGGCTCGCAGAATTGCAGAGTCGTCGC
CCCTTTTTACAACCTGGTCCCGTTTTATTCTGCCGTACCCAGTTTTTGGATTTTTGTCTTCCCCTTCT
TCTCTTTGCTAAACGACCCCTCCAAGATAATTTTTAAAAAACCTTCTCCTTTGCTCACCTTTGCTTCC
CAGCCTTCCCATCCCCCCACCGAAAGCAAATCATTCAACGACCCCCGACCCTCCGACGGCAGGAGCCC
CCCGACCTCCCAGGCGGACCGCCCTCCCTCCCCGCGCGCGGGTTCCGGGCCCGGCGAGAGGGCGCGAG
CACAGCCGAGGCC

PPCPCCPTCTTPPTPCTTTCPPPPPPPPTPCPTTCCCTPT**PPPPPPPPPPPPPPPPP**TPCT**PPPPPPPP**
PPPPPPPPPPPPPPPPPPPPPPPPPPPPPCPPPPPPPPPPCPPPPCPPPPCPPPCPPCPCPPTCTPPCC
PPPCPPPTCPTPCPCCPCCPCCTCCTCCTCCTCTCTPCTCTTCPCTPCCCPPPTPPCCCPPPPPPPPP
CTCCPCCTCCPPPCPPCTPPPPPCCCCPPTPCPPPPPPPCCTPPCTCPCPPPPTTPCPPPPTCPTCPC
CCCTTTTTPCPPCCTPPTCCCPTTTTPTTCTPCCPTPCCCPPTTTTTPPPTTTTTPTCTTCCCCTTCT
TCTCTTTPCTPPPCPPCCCCTCCPPPPTPPTTTTTPPPPPPCCTTCTCCTTTPCTCPCCTTTPCTTCC
CPPCCTTCCCPTCCCCCCPCCPPPPPCPPPTCPTTCPPCPPCCCCCPPCCCTCCPPCPPCPPPPPCCC
CCCPPCCTCCCPPPCPPPCCPCCCTCCCTCCCCPCPCPCPPPTTCCPPPCCCPPCPPPPPPPCPCPPP
CPCPPCCPPPPCC

Had strong polypurine motifs but a long way from the start codon.

SOX6

Four 5’ UTRs in UTRdb. All not validated.

>SOX6-shortest

AGTTGTTAGGAGAGACCATTGGGGATAGGAAAG

PPTTPTTPPPPPPPPCCPTT**PPPPP**T**PPPPPPP**

>SOX6-short

GTCACTTTCATGAATTCAAAGGCAATTTACCAGTGATTTCTGGGTGCTGGGGCTGATATTTTTTGTGC
ATATTTAAGA

PTCPCTTTCPTPPPTTCPPPPPCPPTTTPCCPPTPPTTTCTPPPTPCTPPPPCTPPTPTTTTTTPTPC
PTPTTTPPPP

>SOX6-medium

CCTTGGGGTTAGTTTTAGTCATATTTTTATCTCTATAAAACATCAGGCTGGGAGGTGGTGTGTGCCTG
TAGTCTCAACTGCTAGGGAGCCTGAGGCAGGAAGACTCCTTGAGCACAGGAGTTCAAGGCCAGCCTGT
GCAACATAGTGAGACCCTATCACTCTGGAAAAAAAAAAAAAATCTGCGGAGAAGA

CCTTPPPPTTPPTTTTPPTPPPPPCPTCPPPCTPPPPPPTPPTPTPTPCCTPTPPTCTCPPCTPCTPP
PPPPCCTPPPPCPPPPPPPCTCCTTPPPCPCPPPPPTTCPPPPCCPPCCTPTPCPPCPTPPTPPPPCC
CTPTCPCTCT**PPPPPPPPPPPPPPPP**TCTPCPPPPPPPP

>SOX6-long

AGTTGTTAGGAGAGACCATTGGGGATAGGAAAGATGAAAGGTCATGGTGAGCTTCAAGGACATGAAAG
GTTGTTGTCTCATGTAACAATAGTAGATTGTTTTTTTTCCTAATATTTCTAGCCAGCCCCTAAGTCAG
GTGATGGAACAAATACCTACAGTTTAGTCAGGTGAAACAGGAGTGGGTGGAGGAAGGAAAGAAGAAAA

PPTTPTTPPPPPPPPCCPTTPPPPPTPPPPPPPPTPPPPPPTCPTPPTPPPCTTCPPPPPCPTPPPPP
PTTPTTPTCTCPTPTPPCPPTPPTPPPTTPTTTTTTTTCCTPPTPTTTCTPPCCPPCCCCTPPPTCPP
PTPPTPPPPCPPPTPCCTPCPPTTTPPTCPPPTPPPPCPPPPPTPPPT**PPPPPPPPPPPPPPPPPPP**

27. Gene ontology analysis of pateamine compared to bortezimib of up-regulated proteins for the biological process database (including only terms with 2000 entries or fewer)

Bortezomib	GO:BP	mRNA metabolic process	GO:0016071	2.07E-12
Pateamine	GO:BP	mRNA metabolic process	GO:0016071	1.11E-19
Bortezomib	GO:BP	translation	GO:0006412	1.37E-08
Pateamine	GO:BP	translation	GO:0006412	1.93E-12
Bortezomib	GO:BP	peptide metabolic process	GO:0006518	1.88E-08
Pateamine	GO:BP	peptide metabolic process	GO:0006518	1.22E-10
Bortezomib	GO:BP	peptide biosynthetic process	GO:0043043	2.64E-08
Pateamine	GO:BP	peptide biosynthetic process	GO:0043043	5.04E-12
Bortezomib	GO:BP	posttranscriptional regulation of gene expression	GO:0010608	1.19E-13
Pateamine	GO:BP	posttranscriptional regulation of gene expression	GO:0010608	9.11E-08
Bortezomib	GO:BP	amide biosynthetic process	GO:0043604	1.26E-07
Pateamine	GO:BP	amide biosynthetic process	GO:0043604	2.17E-11
Bortezomib	GO:BP	cellular amide metabolic process	GO:0043603	1.59E-07
Pateamine	GO:BP	cellular amide metabolic process	GO:0043603	4.51E-10
Bortezomib	GO:BP	viral process	GO:0016032	1.94E-07
Pateamine	GO:BP	viral process	GO:0016032	8.09E-15
Bortezomib	GO:BP	cellular protein-containing complex assembly	GO:0034622	5.61E-08
Pateamine	GO:BP	cellular protein-containing complex assembly	GO:0034622	2.54E-07
Bortezomib	GO:BP	symbiotic process	GO:0044403	6.4E-07
Pateamine	GO:BP	symbiotic process	GO:0044403	6.39E-14
Bortezomib	GO:BP	chaperone-mediated protein folding	GO:0061077	1.53E-06
Pateamine	GO:BP	chaperone-mediated protein folding	GO:0061077	4.96E-09
Bortezomib	GO:BP	interspecies interaction between organisms	GO:0044419	1.83E-06
Pateamine	GO:BP	interspecies interaction between organisms	GO:0044419	3.93E-13
Bortezomib	GO:BP	mRNA catabolic process	GO:0006402	2.99E-06
Pateamine	GO:BP	mRNA catabolic process	GO:0006402	3.37E-16
Bortezomib	GO:BP	protein folding	GO:0006457	5.63E-06
Pateamine	GO:BP	protein folding	GO:0006457	7.40E-14
Bortezomib	GO:BP	protein-containing complex assembly	GO:0065003	7.7E-06
Pateamine	GO:BP	protein-containing complex assembly	GO:0065003	1.73E-08
Bortezomib	GO:BP	RNA catabolic process	GO:0006401	9.91E-06
Pateamine	GO:BP	RNA catabolic process	GO:0006401	3.49E-16
Bortezomib	GO:BP	nucleobase-containing compound catabolic process	GO:0034655	7.35E-05
Pateamine	GO:BP	nucleobase-containing compound catabolic process	GO:0034655	2.06E-17
Bortezomib	GO:BP	RNA processing	GO:0006396	4.21E-08
Pateamine	GO:BP	RNA processing	GO:0006396	8.39E-05
Bortezomib	GO:BP	organonitrogen compound biosynthetic process	GO:1901566	9.42E-05

Pateamine	GO:BP	organonitrogen compound biosynthetic process	GO:1901566	4.39E-08
Bortezomib	KEGG	Spliceosome	KEGG:03040	3.29E-05
Pateamine	KEGG	Spliceosome	KEGG:03040	7.3E-05
Bortezomib	GO:BP	telomere organization	GO:0032200	8.45E-05
Pateamine	GO:BP	telomere organization	GO:0032200	0.000114
Bortezomib	GO:BP	heterocycle catabolic process	GO:0046700	0.000231
Pateamine	GO:BP	heterocycle catabolic process	GO:0046700	3.05E-16
Bortezomib	GO:BP	cellular nitrogen compound catabolic process	GO:0044270	0.000236
Pateamine	GO:BP	cellular nitrogen compound catabolic process	GO:0044270	3.22E-16
Bortezomib	GO:BP	aromatic compound catabolic process	GO:0019439	0.000333
Pateamine	GO:BP	aromatic compound catabolic process	GO:0019439	7.20E-16
Bortezomib	GO:BP	DNA biosynthetic process	GO:0071897	0.000192
Pateamine	GO:BP	DNA biosynthetic process	GO:0071897	0.000296
Bortezomib	GO:BP	regulation of mRNA metabolic process	GO:1903311	3.20E-11
Pateamine	GO:BP	regulation of mRNA metabolic process	GO:1903311	0.000496
Bortezomib	GO:BP	telomere maintenance	GO:0000723	0.000522
Pateamine	GO:BP	telomere maintenance	GO:0000723	4.85E-05
Bortezomib	GO:BP	organic cyclic compound catabolic process	GO:1901361	0.000667
Pateamine	GO:BP	organic cyclic compound catabolic process	GO:1901361	3.72E-15
Bortezomib	GO:BP	response to heat	GO:0009408	0.000864
Pateamine	GO:BP	response to heat	GO:0009408	9.41E-05
Bortezomib	GO:BP	RNA localization	GO:0006403	0.001105
Pateamine	GO:BP	RNA localization	GO:0006403	4.78E-06
Bortezomib	GO:BP	'de novo' posttranslational protein folding	GO:0051084	6.13E-05
Pateamine	GO:BP	'de novo' posttranslational protein folding	GO:0051084	0.001194
Bortezomib	GO:BP	cellular response to heat	GO:0034605	0.001357
Pateamine	GO:BP	cellular response to heat	GO:0034605	6.17E-05
Bortezomib	GO:BP	mRNA processing	GO:0006397	8.64E-08
Pateamine	GO:BP	mRNA processing	GO:0006397	0.001522
Bortezomib	KEGG	Protein processing in endoplasmic reticulum	KEGG:04141	0.001722
Pateamine	KEGG	Protein processing in endoplasmic reticulum	KEGG:04141	0.000109
Bortezomib	GO:BP	response to temperature stimulus	GO:0009266	0.001449
Pateamine	GO:BP	response to temperature stimulus	GO:0009266	0.000443
Bortezomib	GO:BP	'de novo' protein folding	GO:0006458	0.000121
Pateamine	GO:BP	'de novo' protein folding	GO:0006458	0.002331
Bortezomib	GO:BP	regulation of translation	GO:0006417	3.09E-09
Pateamine	GO:BP	regulation of translation	GO:0006417	0.002501
Bortezomib	GO:BP	translational initiation	GO:0006413	0.002559
Pateamine	GO:BP	translational initiation	GO:0006413	2.34E-11
Bortezomib	GO:BP	cellular macromolecule catabolic process	GO:0044265	0.002643
Pateamine	GO:BP	cellular macromolecule catabolic process	GO:0044265	3.39E-14
Bortezomib	GO:BP	response to abiotic stimulus	GO:0009628	9.6E-05

Pateamine	GO:BP	response to abiotic stimulus	GO:0009628	0.003017
Bortezomib	GO:BP	regulation of catabolic process	GO:0009894	0.002923
Pateamine	GO:BP	regulation of catabolic process	GO:0009894	0.000307
Bortezomib	GO:BP	positive regulation of DNA biosynthetic process	GO:2000573	0.003265
Pateamine	GO:BP	positive regulation of DNA biosynthetic process	GO:2000573	0.000275
Bortezomib	KEGG	RNA transport	KEGG:03013	0.001316
Pateamine	KEGG	RNA transport	KEGG:03013	0.002563
Bortezomib	GO:BP	response to cytokine	GO:0034097	0.004437
Pateamine	GO:BP	response to cytokine	GO:0034097	7.99E-07
Bortezomib	GO:BP	cellular response to cytokine stimulus	GO:0071345	0.004928
Pateamine	GO:BP	cellular response to cytokine stimulus	GO:0071345	8.76E-08
Bortezomib	GO:BP	mRNA splicing, via spliceosome	GO:0000398	9.50E-10
Bortezomib	GO:BP	RNA splicing, via transesterification reactions with bulged adenosine as nucleophile	GO:0000377	9.50E-10
Pateamine	GO:BP	mRNA splicing, via spliceosome	GO:0000398	0.00505
Pateamine	GO:BP	RNA splicing, via transesterification reactions with bulged adenosine as nucleophile	GO:0000377	0.00505
Bortezomib	GO:BP	RNA splicing, via transesterification reactions	GO:0000375	1.10E-09
Pateamine	GO:BP	RNA splicing, via transesterification reactions	GO:0000375	0.005586
Bortezomib	GO:BP	protein localization to organelle	GO:0033365	0.006345
Pateamine	GO:BP	protein localization to organelle	GO:0033365	1.66E-06
Bortezomib	GO:BP	regulation of cellular catabolic process	GO:0031329	0.000202
Pateamine	GO:BP	regulation of cellular catabolic process	GO:0031329	0.008016
Bortezomib	GO:BP	response to unfolded protein	GO:0006986	0.008828
Pateamine	GO:BP	response to unfolded protein	GO:0006986	8.82E-05
Bortezomib	GO:BP	telomere maintenance via telomere lengthening	GO:0010833	0.009276
Pateamine	GO:BP	telomere maintenance via telomere lengthening	GO:0010833	7.48E-05
Bortezomib	GO:BP	regulation of cellular amide metabolic process	GO:0034248	2.31E-08
Pateamine	GO:BP	regulation of cellular amide metabolic process	GO:0034248	0.01103
Bortezomib	GO:BP	chaperone cofactor-dependent protein refolding	GO:0051085	0.000872
Pateamine	GO:BP	chaperone cofactor-dependent protein refolding	GO:0051085	0.010612
Bortezomib	GO:BP	neutrophil degranulation	GO:0043312	0.000116
Pateamine	GO:BP	neutrophil degranulation	GO:0043312	0.013254
Bortezomib	GO:BP	regulation of cellular response to heat	GO:1900034	0.000469
Pateamine	GO:BP	regulation of cellular response to heat	GO:1900034	0.013167
Bortezomib	GO:BP	macromolecule catabolic process	GO:0009057	0.013714
Pateamine	GO:BP	macromolecule catabolic process	GO:0009057	8.92E-15
Bortezomib	GO:BP	regulation of cellular protein localization	GO:1903827	0.002568
Pateamine	GO:BP	regulation of cellular protein localization	GO:1903827	0.011607
Bortezomib	GO:BP	neutrophil activation involved in immune response	GO:0002283	0.000126
Pateamine	GO:BP	neutrophil activation involved in immune response	GO:0002283	0.014324

Bortezomib	GO:BP	regulation of DNA-templated transcription in response to stress	GO:0043620	0.011047
Pateamine	GO:BP	regulation of DNA-templated transcription in response to stress	GO:0043620	0.003758
Bortezomib	GO:BP	RNA splicing	GO:0008380	4.25E-10
Pateamine	GO:BP	RNA splicing	GO:0008380	0.015434
Bortezomib	GO:BP	regulation of DNA biosynthetic process	GO:2000278	0.004209
Pateamine	GO:BP	regulation of DNA biosynthetic process	GO:2000278	0.011694
Bortezomib	GO:BP	neutrophil activation	GO:0042119	0.000168
Bortezomib	GO:BP	neutrophil mediated immunity	GO:0002446	0.000168
Pateamine	GO:BP	neutrophil activation	GO:0042119	0.018941
Pateamine	GO:BP	neutrophil mediated immunity	GO:0002446	0.018941
Bortezomib	GO:BP	cellular protein localization	GO:0034613	0.02097
Pateamine	GO:BP	cellular protein localization	GO:0034613	1.33E-05
Bortezomib	GO:BP	granulocyte activation	GO:0036230	2.89E-05
Pateamine	GO:BP	granulocyte activation	GO:0036230	0.021984
Bortezomib	GO:BP	response to topologically incorrect protein	GO:0035966	0.022141
Pateamine	GO:BP	response to topologically incorrect protein	GO:0035966	0.00035
Bortezomib	GO:BP	cellular macromolecule localization	GO:0070727	0.02321
Pateamine	GO:BP	cellular macromolecule localization	GO:0070727	1.58E-05
Bortezomib	GO:BP	establishment of protein localization to organelle	GO:0072594	0.023645
Pateamine	GO:BP	establishment of protein localization to organelle	GO:0072594	5.80E-08
Bortezomib	GO:BP	positive regulation of telomere maintenance	GO:0032206	0.015662
Pateamine	GO:BP	positive regulation of telomere maintenance	GO:0032206	0.011788
Bortezomib	GO:BP	intracellular protein transport	GO:0006886	0.029595
Pateamine	GO:BP	intracellular protein transport	GO:0006886	0.000653
Bortezomib	GO:BP	regulation of transcription from RNA polymerase II promoter in response to stress	GO:0043618	0.007996
Pateamine	GO:BP	regulation of transcription from RNA polymerase II promoter in response to stress	GO:0043618	0.023826
Bortezomib	GO:BP	nuclear export	GO:0051168	0.022979
Pateamine	GO:BP	nuclear export	GO:0051168	0.020589
Bortezomib	GO:BP	leukocyte degranulation	GO:0043299	0.000404
Pateamine	GO:BP	leukocyte degranulation	GO:0043299	0.043748
Bortezomib	GO:BP	regulation of RNA binding	GO:1905214	0.045546
Pateamine	GO:BP	regulation of RNA binding	GO:1905214	0.003867
Bortezomib	GO:BP	regulation of telomere maintenance via telomere lengthening	GO:1904356	0.041114
Pateamine	GO:BP	regulation of telomere maintenance via telomere lengthening	GO:1904356	0.03714